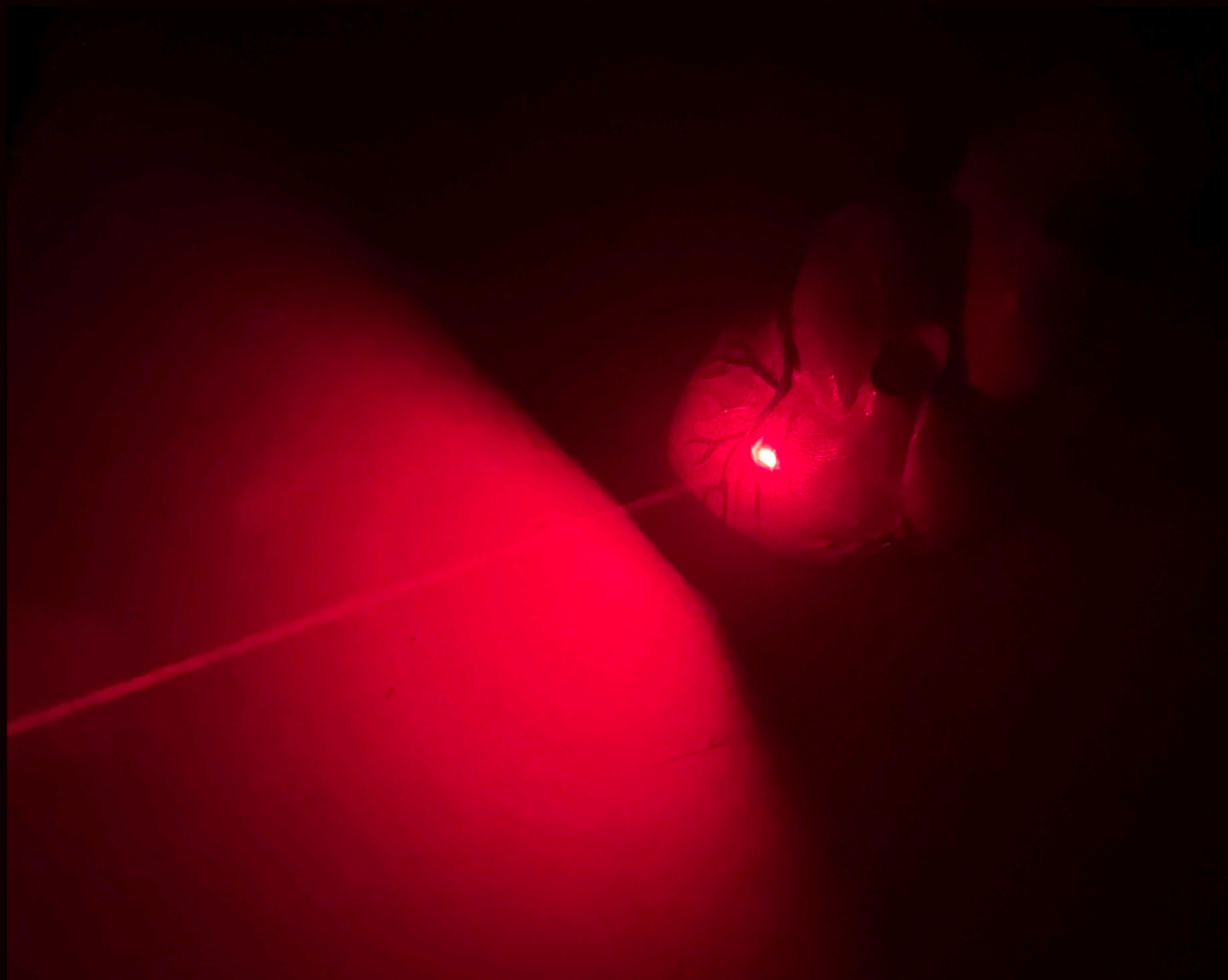


# MICROCIRCULATORY AND MITOCHONDRIAL PO<sub>2</sub> IN DIFFERENT (PATHO-)PHYSIOLOGICAL STATES OF THE RAT HEART

Gianmarco M. Balestra



MICROCIRCULATORY AND MITOCHONDRIAL PO<sub>2</sub> IN DIFFERENT  
(PATHO-)PHYSIOLOGICAL STATES OF THE RAT HEART

Gianmarco M. Balestra

**Microcirculatory and Mitochondrial PO<sub>2</sub>  
in Different (Patho-)Physiological States  
of the Rat Heart**

Gianmarco Maria Balestra

# Microcirculatory and Mitochondrial PO<sub>2</sub> in Different (Patho-)Physiological States of the Rat Heart

Microcirculatoire en mitochondriale PO<sub>2</sub>  
onder verschillende omstandigheden  
van het rattenhart

## Thesis

to obtain the degree of Doctor from the  
Erasmus University Rotterdam  
by command of the  
rector magnificus

Prof. dr. A.L. Bredenoord

and in accordance with the decision of the Doctorate Board.  
The public defence shall be held on

Friday 19 April 2024 at 13.00 hrs  
by

Gianmarco Maria Balestra  
born in Basel, Switzerland.

## Microcirculatory and Mitochondrial PO<sub>2</sub> in Different (Patho-)Physiological States of the Rat Heart

Thesis, Erasmus University, Rotterdam, The Netherlands, with summary in Dutch.

All studies described in this thesis were conducted at:

Laboratory of Experimental Anesthesiology, Erasmus Medical Center, Rotterdam, The  
Netherlands.

Laboratory of Translational Physiology, Academic Medical Center Amsterdam,  
Amsterdam, The Netherlands.

ISBN: 978-94-6496-090-7

Cover concept: Gianmarco Maria Balestra

Cover: Ilse Modder- [www.ilsemodder.nl](http://www.ilsemodder.nl)

Lay-out: Ilse Modder- [www.ilsemodder.nl](http://www.ilsemodder.nl)

Printed by Gildeprint Drukkerijen – [www.gildeprint.nl](http://www.gildeprint.nl)

Copyright © 2024 by Gianmarco M. Balestra

Erasmus University Rotterdam



**Doctoral Committee:**

**Promotors:**

Prof. dr. R.J. Stolker  
Prof. dr. C. Ince

**Other members:**

Prof. dr. D. Merkus  
Prof. dr. M. Singer  
Prof. dr. M. Siegemund

**Co-promotors:**

Dr. E.G. Mik  
Dr. C.J. Zuurbier

*“Le optimiste voit le verre à moitié plein. Le pessimiste voit le verre à moitié vide. Mais aucun des deux (...) se demande pourquoi on leur sert que des demi-verres!”*

*Philippe Geluck*

## TABLE OF CONTENTS

<b>Chapter 1</b>	General Introduction	11
<b>Chapter 2</b>	Microcirculation and mitochondria in sepsis: getting out of breath <i>Current Opinion in Anaesthesiology 2009, 22 (2):184 – 190</i>	23
<b>Chapter 3</b>	Microvascular and mitochondrial PO <sub>2</sub> simultaneously measured by oxygen-dependent delayed luminescence. <i>Biophotonics. 2012 Feb;5(2):140-51.</i>	41
<b>Chapter 4</b>	Oxygenation measurement by multi-wavelength oxygen-dependent phosphorescence and delayed fluorescence: catchment depth and application in intact heart. <i>Journal of Biophotonics 2015, 8 (8): 615–628</i>	63
<b>Chapter 5</b>	Monitoring mitochondrial PO <sub>2</sub> – the next step. <i>Curr Opin Crit Care. 2020 Jun;26(3):289-295.</i>	89
<b>Chapter 6</b>	Mitochondrial oxygen tension within the heart. <i>J Mol Cell Cardiol. 2009 Jun;46(6):943-51.</i>	103
<b>Chapter 7</b>	Increased in vivo mitochondrial oxygenation with right ventricular failure induced by pulmonary arterial hypertension: mitochondrial inhibition as driver of cardiac failure? <i>Respir Res. 2015 Feb 3;16(1):6.</i>	125
<b>Chapter 8</b>	Microcirculatory and mitochondrial oxygenation is preserved in endotoxic shock and resuscitation in rat hearts <i>Submitted</i>	143
<b>Chapter 9</b>	General Discussion	163
<b>Chapter 10</b>	English Summary	175
<b>Chapter 11</b>	Dutch Summary (Nederlandse samenvatting)	181
<b>Chapter 12</b>	Acknowledgements	187
<b>Chapter 13</b>	Publication List	193
<b>Chapter 14</b>	Curriculum Vitae	199
<b>Chapter 15</b>	PhD Portfolio	205

# CHAPTER

General introduction

# 1



## IMPLICATION OF OXYGEN IN HEART DISEASE

Oxygen is the essence for sustainment of aerobic metabolism. It therefore keeps a central position in many physiologic processes. Moreover, several pathophysiological mechanisms are traced back to handling or availability issues of oxygen. Oxygen is being attributed a relevant position in fueling pathologies even when not representing the pivotal causative factor.

Such, in the heart, oxygen contributes to ischemic and septic cardiomyopathy as well as to acutely and chronically failing of hearts [1-3].

The most obvious implication of oxygen is found in **ischemic heart disease** when atheromatous plaque rupture causes thrombotic coronary occlusion. This event induces downstream ischemia resulting in necrosis, apoptosis, stunning and hibernation. While severe and prolonged ischemia leads to necrosis (uncontrolled cell death), a less severe oxygen debt followed by reperfusion may cause stunning (impaired and slowly recovering function) and eventually apoptosis (programmed cell death). In chronic coronary artery disease, in myocardial regions with severely reduced blood flow, oxygen supply may be limited to an amount just enough to sustain viability but not function. As an adaptive reaction cardiomyocytes reduce their cellular metabolism similar to hibernation [4].

In **septic cardiomyopathy**, too, hibernation is being debated as a possible mechanism to explain myocardial dysfunction in severe infection [3]. In addition dysfunctional oxygen handling and hypoxia are discussed as causative mechanisms [5-9]. These two concepts involve altered cellular oxygen handling despite lack of shortage of oxygen and insufficient cellular oxygen availability *per se*. It is still matter of debate which one of these hypotheses represents the main mechanism behind septic organ dysfunction. Some studies point towards an oxygen deficit [6,7] while a larger body of evidence supports altered oxygen handling as a consequence of mitochondrial dysfunction. Evidence of mitochondrial dysfunction has been gathered in several studies at multiple levels of mitochondrial function [10]. Structural damage and compromised biogenesis have been described. Respiratory enzyme inhibition and degree of uncoupling of mitochondrial have been reported at varying extent, however fostering the impression of seemingly inconsistent results, which may be attributed to methodological differences (sepsis model, animal, timing) [8,9,11]. Levels of high energy phosphates have been mainly reported to be in the range of normal [12] but also reduced in patients found to be dying of sepsis [13]. Central to the hypothesis of altered cellular oxygen handling is the assumption of adequate oxygen supply. However only few, indirect and old data support this supposition and none of these studies has measured oxygen directly in the myocardial tissue let say in myocardial mitochondria.

In the **failing heart** due to either ischemic heart disease or pressure overload, induction of hypoxia-inducible factor 1 and 2 (HIF-1/2) triggered by reduced oxygen availability leads to vascular remodeling. Moreover, some studies suggest the metabolic

reprogramming with switch from beta oxidation of fatty acids to carbohydrate fueled energy generation is also influenced by this pathway [14].

It is thus evident that oxygen represents a relevant diagnostic and therapeutic target. Consequently, much interest has been awoken to measure oxygen. This resulted in a wide variety of methods for measuring tissue and microcirculatory oxygenation.

## MEASURING OXYGEN

Direct measurement of oxygen partial pressures ( $pO_2$ ) have been described with polarographic [15] and mass spectrometric electrodes [16], electron paramagnetic resonance (EPR)[17], and oxygen-dependent quenching of phosphorescence [18-20] and fluorescence [21] as well as chemiluminescence [22] and spin label oximetry [23]. These methods markedly differ in accuracy, spatio-temporal resolution and invasiveness.

The largest body of evidence on oxygen levels in the heart originates from studies using polarographic electrodes[15] and mass spectrometry [24].

The **polarographic electrodes** were used either as surface electrodes or invasively inserted needle electrodes. Soon criticism arose due to tissue disruption, formation of hematoma and vasoconstriction found after needle electrode insertion [25,26]. Mapping tissue oxygenation would require inserting multiple electrodes given the fact that only a confined tissue volume is accessible with one electrode. Moreover, inherent to the measurement technique some of the measured oxygen is consumed by the electrode. This instance can alter very small and/or oxygen-deficient samples in a relevant manner. Although thinner needle electrodes and more cautious insertion techniques were developed  $pO_2$  measurements using invasive electrodes yielded lower values than surface electrodes [27-29].

**Mass spectrometric electrodes**, basically share the draw-backs of polarographic electrodes. With regard to the above-mentioned issues these methods are limited in their applicability.

**Electron paramagnetic resonance**, contrary to polarographic electrodes, requires insertion of paramagnetic particles, mostly lithium phthalocyanine or lithium octa-n-butoxynaphthalocyanine (LiPc resp. LiNc-BuO the oxygen-sensitive probe)[30] but not of large electrodes. Their application is thus less invasive however at a tradeoff of longer measurement acquisition times and the need to place the target object inside the EPR spectrometer.

Finally, **phosphorimetry** uses oxygen-dependent quenching of phosphorescence of fluorophores [20]. Our group has chosen this method for its minimal invasiveness, versatile applicability and real-time measurement.

## MEASURING OXYGENATION WITH PHOSPHORIMETRY

For measuring  $PO_2$  different heavy metal-porphyrin compounds, in particular palladium, have been used. Photoexcitation of porphyrins leads to absorption of energy that causes transition of an electron from ground singlet state ( $S_0$ ) to excited singlet state ( $S_1$ ) by elevating one spin to a higher energy level. This absorbed energy can then directly be returned by emission of photons in form of fluorescence (Fig. 1a) or by radiationless transition to the ground state. However, some electrons may relax and switch orientation losing only some of the absorbed energy and thus change to a triplet state ( $T_1$ ), a process called intersystem crossing. From the triplet state the absorbed energy can either be emitted directly, which is called phosphorescence (Fig. 1b), or by prior bidirectional intersystem crossing, which is called delayed fluorescence (Fig. 1c). All emission of the absorbed photons causes a return to the ground state ( $S_0$ ).

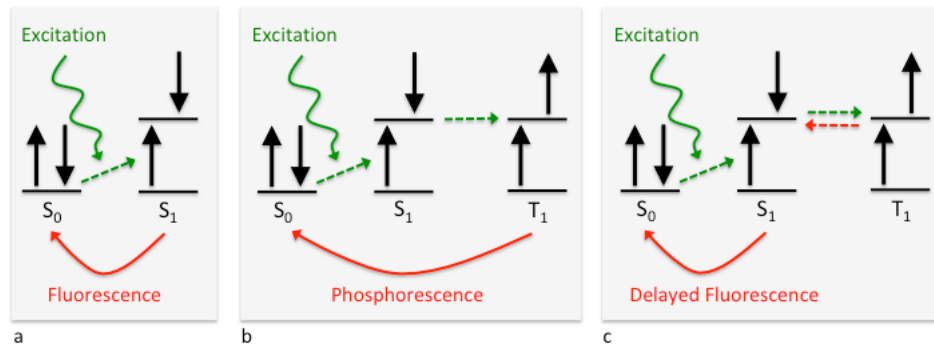


**FIGURE 1** Schematic of Fluorescence, Phosphorescence and delayed Fluorescence

The energy of the excited porphyrin ( $T_1$ ) may however be transferred to the surrounding oxygen ( $O_2$ ). The most common allotrope of oxygen is  $^3O_2$ , a diradical triplet state of a dioxygen molecule, which avidly accepts this energy. Doing so,  $^3O_2$  is elevated to a singlet state  $^1O_2$ . Thus, emission of a photon from the porphyrin ( $T_1$ ) via phosphorescence or delayed fluorescence is quenched. This process is depending on the collision frequency of porphyrin and  $^3O_2$  in function of their concentration (equation 1).

$$(1) \quad [T_1](t) = [T_1]_0 e^{-(k_s - k_q PO_2)t};$$

$[T_1]_0$ :  $T_1$  concentration just after excitation  
 $k_s$ : probability of spontaneous relaxation  
 $k_q$ : quenching probability  
 $PO_2$ : surrounding oxygen tension

This decay formula can also be expressed in function of a lifetime ( $\tau$ ) (equation 2).

$$(2) \quad [T_1](t) = [T_1]_0 e^{-\frac{t}{\tau}}$$

A high concentration of oxygen will therefore lower the number of excited porphyrins ( $T_1$ ) quickly. As a consequence, the emission probability of photons over time is reduced which can be measured as a shorter  $T_1$  lifetime. This association has been determined in the Stern-Volmer relationship (equation 3).

$$(3) \quad \frac{1}{\tau} = \frac{1}{\tau_0} + k_q PO_2$$

$\tau_0$ : time constant of decay in absence of oxygen  
 which is indirectly proportional to  $k_s$

This shows, that the oxygen concentration (expressed as partial pressure) surrounding the excited fluorophore is inverse proportional to the duration of the measured  $T_1$  lifetime. This fact also explains the independence of the measured signal from its intensity, provided a sufficient signal-to-noise ratio allows for its detection.

In our group, we have developed a dual-wavelength phosphorimeter allowing near-simultaneous excitation of a phosphorescent dye at two wavelengths thus allowing measurements of microcirculatory  $pO_2$  at two different depths [31]. This technology was then applied to study oxygenation, in particular of the kidney, in different conditions [32-35]. In 2006 we described the application of this technique for measuring mitochondrial oxygenation [36]. This now opened up new opportunities, namely the measurement of microcirculatory *and* mitochondrial oxygenation *in vivo*.

Few data exist on the transmural distribution of microcirculatory oxygen partial pressures ( $\mu PO_2$ ) and none of parallel measurements of both compartments (microcirculation and mitochondria) *in vivo*.

## AIM OF THE THESIS

In this thesis we developed and characterized a method to measure (near-) simultaneously microcirculatory and mitochondrial oxygenation in heart *in vivo*. Further we investigated the myocardial microcirculatory and mitochondrial oxygenation in two clinically relevant animal models, namely in endotoxemia and right ventricular pressure overload.

The questions addressed are (1) the *in vivo* subcellular and anatomic provenance of the measured signal and (2) the oxygenation level in the microcirculation and mitochondria in physiologic and the above-mentioned pathologic states and their modification due to therapeutic interventions. We hypothesized that in sepsis hypoxia would be found in non-resuscitated animals but no oxygen shortage would be found with supportive therapy indicating oxygen management issues arising from mitochondrial dysfunction or



otherwise termed cytopathic hypoxia. In pressure overload induced right heart failure we expected the substrate switch to be occurring without evidence of hypoxia.

## OVERVIEW OF THE CHAPTERS

In the **second chapter** an overview of microcirculatory involvement and adaptive processes in sepsis is given. The alteration of the microcirculation and mitochondria appear to contribute to the development of sepsis-induced organ failure, although their mutual interplay and contribution to the disease leaves remains to be elucidated. While some clinically available diagnostic tools are available for evaluating the microcirculation, though not being routinely used, there are none for assessing the mitochondria clinically *in vivo*. Only a limited amount of treatment strategies address the microcirculation, none the mitochondria. Some experimental approaches are being studied [37].

The **third chapter** describes the simultaneous measurement of microcirculatory and mitochondrial oxygenation using phosphorimetry. We analyze the crosstalk of the two retrieved measuring signals and influence of noise on measurement. Further the feasibility of this method is tested with measurements of hepatic microcirculatory and mitochondrial oxygenation *in vivo*. And finally, we compare two analysis algorithms for the retrieved phosphorescence signals using either a rectangular distribution method or mono-exponential function [38].

In the **fourth chapter** we characterize the optical properties of the myocardial microcirculatory and mitochondrial oxygenation measurements using oxygen-dependent quenching of the phosphorescence with Oxyphor G2 and protoporphyrin IX as fluorophore, respectively by means of Monte Carlo simulations and *ex vivo* experiments. Further we test the feasibility of measuring changes in microcirculatory and mitochondrial oxygen partial pressures in *in vivo* experiments lasting up to 5 hours [39].

**Chapter five** we point out the importance of taking into consideration cellular function, which still represents a missing piece in the puzzle in the evaluation and therapy of organ dysfunction. The basic principle of the technique to measure mitochondrial oxygenation is outlined as well as its application in experimental studies in animals and some human studies [40].

The **sixth chapter** reports the first measurements of mitochondrial oxygen partial pressure using oxygen-dependent quenching of the phosphorescence in the heart, namely in isolated cardiomyocytes, Langendorff-perfused hearts and *in vivo* hearts. Moreover, the origin of the phosphorescence signal, the correlation with oxygen supply and distribution of mitochondrial oxygen partial pressures retrieved by deconvolution of the phosphorescence signal are presented [41].

In the **seventh chapter** we study the mitochondrial oxygen partial pressures in a rat

model of pulmonary arterial hypertension leading to right ventricular pressure overload and cor pulmonale. It had long been hypothesized that one mechanism of heart failure and the observed metabolic shift was associated with shortage of oxygen at the level of cardiomyocytes [42].

**Chapter eight** investigates how the oxygenation of the microcirculation and mitochondria is affected by endotoxemia and usual clinical supportive therapies in rat hearts *in vivo*. Rats in endotoxemic shock were assigned not to be treated or receive protocol-based treatment with fluid, fluid plus dobutamine, fluid plus levosimendan, fluid plus norepinephrine, fluid plus norepinephrine and dobutamine or levosimendan. Further hemodynamic parameters were collected and troponin levels were used as measure of myocardial damage (Balestra *et al.* submitted).

## REFERENCES

1. Lucero García Rojas EY, Villanueva C, Bond RA. Hypoxia Inducible Factors as Central Players in the Pathogenesis and Pathophysiology of Cardiovascular Diseases. *Front Cardiovasc Med*. Frontiers; 2021;8:709509.
2. Neubauer S. The failing heart—an engine out of fuel. *N Engl J Med*. Massachusetts Medical Society; 2007;356:1140–51.
3. Hollenberg SM, Singer M. Pathophysiology of sepsis-induced cardiomyopathy. *Nat Rev Cardiol*. Nature Publishing Group; 2021;18:424–34.
4. Kloner RA. Stunned and Hibernating Myocardium: Where Are We Nearly 4 Decades Later? *J Am Heart Assoc*. 2020;9:e015502.
5. Graetz TJ, Hotchkiss RS. Sepsis: Preventing organ failure in sepsis — the search continues. Nature Publishing Group. Nature Publishing Group; 2016;13:5–6.
6. Bateman RM, Tokunaga C, Kareco T, Dorscheid DR, Walley KR. Myocardial hypoxia-inducible HIF-1 $\alpha$ , VEGF, and GLUT1 gene expression is associated with microvascular and ICAM-1 heterogeneity during endotoxemia. *AJP: Heart and Circulatory Physiology*. American Physiological Society; 2007;293:H448–56.
7. Østergaard L, Granfeldt A, Secher N, Tietze A, Iversen NK, Jensen MS, et al. Microcirculatory dysfunction and tissue oxygenation in critical illness. *Acta Anaesthesiol Scand*. 2015;59:1246–59.
8. Cimolai MC, Alvarez S, Bode C, Bugger H. Mitochondrial Mechanisms in Septic Cardiomyopathy. *Int J Mol Sci*. Multidisciplinary Digital Publishing Institute; 2015;16:17763–78.
9. Alvarez S, Vico T, Vanasco V. Cardiac dysfunction, mitochondrial architecture, energy production, and inflammatory pathways: Interrelated aspects in endotoxemia and sepsis. *Int. J. Biochem. Cell Biol*. 2016;81:307–14.
10. Wang R, Xu Y, Fang Y, Wang C, Xue Y, Wang F, et al. Pathogenetic mechanisms of septic cardiomyopathy. *J Cell Physiol*. 2022;237:49–58.
11. Stanzani G, Duchon MR, Singer M. The role of mitochondria in sepsis-induced cardiomyopathy. *BBA- Molecular Basis of Disease*. Elsevier; 2018;:1–0.
12. Van Lambalgen AA, van Kraats AA, Mulder MF, Teerlink T, van den BOS GC. High-energy phosphates in heart, liver, kidney, and skeletal muscle of endotoxemic rats. *Am. J. Physiol*. American Physiological Society Bethesda, MD; 1994;266:H1581–7.
13. Brealey D, Brand M, Hargreaves I, Heales S, Land J, Smolenski R, et al. Association between mitochondrial dysfunction and severity and outcome of septic shock. *Lancet*. 2002;360:219–23.
14. Semenza GL. Hypoxia-inducible factor 1 and cardiovascular disease. *Annu. Rev. Physiol*. Annual Reviews; 2014;76:39–56.
15. Clark LC, Wolf R, Granger D, Taylor Z. Continuous recording of blood oxygen tensions by polarography. *Journal of Applied Physiology*. 1953;6:189–93.
16. Hoch G, Kok B. A mass spectrometer inlet system for sampling gases dissolved in liquid phases. *Arch. Biochem. Biophys*. 1963;101:160–70.
17. Swartz HM, Clarkson RB. The measurement of oxygen in vivo using EPR techniques. *Phys Med Biol*. IOP Publishing; 1998;43:1957–75.
18. Wilson DF, Rumsey WL, Green TJ, Vanderkooi JM. The oxygen dependence of mitochondrial oxidative phosphorylation measured by a new optical method for measuring oxygen concentration. *J. Biol. Chem*. 1988;263:2712–8.
19. Lo LW, Koch CJ, Wilson DF. Calibration of oxygen-dependent quenching of the phosphorescence of Pd-meso-tetra (4-carboxyphenyl) porphine: a phosphor with general application for measuring oxygen concentration in biological systems. *Anal. Biochem*. 1996;236:153–60.
20. Vanderkooi JM, Maniara G, Green TJ, Wilson DF. An optical method for measurement of dioxygen concentration based upon quenching of phosphorescence. *J. Biol. Chem*. American Society for Biochemistry and Molecular Biology; 1987;262:5476–82.
21. Opitz N, Weigelt H, Barankay T, Lübbers DW. Application of the optode to measurements of surface PO<sub>2</sub> and PCO<sub>2</sub> of the isolated guinea-pig heart. *Adv. Exp. Med. Biol*. 1977;94:99–105.
22. Oshino R, Oshino N, Tamura M, Kobilinsky L, Chance B. A sensitive bacterial luminescence probe for O<sub>2</sub> in biochemical systems. *Biochim. Biophys. Acta*. 1972;273:5–17.
23. Subczynski WK, Hyde JS. The diffusion-concentration product of oxygen in lipid bilayers using the spin-label T1 method. *Biochim. Biophys. Acta*. Biochim Biophys Acta; 1981;643:283–91.
24. Wilson GJ, MacGregor DC, Holness DE, Lixfeld W, Yasui H. Mass spectrometry for measuring changes in intramyocardial pO<sub>2</sub> and pCO<sub>2</sub>. *Adv. Exp. Med. Biol*. 1973;37A:547–52.
25. Lund N. Skeletal and cardiac muscle oxygenation. *Adv. Exp. Med. Biol*. 1985;191:37–43.
26. Moss AJ. Intramyocardial Oxygen Tension. *Cardiovascular Research*. 1968;2:314–8.
27. Skolasinska K, Harbig K, Lübbers DW, Wodick R. PO<sub>2</sub> and microflow histograms of the beating heart in response to changes in arterial pO<sub>2</sub>. *Basic Res. Cardiol*. 1978;73:307–19.
28. Walfridsson H, Briheim K, Odman S. A multiwire surface oxygen pressure electrode for measurement across zones of normal and damaged tissue. *Int J Clin Monit Comput*. 1985;2:15–20.
29. Boekstegers P, Diebold J, Weiss C. Selective ECG synchronised suction and retroinfusion of coronary veins: first results of studies in acute myocardial ischaemia in dogs. *Cardiovascular Research*. 1990;24:456–64.
30. Zweier JL, Thompson-Gorman S, Kuppusamy P. Measurement of oxygen concentrations in the intact beating heart using electron paramagnetic resonance spectroscopy: a technique for measuring oxygen concentrations in situ. *J. Bioenerg. Biomembr*. 1991;23:855–71.
31. Johannes T, Mik EG, Ince C. Dual-wavelength phosphorimetry for determination of cortical and subcortical microvascular oxygenation in rat kidney. *Journal of Applied Physiology*. 2006;100:1301–10.
32. Johannes T, Mik EG, Nohé B, Raat NJH, Unertl KE, Ince C. Influence of fluid resuscitation on renal microvascular PO<sub>2</sub> in a normotensive rat model of endotoxemia. *Crit Care*. 2006;10:R88.
33. Johannes T, Mik EG, Nohé B, Unertl KE, Ince C. Acute decrease in renal microvascular PO<sub>2</sub> during acute normovolemic hemodilution. *Am. J. Physiol. Renal Physiol*. 2007;292:F796–803.
34. Legrand M, Almac E, Mik EG, Johannes T, Kandil A, Bezemer R, et al. L-NIL prevents renal microvascular hypoxia and increase of renal oxygen consumption after ischemia-reperfusion in rats. *Am. J. Physiol. Renal Physiol*. American Physiological Society; 2009;296:F1109–17.
35. Dyson A, Bezemer R, Legrand M, Balestra GM, Singer M, Ince C. Microvascular and interstitial oxygen tension in the renal cortex and medulla studied in a 4-h rat model of LPS-induced endotoxemia. *Shock*. 2011;36:83–9.
36. Mik EG, Stap J, Sinaasappel M, Beek JF, Aten JA, van Leeuwen TG, et al. Mitochondrial PO<sub>2</sub> measured by delayed fluorescence of endogenous protoporphyrin IX. *Nat Meth*. 2006;3:939–45.

37. Balestra GM, Legrand M, Ince C. Microcirculation and mitochondria in sepsis: getting out of breath. *Current Opinion in Anaesthesiology*. 2009;22:184–90.
38. Bodmer SIA, Balestra GM, Harms FA, Johannes T, Raat NJH, Stolker RJ, et al. Microvascular and mitochondrial PO<sub>2</sub> simultaneously measured by oxygen-dependent delayed luminescence. *J Biophotonics*. WILEY-VCH Verlag; 2012;5:140–51.
39. Balestra GM, Aalders MCG, Specht PAC, Ince C, Mik EG. Oxygenation measurement by multi-wavelength oxygen-dependent phosphorescence and delayed fluorescence: catchment depth and application in intact heart. *J Biophotonics*. WILEY-VCH Verlag; 2015;8:615–28.
40. Mik EG, Balestra GM, Harms FA. Monitoring mitochondrial PO<sub>2</sub>: the next step. *Current Opinion in Critical Care*. 2020;26:289–95.
41. Mik EG, Ince C, Eerbeek O, Heinen A, Stap J, Hooibrink B, et al. Mitochondrial oxygen tension within the heart. *Journal of Molecular and Cellular Cardiology*. 2009;46:943–51.
42. Balestra GM, Mik EG, Eerbeek O, Specht PAC, van der Laarse WJ, Zuurbier CJ. Increased in vivo mitochondrial oxygenation with right ventricular failure induced by pulmonary arterial hypertension: mitochondrial inhibition as driver of cardiac failure? *Respir. Res.* BioMed Central; 2015;16:6.

# CHAPTER

# 2

## Microcirculation and Mitochondria in Sepsis: Getting Out of Breath

Gianmarco M. Balestra  
Matthieu Legrand  
Can Ince

Current Opinion in Anaesthesiology. 2009, 22 (2):184 – 190  
PMID: 19307893 DOI: 10.1097/ACO.0b013e328328d31a



## STRUCTURED ABSTRACT

### Purpose of review

To present the recent findings obtained in clinical and experimental studies examining microcirculatory alterations in sepsis, their link to mitochondrial dysfunction, and current knowledge regarding the impact of these alterations on the outcome of septic patients.

### Recent findings

Interlinked by a mutual cascade effect and driven by the host-pathogen interaction, microcirculatory and mitochondrial functions are impaired during sepsis. Mitochondrial respiration seems to evolve during the course of sepsis, demonstrating a change from reversible to irreversible inhibition. The spatio-temporal heterogeneity of microcirculatory and mitochondrial dysfunction suggests that these processes may be compartmentalized. While a causal relationship between mitochondrial and microcirculatory dysfunction and organ failure in sepsis is supported by an increasing number of studies, adaptive processes have also emerged as part of microcirculatory and mitochondrial alterations. Treatments for improving or preserving microcirculatory and/or mitochondrial function seem to yield a better outcome in patients.

### Summary

Even though there is evidence that microcirculatory and mitochondrial dysfunction plays a role in the development of sepsis-induced organ failure, their interaction and respective contribution to the disease remains poorly understood. Future research is necessary to better define such relationships in order to identify therapeutic targets and refine treatment strategies.

## INTRODUCTION

Sepsis is the main cause of multiple organ dysfunction (MOF) and remains a concern due to its associated high morbidity and mortality [1]. The outcome of patients has only slightly improved during recent decades due to minimal therapeutic advancement. Outcome improvement requires understanding the pathophysiology, recognizing the process early and, finally, finding an effective therapy. The hypothesis of a causative connection between microcirculation and organ dysfunction is not new [2], but only recently have techniques become available that allow for facilitated investigation of the microcirculation also in a clinical setting. Finally, translation of experimental results into clinical trials is complicated; this is mainly due to the observation that the multi-system conditions characterizing sepsis in humans are much more complex than in standardized animal models.

Sepsis arises from an infection that escapes local boundaries and triggers intricate conditions with temporal and compartmental interactions of a multitude of protective or damaging processes. These processes are interlinked and determined by the host-pathogen interaction and lead to a condition termed Microcirculatory and Mitochondrial Distress Syndrome (MMDS) [3]. The purpose of this review is to provide an overview of the current knowledge on how microcirculatory and mitochondrial dysfunction can interact and affect the outcome of sepsis.

## MICROCIRCULATORY ALTERATION IS A HALLMARK OF SEPSIS

The microcirculation, a network of vessels <150  $\mu\text{m}$  in diameter comprising arterioles, capillaries and venules, is critical for supplying tissues with substrates and removing metabolites. The functional capillary density, which dictates perfusion and  $\text{O}_2$  diffusion distance, is the determinant for this function.

In sepsis, both convective and diffusive impairment have been shown to cause significant heterogeneity in oxygen supply [4;5]. Stiff leucocytes and red blood cells, platelet/fibrin clots, and endothelial cell swelling are proposed to be responsible for capillary occlusion. Capillary leakage is a common feature in sepsis and leads to interstitial edema and a positive fluid balance [6]. In addition to being markers of the severity of sepsis, fluid overload and interstitial edema can increase the diffusion distance of oxygen to target cells [7]. Recently, fluid overload has been found to be an independent factor for mortality among septic patients with acute renal failure [8\*]. In fact, the impaired ability of endothelial cells to control permeability by dynamic opening and closing of cell-cell adherence junctions (largely composed of vascular endothelial (VE-) cadherin) is recognized as a potential treatment target [9]. Increased levels of vascular

endothelial growth factor (VEGF), which plays a key role in this mechanism, are found in sepsis. Atrial natriuretic peptide (ANP) has recently been identified as an endogenous factor that counteracts leakage by inhibiting changes in (VE)-cadherin,  $\beta$ -catenin, and p120<sup>cas</sup> levels [10]. ANP has been shown to inhibit NF- $\kappa$ B activation, reduce TNF- $\alpha$  levels, and improve survival in ANP-pretreated, LPS-challenged mice [11]. On the other hand, high levels of pro-ANP are associated with increased mortality [12;13]. An elevated expression of pro-ANP may not only reflect cardiac strain but also the body's effort to limit fluid extravasation.

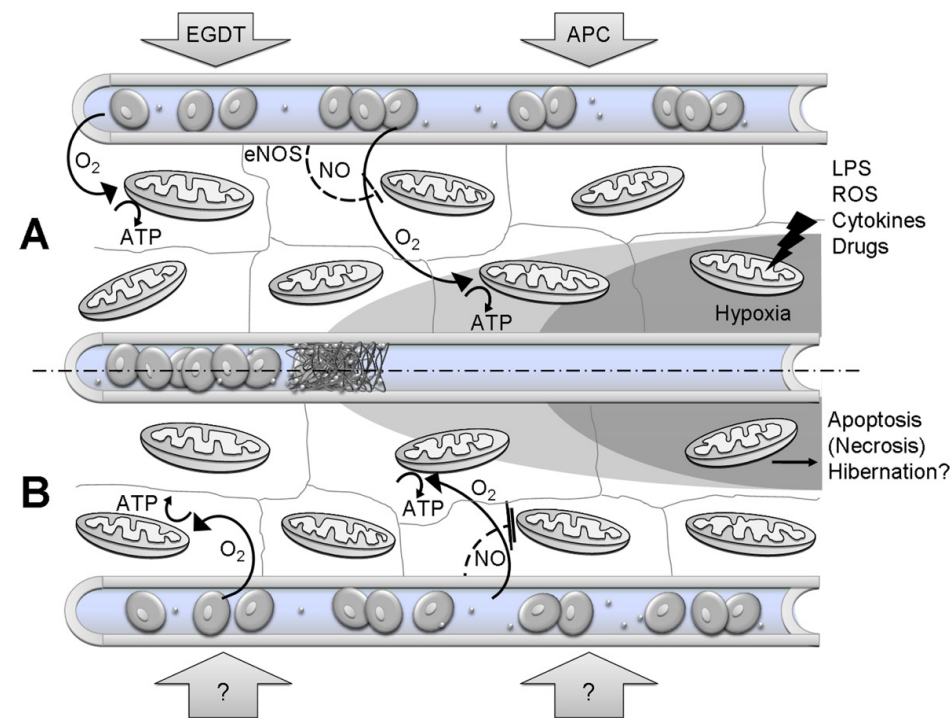


**Figure 1:** Perfusion heterogeneity and mitochondrial dysfunction:

- A Early sepsis: Reversible inhibition of mitochondrial respiration by nitric oxide (NO) augments diffusion distance and thus availability of oxygen ( $O_2$ ) for more distant cells in an otherwise hypoxic area, while a hypoxic core might still persist near not flowing capillaries. Established resuscitation strategies are available (e.g. EGDT, APC).
- B Later sepsis: To an increasing degree presence of irreversible inhibition of mitochondrial respiration (NO, reactive oxygen and nitrogen species in particular peroxynitrite, LPS, cytokines). Multiple damaging factors and persistence of insults trigger apoptosis, to a lesser extent necrosis and eventually hibernation-like state. There are no established therapies for later stage sepsis.

EGDT = Early Goal Directed Therapy; APC = Activated Protein C, LPS = Lipopolysaccharide

The spatio-temporal heterogeneity of dysfunction has not only been found within an organ itself, but also between different microvascular beds, as recently described for the sublingual and intestinal microcirculation in patients with abdominal sepsis [14]. In apparent opposition to the above-mentioned concepts, dysfunction of the microcirculation might not only be viewed as a damaging process, but also as an adaptive and even protective mechanism against systemic spread of the infection. In an elegant study evaluating ascending lower urinary tract infection, prevention of microcirculatory flow disturbance with heparin led to fatal urosepsis [15]. The compartmentalization of microcirculatory dysfunction might be analogous to the compartmentalization of inducible Nitric Oxide Synthase, TNF $\alpha$ , and IL-1 $\beta$  expression in patients with septic shock caused by cellulitis [16], and may occur during specific septic conditions in an attempt to “seal off” the infection, thus avoiding spreading of the infection.

## MICROCIRCULATORY AND MITOCHONDRIAL DYSFUNCTION IN SEPSIS GO HAND IN HAND

The mitochondria are not only the energy suppliers of the cells, but they are also involved in oxygen sensing and cell death signaling pathways (apoptosis and necrosis). In sepsis, they represent a prominent target and source for sepsis-induced organ dysfunction. The predictive importance of mitochondrial dysfunction was demonstrated by Brealey and coworkers, who demonstrated an association of inhibition of complex I and lower ATP levels with worse outcome of septic patients [17]. This finding has been corroborated by a small series of studies performed by Fredriksson *et al.*, who found a two-fold reduction in mitochondria, a lower concentration of energy-rich phosphates, and an increase in anaerobic energy production in the leg, but not in the intercostal muscle, of patients with sepsis-induced multiple organ failure [18]. As microvascular substrate delivery (e.g. oxygen, glucose) decreases, mitochondrial respiration cannot sustain ATP generation. However, unlike in typical ischemia-reperfusion, in sepsis, this process is allowed some time for adaptation. *In vitro* experiments suggest that nitric oxide synthase-derived nitric oxide, produced by neighboring endothelial cells, can diffuse into tissue cells where it inhibits oxygen utilization by cytochrome c oxidases. This results in an increase in oxygen availability to more remote cells via augmentation of its diffusion distance (Fig. 1) [19;20\*\*]. To what extent the acquired defect in oxidative phosphorylation is the result of direct damage to the mitochondria, or adaptive changes due to a failure in substrate supply, is still a matter of debate. The temporary span and scale of the decreased oxygen supply are certainly of fundamental importance to this sequence. In a murine experimental cecal ligation and puncture (CLP) model, competitive inhibition of myocardial cytochrome c oxidase is present during early sepsis, followed by non-competitive inhibition by 48 hours post-CLP [20\*\*; 21]. Downregulated energy

expenditure to a hibernation-like state could be an adaptive mechanism in response to decreases of  $O_2$  and substrate supply. This is suggested by the fact that widespread necrosis is not a feature of sepsis [22\*]. Clarification of whether this previously described disparity in mitochondrial dysfunction [23] is accompanied by microcirculatory alterations would certainly add to our understanding of sepsis-induced organ failure. In summary, increasing evidence links MMDS to septic organ dysfunction and patient outcome. A schematic of how the protagonists may interact and their contribution to organ failure is depicted in Figure 2. Because a better understanding of the sequence of such interactions is required for determining therapeutic windows of opportunity, tools to assess the microcirculation as well as, ideally, mitochondrial function during the course of sepsis are required.

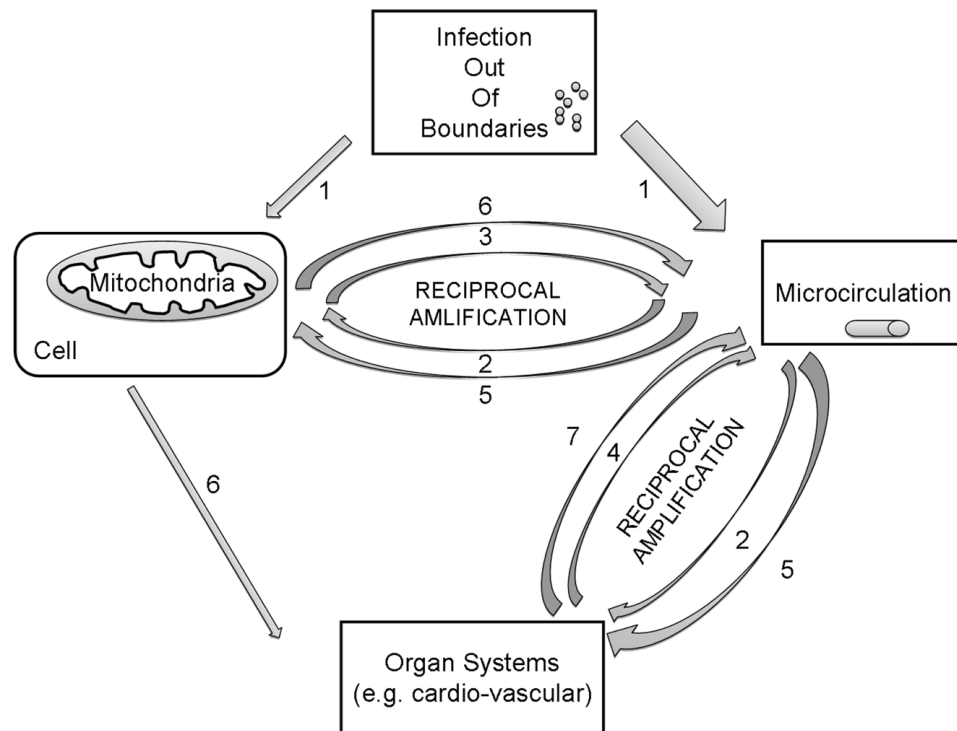


**Figure 2:** Concept of the relationship between the microcirculation, mitochondria and organ systems in causing organ failure in sepsis.

(1) Initial impairment of the microcirculation and to a lesser extent of the mitochondria by host-pathogen interaction. (2) Perfusion heterogeneity of the microcirculation leads to areas with limited substrate supply. (3) Production of reactive oxygen species and mitochondrial dysfunction (diminished ATP production) further impair the microcirculation. (4) Organ/organ system dysfunction leads to additional decrease of microcirculatory flow. (5) Persistent/worsen perfusion heterogeneity negatively affects the mitochondria and organs. (6) Mitochondria trigger apoptosis, necrosis or turn to a hibernation-like state with decreased substrate requirement ( $O_2$ , energy sources). (7) Organ/organ system failure occurs further impairing the microcirculation.

## AVAILABLE DIAGNOSTIC TOOLS

Whereas the macroscopic dimension determines most clinician's perception of sepsis, the microscopic one remains under-recognized and the mitochondrial dimension mostly elusive. There are several clinically applicable tools available for investigation of the microcirculation, but currently none for the mitochondria.

Sidestream dark field (SDF) and Orthogonal Polarization Spectral (OPS) imaging allow direct visualization and semi-quantitative analysis of perfusion heterogeneity [24; 25\*]. They do not, however, provide information on the metabolic state of the imaged tissue. Near-infrared spectroscopy (NIRS) provides information on muscle oxygenation ( $StO_2$ ). While resting  $StO_2$  has been found to be inconclusive in differentiating between septic and non-septic patients, altered recovery in  $StO_2$  after an ischemic challenge has proven to be indicative of sepsis-induced regional microvascular and mitochondrial dysfunction and correlates with organ failure and poor outcome [26-28]. A prospective study is currently being performed to evaluate the changes in  $StO_2$  during Early Goal Directed Therapy (EGDT) and its suitability for guiding early therapy [Annane D, Nardy O. Near Infrared Spectroscopy (NIRS) in Severe Sepsis (OTO-STs), in preparation]. Several other methods, such as laser Doppler flowmetry, tonometry, and sublingual capnography have been used to assess the microcirculation.

## THERAPEUTIC TRIALS

Recognition of the microcirculation and the mitochondria as important players in sepsis raises the question of how they are affected by treatment. In the following portion of this review, we will briefly discuss some aspects of selected therapeutic options and their relative impact on mitochondrial and microcirculatory function and patient outcome.

### Resuscitation goals

The concept behind EGDT is to alleviate the oxygen debt and secondary inflammatory insult inflicted by tissue hypoxia, and this is accomplished by timely and aggressive cardiovascular support [29;30], as corroborated by Rivers's recent study. EGDT appears to reduce the early increase in cytokines and decrease markers of cellular apoptosis [31]. Microcirculatory flow is improved by fluid resuscitation. A finding also observed during passive leg raise testing used to assess fluid responsiveness [32-34]. Applying EGDT, Trzeciak observed an association between the increased microcirculatory flow during resuscitation in the first 6 to 9 hours and reduced organ failure [35\*]. In an endotoxic shock model, the early use of norepinephrine plus volume expansion was associated with a higher proportion of the blood flow being redistributed to the mesenteric area, lower lactate levels, and less infused volume. With respect to the aforementioned associated

harm incurred by fluid overload, the decreased need for volume resuscitation may be of importance [36\*].

### Vasoactive Drugs

Albeit needed to maintain perfusion pressure, use of vasopressors raises concern with respect to their impairment of the microcirculatory system, in particular the intestinal flow [37]. However, mesenteric flow has also been reported as unchanged, while renal and coronary flow, as well as urinary output, were increased by norepinephrine [38]. In fact, norepinephrine was shown to increase global and medullary renal blood flow and restore renal vascular tone to normal levels [39]. In comparison to epinephrine, norepinephrine increased gastric mucosal perfusion less when administered alone, but equally when infused with dobutamine. This result was attributed to the vasodilating effect of dobutamine on the gastric mucosal microcirculation [40]. An analogous effect was observed for intestinal microcirculatory flow, which was improved with norepinephrine plus L-Arginine, but not with either of the drugs alone [41]. In addition, norepinephrine has been found to not only affect the microcirculation, but also to improve hepatic mitochondrial respiration in a porcine endotoxemia model [42]. Yet, when it comes to testing the effect of a different vasopressor on outcome, a recent trial comparing epinephrine with norepinephrine and dobutamine found no significant difference in mortality [43].

Recently, much interest has centered on levosimendan, especially because of its  $\text{Ca}^{2+}$ -sensitizing and  $\text{K}_{\text{ATP}}$  channel-opening effects, which directly influence the microcirculation and mitochondria. In several studies, levosimendan has proved superior to dobutamine or milrinone in augmenting cardiac performance, as well as improving renal, pulmonary, or mesenteric perfusion [44]. In addition, Fries *et al.* demonstrated improved buccal microcirculatory  $\text{pO}_2$  with levosimendan, but not with norepinephrine. In their CLP model, cardiac output was equally improved by both drugs, thus suggesting a mechanism related to their influence on microhemodynamics [45]. However, only one experimental study examined the superiority of levosimendan in reducing mortality, but only versus vehicle [46]. Further studies are therefore required.

Vasodilators, such as nitroglycerine, have been shown to improve microcirculatory perfusion [47]. A recent review concluded that NO donors usually show improvements in the outcomes measured (e.g., mortality, pulmonary hypertension, tissue/organ perfusion), but also lead to lower systemic blood pressure [48]. However, to maximize clinical relevance, further animal experimentation is necessary.

### APC

Activated protein C (APC) administration has generated an animated debate regarding its usefulness. Contrary to the current guidelines [30], a recent Cochrane analysis does not recommend the use of APC [49]. However, APC exhibits multiple beneficial effects

(particularly on the microcirculation and cells), for which it has been dealt as a potentially “ideal” adjunctive drug for sepsis treatment. In fact, APC exhibits anticoagulant, anti-apoptotic, and anti-inflammatory properties, while also providing the protection of an endothelial barrier [50\*]. Decreased damage to the glycocalyx [51], improved functional capillary density of several organs [51-53], sustained tissue oxygenation [54], and preserved or improved organ function [53; 55\*\*] were observed following APC administration in several experimental sepsis models. Furthermore, improved microcirculation has been shown in human sepsis [56]. However, administration of APC before or concomitantly with septic challenge represents a critical limitation of a large number of the experimental studies because such timing is not realistic in the clinic. Studies assessing post-injury treatment are needed to address this issue [57].

## PERSPECTIVES

Currently, several innovative therapeutic strategies for the treatment of sepsis, which also influence microcirculatory and mitochondrial function, are being explored:

### Erythropoietin

Erythropoietin (EPO) has been shown to protect several organs against injury due to ischemia-reperfusion, hemorrhagic shock, and systemic inflammation [58]. A recent study has shown, for the first time, a protective effect of EPO against renal dysfunction when administered contemporaneously with LPS. Maintenance of superoxide dismutase levels and decreased TNF- $\alpha$  levels were observed in response to EPO [59]. Furthermore, in a remarkable murine study, EPO reversed the sepsis-induced decrement of muscle functional capillary density and impaired mitochondrial respiration (measured by NADH fluorescence) within 10 minutes, even when administered 18 hours after CLP [60\*]. Notably, EPO impressively reduced the high mortality (from 70% to 30%) caused by administration of zymosan (a toll-like 2 receptor agonist) in a systemic inflammation model [61]. Outcome studies of EPO in sepsis models remain to be conducted.

### PARP inhibitors

Oxidative and nitrosative stress-induced DNA strand breaks are the primary trigger of poly ADP-ribose polymerase (PARP) activation. PARP is also involved in the upregulation of multiple pro-inflammatory factors. Because it is an energy consuming process, PARP activation can deplete  $\text{NAD}^+$ , thus slowing ATP formation and, therefore, leading to cell dysfunction or death. PARP inhibitors, by maintaining cellular ATP levels, either protect cells against necrosis or divert cell necrosis toward apoptosis [62]. PARP inhibition has been shown to improve microcirculatory flow and to prevent mitochondrial hypoxia in a hepatic ischemia-reperfusion model [63;64] and also to reduce LPS-induced



hyperpermeability in the lung and gut [65]. In several sepsis models, organ dysfunction and outcome could be improved. Several PARP inhibitors have been identified, some of which possess anti-aggregant activity (via competitive antagonism of ADP receptors on thrombocytes). Recently, insulin has been shown to not only reduce hyperglycemia-related ROS generation and DNA damage, but also to act as a direct inhibitor of PARP [66], a fact shedding some light on the mechanism of action of intensive insulin treatment.

### **Cytochrome C**

Two elegant studies highlight the possibility of mitochondrial resuscitation. In a murine CLP model, infusion of exogenous cytochrome c was shown to result in improved cardiac function [67] and prolonged survival [68\*\*]. These findings cannot be simply translated into a human therapeutic strategy, as safety concerns regarding induction of apoptosis and stimulation of reactive oxygen species formation by cytochrome c must first be assessed.

### **TLR4 antagonists**

Toll-like receptor 4 (TLR-4) is involved in LPS recognition and triggers a vigorous inflammatory response [69]. The TLR-4 inhibitors Eritoran, taurolidine, and TAK242 are currently being investigated in clinical trials for their capacity to improve microcirculation and cellular dysfunction, as well as outcome in sepsis models [70-72].

### **Microcirculation and Mitochondria-targeted resuscitation**

The microcirculatory and mitochondrial dysfunction is usually neither assessed in patients nor integrated into the indication for treatment choices. Insights into the adverse effects of therapeutic strategies on the microcirculation and mitochondria as well as their dependence on the phase of disease need to be gained. Future sepsis treatment should account for and focus on microcirculatory and mitochondrial (dys-)function. An integrative multi-marker approach and diagnostic tools comprising new technologies, as well as functional tests for time-gated therapy, must be developed. Dynamic assessment of the recovery of microcirculatory and mitochondrial function during resuscitation could be used to tailor therapy. The components of the microcirculation and mitochondria that should be targeted in order to improve outcome need to be identified. The same applies to the therapeutics used to achieve this goal. Due to the complexity of the process, a well-timed combination of drugs with pleiotropic mechanisms will be most likely to provide beneficial effects.

## CONCLUSION

A growing amount of evidence suggests a causal association of microcirculatory and mitochondrial dysfunction with organ failure and outcome in sepsis. Timely resuscitation has been proven to limit inflammation and organ failure and to improve outcome. Insights into the spatio-temporal association of microcirculatory and mitochondrial dysfunction would add decisive knowledge to the design of effective treatment strategies. Future research should aim at elucidating the interaction between therapy and microcirculatory and mitochondrial function before large clinical trials can be performed. Therapeutic targets to guide such therapies remain to be defined.

## REFERENCES AND RECOMMENDED READING

Papers of particular interest, published within the annual period of review, have been highlighted as:

\* of special interest

\*\* of outstanding interest

1. Vincent JL, Sakr Y, Sprung CL, et al. Sepsis in European intensive care units: results of the SOAP study. *Crit Care Med* 2006, 34:344-353.
2. Freelander SO, Lenhart CH. Clinical observations on the capillary circulation. *Arch Intern Med* 29, 12-32. 1922.
3. Ince C: The microcirculation is the motor of sepsis. *Crit Care* 2005, 9 Suppl 4:S13-S19.
4. Levy MM, Fink MP, Marshall JC, et al. 2001 SCCM/ESICM/ACCP/ATS/SIS International Sepsis Definitions Conference. *Intensive Care Med* 2003, 29:530-538.
5. Spronk PE, Zandstra DF, Ince C. Bench-to-bedside review: sepsis is a disease of the microcirculation. *Crit Care* 2004, 8:462-468.
6. Bagshaw SM, Brophy PD, Cruz D, Ronco C. Fluid balance as a biomarker: impact of fluid overload on outcome in critically ill patients with acute kidney injury. *Crit Care* 2008, 12:169.
7. Hollenberg SM, Ahrens TS, Annane D, et al. Practice parameters for hemodynamic support of sepsis in adult patients: 2004 update. *Crit Care Med* 2004, 32:1928-1948.
- \* 8. Payen D, de Pont AC, Sakr Y, et al. A positive fluid balance is associated with a worse outcome in patients with acute renal failure. *Crit Care* 2008, 12:R74.  
Based on the SOAP cohort, this study proposes the concept of the detrimental effect of a positive fluid balance, especially if the critically ill patient suffers from acute kidney failure.
9. Dejana E, Orsenigo F, Lampugnani MG. The role of adherens junctions and VE-cadherin in the control of vascular permeability. *J Cell Sci.* 2008, 121:2115-2122.
10. Furst R, Bubik MF, Bihari P, et al. Atrial natriuretic peptide protects against histamine-induced endothelial barrier dysfunction in vivo. *Mol.Pharmacol.* 2008, 74:1-8.
11. Ladetzki-Baehs K, Keller M, Kiemer AK, et al. Atrial natriuretic peptide, a regulator of nuclear factor-kappaB activation in vivo. *Endocrinology* 2007, 148:332-336.
12. Morgenthaler NG, Struck J, Christ-Crain M, et al. Pro-atrial natriuretic peptide is a prognostic marker in sepsis, similar to the APACHE II score: an observational study. *Crit Care* 2005, 9:R37-R45.
13. Meyer B, Huelsmann M, Wexberg P, et al. N-terminal pro-B-type natriuretic peptide is an independent predictor of outcome in an unselected cohort of critically ill patients. *Crit Care Med* 2007, 35:2268-2273.
14. Boerma EC, van der Voort PH, Spronk PE, Ince C. Relationship between sublingual and intestinal microcirculatory perfusion in patients with abdominal sepsis. *Crit Care Med* 2007, 35:1055-1060.
- \*\*15. Melican K, Boekel J, Mansson LE, et al. Bacterial infection-mediated mucosal signalling induces local renal ischaemia as a defence against sepsis. *Cell Microbiol.* 2008, 10:1987-1998.  
An elegant study that provides significant insights into the pathophysiology of ascending urinary tract infection. The authors demonstrate how the systemic spread of the infection is prevented by a shutdown of the microcirculation. Prevention of microcirculatory flow deterioration by anticoagulation led to fatal urosepsis.
16. Annane D, Sanquer S, Sqbille V, et al. Compartmentalised inducible nitric-oxide synthase activity in septic shock. *The Lancet* 2000, 355:1143-1148.
17. Brealey D, Brand M, Hargreaves I, et al. Association between mitochondrial dysfunction and severity and outcome of septic shock. *Lancet* 2002, 360:219-223.
18. Fredriksson K, Hammarqvist F, Strigard K, et al. Derangements in mitochondrial metabolism in intercostal and leg muscle of critically ill patients with sepsis-induced multiple organ failure. *Am J Physiol Endocrinol.Metab* 2006, 291:E1044-E1050.
19. Giulivi C, Kato K, Cooper CE. Nitric oxide regulation of mitochondrial oxygen consumption I: cellular physiology. *Am J Physiol Cell Physiol* 2006, 291:C1225-C1231.
- \*\*20. Cooper CE, Giulivi C. Nitric oxide regulation of mitochondrial oxygen consumption II: Molecular mechanism and tissue physiology. *Am J Physiol Cell Physiol* 2007, 292:C1993-C2003.  
Small review series that summarizes, in a well-organized way, the relationship between nitric oxide and mitochondrial respiration. Current knowledge regarding the inhibition of oxygen consumption is described. Spatial and temporal effects are explained, as are their subjacent mechanisms.
21. Levy RJ, Vijayarathay C, Raj NR, et al. Competitive and noncompetitive inhibition of myocardial cytochrome C oxidase in sepsis. *Shock* 2004, 21:110-114.
- \* 22. Singer M. Mitochondrial function in sepsis: acute phase versus multiple organ failure. *Crit Care Med* 2007, 35:S441-S448.  
This review discusses the role of mitochondrial dysfunction in the pathogenesis of multiple organ failure by examining the findings of experimental and clinical studies. The equilibrium of ATP supply and demand in sepsis is evoked, leading to the concept of a hibernation-like state characterized by decreased mitochondrial function.
23. Porta F, Takala J, Weikert C, et al. Effects of prolonged endotoxemia on liver, skeletal muscle and kidney mitochondrial function. *Crit Care* 2006, 10:R118.
24. Goedhart PT, Khalilzada M, Bezemer R, et al. Sidestream Dark Field (SDF) imaging: a novel stroboscopic LED ring-based imaging modality for clinical assessment of the microcirculation. *Optics Express* 2007, 15:15101-15114.
- \* 25. De Backer D, Hollenberg S, Boerma C, et al. How to evaluate the microcirculation: report of a round table conference. *Crit Care* 2007, 11:R101.  
Consensus paper on the standards required for the evaluation of microcirculatory images.
26. Creteur J, Carollo T, Soldati G, et al. The prognostic value of muscle StO2 in septic patients. *Intensive Care Med* 2007, 33:1549-1556.
27. Doerschug KC, Delsing AS, Schmidt GA, Haynes WG. Impairments in microvascular reactivity are related to organ failure in human sepsis. *Am J Physiol Heart Circ Physiol* 2007, 293:H1065-H1071.
28. Pareznik R, Knezevic R, Voga G, Podbregar M. Changes in muscle tissue oxygenation during stagnant ischemia in septic patients. *Intensive Care Med* 2006, 32:87-92.
29. Rivers E, Nguyen B, Havstad S, et al. Early goal-directed therapy in the treatment of severe sepsis and septic shock. *N Engl J Med* 2001, 345:1368-1377.

- 2
30. Dellinger RP, Levy MM, Carlet JM, *et al.* Surviving Sepsis Campaign: international guidelines for management of severe sepsis and septic shock: 2008. *Crit Care Med* 2008, 36:296-327.
31. Rivers EP, Kruse JA, Jacobsen G, *et al.* The influence of early hemodynamic optimization on biomarker patterns of severe sepsis and septic shock. *Crit Care Med* 2007, 35:2016-2024.
32. Monnet X, Rienzo M, Osman D, *et al.* Passive leg raising predicts fluid responsiveness in the critically ill. *Crit Care Med* 2006, 34:1402-1407.
33. Pottelcher J, Deruddre S., Georger J.F., *et al.* Both passive leg raising and volume expansion improve sublingual microcirculation in preload-dependent septic patients. *Intensive Care Med* 34[Supplement 1], S103. 2008.
34. Luengo C, Losser MR, Legrand M, *et al.* Fluid resuscitation improves sublingual microcirculatory flow in septic shock patients. *Intensive Care Med* 34[Supplement 1], S103. 2008.
- \* 35. Trzeciak S, McCoy JV, Phillip DR, *et al.* Early increases in microcirculatory perfusion during protocol-directed resuscitation are associated with reduced multi-organ failure at 24 h in patients with sepsis. *Intensive Care Med* 2008.
- In an EGDT setting, increased microcirculatory flow during resuscitation was associated with reduced organ failure at 24 h, without substantial differences in global hemodynamics. The authors conclude that these findings support the hypothesis that targeting the microcirculation distinct from the macrocirculation could potentially improve organ failure in sepsis.
- \* 36. Sennoun N, Monternont C, Gibot S, *et al.* Comparative effects of early versus delayed use of norepinephrine in resuscitated endotoxic shock. *Critical Care Medicine* 2007, 35:1736-1740.
- The authors conclude that early use of norepinephrine might lead to a decreased need for fluid resuscitation, while providing better tissue oxygenation and mesenteric flow. This study shows that different EGDT designs might be of interest.
37. Krejci V, Hildebrand LB, Sigurdsson GH. Effects of epinephrine, norepinephrine, and phenylephrine on microcirculatory blood flow in the gastrointestinal tract in sepsis. *Crit Care Med* 2006, 34:1456-1463.
38. Di Giantomasso D, Morimatsu H, May CN, Bellomo R. Increasing renal blood flow: low-dose dopamine or medium-dose norepinephrine. *Chest* 2004, 125:2260-2267.
39. Di Giantomasso D, Morimatsu H, May CN, Bellomo R. Intrarenal blood flow distribution in hyperdynamic septic shock: Effect of norepinephrine. *Crit Care Med* 2003, 31:2509-2513.
40. Duranteau J, Sitbon P, Teboul JL, *et al.* Effects of epinephrine, norepinephrine, or the combination of norepinephrine and dobutamine on gastric mucosa in septic shock. *Crit Care Med* 1999, 27:893-900.
41. Nakajima Y, Baudry N, Duranteau J, Vicaud E. Effects of vasopressin, norepinephrine, and L-arginine on intestinal microcirculation in endotoxemia. *Crit Care Med* 2006, 34:1752-1757.
42. Regueira T, Banziger B, Djafarzadeh S, *et al.* Norepinephrine to increase blood pressure in endotoxaemic pigs is associated with improved hepatic mitochondrial respiration. *Crit Care* 2008, 12:R88.
43. Annane D, Vignon P, Renault A, *et al.* Norepinephrine plus dobutamine versus epinephrine alone for management of septic shock: a randomised trial. *Lancet* 2007, 370:676-684.
44. Pinto BB, Rehberg S, Ertmer C, Westphal M. Role of levosimendan in sepsis and septic shock. *Curr Opin Anaesthesiol* 2008, 21:168-177.
45. Fries M, Ince C, Rossaint R, *et al.* Levosimendan but not norepinephrine improves microvascular oxygenation during experimental septic shock. *Crit Care Med* 2008, 36:1886-1891.
46. Rehberg S, Ertmer C, Lange M, *et al.* Combined Levosimendan and vasopressin prolongs survival in ovine septic shock. *Crit Care Med* 35[12], A61. 2007.
47. Spronk PE, Ince C, Gardien MJ, *et al.* Nitroglycerin in septic shock after intravascular volume resuscitation. *Lancet* 2002, 360:1395-1396.
48. Lamontagne F, Meade M, Ondiveeran HK, *et al.* Nitric oxide donors in sepsis: a systematic review of clinical and *in vivo* preclinical data. *Shock* 2008;30:653-659.
49. Marti-Carvajal A, Salanti G, Cardona AF. Human recombinant activated protein C for severe sepsis. *Cochrane.Database.Syst.Rev.* 2008,CD004388.
- \* 50. Mosnier LO, Zlokovic BV, Griffin JH. The cytoprotective protein C pathway. *Blood* 2007, 109:3161-3172.
- Excellent review highlighting the different pathways modulated by APC.
51. Marechal X, Favory R, Joulin O, *et al.* Endothelial glycocalyx damage during endotoxemia coincides with microcirculatory dysfunction and vascular oxidative stress. *Shock* 2008, 29:572-576.
52. Hoffmann JN, Vollmar B, Laschke MW, *et al.* Microhemodynamic and cellular mechanisms of activated protein C action during endotoxemia. *Crit Care Med* 2004, 32:1011-1017.
53. Favory R, Lancel S, Marechal X, *et al.* Cardiovascular protective role for activated protein C during endotoxemia in rats. *Intensive Care Med* 2006, 32:899-905.
54. Gierer P, Hoffmann JN, Mahr F, *et al.* Activated protein C reduces tissue hypoxia, inflammation, and apoptosis in traumatized skeletal muscle during endotoxemia. *Crit Care Med* 2007, 35:1966-1971.
- \*\*55. Gupta A, Berg DT, Gerlitz B, *et al.* Role of protein C in renal dysfunction after polymicrobial sepsis. *J Am Soc.Nephrol.* 2007, 18:860-867.
- Very nicely conducted study, and one of the rare experimental studies assessing late APC administration (10h after CLP). APC treatment reduced blood urea nitrogen, renal pathology, and chemokine expression, and dramatically reduced induction of inducible nitric oxide synthase and caspase-3 activation in the kidney.
56. De Backer D, Verdant C, Chierago M, *et al.* Effects of drotrecogin alfa activated on micro circulatory alterations in patients with severe sepsis. *Critical Care Medicine* 2006, 34:1918-1924.
57. Regnault V, Levy B. Recombinant activated protein C in sepsis: endothelium protection or endothelium therapy? *Crit Care* 2007, 11:103.
58. Thiemermann C. Beneficial effects of erythropoietin in preclinical models of shock and organ failure. *Crit Care* 2007, 11:132.
59. Mitra A, Bansal S, Wang W, *et al.* Erythropoietin ameliorates renal dysfunction during endotoxaemia. *Nephrol.Dial.Transplant.* 2007, 22:2349-2353.
- \* 60. Kao R, Xenocostas A, Rui T, *et al.* Erythropoietin improves skeletal muscle microcirculation and tissue bioenergetics in a mouse sepsis model. *Crit Care* 2007, 11:R58.
- This study approaches a clinical, realistic setting by choosing to administer EPO 18h after CLP. The observation of parallel recovery of microcirculatory and mitochondrial function suggests a cause-effect relationship. However, further investigations are required for confirmation.
61. Cuzzocrea S, Di Paola R, Mazzon E, *et al.* Erythropoietin reduces the development of nonseptic shock

- induced by zymosan in mice. *Crit Care Med* 2006, 34:1168-1177.
62. Gero D, Szabo C. Poly(ADP-ribose) polymerase: a new therapeutic target? *Curr Opin Anaesthesiol* 2008, 21:111-121.
  63. Roesner JP, Vagts DA, Iber T, *et al*. Protective effects of PARP inhibition on liver microcirculation and function after haemorrhagic shock and resuscitation in male rats. *Intensive Care Med* 2006, 32:1649-1657.
  64. Szijarto A, Batmunkh E, Hahn O, *et al*. Effect of PJ-34 PARP-inhibitor on rat liver microcirculation and antioxidant status. *J Surg Res* 2007, 142:72-80.
  65. Szabo A, Salzman AL, Szabo C. Poly (ADP-ribose) synthetase activation mediates pulmonary microvascular and intestinal mucosal dysfunction in endotoxin shock. *Life Sci*. 1998, 63:2133-2139.
  66. Horvath EM, Benko R, Gero D, *et al*. Treatment with insulin inhibits poly(ADP-ribose)polymerase activation in a rat model of endotoxemia. *Life Sci*. 2008, 82:205-209.
  67. Piel DA, Gruber PJ, Weinheimer CJ, *et al*. Mitochondrial resuscitation with exogenous cytochrome c in the septic heart. *Crit Care Med* 2007, 35:2120-2127.
  - \*\*68. Piel DA, Deutschman CS, Levy RJ. Exogenous cytochrome C restores myocardial cytochrome oxidase activity into the late phase of sepsis. *Shock* 2008, 29:612-616.  
Using an innovative approach, the authors directly target mitochondrial dysfunction and show that mitochondrial activity can be recovered, leading to better myocardial function and survival.
  69. Gao H, Evans TW, Finney SJ. Bench-to-bedside review: sepsis, severe sepsis and septic shock- does the nature of the infecting organism matter? *Crit Care* 2008, 12:213.
  70. Mullarkey M, Rose JR, Bristol J, *et al*. Inhibition of endotoxin response by e5564, a novel Toll-like receptor 4-directed endotoxin antagonist. *J Pharmacol Exp Ther*. 2003, 304:1093-1102.
  71. Frieling H, Lauer KS, Grundling M, *et al*. Peritoneal instillation of taurilidone or polihexanide modulates intestinal microcirculation in experimental endotoxemia. *Int J Colorectal Dis*. 2007, 22:807-817.
  72. Sha T, Sunamoto M, Kitazaki T, *et al*. Therapeutic effects of TAK-242, a novel selective Toll-like receptor 4 signal transduction inhibitor, in mouse endotoxin shock model. *Eur J Pharmacol*. 2007, 571:231-239.

# CHAPTER

# 3

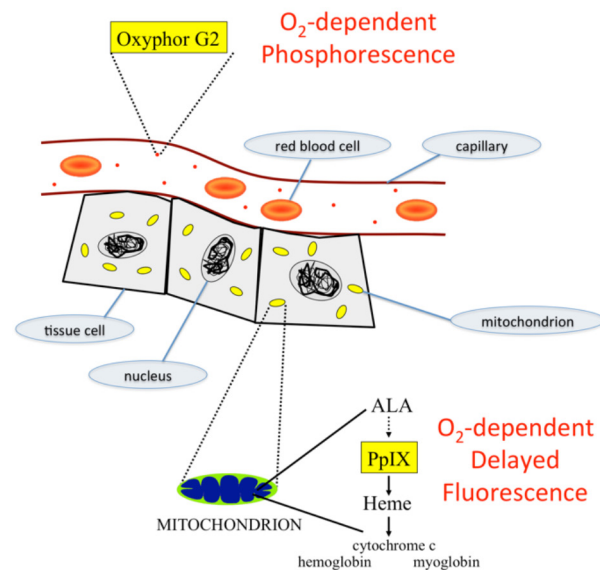
## Microvascular and mitochondrial $PO_2$ simultaneously measured by oxygen-dependent delayed luminescence

Sander I. A. Bodmer  
Gianmarco M. Balestra  
Floor A. Harms  
Tanja Johannes  
Nicolaas J. H. Raat  
Robert J. Stolker  
Egbert G. Mik



## ABSTRACT

Measurement of tissue oxygenation is a complex task and various techniques have led to a wide range of tissue PO<sub>2</sub> values and contradictory results. Tissue is compartmentalized in microcirculation, interstitium and intracellular space and current techniques are biased towards a certain compartment. Simultaneous oxygen measurements in various compartments might be of great benefit for our understanding of determinants of tissue oxygenation. Here we report simultaneous measurement of microvascular PO<sub>2</sub> ( $\mu$ PO<sub>2</sub>) and mitochondrial PO<sub>2</sub> (mitoPO<sub>2</sub>) in rats. The  $\mu$ PO<sub>2</sub> measurements are based on oxygen-dependent quenching of phosphorescence of the near-infrared phosphor Oxyphor G2. The mitoPO<sub>2</sub> measurements are based on oxygen-dependent quenching of delayed fluorescence of protoporphyrin IX (PpIX). Favorable spectral properties of these porphyrins allow simultaneous measurement of the delayed luminescence lifetimes. A dedicated fiber-based time-domain setup consisting of a tunable pulsed laser, 2 red-sensitive gated photomultiplier tubes and a simultaneous sampling data-acquisition system is described in detail. The absence of cross talk between the channels is shown and the feasibility of simultaneous  $\mu$ PO<sub>2</sub> and mitoPO<sub>2</sub> measurements is demonstrated in rat liver in vivo. It is anticipated that this novel approach will greatly contribute to our understanding of tissue oxygenation in physiological and pathological circumstances.



## 1. INTRODUCTION

The study into the determinants of tissue oxygenation in physiological and pathological circumstances is a complex field of ongoing research. Tissue oxygen tension (tPO<sub>2</sub>) is a key parameter for physiological function. Because of its importance many techniques have been developed to measure tPO<sub>2</sub> in vivo [1]. Concerning oxygenation, tissue can be regarded to consist of three main compartments, the microcirculation, the interstitial space and the intracellular space. Due to the technological and physical-chemical background of the available techniques to measure tPO<sub>2</sub>, each is biased towards a certain compartment. Oxygen electrodes [2] tend to measure interstitial PO<sub>2</sub> while e.g. phosphorescence quenching [3] and electron paramagnetic resonance oxime-try [4] are biased towards the microcirculation. Since oxygen gradients exist between the compartments this results in a bias towards a specific PO<sub>2</sub> range. This bias, together with technical differences like response time and sample volume, have made the interpretation and comparison of in vivo oxygen measurements difficult [5]. Therefore, the simultaneous measurement of PO<sub>2</sub> in different tissue compartments is needed to further our understanding of oxygen delivery and utilization under various pathophysiological circumstances.

Oxygen-dependent quenching of phosphorescence is a powerful method for quantitative measurement of PO<sub>2</sub> in biological samples [6]. Pd-meso-tetra-(4-carboxyphenyl)-tetrabenzoporphyrin (Oxyphor G2) is a relatively new phosphor which is excellently suited for oxygen measurements in vivo [7 – 9]. It is highly soluble in blood plasma, where it binds to albumin and confines to the circulation [10]. Upon intravascular injection oxygen-dependent phosphorescence lifetimes can be measured at the surface of tissues and organs using e.g. fiber-based phosphorimeters [11, 12]. In this way, Oxyphor G2 has been successfully used for measurement of the distribution of microvascular oxygen pressure (mPO<sub>2</sub>) in e.g. solid tumors [13] and kidney [14, 15]. Oxyphor G2 has its absorption maxima at 440 and 632 nm and its emission near 800 nm.

Recently we reported that the delayed fluorescence lifetime of endogenous PpIX can be used to measure mitochondrial PO<sub>2</sub> (mitoPO<sub>2</sub>) in cultured cells [16] and in vivo [17 – 19]. Administration of the precursor 5-aminolevulinic acid (ALA) increases the intramitochondrial levels of PpIX, and mitoPO<sub>2</sub> can subsequently be measured by its oxygen-dependent delayed fluorescence lifetime. Delayed fluorescence has much in common with phosphorescence and it shares the useful possibility to determine heterogeneity in PO<sub>2</sub> within a volume of tissue with high temporal resolution [20, 21]. Moreover, the basic setup for delayed fluorescence lifetime measurements resembles the equipment for phosphorescence quenching experiments. Therefore, simultaneous measurement of phosphorescence and delayed fluorescence should be possible. The spectral properties of Oxyphor G2 and PpIX are very favorable in this respect with having a common excitation band (632 nm) and widely separated emission bands (~800 nm for

Oxyphor G2 and ~690 nm for PpIX). The successful combination of the two techniques would provide a powerful means to measure simultaneously mPO<sub>2</sub> and mitoPO<sub>2</sub> *in vivo*.

Accordingly, we have developed a delayed luminescence lifetime technique that quantitatively and simultaneously measures mPO<sub>2</sub> using the oxygen-dependent optical properties of injectable Oxyphor G2 and mitoPO<sub>2</sub> using the oxygen-dependent optical properties of ALA-enhanced PpIX. In this paper we describe in detail the setup and the applicability of this technique for simultaneous measurements of mPO<sub>2</sub> and mitoPO<sub>2</sub> in intact tissue. The lack of cross-over in the detection channels is demonstrated *in vivo* in the rat. Ultimately, we provide the first simultaneous measurements of mPO<sub>2</sub> and mitoPO<sub>2</sub> in the rat liver *in vivo*.

## 2. MATERIALS AND METHODS

### 2.1 The measurement concept

Both Oxyphor G2 and PpIX possess a first excited triplet state (T<sub>1</sub>) that reacts strongly with oxygen. Population of T<sub>1</sub> occurs upon photo excitation with light at one of the porphyrin-specific absorption bands. Energy transfer between the excited porphyrin and oxygen results in an oxygen-dependent T<sub>1</sub> lifetime. Spontaneous relaxation of the T<sub>1</sub> state to the ground state (S<sub>1</sub>) produces delayed luminescence (i.e. phosphorescence or delayed fluorescence) that can be used to measure the T<sub>1</sub> lifetime (figure 1). The lifetime of the delayed luminescence is quantitatively related to the oxygen tension by the Stern-Volmer relationship:

$$PO_2 = \frac{\frac{1}{\tau} - \frac{1}{\tau_0}}{k_q} \quad (1)$$

where PO<sub>2</sub> is the oxygen tension (in mmHg), τ is the measured decay time, k<sub>q</sub> is the quenching constant (in mmHg<sup>-1</sup>s<sup>-1</sup>) and τ<sub>0</sub> is the lifetime at an oxygen pressure of zero.

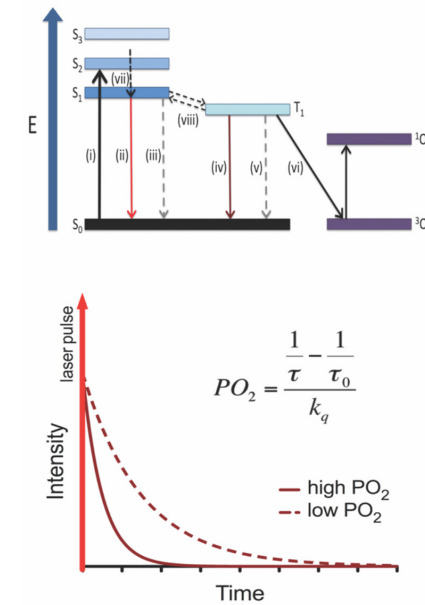


**Figure 1** Jablonski diagram of states and state transitions of PpIX and its interaction with oxygen (upper panel) and the principle of measuring oxygen tension (PO<sub>2</sub>) by oxygen dependent quenching of delayed luminescence (lower panel). S<sub>0</sub>, S<sub>1</sub>, S<sub>2</sub> and S<sub>3</sub> represent the ground state and first, second and third excited singlet states, respectively. T<sub>1</sub> represent the first excited triplet states of PpIX and <sup>3</sup>O<sub>2</sub> and <sup>1</sup>O<sub>2</sub> are the triplet ground state and excited singlet state of oxygen. Absorption (i), fluorescence and delayed fluorescence (ii), radiationless transitions (iii and v), phosphorescence (iv), energy transfer (vi), internal conversion (vii) and bi-directional intersystem crossing (viii). The inserted equation in the lower panel is the Stern-Volmer relationship in which PO<sub>2</sub> is the oxygen tension, τ is the measured lifetime, k<sub>q</sub> is the quenching constant and τ<sub>0</sub> is the lifetime in the absence of oxygen.

Oxyphor G2 is a water-soluble synthetic porphyrin especially developed as oxygen-sensitive phosphorescent dye. Absorption maxima of Oxyphor G2 are 440 and 632 nm and emission peaks around 800 nm. The calibration constants of Oxyphor G2 for *in vivo* conditions are k<sub>q</sub> = 270 mmHg<sup>-1</sup>s<sup>-1</sup> and τ<sub>0</sub> = 250μs and the quantum efficiency of phosphorescence is approximately 12% [9]. The oxygen-dependent quenching of phosphorescence of Oxyphor G2 has been successfully used for microvascular (μPO<sub>2</sub>) measurements [11, 13-15] and PO<sub>2</sub> measurements in macrovessels [22]. To this end, Oxyphor G2 is injected into the blood stream of experimental animals where the probe binds to albumin and is confined to the circulation [10]. Typical *in vivo* concentrations of Oxyphor G2 for microvascular oxygen measurements are around 1 nmol/g (tissue wet weight).

Protoporphyrin IX (PpIX) is the final precursor of heme in the heme biosynthetic pathway. PpIX is synthesized in the mitochondria [23] and administration of its precursor 5-aminolevulinic acid (ALA) to cells and organisms substantially enhances

PpIX concentration [24]. Since the conversion of PpIX to heme is a rate-limiting step, administration of ALA causes accumulation of PpIX in the mitochondria [19]. Besides the absorption maximum around 420 nm the absorption spectrum of PpIX contains several smaller peaks including one around 634 nm (figure 2).

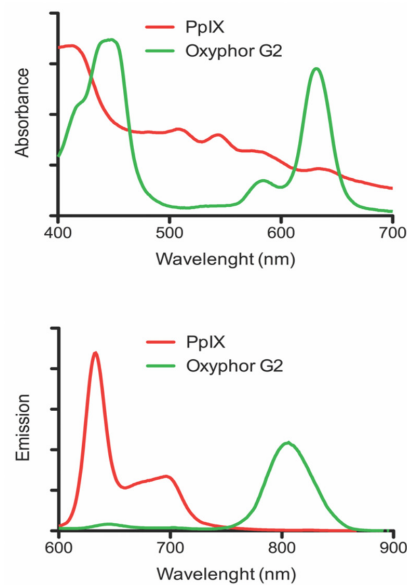


**Figure 2** Absorption spectra (upper panel) and emission spectra (lower panel) of Oxyphor G2 and PpIX.

The fluorescence spectrum is typically two-peaked. Because of the spectral overlap with the excitation pulse only the peak around 690 nm is used for delayed fluorescence detection. The oxygen-dependent delayed fluorescence of PpIX has been successfully introduced as a technique for mitochondrial oxygen measurements [16, 18, 19]. The calibration constants of PpIX for in vivo conditions are  $k_q = 830 \text{ mmHg}^{-1}\text{s}^{-1}$  and  $\tau_0 = 0.8 \text{ ms}$ . ALA-induced PpIX levels have been reported to be in the order of 20 nmol/g (tissue wet weight) in liver [25].

Both Oxyphor G2 and PpIX can be effectively excited with red light at a wavelength around 632 nm. This allows simultaneous excitation within a single measurement volume. The emission peaks are well separated without spectral overlap. Therefore, in principle, these spectral properties are excellently suited for simultaneous excitation and separate detection of the two phosphors. The intravascular localization of Oxyphor G2 combined with the mitochondrial localization of PpIX therefore enables simultaneous measurement of  $\mu\text{PO}_2$  and  $\text{mitoPO}_2$  (figure 3).

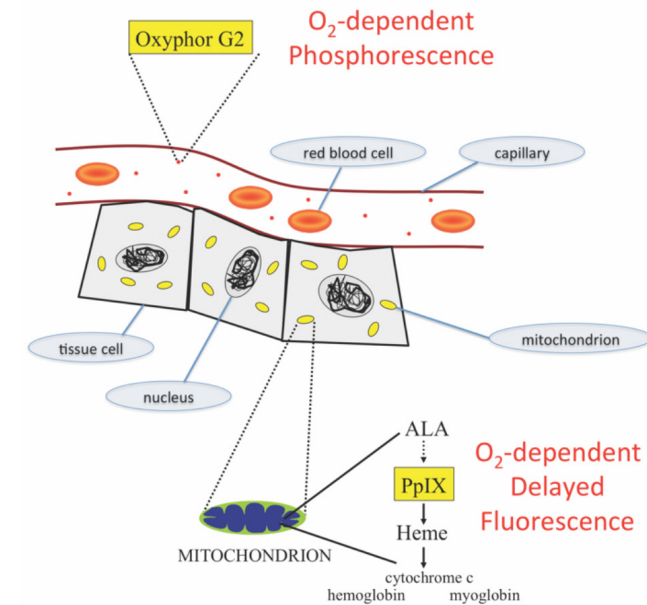


**Figure 3** Schematic representation of the measuring concept. Oxyphor G2 is directly injected into the bloodstream and is used as microvascular oxygen probe by means of oxygen-dependent quenching of phosphorescence. PpIX is induced in the mitochondria by administration of its precursor ALA and is used as mitochondrial oxygen probe by means of oxygen-dependent quenching of delayed fluorescence.

## 2.2 Delayed luminescence setup

A schematic drawing of the experimental setup is shown in figure 4. A compact computer-controlled tunable laser (Opolette 355-I, Opotek, Carlsbad, CA, USA), providing pulses with a specified duration of 4-10 ns and typically 2-4 mJ/pulse over the tunable range of 410 to 670 nm, was used as excitation source. The laser was coupled into a Fiber Delivery System (Opotek, Carlsbad, CA, USA) consisting of 50 mm planoconvex lens, X-Y fiber mount and a 2-meter fiber with a core diameter of 1000  $\mu\text{m}$ . This fiber was coupled to the excitation branch of a bifurcated reflection probe (FCR-7IR400-2-ME, Avantes b.v., Eerbeek, The Netherlands) by an In-Line Fiber Optic Attenuator (FOA-Inline, Avantes b.v., Eerbeek, The Netherlands). The light output of the excitation branch was set at 200  $\mu\text{W}$ /pulse as measured by a FieldMate laser power meter with PowerMax PS19 measuring head (Coherent Inc., Santa Clara, CA, USA). The emission branch of the reflection probe was coupled to a bifurcated fiber assembly (Model 77533, Newport, Irvine, CA, USA), which acted as splitter for the two detection channels.



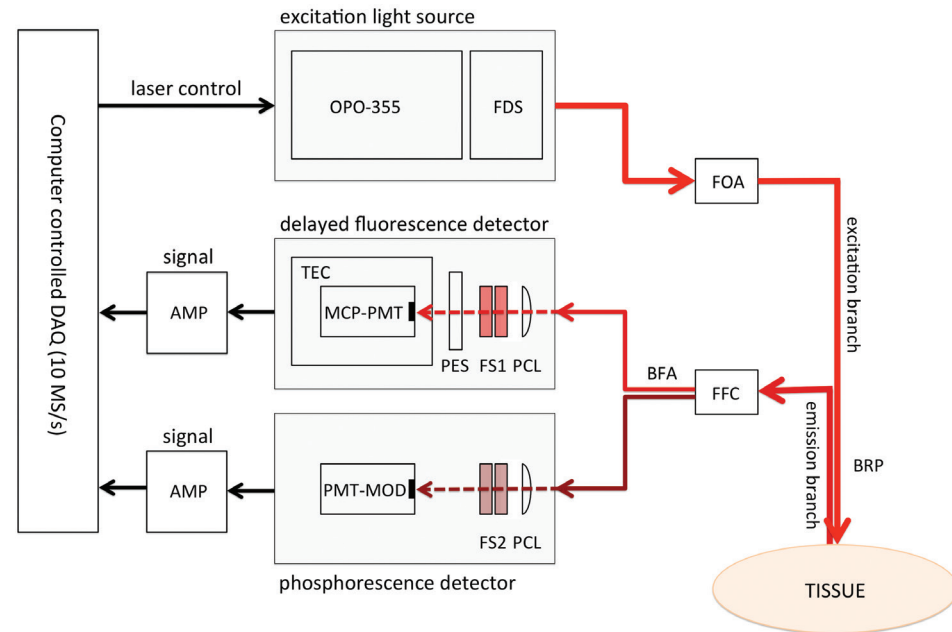


**Figure 4** Schematic drawing of the experimental setup. OPO-355: Opolette 355-I, FDS: Fiber Delivery System, FOA: Fiber Optic Attenuator, BFP: Bifurcated Reflection Probe, FFC: Fiber to Fiber Coupling, BFA: Bifurcated Fiber Assembly, PCL: Plano Convex Lens, FS1 & FS2: Filter Sets, PES: Protective Electronic Shutter, MCP-PMT: Micro Channel Plate Photomultiplier Tube, TEC: Thermo Electric Cooling, PMT-MOD: Photomultiplier Module, AMP: Amplifier, DAQ: Data Acquisition.

The PpIX signal was detected by a gated microchannel plate photomultiplier tube (MCP-PMT R5916U series, Hamamatsu Photonics, Hamamatsu, Japan). The MCP-PMT was custom adapted with an enhanced red-sensitive photocathode having a quantum efficiency of 24% at 650 nm. The MCP-PMT was mounted on a gated socket assembly (E3059-501, Hamamatsu Photonics, Hamamatsu, Japan) and cooled to  $-30\text{ }^{\circ}\text{C}$  by a thermoelectric cooler (C10373, Hamamatsu Photonics, Hamamatsu, Japan). The MCP-PMT was operated at a voltage in the range of 2300V-3000V by a regulated high-voltage DC power supply (C4848-02, Hamamatsu Photonics, Hamamatsu, Japan). One branch of the bifurcated fiber (splitter) was fit into an Oriel Fiber Bundle Focusing Assembly (Model 77799, Newport, Irvine, CA, USA) which was coupled to the MCP-PMT by an in-house built optics consisting of a filter-holder, a plano convex lens (BK-7, OptoSigma, Santa Ana, CA, USA) with focal length of 90 mm and an electronic shutter (04 UTS 203, Melles Griot, Albuquerque, NM, USA). The shutter was controlled by an OEM Shutter Controller Board (59 OSC 205, Melles Griot, Albuquerque, NM, USA) and served as protection for the PMT, which was configured for the “normally on” mode. The PpIX emission light was filtered by a combination of a 590 nm longpass filter (OG590, Newport, Irvine, CA, USA)

and a broadband ( $675 \pm 25\text{ nm}$ ) bandpassfilter (Omega Optical, Brattleboro, VT, USA).

The Oxyphor G2 signal was detected by a photomultiplier module with gate function (H10304-20-NN, Hamamatsu Photonics, Hamamatsu, Japan). The second branch of the bifurcated fiber (splitter) was fit into an Oriel Fiber Bundle Focusing Assembly (Model 77799, Newport, Irvine, CA, USA) which was coupled to the PMT-module by an in-house built optics consisting of a filter-holder, a plano convex lens (BK-7, OptoSigma, Santa Ana, CA, USA) with focal length of 90 mm. The Oxyphor G2 emission light was filtered by a combination of a 715 nm longpass filter (RG715, Newport, Irvine, CA, USA) and a  $790 \pm 20\text{ nm}$  bandpassfilter (Omega Optical, Brattleboro, VT, USA).

The output currents of the photomultipliers were voltage-converted by in-house built amplifiers with an input impedance of 440 ohm, 400 times voltage amplification and a bandwidth around 20 Mhz. Data-acquisition was performed by a PC-based data-acquisition system containing a 10 MS/s simultaneous sampling data-acquisition board (NI-PCI-6115, National Instruments, Austin, TX). The amplifiers were coupled to the DAQ-board by a BNC interface (BNC-2090A, National Instruments, Austin, TX). The data-acquisition ran at a rate of 10 mega samples per second and 64 laser pulses (repetition rate 20 Hz) were averaged prior to analysis. Control of the setup and analysis of the data was performed with software written in LabView (Version 8.6, National Instruments, Austin, TX, USA).

### 2.3 Analysis of delayed luminescence

In case of non-homogeneous oxygen tension, the delayed luminescence signal can in general be described by an integral over an exponential kernel:

$$y(t) = \int_0^t \exp(-\lambda t) f(\lambda) d\lambda \quad (2)$$

where  $f(\lambda)$  denotes the spectrum of reciprocal lifetimes within the finite data set  $y(t)$ . Mono-Exponential Analysis (MEA) in generally overestimates the average lifetime and consequently underestimates the  $\text{PO}_2$  within the sample volume [11]. A much better estimation of the average  $\text{PO}_2$  and an indication of its heterogeneity can be obtained by the approach described by Golub et al. [20]. They demonstrated that the heterogeneity in oxygen pressure could be analyzed by fitting distributions of quencher concentration to the delayed luminescence data. Corresponding to their work, the fitting function for a simple rectangular distribution with a mean  $\text{PO}_2$   $Q_m$  and a  $\text{PO}_2$  range from  $Q_m - \delta$  till  $Q_m + \delta$  is:

$$Y_R = \exp\left(-\left(k_0 + k_q Q_m\right)t\right) \cdot \frac{\sinh(k_q \delta t)}{k_q \delta t} \quad (3)$$

where  $Y(t)$  is the normalized delayed fluorescence data,  $k_0$  is the first-order rate constant for delayed fluorescence decay in the absence of oxygen,  $k_q$  is the quenching constant

and  $\delta$  is half the width of the rectangular distribution. In terms of quenching constants and the Stern-Volmer relationship, equation 3 can be rewritten as:

$$Y_R = \exp\left(-\left(\frac{1}{\tau_0} + k_q \langle PO_2 \rangle\right)t\right) \cdot \frac{\sinh(k_q \delta t)}{k_q \delta t} \quad (4)$$

where  $\langle PO_2 \rangle$  is the mean PO<sub>2</sub> within the sample volume and  $\tau_0$  the lifetime in the absence of oxygen. The standard deviation ( $\sigma$ ) can be retrieved from  $\delta$  by:

$$\sigma = \frac{\delta}{\sqrt{3}} \quad (5)$$

This approach was successfully used by our group in phosphorescence lifetime measurements [11]. Recently we demonstrated that the approach is also useful for delayed fluorescence lifetime measurements in the case of complex underlying lifetime distributions [17]. Analysis of the delayed luminescence signals by means of equations 3-4 is referred to as the Rectangular Distribution Method (RDM).

Analysis of the photometric signals, by means of MEA and RDM, was performed with software written in LabView (Version 8.6, National Instruments, Austin, TX, USA), using the Marquart-Levenberg non-linear fit procedure.

#### 2.4 Analysis of influence of noise

Signal-to-noise ratio (SNR) in time domain lifetime measurements is commonly defined as the ratio of maximal signal amplitude (at the start of the decay) to the maximum signal of the noise (peak-to-peak). The negative effects of noise on the accuracy of the measurement are inversely related to the lifetime. Therefore, the presence of noise especially degrades measurement accuracy at higher PO<sub>2</sub> levels.

Because the quenching constants of PpIX and Oxyphor G2 are not the same, the effect of noise on the accuracy of  $\mu PO_2$  and mitoPO<sub>2</sub> measurements differs. We analyzed the relationship between measurement accuracy, PO<sub>2</sub> and SNR of the two channels by means of computer simulations. In steps of 10 mmHg, over a PO<sub>2</sub> range of 0-300 mmHg, we simulated delayed fluorescence and phosphorescence traces. SNR was varied by adding different amounts of Poisson distributed noise to the simulated decays (SNR 5, 10, 20 and 50). The PO<sub>2</sub> was calculated back from the noisy signal by lifetime analysis. The noise-induced error was calculated as the absolute difference between simulated PO<sub>2</sub> and recovered PO<sub>2</sub>. We performed 500 simulation runs per PO<sub>2</sub> step and defined the potential noise-induced error as the maximum error occurring during these 500 runs.

#### 2.5 Measurement of spectral properties

Absorption spectra were recorded using a Hitachi U-3000 Spectrophotometer (Hitachi High-Technologies Corporation, Tokyo, Japan). Emission spectra were recorded using a Hitachi F-4500 Fluorescence Spectrophotometer (Hitachi High-Technologies

Corporation, Tokyo, Japan). Both Oxyphor G2 and PpIX were dissolved in phosphate buffered saline containing 4% bovine serum albumin (Sigma-Aldrich, St. Louis, MO, USA) to a final concentration of 10  $\mu$ M. Emission spectra were recorded after deoxygenating the sample by flushing with nitrogen.

#### 2.6 Animal preparation

The experimental protocol was approved by the Animal Research Committee of the Erasmus MC - University Medical Center Rotterdam. Animal care and handling were performed in accordance with the guidelines for Institutional and Animal Care and Use Committees (IACUC) and done by trained staff of the Erasmus Experimental Animal Facility.

A total of 15 male Wistar rats (Charles River, Wilmington, MA) with a bodyweight of 275-325 gram were used. Rats received either a combination of 200 mg/kg 5-aminolevulinic acid (ALA, Sigma-Aldrich, St. Louis, MO, USA) and 0.4 mg/kg Oxyphor G2 (Oxygen Enterprises, Philadelphia, PA, USA) ( $n = 10$ ) or only Oxyphor G2 ( $n = 5$ ). In order to ensure an optimal mitochondrial PpIX concentration, ALA was administered by intraperitoneal injection 2.5 hours before start of experimental procedures. Animals were anesthetized by an intraperitoneal injection of a mixture of Ketamine (90 mg/kg, Alfasan, Woerden, The Netherlands), Medetomidine (0.5 mg/kg, Sedator Eurovet Animal Health BV, Bladel, The Netherlands) and Atropine (0.05 mg/kg, Centrofarm Services BV, Etten-Leur, The Netherlands). A continuous intravenous infusion of Ketamine (50 mg/kg/hr) was used for maintaining anesthesia. A tracheotomy was performed prior to starting mechanical ventilation. Mechanical ventilation, using a Babylog 8000 ventilator (Dräger, Dräger Medical Netherlands BV, Zoetermeer, The Netherlands), was controlled and adjusted on end-tidal PCO<sub>2</sub> (~ 35 mmHg).

A catheter (sterilized 0.9 mm diameter polyethylene catheter) was inserted in the right jugular vein for intravenous administration of anesthetics, Oxyphor G2 and fluids (0.9% NaCl, 5 mL kg<sup>-1</sup> h<sup>-1</sup>). A similar catheter was placed in the right carotid artery to monitor arterial blood pressure (MAP) using a Powerlab 8/30 data-acquisition system with LabChart Pro (ADInstruments, Bella Vista NSW, Australia). This catheter was also used for taking arterial blood gases. The animal was placed onto a heating pad and body temperature was rectally measured and kept around 37 °C.

A midline laparotomy was performed to gain access to the liver for measuring  $\mu PO_2$  and mitoPO<sub>2</sub>. Before infusion of Oxyphor G2, 20 minutes prior to the start of the actual oxygen measurements, signals were recorded for examination of cross talk between the channels. This was repeated after administration of Oxyphor G2. Measurements were performed in dimmed light, after assuring proper positioning of the reflection probe. ALA was dissolved in phosphate buffered saline (PBS) and adjusted to pH 7.4 prior to injection. Oxyphor G2 was dissolved in PBS (1.25 mg/ml) as stock solution.

Variations in inspired oxygen fraction (FIO<sub>2</sub>) were made during the protocol at set time points by mixtures of oxygen and nitrogen. Instrumentation and Oxyphor G2 administration

were performed while breathing 40% oxygen (0.4 FiO<sub>2</sub>). After first measurements at 0.4 FiO<sub>2</sub>, FiO<sub>2</sub> was set to 1.0 and after a stabilization period of 20 min the second measurements were performed. Then FiO<sub>2</sub> was set to 0.2 and again after a stabilization period of 20 min the third measurements were performed. In the time control group (n = 5) FiO<sub>2</sub> was set to 0.4 during the entire experiment. At the end of the experimental protocol animals were euthanized by an overdose of Euthasol (ST Farma, Raamsdonksveer, The Netherlands).

### 2.7 Statistical analysis

Data are expressed as mean ± standard deviation (s.d.) unless stated otherwise. Repeated-measures analysis of variance, one-way ANOVA with Bonferroni posttest, was used to analyze the effect of changes in FiO<sub>2</sub> on physiological parameters. Two-way ANOVA for repeated measurements with Bonferroni posttest was used to analyze differences between μPO<sub>2</sub> and mitoPO<sub>2</sub> at the various FiO<sub>2</sub> settings. *P* < 0.05 was considered significant.

## 3. RESULTS

In order to measure signals of different porphyrins simultaneously, it is mandatory that the readings do not mutually interfere. The wide spectral separation of the emissions of PpIX and Oxyphor G2, 690 nm and 790 nm respectively, indicate this should be possible to achieve. Indeed, as is shown in figure 5, there was no interference of the two signals. Injection of ALA induced a clear delayed fluorescence signal in the 690 nm channel, indicating buildup of mitochondrial PpIX within the liver. In contrast, ALA administration did not induce any signal in the 790 nm channel. While injection of Oxyphor G2 induced a readily measurable phosphorescence signal at 790 nm, it was not detectable in the 690 nm channel. In both channels a faint decaying signal was observed in the absence of porphyrins. This background was not oxygen-sensitive and most probably originated from the glass in the fiber optic. Overall this background accounted to less than 5% of the total signal and no background corrections were made in the signal analysis.

Noise is inevitably present in real signals and generally has a negative effect on the accuracy of measurements. Because the quenching constants for μPO<sub>2</sub> and mitoPO<sub>2</sub> differ, the dynamic range of measure lifetimes differs between the channels. Interpretation of simultaneous measurements could be hampered by inter channel differences in noise sensitivity. Therefore, we analyzed the relationship between accuracy, PO<sub>2</sub> and SNR by means of computer simulations (figure 6). It is evident that both channels behave differently, with the delayed fluorescence measurement being more sensitive to the deleterious effects of noise. However, in practice, SNR > 20 is readily achieved for both PpIX and Oxyphor G2. In that case, the noise-induced potential error in both channels is below 2% over a large PO<sub>2</sub> range.

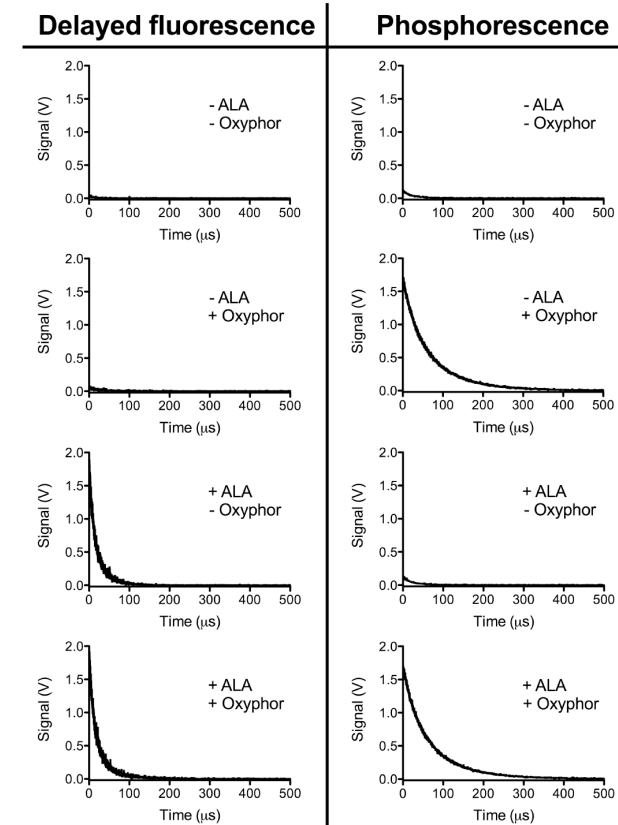


**Figure 5** Signals obtained from both channels with and without various combinations of probes. Delayed fluorescence at 690 nm and phosphorescence at 790 nm simultaneously measured after excitation at 632 nm. ALA: 200 mg/kg 5-aminolevulinic acid, Oxyphor: 0.4 mg/kg Oxyphor G2

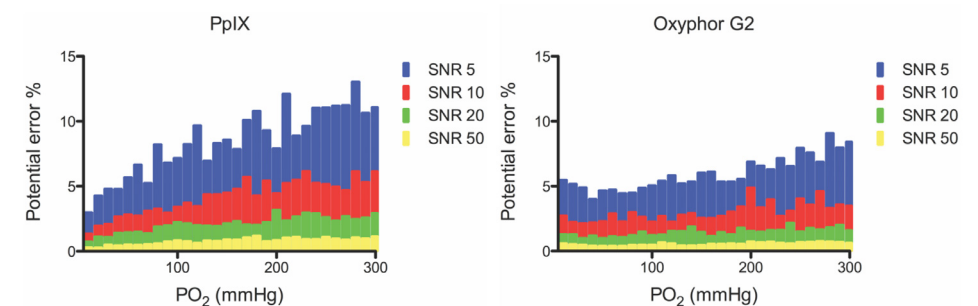


**Figure 6** Noise-induced potential error in PO<sub>2</sub> retrieval as result of the presence of noise in delayed fluorescence (upper panel) and phosphorescence (lower panel) signals. SNR: signal-to-noise ratio.

In general, the oxygen tension in tissue is non-homogeneous because of the existence of oxygen gradients as a result of oxygen consumption and diffusion. Delayed luminescence of oxygen-sensitive probes is therefore not decaying mono-exponentially but the photometric signals contain lifetime distributions. Figure 7 shows an example of a phosphorescence trace from Oxyphor G2 measured in rat liver at 0.4 FiO<sub>2</sub> (= 40% oxygen). Mono-exponential analysis (MEA) resulted in a poor fit and, compared to the rectangular distribution method (RDM), resulted in a relatively long phosphorescence lifetime. In the case of MEA the lifetime was 96.8 μs, corresponding to a μPO<sub>2</sub> of 23.4 mmHg. The RDM resulted in a lifetime of 69.8 μs, corresponding to an average μPO<sub>2</sub> of 38.2 mmHg. The remaining small difference between data and RDM curve fit at early times reflects the fact that a rectangular distribution is only an estimation of the real oxygen distribution.

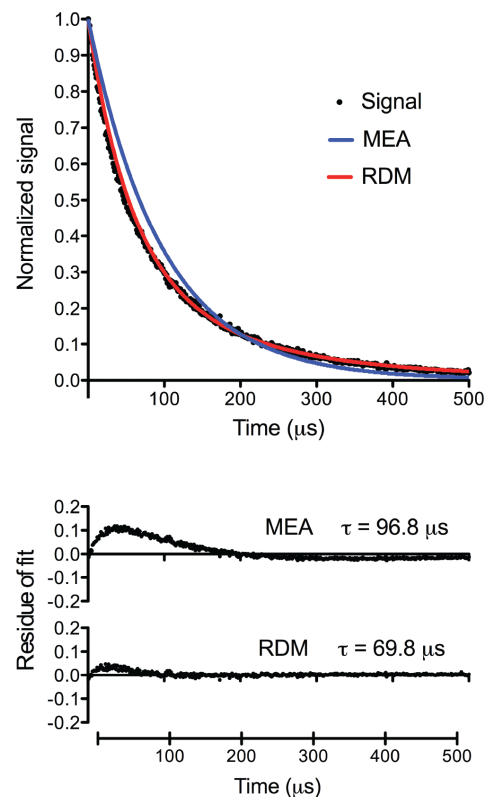


**Figure 7** Example of two different fit procedures on a phosphorescence signal measured in vivo rat liver at 0.4 FiO<sub>2</sub>. Raw phosphorescence decay data and the corresponding curves of two fit procedures (upper panel). Residue of fit (difference between data and fit) for both fit procedures and the obtained phosphorescence lifetimes. MEA, mono-exponential analysis; RDM, rectangular distribution method.

An example of a simultaneous measurement of PpIX delayed fluorescence and Oxyphor G2 phosphorescence is shown in Figure 8. Both signals showed clear oxygen-sensitivity, with the lifetime becoming visually longer at a lower inspired oxygen fraction. The lifetimes of PpIX delayed fluorescence were 17.9 μs at 1.0 FiO<sub>2</sub> and 39.4 μs at 0.2 FiO<sub>2</sub>, corresponding to an average mitoPO<sub>2</sub> of 65.8 mmHg and 29.1 mmHg respectively. The lifetimes of Oxyphor G2 phosphorescence were 44.1 μs at 1.0 FiO<sub>2</sub> and 59.9 μs at 0.2 FiO<sub>2</sub>, corresponding to an average μPO<sub>2</sub> of 69.2 mmHg and 47.0 mmHg respectively.

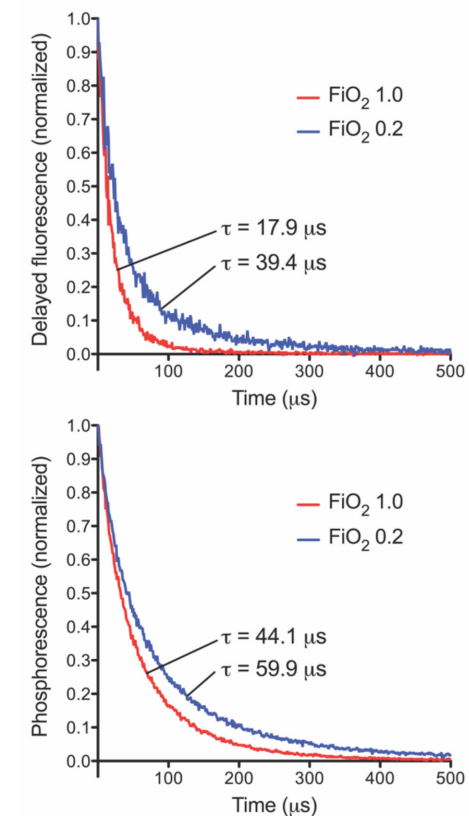


**Figure 8** Examples of delayed luminescence data measured at two different inspired oxygen fractions (FiO<sub>2</sub>). Delayed fluorescence from PpIX (upper panel) and phosphorescence from Oxyphor G2 (lower panel). Lifetimes were obtained by RDM analysis.

Simultaneous measurements of liver mitoPO<sub>2</sub> and μPO<sub>2</sub> at three FiO<sub>2</sub> steps were performed in a series of 5 rats. An overview of physiological variables is given in Table 1. Arterial PO<sub>2</sub>, as measured by bloodgas analysis, significantly differed between the FiO<sub>2</sub> steps, being approximately 5 times higher at 1.0 FiO<sub>2</sub> compared to 0.2 FiO<sub>2</sub>. From the

other variables only the MAP at 0.2 FiO<sub>2</sub> is significantly lower than MAP at 0.4 and 1.0 FiO<sub>2</sub>. End-tidal CO<sub>2</sub> and temperature were actively controlled by ventilation and external heating. Heart rate and hemoglobin concentration were stable during the FiO<sub>2</sub> steps.

**Table 1** Physiological values measured during in vivo experiments at FiO<sub>2</sub> of 0.2, 0.4 and 1.0. A significant difference (\*) was noted in the arterial PO<sub>2</sub> between the FiO<sub>2</sub> steps and in the MAP between FiO<sub>2</sub> of 0.2 and the other steps. No significant difference was measured between conditions for the remaining physiological variables.

Physiological variables	FiO <sub>2</sub> = 0.2	FiO <sub>2</sub> = 0.4	FiO <sub>2</sub> = 1.0
PO <sub>2</sub> (mmHg)*	93 ± 12	191 ± 15	481 ± 35
EtCO <sub>2</sub> (mmHg)	36 ± 2	34 ± 4	33 ± 3
Hb (mmol/L)	8.0 ± 0.4	8.2 ± 0.7	8.1 ± 0.9
MAP (mmHg)*	87 ± 15	109 ± 10	105 ± 10
Temp (°C)	37.1 ± 0.6	36.9 ± 0.5	37.0 ± 0.7
HR (beats/min)	248 ± 9	256 ± 18	251 ± 16

Figure 9 shows the results of the simultaneous measurements of mitoPO<sub>2</sub> and μPO<sub>2</sub> at various FiO<sub>2</sub> settings. Both mitoPO<sub>2</sub> and μPO<sub>2</sub> increased at higher FiO<sub>2</sub>, and there were significant differences between 0.2 FiO<sub>2</sub> and 1.0 FiO<sub>2</sub> and between 0.4 FiO<sub>2</sub> and 1.0 FiO<sub>2</sub>. Furthermore, at all FiO<sub>2</sub> settings the average mitoPO<sub>2</sub> was a little lower than the average μPO<sub>2</sub> but only at 1.0 FiO<sub>2</sub> this difference was statistically significant. The standard deviation, as a measure of heterogeneity obtained from the RDM, was significantly higher for μPO<sub>2</sub> compared to mitoPO<sub>2</sub> at all FiO<sub>2</sub> settings. At 1.0 FiO<sub>2</sub> the heterogeneity in μPO<sub>2</sub> was significantly higher compared to the heterogeneity in μPO<sub>2</sub> at 0.2 FiO<sub>2</sub>. In the time control group at 0.4 FiO<sub>2</sub> μPO<sub>2</sub> and mitoPO<sub>2</sub> and their heterogeneity were stable over time and similar to the experimental group at 0.4 FiO<sub>2</sub>.

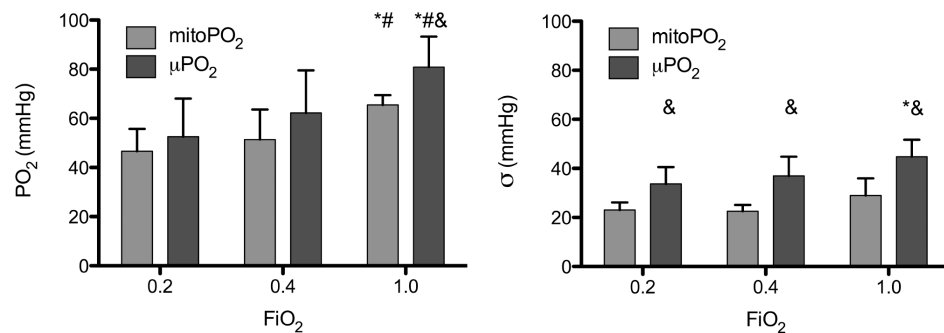


**Figure 9** Microvascular and mitochondrial PO<sub>2</sub> in rat liver at different FiO<sub>2</sub> values. Average PO<sub>2</sub> as obtained by RDM analysis (upper panel) and corresponding standard deviation (lower panel). Significantly different compared to (\*) 0.2 FiO<sub>2</sub>, (#) 0.4 FiO<sub>2</sub> and (&) mitoPO<sub>2</sub>.

## 4. DISCUSSION AND CONCLUSION

In this work, we present a method to simultaneously measure oxygen tension in the mitochondria and microcirculation within intact living tissue. The method is based on a combination of oxygen-dependent quenching of delayed fluorescence of ALA-enhanced mitochondrial PpIX and oxygen-dependent quenching of phosphorescence of the exogenous dye Oxyphor G2. We comprehensively describe a time-domain based measurement system consisting of a tunable pulsed laser and two gated red-sensitive photomultipliers. The measurement equipment is fiber-based and can be easily used in (patho)physiological studies in small and large experimental animals. We demonstrate that the in vivo measured signals of PpIX and Oxyphor G2 do not interfere and that SNR ≥ 20 reduces noise-induced inaccuracy of both channels below 2%. Furthermore, we provide data of the first simultaneous measurements of mitoPO<sub>2</sub> and μPO<sub>2</sub>, measured in rat liver in vivo during ventilation with various inspired oxygen fractions. To analyze the complex photometric signals we used RDM analysis, which provides the mean and standard deviation of the PO<sub>2</sub> in the measurement volume.

Our view on tissue oxygenation has gradually changed over years with the advent of novel technology to measure oxygen in tissues. Oxygen is supplied from blood to the tissues by passive diffusion and the site for oxygen exchange is the microcirculation. Although classically the capillary network was identified as the most likely site for oxygen to leave the bloodstream, a more modern view is that oxygen has the ability to diffuse from any microvessel along a large enough oxygen gradient [26]. Surrounding the microcirculation and in between the tissue cells is the interstitial space. Recent studies in resting skeletal muscle have indicated the existence of only a small gradient between microvessels and interstitium [27, 28]. The intracellular PO<sub>2</sub> and its influence on metabolism in vivo remains the most difficult to measure. Measurements of intracellular PO<sub>2</sub> have mostly been indirect, e.g. via measurement of myoglobin saturation [29]. Only recently it has become possible to measure directly PO<sub>2</sub> in mitochondria of living intact tissue [18, 19].

Since mitochondria are the oxygen consuming and energy producing organelles of cells, the development of a technique to measure mitoPO<sub>2</sub> removes the last hurdle in our ability to comprehensively measure tissue oxygenation. Especially in combination with microvascular PO<sub>2</sub> measurements it might be possible to gain direct insight in oxygen gradients and oxygen consumption. We previously used a combination of endogenously enhanced PpIX and Oxyphor G2 to measure, in cell suspensions, mitoPO<sub>2</sub> and extracellular PO<sub>2</sub> in culture medium [16]. These measurements were performed in cuvettes with separate devices that, unfortunately, could not be integrated into a useful in vivo measurement system. Therefore, we developed a dedicated fiber-based setup that allows simultaneous measurement of mitoPO<sub>2</sub> and μPO<sub>2</sub> in intact tissue using PpIX and Oxyphor G2.

In the current study we focused on the rat liver, since we have extensively evaluated the mitoPO<sub>2</sub> measurements in this type of tissue [19]. The measured mitoPO<sub>2</sub> values in the current study are very similar to our previously reported results. In light of the fact that intracellular PO<sub>2</sub> is generally expected to be low (several mmHg) as a result of mitochondrial oxygen consumption, we were surprised to find such high mitoPO<sub>2</sub>. However, mitoPO<sub>2</sub> values were well in the range of reported tissue PO<sub>2</sub> values measured by microoxygen electrodes [30]. In our current study we can directly compare our mitoPO<sub>2</sub> measurements with the well-established phosphorescence lifetime technique. This direct comparison learns that only a small difference between mitoPO<sub>2</sub> and μPO<sub>2</sub> exists in liver. This latter is not surprising due to the anatomical structure of the liver, with very close proximity of tissue cells to blood and overall high blood supply. Furthermore, our findings fit well in the current view that tissue PO<sub>2</sub> might be much higher than classically reported with invasive techniques [31]. Indeed, a recent study using minimally invasive 19F MRI in a rat model found tissue PO<sub>2</sub> levels well above 50 mmHg in several organs including liver [32]. The standard deviation in μPO<sub>2</sub> obtained from the RDM analysis is larger than that for the mitoPO<sub>2</sub>. This is most likely due to the size of the reflection probe. The measurement volume likely contains multiple microvessels that represent heterogenous PO<sub>2</sub>.

Overall, our study shows that implementation of the technique to measure simultaneously μPO<sub>2</sub> and mitoPO<sub>2</sub> by oxygen-dependent delayed luminescence is feasible, based on a combination of exogenous Oxyphor G2 and endogenous PpIX. With ongoing evaluation of the use of the mitoPO<sub>2</sub> technique in other organs and tissues it is expected that this approach will greatly contribute to further our understanding of oxygen transport and oxygen metabolism in health and disease.

### Acknowledgements

This work was financially supported by the Young Investigator Grant 2009 (awarded to E.G.M.) from the Dutch Society of Anesthesiology. The authors thank Jacqueline Voorbeijtel and Patricia Specht for their expert biotechnical help. The authors thank dr. G.A. Koning and the Laboratory of Experimental Surgical Oncology of the Erasmus MC for help with the spectral measurements.

## REFERENCES

1. Springett R, Swartz HM. Measurements of Oxygen In Vivo: Overview and Perspectives on Methods to Measure Oxygen Within Cells and Tissues. Mary Ann Liebert, Inc. 2 Madison Avenue Larchmont, NY 10538 USA; 2007.
2. Lübbers DW, Baumgärtl H. Heterogeneities and profiles of oxygen pressure in brain and kidney as examples of the pO<sub>2</sub> distribution in the living tissue. *Kidney Int.* 1997;51:372–80.
3. Sinaasappel M, Donkersloot C, van Bommel J, Ince C. PO<sub>2</sub> measurements in the rat intestinal microcirculation. *Am. J. Physiol. American Physiological Society* Bethesda, MD; 1999;276:G1515–20.
4. Swartz HM, Clarkson RB. The measurement of oxygen in vivo using EPR techniques. *Phys Med Biol.* IOP Publishing; 1998;43:1957–75.
5. Swartz HM, Dunn J. The difficulties in comparing in vivo oxygen measurements: turning the problems into virtues. *Adv. Exp. Med. Biol.* Springer, Boston, MA; 2005;566:295–301.
6. Vanderkooi JM, Maniara G, Green TJ, Wilson DF. An optical method for measurement of dioxygen concentration based upon quenching of phosphorescence. *J. Biol. Chem. American Society for Biochemistry and Molecular Biology*; 1987;262:5476–82.
7. Vladimir Rozhkov, David Wilson A, Vinogradov S. Phosphorescent Pd Porphyrin–Dendrimers: Tuning Core Accessibility by Varying the Hydrophobicity of the Dendritic Matrix. *American Chemical Society*; 2002.
8. Vinogradov SA, Lo L-W, Wilson DF. Dendritic Polyglutamic Porphyrins: Probing Porphyrin Protection by Oxygen-Dependent Quenching of Phosphorescence. *Chemistry – A European Journal.* John Wiley & Sons, Ltd; 1999;5:1338–47.
9. Dunphy I, Vinogradov SA, Wilson DF. Oxyphor R2 and G2: phosphors for measuring oxygen by oxygen-dependent quenching of phosphorescence. *Anal. Biochem.* 2002;310:191–8.
10. Poole DC, Behnke BJ, McDonough P, McAllister RM, Wilson DF. Measurement of muscle microvascular oxygen pressures: compartmentalization of phosphorescent probe. *Microcirculation.* John Wiley & Sons, Ltd; 2004;11:317–26.
11. Johannes T, Mik EG, Ince C. Dual-wavelength phosphorimetry for determination of cortical and subcortical microvascular oxygenation in rat kidney. *Journal of Applied Physiology.* 2006;100:1301–10.
12. Vinogradov SA, Fernandez-Seara MA, Dupan BW, Wilson DF. A method for measuring oxygen distributions in tissue using frequency domain phosphorimetry. *Comparative Biochemistry and Physiology Part A: Molecular & Integrative Physiology.* 2002;132:147–52.
13. Ziemer LS, Lee WMF, Vinogradov SA, Sehgal C, Wilson DF. Oxygen distribution in murine tumors: characterization using oxygen-dependent quenching of phosphorescence. *J. Appl. Physiol. American Physiological Society*; 2005;98:1503–10.
14. Johannes T, Ince C, Klingel K, Unertl KE, Mik EG. Iloprost preserves renal oxygenation and restores kidney function in endotoxemia-related acute renal failure in the rat. *Critical Care Medicine.* 2009;37:1423–32.
15. Johannes T, Mik EG, Nohé B, Raat NJH, Unertl KE, Ince C. Influence of fluid resuscitation on renal microvascular PO<sub>2</sub> in a normotensive rat model of endotoxemia. *Crit Care.* 2006;10:R88.
16. Mik EG, Stap J, Sinaasappel M, Beek JF, Aten JA, van Leeuwen TG, et al. Mitochondrial PO<sub>2</sub> measured by delayed fluorescence of endogenous protoporphyrin IX. *Nat Meth.* 2006;3:939–45.

17. Harms FA, de Boon WMI, Balestra GM, Bodmer SIA, Johannes T, Stolker RJ, et al. Oxygen-dependent delayed fluorescence measured in skin after topical application of 5-aminolevulinic acid. Sterenberg HJCM, Bendsoe N, Svanberg K, editors. *J Biophotonics*. WILEY-VCH Verlag; 2011;4:731–9.
18. Mik EG, Ince C, Eerbeek O, Heinen A, Stap J, Hooibrink B, et al. Mitochondrial oxygen tension within the heart. *Journal of Molecular and Cellular Cardiology*. 2009;46:943–51.
19. Mik EG, Johannes T, Zuurbier CJ, Heinen A, Houben-Weerts JHPM, Balestra GM, et al. In vivo mitochondrial oxygen tension measured by a delayed fluorescence lifetime technique. *Biophys. J.* Elsevier; 2008;95:3977–90.
20. Golub AS, Popel AS, Zheng L, Pittman RN. Analysis of phosphorescence in heterogeneous systems using distributions of quencher concentration. *Biophys. J.* 1997;73:452–65.
21. Johannes T, Mik EG, Ince C. Nonresuscitated endotoxemia induces microcirculatory hypoxic areas in the renal cortex in the rat. *Shock*. 2009;31:97–103.
22. Mik EG, Johannes T, Ince C. Monitoring of renal venous PO<sub>2</sub> and kidney oxygen consumption in rats by a near-infrared phosphorescence lifetime technique. *Am. J. Physiol. Renal Physiol.* American Physiological Society; 2008;294:F676–81.
23. Poulson R. The enzymic conversion of protoporphyrinogen IX to protoporphyrin IX in mammalian mitochondria. *J. Biol. Chem.* 1976;251:3730–3.
24. Fukuda H, Casas A, Batlle A. Aminolevulinic acid: from its unique biological function to its star role in photodynamic therapy. *Int. J. Biochem. Cell Biol.* Pergamon; 2005;37:272–6.
25. van den Boogert J, van Hillegersberg R, de Rooij FW, de Bruin RW, Edixhoven-Bosdijk A, Houtsmuller AB, et al. 5-Aminolaevulinic acid-induced protoporphyrin IX accumulation in tissues: pharmacokinetics after oral or intravenous administration. *Journal of Photochemistry and Photobiology B: Biology*. 1998;44:29–38.
26. Pittman RN. Oxygen gradients in the microcirculation. *Acta Physiol (Oxf)*. John Wiley & Sons, Ltd; 2011;202:311–22.
27. Wilson DF, Finikova OS, Lebedev AY, Apreleva S, Pastuszko A, Lee WMF, et al. Measuring Oxygen in Living Tissue: Intravascular, Interstitial, and “Tissue” Oxygen Measurements. *Oxygen Transport to Tissue XXXII*. Springer, Boston, MA; 2011. pp. 53–9.
28. Wilson DF, Lee WMF, Makonnen S, Finikova O, Apreleva S, Vinogradov SA. Oxygen pressures in the interstitial space and their relationship to those in the blood plasma in resting skeletal muscle. *Journal of Applied Physiology*. American Physiological Society; 2006.
29. Molé PA, Chung Y, Tran TK, Sailasuta N, Hurd R, Jue T. Myoglobin desaturation with exercise intensity in human gastrocnemius muscle. *Am. J. Physiol. Regul. Integr. Comp. Physiol.* American Physiological Society Bethesda, MD; 1999.
30. van Wagenveld BA, Van Gulik European surgical TM, 1998. Intrahepatic Tissue pO<sub>2</sub> during Continuous or Intermittent Vascular Inflow Occlusion in a Pig Liver Resection Model. *karger.com*.
31. Wilson DF. Quantifying the role of oxygen pressure in tissue function. *AJP: Heart and Circulatory Physiology*. American Physiological Society; 2008;294:H11–3.
32. Liu S, Shah SJ, Wilmes LJ, Feiner J, Kodibagkar VD, Wendland MF, et al. Quantitative tissue oxygen measurement in multiple organs using 19F MRI in a rat model. *Magn. Reson. Med.* John Wiley & Sons, Ltd; 2011;66:1722–30.

# CHAPTER

# 4

Oxygenation measurement  
by multi-wavelength oxygen-  
dependent phosphorescence and  
delayed fluorescence:  
catchment depth and application  
in intact heart

Balestra GM  
Aalders MCG  
Specht PAC  
Ince C  
Mik EG. J

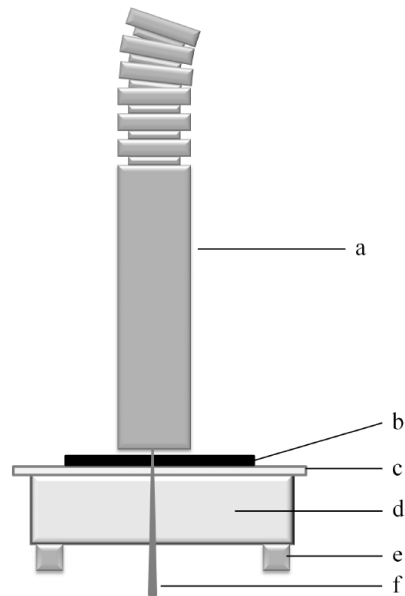
Journal of Biophotonics. 2015, 8 (8): 615–628  
PMID: 25250821 DOI: 10.1002/jbio.201400054.





## ABSTRACT

Oxygen delivery and metabolism represent key factors for organ function in health and disease. We describe the optical key characteristics of a technique to comprehensively measure oxygen tension ( $PO_2$ ) in myocardium, using oxygen-dependent quenching of phosphorescence and delayed fluorescence of porphyrins, by means of Monte Carlo simulations and *ex vivo* experiments. Oxyphor G2 (microvascular  $PO_2$ ) was excited at 442 nm and 632 nm and protoporphyrin IX (mitochondrial  $PO_2$ ) at 510 nm. This resulted in catchment depths of 161 (86)  $\mu\text{m}$ , 350 (307)  $\mu\text{m}$  and 262 (255)  $\mu\text{m}$  respectively, as estimated by Monte Carlo simulations and *ex vivo* experiments (brackets). The feasibility to detect changes in oxygenation within separate anatomical compartments is demonstrated in rat heart *in vivo*.



Schematic of *ex vivo* measurements.

## 1. INTRODUCTION

Insight in oxygen delivery and utilization are key factors for understanding organ function. Inadequate oxygen availability plays a role in physiological as well as pathophysiological conditions, like sepsis [1-6] and ischemia-reperfusion [7-12]. A variety of methods for measuring tissue and microcirculatory oxygenation are available [13-17]. They all differ significantly in accuracy, spatio-temporal resolution and invasiveness. Oxygen-dependent quenching of phosphorescence, as described by Wilson et al. in 1987 [18], is one of the methods to quantitatively determine oxygen partial pressures ( $PO_2$ ) within living tissues in a non-destructive way. Our group has been using this method for its minimal invasiveness, versatile applicability and real-time measurement. The method relies on injection of a phosphorescent dye in the circulation which enables measurement of microvascular oxygen tension ( $\mu PO_2$ ) using the phosphorescence lifetime approach [18]. The practical implementations range from *in vivo* microscopy [15,19,20] and two-photon laser scanning [21,22] to fiber-based measurement in thick tissue [23,24] and large blood vessels [25].

Oxygenation in tissue is heterogeneous, with heterogeneity arising e.g. from local oxygen gradients in microcirculation and interstitium [16,26]. Heterogeneity also arises from differences in anatomical compartments within tissues and organs, e.g. renal cortex and medulla [24] and intestinal serosa and mucosa [27-31]. Oxygen-dependent quenching of phosphorescence has been proven to be a valuable tool to study this heterogeneity. For example, two-photon microscopy [21,22] and optical tomography [32] allow visualization of oxygen levels in tissue. However, these approaches find their limitations in acquisition time and the need to immobilize the tissue. Dual-wavelength phosphorimetry uses near-simultaneous excitation of a phosphorescent dye at two wavelengths. Based on wavelength-dependent penetration depth of light in tissue this method enables measurement of  $\mu PO_2$  at two different depths in tissue using the phosphorescent dye Oxyphor G2 [24]. While providing less spatial resolution than microscopy and tomography, the temporal resolution is unmatched. Moreover, its use is not restricted to immobilized tissues and the technique can in principle even be applied on beating heart. Dual-wavelength phosphorimetry has been used to study microvascular oxygenation in the kidney under different pathophysiological conditions [2,33-35].

Recently, we have developed a break-through method for non-invasive measurement of mitochondrial oxygenation using oxygen-dependent quenching of delayed fluorescence of the endogenous molecule protoporphyrin IX (PpIX) [36-38]. It is based on enhancement of mitochondrial PpIX levels by administration of the precursor 5-aminolevulinic acid. Administration of 5-aminolevulinic acid is in itself non-toxic and delayed fluorescence lifetime measurements are applicable in man [39]. Phosphorescence and delayed fluorescence have much in common and are

both a type of oxygen-dependent luminescence. The technical feasibility to combine phosphorescence-based  $\mu\text{PO}_2$  measurements with delayed fluorescence-based  $\text{mitoPO}_2$  measurements, by means of a dual-dye technique, has been demonstrated [40]. A next logical step in the evolution of the technology would be the exploration of the usefulness of multi-wavelength excitation in combination with this dual-dye approach.

The present work was designed to characterize multi-wavelength excitation of phosphorescence of Oxyphor G2 and delayed fluorescence of PpIX for the measurement of  $\mu\text{PO}_2$  and  $\text{mitoPO}_2$  in intact *in vivo* rat heart. To this end, Monte Carlo Simulations (MCS) were performed to estimate the wavelength-dependent catchment depths in myocardial tissue, based on absorption of excitation light and emission of phosphorescence and delayed fluorescence. As verification of the MCS, the catchment depths of phosphorescence and delayed fluorescence measurements in rat myocardium were also assessed by *ex vivo* experiments. Furthermore, we tested the practical feasibility of the multi-wavelength approach in an *in vivo* experiment of non-resuscitated endotoxemia in rat.

## 2. MATERIAL AND METHODS

### 2.1 Monte Carlo simulations

The Monte Carlo Simulations (MCS) for excitation light propagation were run on a standard program for Monte Carlo modeling of light transport in multi-layered turbid media as are biologic tissues. A Monte Carlo program, MCML, was used, which was extensively described in the articles of the designers [41].

In short, photons, each with a certain “photon weight”, are launched from an infinitely narrow photon beam into a layered medium with user-defined optical properties of absorption, scattering, and anisotropy, the probability function for the cosine of the deflection angle. For a short description of the optical parameters see figure 1. In the MCL program, the Henyey-Greenstein function is used. The photon takes steps between scattering and absorption interactions with the tissue. The steps are based on the probability of photon movement before interaction by absorption and scattering. During each step as the photon propagates, the photon deposits a fraction of its weight into the local bin at its position. Each bin in the array of bins accumulates the photon weight deposited due to absorption by all N photons in that bin. After all N photons have been propagated each bin contains an accumulated weight of absorbed photons. Dividing each weight by the total number of photons (N) and by the volume of that particular bin yields the concentration of absorbed energy.

After the pencil beam simulation, a convolution program (CONV) which uses the MCML output file to convolve for photon beams of any size in a Gaussian or flat field shape is used to obtain the deposited energy for our geometry [42].

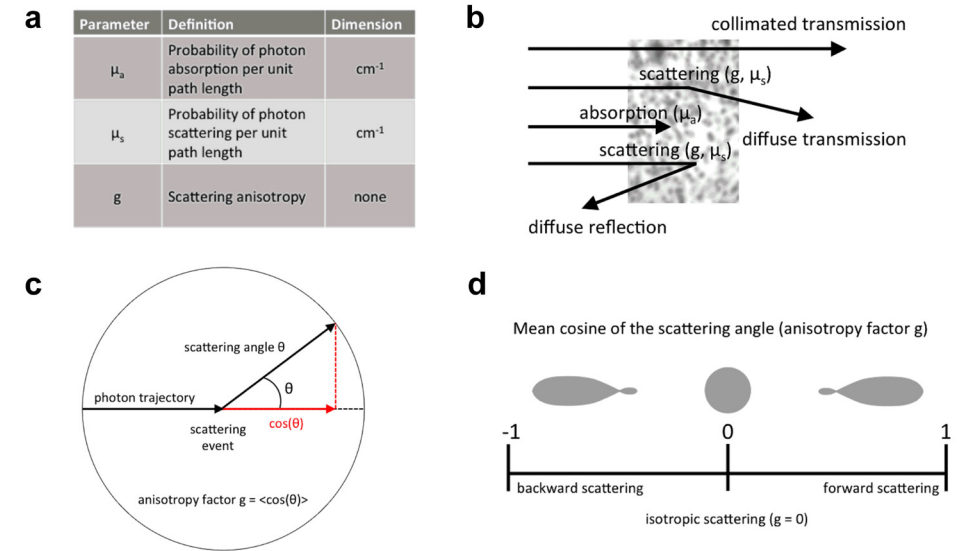


**Figure 1** Tissue optical parameters

a)  $\mu_a$ : absorption coefficient,  $\mu_s$ : scattering coefficient and  $g$ : anisotropy factor. b) Types of tissue-light interactions and the corresponding relevant parameters. c) Definition of the anisotropy factor as the average cosine of the deflection angle in scattering events. d) Graphical explanation of the impact of the anisotropy factor  $g$  on the scattering pattern in tissue.

A second Monte Carlo program (MCMLconsole), written in Labview (National Instruments, TX, USA), based on the MCML program, was used to calculate the propagation of the porphyrin fluorescence through the tissue. Again, the tissue slab is defined with optical properties. The deposited energy is used as a source file for the phosphorescence and delayed fluorescence Monte-Carlo. Each bin (volume element in the tissue) is used as an isotropic source; the deposited weight is used as weighting factor. The remaining weight and exit angle of the photons which escape at the surface are recorded.

For the MCS a model with a myocardial tissue slab with air above and a semi-infinite layer of blood below was designed. The dimensions of the rat tissue slab were retrieved from *in vivo* echocardiographic measurements of the left anterior wall of rat hearts. Diastolic left anterior wall thickness was found to amount to 1200-2000  $\mu\text{m}$  and right ventricular free wall to 600  $\mu\text{m}$  [6,43-48]. Using the maximal retrieved thickness, namely a myocardial layer of 2000  $\mu\text{m}$ , was chosen for the model.

The present model of oxygen-dependent quenching of phosphorescence and delayed fluorescence for non-invasive measurement of oxygen partial pressures in the microcirculation ( $\mu\text{PO}_2$ ) and mitochondria ( $\text{mitoPO}_2$ ) involved two oxygen-sensitive porphyrins (see below). Corresponding to the excitation wavelengths of the porphyrins three excitation wavelengths were used for the MCS: 440 nm, 510 nm and 632 nm.

**Table 1** Optical properties from the literature

Organ	Species	Remark	Wavelength ( $\lambda$ ) [nm]	Absorption Coefficient ( $\mu_a$ ) [ $cm^{-1}$ ]	Scattering Coefficient ( $\mu_s$ ) [ $cm^{-1}$ ]	Anisotropy Factor ( $g$ )	Ref.
Liver	porcine	homogenized	440	20	110	0.8	[49]
	porcine	homogenized	510	7.5	90	0.88	[49]
	porcine	homogenized	630	5	80	0.9	[49]
	porcine	homogenized	700	1.5	70	0.92	[49]
	porcine	homogenized	800	0.8	60	0.92	[49]
Myocardium	porcine	-	440	(15)*	-	-	[50]
	porcine	blood-free	450	14.7	(110-120)#	(0.9) $^{\S}$	[51]
	porcine	-	510	6	(140)#	(0.9) $^{\S}$	[50]
	porcine	blood-free	510	7.5	-	-	[51]
	porcine	-	514	10	-	-	[52]
	human	-	515	10	-	-	[53]
	porcine	-	544	9.5	119	(0.9) $^{\S}$	[51]
	canine	-	630	2	160	0.93	[54]
	porcine	-	630	2	-	-	[50]
	porcine	-	700	1	110	0.91	[50]
	canine	-	790	0.95	164	0.94	[73]
	porcine	-	800	0.6	110	0.93	[50]
	Blood	human	Hct 0.84%	440	20	33	0.9
human		Hct 0.84%	510	2	40	0.98	[55]
porcine		Lysed	510	1.2	40	0.996	[56]
human		Hct 0.84%	630	0.2	61	0.99	[55]
porcine		Lysed	630	0.3	34	0.995	[56]
human		Hct 0.84%	700	0.03	65	0.99	[55]
human		Hct 0.84%	800	0.06	56	0.99	[55]
canine		Whole blood	800	-	-	0.98	[74]

\* extrapolated from Fig.3 of Ref.[50]; # corrected scattering coefficient;  $^{\S}$ estimated

According to these excitation wavelengths optical properties of myocardial tissue and blood were retrieved from the literature [49-61]. Due to the scarce primary data for myocardial tissue, striated muscle and liver data were also gathered for comparison due to their similar absorption and scattering properties (table 1, 2). This approach allowed an estimation of the optical properties of myocardium within a confidence interval. Thus, the MCS input parameters were chosen by the boundaries of the ranges of the optical properties retrieved from the literature (table 3). An approximately homogenous distribution of the porphyrins across the myocardial wall was assumed.

**Table 2** Index of Refraction for Monte Carlo Simulations

Organ	Remark	Species	Wavelength ( $\lambda$ ) [nm]	Index of Refraction ( $n$ )	Ref.
Myocardium	LV (postmortem)	human	1300	1.382±0.007	[57]
	LV	canine	632	1.40	[57]
Striated Muscle		bovine	440	1.42±0.005	[58]
		bovine	510	1.412±0.005	[58]
		bovine	592	1.382±0.004	[59]
		human	632	1.40	[58]
		bovine	632	1.412±0.006	[58]
		porcine	632.8	1.38±0.007	[75]
		porcine	632.8	1.46±0.008	[75]
		bovine	700	1.395	[58]
Blood	Unspecified	human	632.8	1.426±0.007	[75]
	Whole blood (n=1)	human	820	1.485	[61]
	Whole blood (n=1)	human	820	1.397	[61]
	Lysed	porcine	440	1.3975	[56]
	Lysed	porcine	510	1.393	[56]
	Lysed	porcine	632	1.393	[56]
	Lysed	porcine	700	1.393	[56]
	Lysed	porcine	800	1.393	[56]

**Table 3** Selected input ranges for Monte Carlo simulations

Wavelength ( $\lambda$ ) [nm]	Absorption Coefficient ( $\mu_a$ ) [ $cm^{-1}$ ]	Scattering Coefficient ( $\mu_s$ ) [ $cm^{-1}$ ]	Anisotropy Factor ( $g$ )	Index of Refraction ( $n$ ) myocardium	Index of Refraction ( $n$ ) blood
440	10-20	110-220	0.9	1.42	1.397
510	6-10	80-100	0.9	1.41	1.393
632	2-5	80-160	0.93	1.40	1.393

4 distinct sets of MCS were run for each excitation wavelength (table 4, 5). Using the output of the convolution program phosphorescence and delayed fluorescence were computed in layers of 100  $\mu m$  for better resolution. Thus 20 MCML console runs were needed per wavelength and input set to cover the complete tissue slab thickness.

**Table 4** Input values for Monte Carlo simulations

Wavelength ( $\lambda$ ) [nm]	Number of Simulation	Absorption Coefficient ( $\mu_a$ ) [ $\text{cm}^{-1}$ ]	Scattering Coefficient ( $\mu_s$ ) [ $\text{cm}^{-1}$ ]	Anisotropy Factor (g)
440	1	10	110	0.9
	2	10	220	0.9
	3	20	110	0.9
	4	20	220	0.9
510	1	6	80	0.9
	2	6	100	0.9
	3	10	80	0.9
	4	10	100	0.9
632	1	2	80	0.93
	2	2	160	0.93
	3	5	80	0.93
	4	5	160	0.93

**Table 5** Input parameters for Monte Carlo simulations

Absorption		
MCML	Number of photons	$10^7$
	Bin size	$100 \mu\text{m}$ (dz; dr) <sup>#</sup>
	Number of bins	50; 30; 2 (dz; dr; da) <sup>#</sup>
	Tissue slab thickness	$2000 \mu\text{m}$
	$\mu_a$ ; $\mu_s$ ; g; n	According to table 3 and 4
CONV	Beam type	Gaussian
	Energy of the beam	$200 \mu\text{J}$
	Beam radius	$200 \mu\text{m}$
	Convolution type	Absorption in r & z (Arz) <sup>#</sup>
Phosphorescence and delayed fluorescence		
MCML Console	Number of photons	$125 \times 10^6$
	Input data	Arz-file
	Openings angle of detection camera	$26.1^\circ$
	Layer thickness	$100 \mu\text{m}$
	Bin size	dr = $100 \mu\text{m}$ , dz = $0 \mu\text{m}$ <sup>#</sup>
	Number of bins	250
	Optical parameters	According to table 1, 2 and Arz-file

<sup>#</sup> z, r and a stand for z-axis, radial and angle direction

## 2.2 Phosphorescent and delayed fluorescent molecules

In the MCS model and subsequent *ex vivo* and *in vivo* experiments two oxygen-sensitive porphyrins were involved:

The first, a dye used for measuring  $\mu\text{PO}_2$ , was Pd-meso-tetra-(4-carboxyphenyl)-tetrabenzoporphyrin (Oxyphor G2, Oxygen Enterprises Ltd, Philadelphia, PA), a phosphorescent polyglutamic Pd-porphyrin-dendrimer dye [62]. Oxyphor G2 is a negatively charged, large, water-soluble molecule (2.4 kDa) that binds to albumin and therefore stays primarily in the microcirculation [63,64]. Oxyphor G2 can be excited at 440 nm and 632 nm thus allowing measurements at two different depths. Its emission of phosphorescence occurs around 800 nm [65].

The second, used for measuring  $\text{mitoPO}_2$ , was Protoporphyrin IX. This endogenous porphyrin is the final precursor of heme in the heme biosynthetic pathway. It is synthesized inside the mitochondria [66] and used for the measurement of mitochondrial oxygenation by delayed fluorescence. Its synthesis can be enhanced by administration of PpIX precursor 5-aminolevulinic acid hydrochloride. PpIX is excited at 510 nm and exhibits a two-peaked emission with maxima around 630 and 700 nm [36].

## 2.3 *Ex vivo* penetration measurements

In order to experimentally assess the capability of exciting and detecting the porphyrins at a defined depth we used a previously described approach [24]. Slices of myocardial tissue on a microscope slide were placed between the fiber-optic light guide (setup described below) and an airtight sealed cuvette filled with Protoporphyrin IX ( $10 \mu\text{M}$ ) or Oxyphor G2 ( $20 \mu\text{M}$ ), both dissolved in a 4% albumin solution (Bovine serum albumin, Sigma, St. Louis, MO) (figure 2). To prevent oxygen-dependent changes in the signal, the chambers were enzymatically oxygen-depleted by catalase (catalase from bovine liver, Sigma, St. Louis, MO) and glucose-oxidase (glucose oxidase from aspergillus niger, Sigma, St. Louis, MO) [67]. The myocardial slices were cut from 8 freshly harvested hearts from male Wistar rats, which were not pre-treated with Oxyphor G2 or aminolevulinic acid. The slices were cut by means of a custom-made razor blade cutting device. The slice thickness was measured using a micrometer. The phosphorescence and delayed fluorescence emission intensity returning through the myocardial slices after excitation with 440 nm, 510 nm and 632 nm light was measured in 22 slices ranging from 200 to 2300  $\mu\text{m}$ . All experiments were performed at room temperature ( $25^\circ\text{C}$ ).

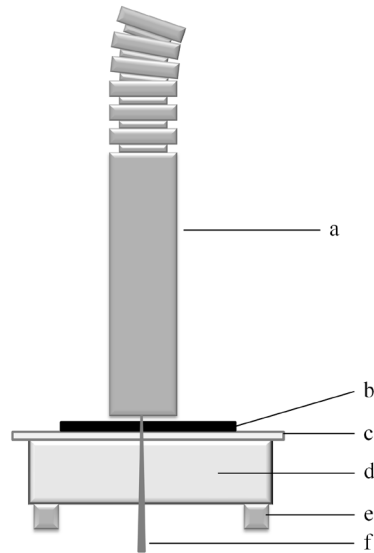


**Figure 2** Schematic of *ex vivo* measurements  
a) fiber, b) tissue slice, c) microscope slide, d) cuvette, e) cuvette holder, f) excitation light

#### 2.4 Laser setup, phosphorescence and delayed fluorescence lifetime measurements

We developed a multi-wavelength phosphorimeter allowing near-simultaneous excitation of Oxyphor G2 at 440 nm and 632 nm (emission at 800 nm). The validation experiments for interchannel differences and accuracy of oxygen measurement have been published earlier [24]. In this experiment we used a modified system of the one we published earlier which allowed, in addition to the above mentioned two wavelengths, near-simultaneous measurements of PpIX excitation at 510 nm (emission at 690 nm). The excitation source consisted of an Opolette 355-I (Opotek, Carlsbad, CA, USA), a compact computer-controlled fast tunable laser which emits laser pulses with a specified duration of 4-10 ns and typically 2-4 mJ/pulse over a tunable range of 410 to 670 nm. The laser was coupled into a Fiber Delivery System (Opotek, Carlsbad, CA, USA) consisting of 50 mm plano-convex lens, X-Y fibermount and a 2 meter fiber with a core diameter of 1000 $\mu$ m. This fiber was coupled to a custom-made reflection probe by an in-line Fiber Optic Attenuator (FOA-Inline, Avantes b.v., Eerbeek, The Netherlands). The reflection probe consisted of a probe with 6 fibers for guiding the excitation light to the tissue and a 7<sup>th</sup> fiber for guiding the reflected light (FCR-7IR400-2-ME,  $r=0.02$ cm, acceptance angle 26.1 $^\circ$ ; Avantes, Eerbeek, Netherlands) to the detector (Figure 3). The PpIX and the Oxyphor G2 emission light were filtered by a combination of a long-pass and a bandpassfilter. For PpIX a 590 nm (OG590, Newport, Irvine, CA, USA) and a 675  $\pm$  25 nm (Omega Optical, Brattleboro, VT, USA) filter were used. While for Oxyphor G2 we used a 715 nm (RG715, Newport, Irvine, CA, USA) and a 790  $\pm$  20 nm filter (Omega

Optical, Brattleboro, VT, USA). 200  $\mu$ J were used per excitation pulse. The acceptance angle resulted in an illuminated area of 0.5 to 1 mm<sup>2</sup>, assuming a fiber-tissue distance of 1 to 1.5 mm.

In both fluorophors, when excited by a light pulse, the intensity of phosphorescence and delayed fluorescence, respectively, decrease at a rate dependent on the surrounding oxygen pressure. The relationship between the measured decay time and the PO<sub>2</sub> is given by the Stern-Volmer relation:

$$pO_2 = (1/\tau - 1/\tau_0)/k_q \quad (1)$$

Where  $\tau$  is the measured decay time,  $\tau_0$  is the decay time at an oxygen pressure of zero, and  $k_q$  is the quenching constant.

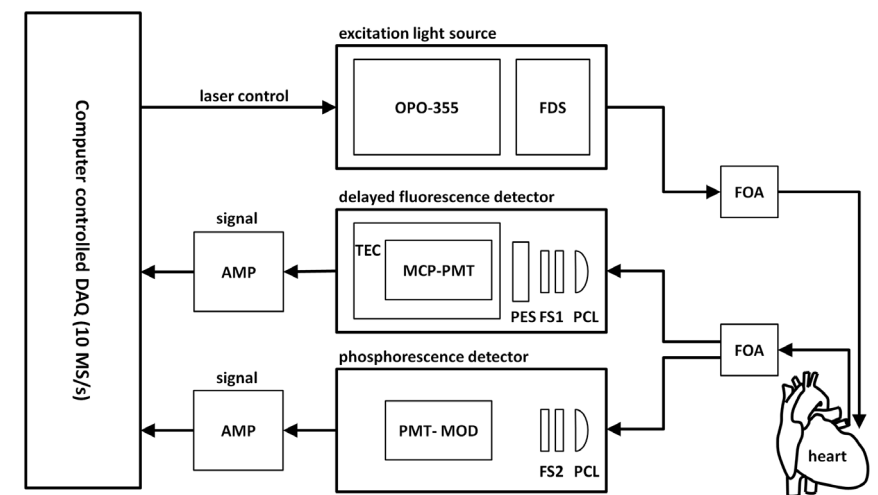


**Figure 3** Schematic design of the setup  
OPO-355: Opolette 355-I, FDS: Fiber Delivery System, FOA: Fiber Optic Attenuator, BFP: Bifurcated Reflection Probe, FFC: Fiber to Fiber Coupling, BFA: Bifurcated Fiber Assembly, PCL: Plano Convex Lens, FS1 & FS2: Filter Sets, PES: Protective Electronic Shutter, MCP-PMT: Micro Channel Plate Photomultiplier Tube, TEC: Thermo Electric Cooling, PMT-MOD: Photomultiplier Module, AMP: Amplifier, DAQ: Data Acquisition. As earlier published [40].

#### 2.5 *In vivo* experiment

This study was approved and reviewed by the Animal Research Committees of the Academic Medical Center at the University of Amsterdam and Erasmus Medical Center at the University of Rotterdam. Care and handling of the animals are in accordance with

the guidelines for Institutional and Animal Care and Use Committees.

90 minutes before starting instrumentation of the rat ( $n=1$ ), buffered PpIX-precursor 5-aminolevulinic acid hydrochloride (200 mg/kg) was administered intraperitoneally. The rat was anesthetized with an intraperitoneal injection of pentobarbital (60 mg/kg; Apotheek Faculteit Dierengeneeskunde Rotterdam, NL) and sufentanil (20  $\mu\text{g}/\text{kg}$ ; Janssen-Cilag BV, Tilburg, NL). Propofol (10 mg/kg/h; Fresenius Kabi, Nederland BV, Schelle, Belgium) and sufentanil (7.5  $\mu\text{m}/\text{kg}/\text{h}$ ) were used for maintenance of the anesthesia. After tracheotomy the animal was mechanically ventilated with the inspired oxygen fraction titrated to an arterial  $\text{PO}_2$  of 100 mmHg. A catheter was inserted in the right carotid artery and used for continuous measurement of arterial blood pressure and heart rate. The right jugular vein was then cannulated and the catheter tip inserted to a depth close to the right atrium, allowing continuous monitoring of the central venous pressure. Pressures were measured by use of a disposable transducer (Combitrans disposable transducer; BBraun Medical B.V., Oss, NL) connected to a HEMO POD of a standard intensive care patient monitor (Siemens SC9000, Siemens Medical Systems). A tail vein was cannulated and used for administration of maintenance fluid (10 ml/kg/h Ringer's solution). Lateral thoracotomy and pericardiotomy was performed and the optical fiber for phosphorescence and delayed fluorescence measurements was placed 1 mm above surface of the antero-lateral wall of the left ventricle. The operation field was then covered with aluminum foil throughout the entire experiment to prevent the phosphorescence and delayed fluorescence signals being influenced by room light. To detect changes in microcirculatory  $\text{PO}_2$  Oxyphor G2 (1mg/kg; dissolved in normal saline) was infused. Baseline measurements were taken after a 15-minute stabilization time. Then lipopolysaccharide (LPS from E.coli; O127:B8, Sigma, St.Louis, MO; 2.5 mg/kg) was infused over 15 minutes. After accomplishment of the LPS-infusion, oxygenation measurements were performed in triple readings (30 s apart), and repeated at intervals of 30 minutes up to a total time of 5 hours from the baseline. After the protocol was finished the animal was euthanatized by pentobarbital overdose.

### 3.6 Statistics

Statistical analysis was performed using GraphPad Prism (5.0, GraphPad Software, San Diego, CA, USA). To test the differences of means of penetration depths by 2-tailed Mann Whitney tests was applied. Differences of absorbed dose of phosphorescence and delayed fluorescence according to wavelength and depth in the tissue were compared using a two-way ANOVA for repeated measures. Differences with a p-value of  $< 0.05$  were considered statistically significant. Results are reported as mean  $\pm$  SEM.

## 3. RESULTS

### 3.1 Monte Carlo simulations

Figure 4 shows the results of the MC simulation of light absorption in the myocardial tissue in the laser beam center. Blue light (440 nm) displayed a steep exponential decrease of absorbed dose as a function of tissue depth. The predominant part of the absorption took place within the first 500  $\mu\text{m}$ . For red light (632 nm) the absorption had a flatter course and was more evenly distributed in the calculated tissue, while excitation with green (510 nm) displayed an intermediate course between the former two. The comparison of the absorption curves of 440 nm, 510 nm and 632 nm showed a significant difference ( $*p < 0.05$ ) of absorbed dose between these wavelengths from 0 to 400  $\mu\text{m}$ . At a depth of 500  $\mu\text{m}$  the absorbed dose of 632 nm was significantly different from 440 nm or 510 nm ( $\# p < 0.01$ ). Below 500  $\mu\text{m}$  the absorbed dose was similar for the three wavelengths.

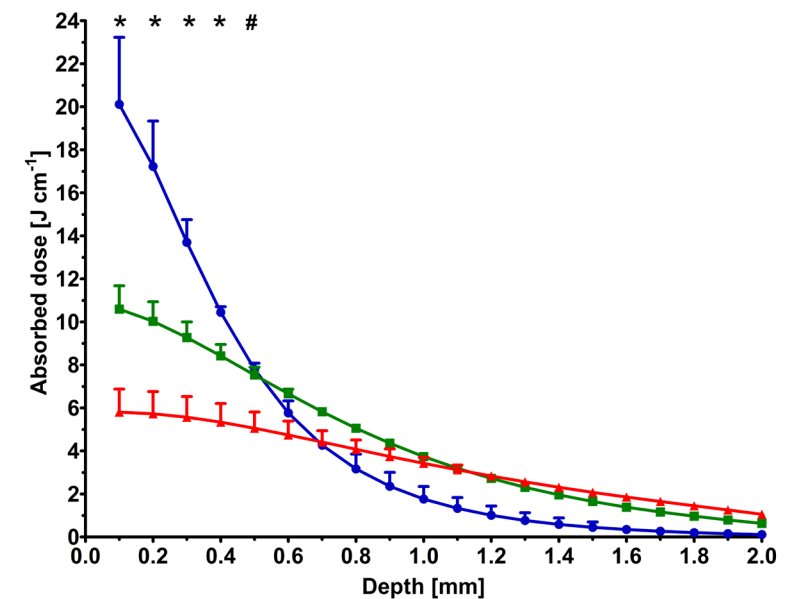


**Figure 4** Monte Carlo simulation of absorption. Results of the MC simulation of light absorption [ $\text{J cm}^{-1}$ ] of 440 nm (circles), 510 nm (squares) and 632 nm (triangles) in the myocardial tissue.

The next step was to model detection of phosphorescence and delayed fluorescence as result of the absorbed light. Figure 5 shows the plot of the MCS-derived intensity of phosphorescence and delayed fluorescence in the beam center of a simulated excitation

pulse. 3 areas from which the signals originate can be identified. While excitation with blue (440 nm) and red light (632 nm) led to superficial and deeper signal origin respectively, green (510 nm) again took an intermediate position. Two-way ANOVA for repeated measures yielded a significant difference for the comparison of the slopes of the simulated and measured data for 440 nm at a depth of 100  $\mu\text{m}$  (\* $p < 0.05$ ). This fact is mainly due to technical issues of the *ex vivo* experiment, which is discussed below. Comparison of the 510 nm and 632 nm slopes showed there was no significant difference.

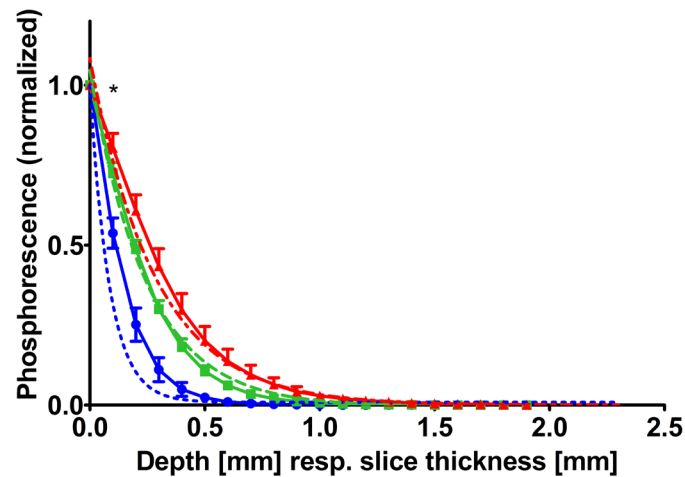


**Figure 5** Comparison of Monte Carlo simulations and *ex vivo* measurements. The MCS of phosphorescence after excitation with 440 nm (circles), 510 nm (squares) and 632 nm (triangles) matched well with the non-linear fit (NLF) of the *ex vivo* measurements with 440 nm (hyphen), 510 nm (dash) and 632 nm (hyphen-dash).

In order to grasp a sense of the dimension of overlay of the measured phosphorescence and delayed fluorescence signals the area under the curve (AUC) of the slopes of the MCS were calculated using GraphPad Prism. Computation of the AUC resulted in  $0.15 \pm 0.02$  mm,  $0.24 \pm 0.02$  mm, and  $0.32 \pm 0.04$  mm for 440 nm, 510 nm and 632 nm respectively. Very similar AUC values resulted from the *ex vivo* derived slopes (only one slope per excitation wavelength): 0.11 mm, 0.26 mm, 0.31 mm. From these calculations it can be seen that 45.6% (33.7%) of the signal originating from excitation with 632 nm overlaps with the signal from excitation with 440 nm (*ex vivo*). Therefore, more than half of this signal arises from deeper strata than when exciting with 440 nm, thus providing additional information of another biological compartment. For (patho-)physiological experiments it is interesting to compare  $\mu\text{PO}_2$  and  $\text{mitoPO}_2$ . Therefore, it is important to know the origin and overlap of the signals gathered after excitation with 440 nm, 632 nm

and 510 nm respectively. The myocardial volume excited with 440 nm, providing information about superficial  $\mu\text{PO}_2$ , is small compared to the one excited with 510 nm, measuring  $\text{mitoPO}_2$ . The signal originating from an excitation with 440 nm represents 61.1% (40.9%) of the  $\text{mitoPO}_2$  signal, thus 38.9% (59.1%) of the signal is derived from mitochondria in deeper tissue layers. On the other hand, the  $\text{mitoPO}_2$  signal covers 74.6% (82.6%) of the myocardial volume excited with 632 nm, the deep  $\mu\text{PO}_2$ .

### 3.2 *Ex vivo* experiment

Due to difficulties in cutting slices of equal thickness from fresh tissue the data in figure 6 are presented as individual data points instead of repeated measurements. Similar to the MCS-derived results, phosphorescence and delayed fluorescence measured with the multi-wavelength setup showed an exponential decrease of intensity as a function of myocardial slice thickness. A good match was found between the intensities of emission of phosphorescence measured with the phosphorimeter and the MCS-derived results (figure 5). The determined catchment depths (defined as  $1/e$  of the intensity drop) with MCS were  $161 \pm 2$   $\mu\text{m}$ ,  $262 \pm 1$   $\mu\text{m}$  and  $350 \pm 4$   $\mu\text{m}$  for 440 nm, 510 nm and 632 nm respectively. These values were very similar to the depths estimated from the *ex vivo* experiments. In these experiments catchment depths of approximately 86  $\mu\text{m}$ , 255  $\mu\text{m}$  and 307  $\mu\text{m}$  for 440 nm, 510 nm and 632 nm were found (figure 7). While the MCS with 510 nm and 632 nm showed no significant difference in catchment depth as compared to the *ex vivo* measurements ( $p = 0.87$  and  $p = 0.41$  resp.), a small but significant difference of the mean catchment depth of the MCS and *ex vivo* measurements was found for 440 nm (#  $p = 0.03$ ).

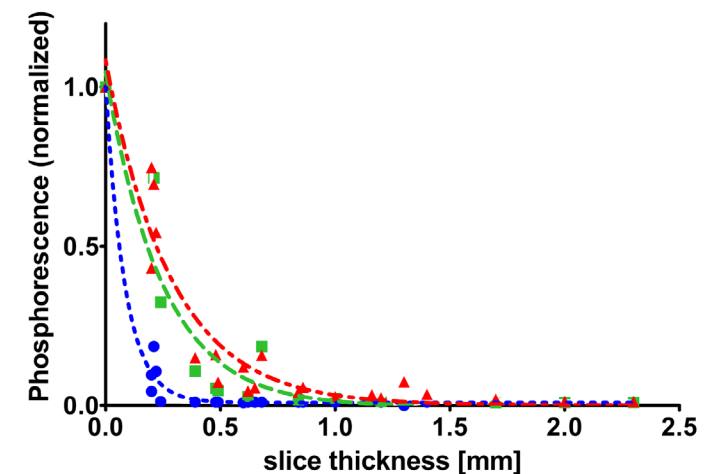


**Figure 6** *Ex vivo* measurements of phosphorescence and delayed fluorescence. Circles, squares and triangles represent normalized phosphorescence averaged from 3 consecutive measurements after excitation with 440 nm, 510 nm and 632 nm, respectively, measured through fresh myocardial tissue slices of different thicknesses. A non-linear regression by least square method (NLF) of the *ex vivo* measurements with 440 nm (hyphen), 510 nm (dash) and 632 nm (hyphen-dash) was used for curve fitting.

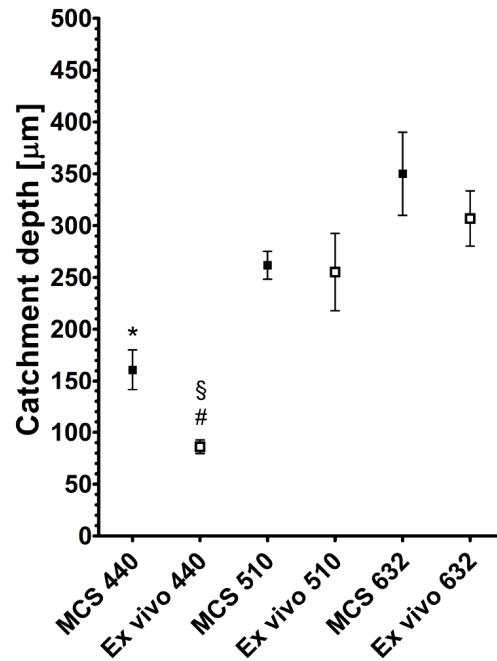


**Figure 7** Comparison of the catchment depths. Mean and SEM of the catchment depths are shown of MCS (filled squares) and *ex vivo* experiments (empty squares). The catchment depth of the *ex vivo* experiments was calculated from the NLF-fitted curve. The catchment depth of the MCS with 440 nm differed significantly from the catchment depth of MCS with 510 nm as well as with 632 nm (\*  $p=0.0286$  each). The catchment depth of the 440 nm *ex vivo* experiments was significantly lower than the other catchment depths (#  $p<0.05$  versus MCS 440 nm; §  $p<0.01$  versus MCS 510nm and 632 nm).

### 3.3 *In vivo* experiment

In this experiment we investigated the applicability of the multi-wavelength phosphorimeter in a model of non-resuscitated endotoxemia in rat. Distinct microcirculatory and mitochondrial phosphorescence and delayed fluorescence signals were measurable throughout the whole experiment lasting for 5 hours. Infusion of LPS induced a substantial drop of mean arterial pressure (MAP). While MAP remained low, cardiac output raised over time, thus characterizing the distributive shock. Heart rate remained stable for 4 hours only to drop in the last hour, herewith reflecting the severity of the chosen model and imminent death of the animal (figure 8).

In figure 9 the microcirculatory and mitochondrial oxygenation measured on the antero-lateral wall of the left ventricle as well as the arterial  $PO_2$  and central-venous saturation ( $ScvO_2$ ) are depicted. Because of an arterial oxygen saturation of 86% at the 2.5 h blood gas analysis (T150; data not shown) we increased the inspired oxygen fraction from 30% to 40%. This explains the increase of arterial  $PO_2$ . The  $mitoPO_2$  and both  $\mu PO_2$

slopes showed a decline over time, a stabilization of the oxygenation drop after increase of the  $FiO_2$  and a limited rise at the very end of the experiment. The  $mitoPO_2$  fell before a reduction of the deep and later also superficial  $\mu PO_2$  could be measured. This sequence reflects the difference of the compartments measured, the subepicardial being more sensitive to hypoperfusion than the superficial epimyocardial compartment [68]. The increase of  $mitoPO_2$  and  $ScvO_2$  at T210 suggest a lower  $O_2$ -consumption compatible with endotoxemia. The final drop of the  $ScvO_2$  at T300 probably reflects a “pre-terminal” hypoperfusion state compatible with a prolonged hyperdynamic shock leading to an insufficient  $O_2$  delivery.

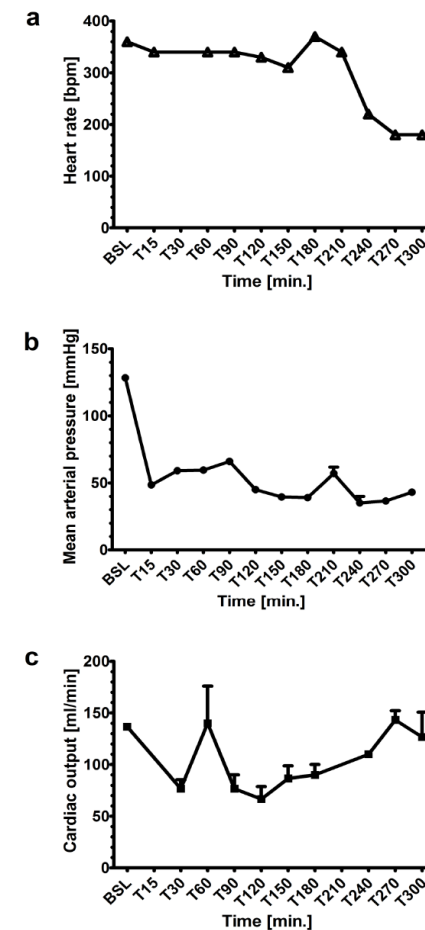


**Figure 8** Macrohemodynamics a) heart rate [bpm], b) mean arterial pressure [mmHg], c) cardiac output [ml/min.], triple measurements per time point. BSL = baseline measurement



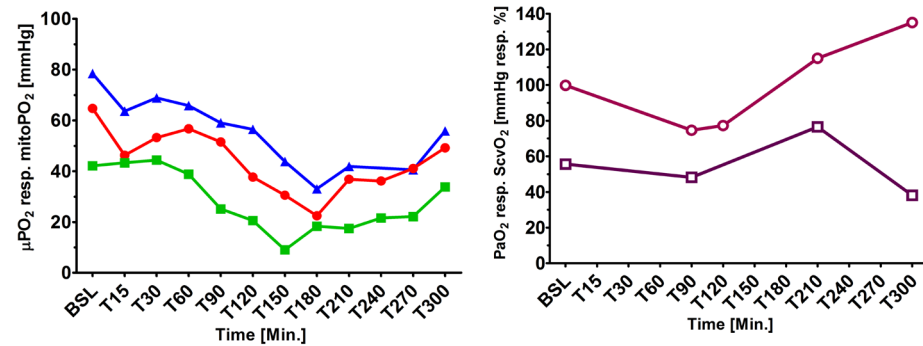


**Figure 9** Oxygenation measurements in endotoxemic rat

a) Microcirculatory and mitochondrial oxygenation measured by phosphorescence: superficial myocardial microcirculatory  $\text{PO}_2$  (blue circles), subepicardial microcirculatory  $\text{PO}_2$  (red triangles), mitochondrial  $\text{PO}_2$  (green squares). b) Systemic oxygenation parameters: arterial  $\text{PO}_2$  (open circles), central venous saturation (open squares). BSL = baseline measurement; resp. = respectively

## 4. DISCUSSION

In the present study we evaluated and validated a system of multi-wavelength phosphorimetry for the measurement of microcirculatory and mitochondrial oxygenation in rat heart. We can summarize the main findings as follows:

- 1) Three separate phosphorescence signals could be identified in Monte Carlo simulations and *ex vivo* experiments. Excitation with 440, 632 and 510 nm respectively resulted in a superficial microcirculatory, a deep microcirculatory and a mitochondrial signal.
- 2) We found an excellent correlation of the calculated MCS- and measured *ex vivo*-results.
- 3) The respective signals originated from depths of up to 161, 350 and 262  $\mu\text{m}$  (MCS) and 86, 307 and 255  $\mu\text{m}$  (*ex vivo* experiments).
- 4) Excitation with 440 nm led to the emission of a phosphorescence signal from a myocardial volume comprised in the volume excited with 510 nm and 632 nm. Approximately 39% and 50% of the signal after excitation with 510 nm and 632 nm respectively arose from deeper strata compared to excitation with 440 nm.
- 5) Using multi-wavelength phosphorimetry we were able to detect changes in microcirculatory and mitochondrial  $\text{PO}_2$  in *in vivo* experiments lasting up to 5 hours.
- 6) The measured signals reflected biologically distinct compartments.

By the use of two methods, MCS and *ex vivo* experiments, we could characterize the presented system of multi-wavelength phosphorimetry. The two methods' results were

well matching. These findings allow grasping a sense of the origin of the measured signal of *in vivo* experiments. For this purpose not only the wavelength-dependent catchment depths in myocardial tissue but also the signal overlay of the measured phosphorescence and delayed fluorescence are essential.

There was an excellent correlation of the calculated and measured phosphorescence and delayed fluorescence intensity profiles. Only for the excitation with 440 nm there is a notable lower penetration depth in the *ex vivo* experiments in comparison to the Monte Carlo simulation. This difference most probably originates from a technical limitation. Due to the large amount of absorption of the 440 nm excitation signal in the first 400  $\mu\text{m}$  the measured phosphorescence signal and derived penetration depth highly depends on measurements with very thin slices. The fabrication of very thin slices ( $\leq 200 \mu\text{m}$ ) from fresh myocardial tissue was affected by the limits of accuracy of how these could be cut and measured with the micrometer. Considering the near-perfect match of the measurements after excitation with 510 and 632 nm, we think the *ex vivo*-measured catchment depth for excitation with 440 nm is somewhat underestimated.

Previously, our laboratory calculated light penetration into gut tissue using Monte-Carlo simulations. The aim was to model the catchment depth and thus estimate the measured depth of microcirculatory  $\text{PO}_2$  measurements using Pd-porphyrin, a tracer which is excited at 520nm. In these experiments a catchment depth of 500  $\mu\text{m}$  was found [28]. For Oxyphor G2, earlier experiments measuring  $\mu\text{PO}_2$  in murine tumors have claimed a general penetration depth for excitation light of more than a centimeter through the skin of a mouse [62]. Johannes, on the other hand, using an *ex vivo* approach of stacked tissue slices determined in rat kidneys catchment depths of 700  $\mu\text{m}$  for excitation with 440nm and as much as 4000  $\mu\text{m}$  for 632 nm [24]. Our calculated and measured penetration depths differ from the above-mentioned experiments. This difference can be attributed to the diverseness of the tissues studied. The myocardium has, compared to gut, skin, mammary tumors and kidney a high density of myoglobin and cytochromes, which have a significant impact on absorption and scattering properties of myocardial tissue.

One might argue that the catchment depths have been overestimated as we did not account for additional absorption by other fluorophores and hemoglobin. However, for the *ex vivo*-experiments the hearts were not washed free of erythrocytes. It may be assumed that a beating heart has higher tissue blood content during diastole, than the tissue slices used, while in systole the blood content might even be lower. Thus, the post-mortem tissue blood content is considered an in between value.

We can assume that a rat weighting 300g has a circulating blood volume of 18ml. Its heart weighs approximately 1g and contains between 50 and 130  $\mu\text{l}$  of blood in the microcirculation [69-71]. Due to technical improvement of the excitation/detection system used for these experiments we could reduce the Oxyphor G2 dose from 1.8 mg/kg to 1 mg/kg leading to a 45% reduction of fluorophore concentration with respect to

our earlier published work [24]. Thus, infusion of 1 mg/kg of Oxyphor G2 will result in a 17mM whole blood concentration. Earlier, we had calculated the attenuation of tissue penetration of excitation light due to Oxyphor in kidneys [24]. Applying Beer's law and assuming different photon path lengths from 3 to 10-times longer than measured we estimated the attenuation due to the phosphor less than 30%. Because of the lower tissue concentration in the present study in combination with the much higher intrinsic absorption of heart tissue, the influence of the presence of Oxyphor G2 can be neglected.

Moreover, the lower fluorophore concentration and higher sensitivity of the phosphorimeter prevented any (visually assessed) macroscopic phototoxicity to occur. This dose- and time-dependent phenomenon has been described earlier [72]. However, already in our previous publication by Johannes, which made use of higher Oxyphor doses and flash intensities, no macroscopic phototoxicity was observed [24]. Also for PpIX phototoxicity has been described. We have addressed PpIX phototoxicity earlier [36].

Finally, in this study we present for the first time the data of an *in vivo* experiment, in which we measured microcirculatory and mitochondrial oxygenation in the heart in a near-simultaneous manner. The multi-wavelength phosphorimeter resulted to be applicable in a model of non-resuscitated endotoxemia in rat and distinct microcirculatory and mitochondrial oxygenation signals were measurable throughout the whole experiment lasting for 5 hours. The mitoPO<sub>2</sub> fell before a reduction of the deep and later also superficial μPO<sub>2</sub> could be measured. This sequence reflects the difference of the compartments measured, the subepicardial being more sensitive to hypoperfusion than the superficial epimyocardial compartment. This individual behavior suggests that anatomically distinct compartments can be measured by the use of multi-wavelength phosphorimetry.

## 5. CONCLUSION

With this work we provide the optical basis of multi-wavelength phosphorimetry in the heart, using of two methods, MCS and *ex vivo* experiments. This technique adopted to measure microcirculatory and mitochondrial oxygenation in myocardial tissue, using oxygen-dependent quenching of phosphorescence and delayed fluorescence of porphyrins, gives access to the key compartments of the oxygen pathway in the body. The knowledge of the wavelength-dependent catchment depths in myocardial tissue and signal overlay of the measured luminescence are essential for pathophysiological interpretation of *in vivo* experiments. This study further demonstrates the applicability of optical oxygen measurements based on phosphorescence and delayed fluorescence lifetime quenching in an *in vivo* experiment of non-resuscitated endotoxemia in rat.

## REFERENCES

1. Carré JE, Singer M. Cellular energetic metabolism in sepsis: The need for a systems approach. *Biochimica et Biophysica Acta (BBA) - Bioenergetics*. 2008;1777:763–71.
2. Johannes T, Mik EG, Nohé B, Raat NJH, Unertl KE, Ince C. Influence of fluid resuscitation on renal microvascular PO<sub>2</sub> in a normotensive rat model of endotoxemia. *Crit Care*. 2006;10:R88.
3. Johannes T, Mik EG, Ince C. Nonresuscitated endotoxemia induces microcirculatory hypoxic areas in the renal cortex in the rat. *Shock*. 2009;31:97–103.
4. Johannes T, Mik EG, Klingel K, Dieterich H-J, Unertl KE, Ince C. Low-dose dexamethasone-supplemented fluid resuscitation reverses endotoxin-induced acute renal failure and prevents cortical microvascular hypoxia. *Shock*. 2009;31:521–8.
5. Legrand M, Bezemer R, Kandil A, Demirci C, Payen D, Ince C. The role of renal hypoperfusion in development of renal microcirculatory dysfunction in endotoxemic rats. *Intensive Care Med*. 2011;37:1534–42.
6. Dyson A, Rudiger A, Singer M. Temporal changes in tissue cardiorespiratory function during faecal peritonitis. *Intensive Care Med*. Springer-Verlag; 2011;37:1192–200.
7. Legrand M, Mik EG, Johannes T, Payen D, Ince C. Renal hypoxia and dysoxia after reperfusion of the ischemic kidney. *Mol. Med. BioMed Central*; 2008;14:502–16.
8. Hengst den WA, Gielis JF, Lin JY, Van Schil PE, De Windt LJ, Moens AL. Lung ischemia-reperfusion injury: a molecular and clinical view on a complex pathophysiological process. *Am. J. Physiol. Heart Circ. Physiol.* American Physiological Society Bethesda, MD; 2010;299:H1283–99.
9. Scheeren TWL, Martin K, Maruschke M, Hakenberg OW. Prognostic value of intraoperative renal tissue oxygenation measurement on early renal transplant function. *Transpl Int*. 2011;24:687–96.
10. Jespersen SN, Østergaard L. The roles of cerebral blood flow, capillary transit time heterogeneity, and oxygen tension in brain oxygenation and metabolism. *J Cereb Blood Flow Metab.* SAGE PublicationsSage UK: London, England; 2012;32:264–77.
11. Li Y, Cai M, Xu Y, Swartz HM, He G. Late phase ischemic preconditioning preserves mitochondrial oxygen metabolism and attenuates post-ischemic myocardial tissue hyperoxygenation. *Life Sci.* Elsevier Inc; 2011;88:57–64.
12. Cai M, Li Y, Xu Y, Swartz HM, Chen C-L, Chen Y-R, et al. Endothelial NOS activity and myocardial oxygen metabolism define the salvageable ischemic time window for ischemic postconditioning. *Am. J. Physiol. Heart Circ. Physiol.* American Physiological Society Bethesda, MD; 2011;300:H1069–77.
13. Dyson A, Singer M. Tissue oxygen tension monitoring: will it fill the void? *Current Opinion in Critical Care*. 2011;17:281–9.
14. Golub AS, Pittman RN. PO<sub>2</sub> measurements in the microcirculation using phosphorescence quenching microscopy at high magnification. *AJP: Heart and Circulatory Physiology.* American Physiological Society; 2008;294:H2905–16.
15. Pittman RN, Golub AS, Carvalho H. Measurement of oxygen in the microcirculation using phosphorescence quenching microscopy. *Adv. Exp. Med. Biol.* Springer, Boston, MA; 2010;662:157–62.
16. Pittman RN. Oxygen gradients in the microcirculation. *Acta Physiol (Oxf).* John Wiley & Sons, Ltd; 2011;202:311–22.

17. Sakr Y. Techniques to assess tissue oxygenation in the clinical setting. *Transfus Apher Sci.* 2010;43:79–94.
18. Vanderkooi JM, Maniara G, Green TJ, Wilson DF. An optical method for measurement of dioxygen concentration based upon quenching of phosphorescence. *J. Biol. Chem. American Society for Biochemistry and Molecular Biology*; 1987;262:5476–82.
19. Torres Filho IP, Intaglietta M. Microvessel PO<sub>2</sub> measurements by phosphorescence decay method. *Am. J. Physiol. American Physiological Society Bethesda, MD*; 1993;265:H1434–8.
20. Sinaasappel M, Donkersloot C, van Bommel J, Ince C. PO<sub>2</sub> measurements in the rat intestinal microcirculation. *Am. J. Physiol. American Physiological Society Bethesda, MD*; 1999;276:G1515–20.
21. Mik EG, van Leeuwen TG, Raat NJ, Ince C. Quantitative determination of localized tissue oxygen concentration in vivo by two-photon excitation phosphorescence lifetime measurements. *J. Appl. Physiol. American Physiological Society*; 2004;97:1962–9.
22. Sakadžić S, Roussakis E, Yaseen MA, Mandeville ET, Srinivasan VJ, Arai K, et al. Two-photon high-resolution measurement of partial pressure of oxygen in cerebral vasculature and tissue. *Nat Meth. Nature Publishing Group*; 2010;7:755–9.
23. Mik EG, Donkersloot C, Raat NJ, Ince C. Excitation pulse deconvolution in luminescence lifetime analysis for oxygen measurements in vivo. *Photochem Photobiol.* 2002;76:12–21.
24. Johannes T, Mik EG, Ince C. Dual-wavelength phosphorimetry for determination of cortical and subcortical microvascular oxygenation in rat kidney. *Journal of Applied Physiology.* 2006;100:1301–10.
25. Mik EG, Johannes T, Ince C. Monitoring of renal venous PO<sub>2</sub> and kidney oxygen consumption in rats by a near-infrared phosphorescence lifetime technique. *Am. J. Physiol. Renal Physiol. American Physiological Society*; 2008;294:F676–81.
26. Zheng L, Golub AS, Pittman RN. Determination of PO<sub>2</sub> and its heterogeneity in single capillaries. *Am. J. Physiol. American Physiological Society Bethesda, MD*; 1996;271:H365–72.
27. Siegemund M, van Bommel J, Stegenga ME, Studer W, van Iterson M, Annaheim S, et al. Aortic cross-clamping and reperfusion in pigs reduces microvascular oxygenation by altered systemic and regional blood flow distribution. *Anesthesia & Analgesia.* 2010;111:345–53.
28. Sinaasappel M, van Iterson M, Ince C. Microvascular oxygen pressure in the pig intestine during haemorrhagic shock and resuscitation. *The Journal of Physiology.* 1999;514 ( Pt 1):245–53.
29. van Iterson M, Sinaasappel M, Burhop K, Trouwborst A, Ince C. Low-volume resuscitation with a hemoglobin-based oxygen carrier after hemorrhage improves gut microvascular oxygenation in swine. *J Lab Clin Med.* 1998;132:421–31.
30. van Iterson M, Siegemund M, Burhop K, Ince C. Hemoglobin-based oxygen carrier provides heterogeneous microvascular oxygenation in heart and gut after hemorrhage in pigs. *J Trauma.* 2003;55:1111–24.
31. van Iterson M, Bezemer R, Heger M, Siegemund M, Ince C. Microcirculation follows macrocirculation in heart and gut in the acute phase of hemorrhagic shock and isovolemic autologous whole blood resuscitation in pigs. *Transfusion.* 2012;52:1552–9.
32. Apreleva SV, Wilson DF, Vinogradov SA. Tomographic imaging of oxygen by phosphorescence lifetime. *Appl Opt. Optica Publishing Group*; 2006;45:8547–59.
33. Johannes T, Mik EG, Nohé B, Unertl KE, Ince C. Acute decrease in renal microvascular PO<sub>2</sub> during acute normovolemic hemodilution. *Am. J. Physiol. Renal Physiol.* 2007;292:F796–803.
34. Legrand M, Almac E, Mik EG, Johannes T, Kandil A, Bezemer R, et al. L-NIL prevents renal microvascular hypoxia and increase of renal oxygen consumption after ischemia-reperfusion in rats. *Am. J. Physiol. Renal Physiol. American Physiological Society*; 2009;296:F1109–17.
35. Dyson A, Bezemer R, Legrand M, Balestra GM, Singer M, Ince C. Microvascular and interstitial oxygen tension in the renal cortex and medulla studied in a 4-h rat model of LPS-induced endotoxemia. *Shock.* 2011;36:83–9.
36. Mik EG, Stap J, Sinaasappel M, Beek JF, Aten JA, van Leeuwen TG, et al. Mitochondrial PO<sub>2</sub> measured by delayed fluorescence of endogenous protoporphyrin IX. *Nat Meth.* 2006;3:939–45.
37. Mik EG, Johannes T, Zuurbier CJ, Heinen A, Houben-Weerts JHPM, Balestra GM, et al. In vivo mitochondrial oxygen tension measured by a delayed fluorescence lifetime technique. *Biophys. J. Elsevier*; 2008;95:3977–90.
38. Mik EG, Ince C, Eerbeek O, Heinen A, Stap J, Hooibrink B, et al. Mitochondrial oxygen tension within the heart. *Journal of Molecular and Cellular Cardiology.* 2009;46:943–51.
39. Harms FA, de Boon WMI, Balestra GM, Bodmer SIA, Johannes T, Stolker RJ, et al. Oxygen-dependent delayed fluorescence measured in skin after topical application of 5-aminolevulinic acid. *Sterenberg HJCM, Bendsoe N, Svanberg K, editors. J Biophotonics. WILEY-VCH Verlag*; 2011;4:731–9.
40. Bodmer SIA, Balestra GM, Harms FA, Johannes T, Raat NJ, Stolker RJ, et al. Microvascular and mitochondrial PO<sub>2</sub> simultaneously measured by oxygen-dependent delayed luminescence. *J Biophotonics. WILEY-VCH Verlag*; 2012;5:140–51.
41. Wang L, Jacques SL, Zheng L. MCML--Monte Carlo modeling of light transport in multi-layered tissues. *Comput Methods Programs Biomed.* 1995;47:131–46.
42. Wang L, Jacques SL, Zheng L. CONV--convolution for responses to a finite diameter photon beam incident on multi-layered tissues. *Comput Methods Programs Biomed.* 1997;54:141–50.
43. Stein AB, Tiwari S, Thomas P, Hunt G, Levent C, Stoddard MF, et al. Effects of anesthesia on echocardiographic assessment of left ventricular structure and function in rats. *Basic Res. Cardiol. Steinkopff-Verlag*; 2007;102:28–41.
44. Hardziyenka M, Campian ME, de Bruin-Bon HACMR, Michel MC, Tan HL. Sequence of echocardiographic changes during development of right ventricular failure in rat. *J Am Soc Echocardiogr.* 2006;19:1272–9.
45. Kawahara Y, Tanonaka K, Daicho T, Nawa M, Oikawa R, Nasa Y, et al. Preferable anesthetic conditions for echocardiographic determination of murine cardiac function. *J Pharmacol Sci. The Japanese Pharmacological Society*; 2005;99:95–104.
46. Watson LE, Sheth M, Denyer RF, Dostal DE. Baseline echocardiographic values for adult male rats. *J Am Soc Echocardiogr.* 2004;17:161–7.
47. Cantor EIJ, Babick AP, Vasanji Z, Dhalla NS, Netticadan T. A comparative serial echocardiographic analysis of cardiac structure and function in rats subjected to pressure or volume overload. *Journal of Molecular and Cellular Cardiology.* 2005;38:777–86.
48. Sjaastad I, Sejersted OM, Illebekk A, Bjornerheim R. Echocardiographic criteria for detection of postinfarction congestive heart failure in rats. *J. Appl. Physiol. American Physiological Society Bethesda, MD*; 2000;89:1445–54.
49. Ritz JP, Roggan A, Isbert C, Müller G, Buhr HJ, Germer CT. Optical properties of native and coagulated

- porcine liver tissue between 400 and 2400 nm. *Lasers Surg Med*. John Wiley & Sons, Ltd; 2001;29:205–12.
50. Swartling J, Pålsson S, Platonov P, Olsson SB, Andersson-Engels S. Changes in tissue optical properties due to radio-frequency ablation of myocardium. *Med Biol Eng Comput*. Springer-Verlag; 2003;41:403–9.
  51. Gandjbakhche AH, Bonner RF, Arai AE, Balaban RS. Visible-light photon migration through myocardium in vivo. *Am. J. Physiol. American Physiological Society* Bethesda, MD; 1999;277:H698–704.
  52. Cheong WF, Prah SA, Welch AJ. Review of the Optical Properties of Biological Tissues. *IEEE Journal of Quantum Electronics*. 1990;26:2166–85.
  53. Marchesini R, Bertoni A, Andreola S, Melloni E, Sichirollo AE. Extinction and absorption coefficients and scattering phase functions of human tissues in vitro. *Appl Opt*. Optica Publishing Group; 1989;28:2318–24.
  54. Pickering JW, Bosman S, Posthumus P, Blokland P, Beek JF, van Gemert MJ. Changes in the optical properties (at 632.8 nm) of slowly heated myocardium. *Appl Opt*. Optica Publishing Group; 1993;32:367–71.
  55. Friebel M, Roggan A, Müller G, Meinke M. Determination of optical properties of human blood in the spectral range 250 to 1100 nm using Monte Carlo simulations with hematocrit-dependent effective scattering phase functions. *J. Biomed. Opt. SPIE*; 2006;11:34021.
  56. Faber DJ, Aalders MCG, Mik EG, Hooper BA, van Gemert MJC, van Leeuwen TG. Oxygen saturation-dependent absorption and scattering of blood. *Phys Rev Lett. American Physical Society*; 2004;93:028102.
  57. Tearney GJ, Brezinski ME, Southern JF, Bouma BE, Hee MR, Fujimoto JG. Determination of the refractive index of highly scattering human tissue by optical coherence tomography. *Opt Lett*. 1995;20:2258.
  58. Bolin FP, Preuss LE, Taylor RC, Ference RJ. Refractive index of some mammalian tissues using a fiber optic cladding method. *Appl Opt*. Optica Publishing Group; 1989;28:2297–303.
  59. Dirckx JJJ, Kuypers LC, Decraemer WF. Refractive index of tissue measured with confocal microscopy. *J. Biomed. Opt. SPIE*; 2005;10:44014.
  60. Duprez D, De Buyzere M, Dhondt E, Clement DL. Impaired microcirculation in heart failure. *Int J Microcirc Clin Exp*. 1996;16:137–42.
  61. Xu X, Wang RK, Elder JB, Tuchin VV. Effect of dextran-induced changes in refractive index and aggregation on optical properties of whole blood. *Phys Med Biol. IOP Publishing*; 2003;48:1205–21.
  62. Vinogradov SA, Lo LW, Jenkins WT, Evans SM, Koch C, Wilson DF. Noninvasive imaging of the distribution in oxygen in tissue in vivo using near-infrared phosphors. *Biophys. J*. 1996;70:1609–17.
  63. Poole DC, Behnke BJ, McDonough P, McAllister RM, Wilson DF. Measurement of muscle microvascular oxygen pressures: compartmentalization of phosphorescent probe. *Microcirculation*. John Wiley & Sons, Ltd; 2004;11:317–26.
  64. Ziemer LS, Lee WMF, Vinogradov SA, Sehgal C, Wilson DF. Oxygen distribution in murine tumors: characterization using oxygen-dependent quenching of phosphorescence. *J. Appl. Physiol. American Physiological Society*; 2005;98:1503–10.
  65. Dunphy I, Vinogradov SA, Wilson DF. Oxyphor R2 and G2: phosphors for measuring oxygen by oxygen-dependent quenching of phosphorescence. *Anal. Biochem*. 2002;310:191–8.
  66. Poulson R. The enzymic conversion of protoporphyrinogen IX to protoporphyrin IX in mammalian mitochondria. *J. Biol. Chem*. 1976;251:3730–3.
  67. Lo LW, Koch CJ, Wilson DF. Calibration of oxygen-dependent quenching of the phosphorescence of Pd-meso-tetra (4-carboxyphenyl) porphine: a phosphor with general application for measuring oxygen concentration in biological systems. *Anal. Biochem*. 1996;236:153–60.
  68. Duncker DJ, Bache RJ. Regulation of coronary vasomotor tone under normal conditions and during acute myocardial hypoperfusion. *Pharmacol. Ther*. 2000;86:87–110.
  69. Streif JUG, Nahrendorf M, Hiller K-H, Waller C, Wiesmann F, Rommel E, et al. In vivo assessment of absolute perfusion and intracapillary blood volume in the murine myocardium by spin labeling magnetic resonance imaging. *Magn. Reson. Med*. John Wiley & Sons, Ltd; 2005;53:584–92.
  70. Kahler E, Waller C, Rommel E, Belle V, Hiller KH, Voll S, et al. Perfusion-corrected mapping of cardiac regional blood volume in rats in vivo. *Magn. Reson. Med*. John Wiley & Sons, Ltd; 1999;42:500–6.
  71. Kwon Y. *Handbook of Essential Pharmacokinetics, Pharmacodynamics and Drug Metabolism for Industrial Scientists*. 1st ed. San Diego, California: Springer US; 2001.
  72. Stepinac TK, Chamot SR, Rungger-Brändle E, Ferrez P, Munoz J-L, van den Bergh H, et al. Light-induced retinal vascular damage by Pd-porphyrin luminescent oxygen probes. *Invest Ophthalmol Vis Sci. The Association for Research in Vision and Ophthalmology*; 2005;46:956–66.
  73. Beek JF, Blokland P, Posthumus P, Aalders M, Pickering JW, Sterenborg HJ, et al. In vitro double-integrating-sphere optical properties of tissues between 630 and 1064 nm. *Phys Med Biol*. 1997;42:2255–61.
  74. Steinke JM, Shepherd AP. Diffusion model of the optical absorbance of whole blood. *J Opt Soc Am A. Optica Publishing Group*; 1988;5:813–22.
  75. Li H, Xie S. Measurement method of the refractive index of biotissue by total internal reflection. *Appl Opt*. Optica Publishing Group; 1996;35:1793–5.

# CHAPTER

# 5

## Monitoring mitochondrial PO<sub>2</sub> – the next step

Egbert G. Mik  
Gianmarco M. Balestra  
Floor A. Harms

Curr Opin Crit Care. 2020 Jun;26(3):289-295.  
PMID: 32348095 DOI: 10.1097/MCC.0000000000000719.



## ABSTRACT

### Purpose of review

To fully exploit the concept of hemodynamic coherence in resuscitating critically ill one should preferably take into account information about the state of parenchymal cells. Monitoring of mitochondrial oxygen tension (mitoPO<sub>2</sub>) has emerged as a clinical means to assess information of oxygen delivery and oxygen utilization at the mitochondrial level. This review will outline the basics of the technique, summarize its development and describe the rationale of measuring oxygen at the mitochondrial level.

### Recent findings

Mitochondrial oxygen tension can be measured by means of the protoporphyrin IX-Triplet State Lifetime Technique (PpIX-TSLT). After validation and use in preclinical animal models the technique has recently become commercially available in the form of a clinical measuring system. This system has now been used in a number of healthy volunteer studies and is currently being evaluated in studies in perioperative and intensive care patients in several European university hospitals.

### Summary

PpIX-TSLT is a non-invasive and safe method to assess aspects of mitochondrial function at the bedside. It allows doctors to look beyond the macro and microcirculation and to take the oxygen balance at the cellular level into account in treatment strategies.

### KEY POINTS

- Mitochondria are important energy producing organelles at risk in perioperative and Intensive care medicine
- Mitochondrial oxygen tension can be non-invasively and safely measured using the optical properties of protoporphyrin IX
- Mitochondrial oxygen monitoring is feasible at the bedside and provides unique parameters and information
- Mitochondrial oxygen monitoring provides a new tool for research in resuscitation, transfusion, and pathophysiology

## INTRODUCTION

Resuscitating critically ill patients from different states of shock is a key strategy in critical care but remains a challenge. Targeting the normalization of systemic hemodynamic parameters does not lead to improved outcomes [1–5]. Over the last two decades, considerable attention has been given to the role of microcirculatory dysfunction as substrate for such failure, leading to the concept of ‘hemodynamic coherence’ [6,7]. Hemodynamic coherence is the coherence between the macrocirculation, microcirculation and ultimately the parenchymal cells, leading to an optimal balance of supply and demand of oxygen and nutrients to the tissues. Loss of hemodynamic coherence is associated with increased morbidity and mortality [8–10], as recently confirmed again in cardiogenic shock patients [11]\*. The treatment strategy can have an effect on the occurrence of loss of hemodynamic coherence [12]\*. As the ultimate goal of optimizing macrocirculatory and microcirculatory hemodynamics is providing parenchymal cells with an optimal milieu intérieur, a missing piece of the puzzle remains information from the tissue cells. Especially information from the mitochondria, a key cell organelle and ultimate destination of oxygen could be very helpful. Using an optical technique, it is now possible to get quantitative information about the oxygen tension in mitochondria and their oxygen utilization. This review will describe the rationale of taking into account mitochondrial measurements in perioperative and intensive care medicine and summarize the development of a clinically applicable technique for assessing mitochondrial oxygen tension and respiration.

## MITOCHONDRIAL FUNCTION

Mitochondria are double-membrane organelles that play pivotal roles in cellular physiology. Our understanding of their functions and complex interplay with their surrounding has been boosted in the last two decades and is still growing [13]. Mitochondria are well known as the powerhouses of the cells but they take part in other important cellular processes as well. For example, mitochondria are involved in programmed cell death via opening of the permeability transition pore and cytochrome c release [14,15]. Also, mitochondria might play a role in intracellular calcium homeostasis [16] as they possess calcium uniporters [17,18] and mitochondrially generated reactive oxygen species (ROS) act as cell-signaling molecules involved in metabolic adaptation [19], apoptosis [20] and autophagy [21]. Notwithstanding all other important functions, it is the ATP production by oxidative phosphorylation that is clinically in the foreground. Mitochondria are the primary consumers of oxygen and are responsible for approximately 98% of total body oxygen consumption. Oxygen is ultimately used at complex IV of the electron transport chain in the inner mitochondrial membrane. Reduced nicotinamide

adenine dinucleotide (NADH) and flavin adenine dinucleotide (FADH<sub>2</sub>), generated in the Krebs cycle, are transferred from carrier molecules to the electron transport chain on complex I and II, respectively. The resulting electron transport through the chain causes protons to be pumped to the intermembrane space. This proton pumping causes an electrochemical potential over the inner membrane that is used to convert ADP to ATP by ATP synthase. ATP is the energy currency of the cells and used for driving cellular processes like maintaining membrane potentials, protein synthesis and replication.

## THREATS TO MITOCHONDRIAL FUNCTION

In the perioperative and intensive care setting, many factors pose a threat to mitochondrial integrity and function, as set out in a recent review [22]. Both internal and external threats can be identified (Fig. 1). Such altered mitochondrial function, for example, diminished respiration and ATP production, does not necessarily mean dysfunction because of damage. It can be an adaptive response to threats, for example, prolonged hypoxia because of oxygen-conformance or metabolic reprogramming [23,24], which extends seamlessly to a dysfunctional state and responds to resuscitation [25]. The functional consequences of such oxygen-dependent adaptation for cell and organ functions remain largely unknown, as well as its effects on microvascular perfusion. Thus, it remains unclear whether microvascular perfusion disturbances in critical illness are caused by dysfunction and should be a target of treatment, or merely are an epiphenomenon caused by altered cellular metabolism and diminished oxygen demand. Direct measurement of aspects of mitochondrial function could, therefore, be helpful and mitochondrial oxygen is a parameter of great interest in this respect.

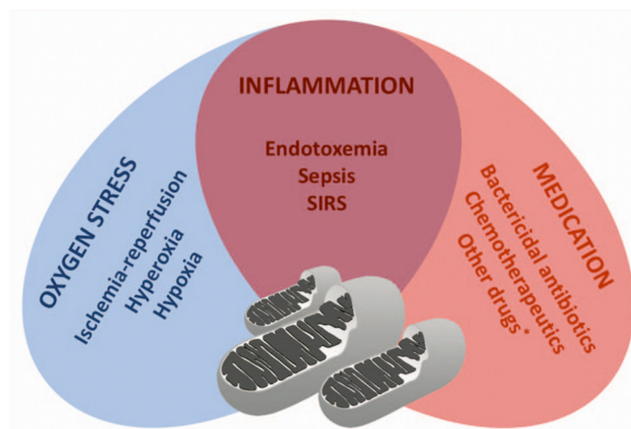


**Figure 1.** Threats to mitochondria in perioperative and intensive care medicine. \*Drugs like statins, metformin, propofol, amiodarone and many others.

## MEASURING MITOPO<sub>2</sub>

The measurement of mitoPO<sub>2</sub> has been made possible by the introduction of an optical technique, called the Protoporphyrin IX – Triplet State Lifetime Technique (PpIX-TSLT). Protoporphyrin IX is the final precursor in the heme biosynthetic pathway and is synthesized in the mitochondria [26] and shows a bright red prompt fluorescence when illuminated with blue or green light. This fluorescence is, for example, used in photodynamic diagnosis to visualize tumor during surgical resection [27]. Key in the development of PpIX-TSLT was the discovery of the existence of a more long-lived red emission from protoporphyrin IX, called delayed fluorescence [28]. Although prompt fluorescence intensity decays with a nanosecond lifetime, delayed fluorescence lasts microseconds to milliseconds.

## OXYGEN-DEPENDENT DELAYED FLUORESCENCE

The delayed fluorescence lifetime is dependent on the oxygen concentration. Higher oxygen concentrations result in a shorter lifetimes, whereas low oxygen concentrations leads to long lifetimes. The molecular mechanisms involved in this oxygen-dependent quenching of delayed fluorescence have been described elsewhere [29]. In short, photoexcitation of PpIX leads to population of an excited triplet state. Relaxation to the ground state can be spontaneous and result in the emission of a photon (delayed fluorescence). Alternatively, the energy can be transferred to an oxygen molecule upon collision and relaxation occurs without emission of a photon. More oxygen leads to more collisions and a higher collision rate, and therefore, results in a faster decaying delayed fluorescence signal (quenching). The delayed fluorescence lifetime can be converted to partial pressure of oxygen by the Stern–Volmer equation [30].

## FROM CULTURED CELLS TO IN VIVO

In 2006, the technique for measuring mitochondrial PO<sub>2</sub> by delayed fluorescence of protoporphyrin IX was first described [28]. In this pivotal study, 5-aminolevulinic acid (ALA) was administered to several types of cell cultures and the mitochondrial localization of ALA-induced PpIX was demonstrated, together with the presence of oxygen-dependent delayed fluorescence from cell suspensions. Also, direct simultaneous measurement of mitoPO<sub>2</sub> and extracellular PO<sub>2</sub> showed that only shallow oxygen gradients exist over the cell membrane. Some years later, it was demonstrated that the technique could be extended to in-vivo use [31]. Intravenous administration of ALA led to detectable oxygen-dependent delayed fluorescence in rat liver [31] and heart [32]. The technique has been

used in several preclinical pathophysiological studies [23,33–35]. As the technique was feasible in humans, but systemic administration of ALA was considered an obstacle, topical administration of ALA was tested for mitoPO<sub>2</sub> measurements (Fig. 2). For practical and clinical reasons, the skin was considered an ideal target organ for such measurements. Indeed, topical application of ALA to skin induced sufficient oxygen-dependent delayed fluorescence [36] and allowed local mitoPO<sub>2</sub> measurements [37] in rats. In a pig model, we demonstrated that, unlike tissue oxygenation measured with near-infrared spectroscopy, cutaneous mitoPO<sub>2</sub> is a sensitive parameter for detecting the physiologic limit of hemodilution on an individual level [34]. The skin is especially interesting since, like the gastrointestinal tract [38], it can be regarded as the canary of the body.

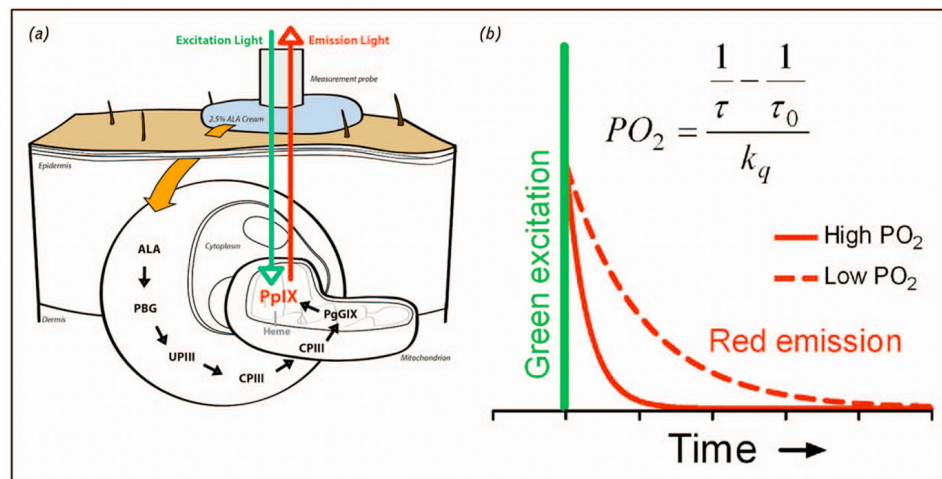


**Figure 2.** (a) Principle of protoporphyrin IX-Triplet State Lifetime Technique. The pathway by which topical ALA administration enhances mitochondrial PpIX levels and the principle of delayed fluorescence detection after an excitation pulse with green (510nm) light. Emission light is the delayed fluorescence (red light, 630–700nm) and its lifetime is oxygen-dependent. (b) PpIX emits delayed fluorescence after excitation by a pulse of green (510nm) light. The delayed fluorescence lifetime is oxygen-dependent according to the Stern–Volmer equation (inset), in which  $k_q$  is the quenching constant and  $\tau_0$  is the lifetime at zero oxygen. ALA, 5-aminolevulinic acid; CPIII, coproporphyrinogen III; PBG, porphobilinogen; PO<sub>2</sub>, oxygen tension; PpIX, protoporphyrin IX; UPIII, uroporphyrinogen II. Reproduced with permission from Harms *et al.* [60].

## HUMAN USE (CELLULAR OXYGEN METABOLISM)

A clinical prototype of PpIX-TSLT was successfully tested in a healthy volunteer study [39] and triggered the development of the COMET system. COMET is an acronym of Cellular Oxygen METabolism and is a monitoring system developed by Photonics Healthcare in Utrecht, The Netherlands. The system is CE-marked and allows, in combination with

its SkinSensor, repetitive noninvasive measurements of mitoPO<sub>2</sub> in human skin [40]. To prime the skin for delayed fluorescence measurements, a ALA-containing plaster is applied to the skin (Alacare, photonamic & Co. KG, Pinneberg, Germany). Although sufficient induction of PpIX by this plaster takes several hours, it provides a practical way of applying ALA to the skin in a clinical setting. The COMET system has by now been tested in several healthy volunteer studies [41,42\*] and is currently being evaluated in clinical studies, both in perioperative and intensive care setting [22,40,43]. Importantly, the use of COMET is not limited to mitoPO<sub>2</sub> measurements in skin. The system has been used to demonstrate the feasibility of assessing the mucosal oxygenation in the gastrointestinal system via endoscopy [44\*]. To this end, the ALA was administered systemically, via the oral route, and oxygen-dependent delayed fluorescence was measured via an optical fiber through the working channel of an endoscope. The authors propose to use mitoPO<sub>2</sub> measurements as a functional test in the workup for the diagnosis of chronic mesenteric ischemia, but since the gut is very sensitive for shock [45], such an approach might ultimately also be of benefit for resuscitation purposes in the intensive care.

## THE MYTH OF LOW MITOPO<sub>2</sub>

As oxygen transport from microcirculation into the tissue cells is driven by diffusion, it is generally anticipated, according to the classical oxygen cascade that mitochondrial oxygen tension should be very low (several mmHgs) to create a big enough oxygen gradient [46,47]. However, average mitoPO<sub>2</sub> measured with the PpIX-TSLT technique appears to be, depending on the specific tissue, close to microvascular oxygen tension [33,48] and known values for tissue and/or interstitial oxygen levels [49,50\*\*]. In fact, mitoPO<sub>2</sub> is unlikely to be an order of magnitude lower than microvascular and interstitial oxygen tension. First, oxygen does not disappear stepwise so several mitochondria will see aPO<sub>2</sub> close to intravascular values. Second, larger vessels (not only capillaries) also contribute to diffusional oxygen delivery [51] so some mitochondria might see a PO<sub>2</sub> higher than the oxygen tension in the capillaries. Third, the oxygen gradient over the cell membrane is small [28] and will not cause mitoPO<sub>2</sub> to be substantially lower than interstitial PO<sub>2</sub>. Typically reported cutaneous mitoPO<sub>2</sub> values under baseline circumstances are 40–70 mmHg and considered to be matching well with other measurements in skin [50\*\*]. Importantly, we demonstrated in both a preclinical [34] and clinical setting [40] that mitoPO<sub>2</sub> provides different information than hemoglobin saturation-based techniques like near-infrared spectroscopy. In situations, where visible light spectroscopy and near-infrared spectroscopy failed to show any response on a perturbation, mitoPO<sub>2</sub> clearly dropped to indicate cellular distress.



## A POTENTIAL NEW TRANSFUSION TRIGGER

In current clinical practice, optimization of hemodynamics and tissue oxygen delivery in perioperative and intensive care patients is focusing on the administration of fluids, blood transfusion and vasoactive medication, targeting normal systemic hemodynamic parameters such as blood pressure, cardiac output, hemoglobin levels and venous saturation. For example, the management of acute anemia is mainly focused on the use of allogeneic blood transfusion guided on specific hemoglobin levels instead of a patient's personal need. Allogeneic blood transfusion itself is not without risks and has been shown to be an independent factor for an increased mortality and morbidity [52,53]. Transfusion guidelines use hemoglobin levels to indicate the need for blood transfusion. Such guidelines are based on data of large groups and incorporate a safety margin that might lead to unnecessary transfusion in individual cases. As ultimately the mitochondria are the target for oxygen delivery, it seems reasonable to use mitoPO<sub>2</sub> as a measure for an individual's transfusion need. This presupposition was fostered by the finding that in hemodiluted pigs mitoPO<sub>2</sub> dropped as a result of ongoing hemodilution. Reaching the physiological limit of an individual pig, mitoPO<sub>2</sub> acutely dropped and this drop preceded other signs of inadequate oxygen delivery, like a rise in serum lactate. Thus, mitoPO<sub>2</sub> measurements can be useful as a novel transfusion trigger for personalized transfusion medicine. Studies that show that this drop in mitoPO<sub>2</sub> can be reversed by transfusion of autologous blood and that mitoPO<sub>2</sub> could indeed be a potential physiological transfusion trigger are under way.

## UNRAVELING THE OXYGEN BALANCE

Fluid resuscitation, based on systemic hemodynamic parameters remains key in the treatment of sepsis shock. The substantiation for this type of treatment is based on the hypothesis that the development of septic shock and multiorgan failure is caused by tissue hypoxia because of a higher metabolic rate together with impaired diffusion processes in the microcirculation [54]. However, many clinical trials have failed to demonstrate benefits of resuscitation on hemodynamic parameters, such as blood pressure, central venous pressure, cardiac output and central venous saturation [3,4,55,56]. This suggests that other mechanism, such as mitochondrial dysfunction, also play a role in the pathogenesis of sepsis shock. However, the literature about mitochondrial dysfunction in sepsis shows conflicting results [57\*\*], most likely because of the lack of a valid and reliable measurement method to monitor mitochondrial dysfunction [58]. Therefore, we suggested PpIX-TSLT as a possible noninvasive monitoring tool for measuring mitoPO<sub>2</sub> and mitochondrial oxygen consumption (mitoVO<sub>2</sub>) *in vivo*. Oxygen consumption is determined by a dynamic mitoPO<sub>2</sub> measurement, measuring mitoPO<sub>2</sub> every second

for approximately 90 s, while microvascular oxygen supply is blocked by applying pressure on the skin with the measuring probe. mitoVO<sub>2</sub> can then be derived from the resulting oxygen disappearance curve [59]. We demonstrated the feasibility to measure the mitoPO<sub>2</sub> and mitoVO<sub>2</sub> in an endotoxemic model of acute critical illness [60]. In this study, we observed a decreased mitochondrial oxygen consumption in endotoxemic rats independently of the fact whether mitoPO<sub>2</sub> was reduced or restored by fluid resuscitation, suggesting that endotoxemia had a lasting effect on mitochondrial function, even in the absence of evident hemodynamic shock. Another recent study compared the PpIX-TSLT measurements with a widely used 'ex vivo' mitochondrial respirometry technique. The same decrease in mitoPO<sub>2</sub> and mitochondrial oxygen consumption were measured with the PpIX-TSLT after the induction of sepsis, but 'ex vivo' mitochondrial function measurements remained unchanged before and after induction of sepsis. This results are probably caused by a higher sensitivity of the 'in vivo' PpIX-TSLT measurements compared with the classic 'ex vivo' measurements. After demonstrating the feasibility of cutaneous mitoVO<sub>2</sub> measurements, it remained important to demonstrate that cutaneous mitoPO<sub>2</sub> and mitoVO<sub>2</sub>, at least to some extent, reflect such mitochondrial parameters in other vital organs. Therefore, we conducted a study that compared the values and responses of cutaneous mitoPO<sub>2</sub> and mitoVO<sub>2</sub> with liver and gastrointestinal tract [61]. The results showed that the absolute value of mitoPO<sub>2</sub> and mitoVO<sub>2</sub> in the skin may differ from other organs, but that the trend of a decreased mitoPO<sub>2</sub> and mitoVO<sub>2</sub> was observed in all studied organs after the administration of endotoxin.

## CONCLUSION

Mitochondria are the ultimate destination of oxygen delivery. Measurement of oxygen and oxygen utilization at the mitochondrial level is expected to be of benefit for guiding therapies aimed at restoring or optimizing tissue oxygenation and ultimately organ function. PpIX-TSLT is a noninvasive and well tolerated technique to measure mitoPO<sub>2</sub> and mitoVO<sub>2</sub>. The COMET system allows bedside use of this technique, providing a next step in monitoring.

## REFERENCES AND RECOMMENDED READING

Papers of particular interest, published within the annual period of review, have been highlighted as: \* of special interest \*\* of outstanding interest

1. Asfar P, Meziani F, Hamel JF, et al., SEPSISPAM Investigators. High versus low blood-pressure target in patients with septic shock. *N Engl J Med* 2014; 370:1583–1593.
2. Holst LB, Haase N, Wetterslev J, et al. Lower versus higher hemoglobin threshold for transfusion in septic shock. *N Engl J Med* 2014; 371:1381–1391.
3. Arise Investigators. Group ACT, Peake SL, et al. Goal-directed resuscitation for patients with early septic shock. *N Engl J Med* 2014; 371: 1496–1506.
4. ProCESS Investigators. Yealy DM, Kellum JA, et al. A randomized trial of protocol-based care for early septic shock. *N Engl J Med* 2014; 370:1683–1693.
5. Mouncey PR, Osborn TM, Power GS, et al., ProMISe Trial Investigators. Trial of early, goal-directed resuscitation for septic shock. *N Engl J Med* 2015; 372:1301–1311.
6. Ince C. Hemodynamic coherence and the rationale for monitoring the microcirculation. *Crit Care* 2015; 19 Suppl 3:S8.
7. Ince C, Mik EG. Microcirculatory and mitochondrial hypoxia in sepsis, shock, and resuscitation. *J Appl Physiol* (1985) 2016; 120:226–235.
8. De Backer D, Donadello K, Sakr Y, et al. Microcirculatory alterations in patients with severe sepsis: impact of time of assessment and relationship with outcome. *Crit Care Med* 2013; 41:791–799.
9. Sakr Y, Dubois MJ, De Backer D, et al. Persistent microcirculatory alterations are associated with organ failure and death in patients with septic shock. *Crit Care Med* 2004; 32:1825–1831.
10. 10. Trzeciak S, McCoy JV, Phillip Dellinger R, et al., Microcirculatory Alterations in Resuscitation and Shock (MARS) investigators. Early increases in microcirculatory perfusion during protocol-directed resuscitation are associated with reduced multiorgan failure at 24 h in patients with sepsis. *Intensive Care Med* 2008; 34:2210–2217.
11. \* Wijntjens GW, Fengler K, Fuernau G, et al. Prognostic implications of microcirculatory perfusion versus macrocirculatory perfusion in cardiogenic shock: a CULPRIT-SHOCK substudy. *Eur Heart J Acute Cardiovasc Care* 2019; 9:108–119.  
Substudy in 66 patients of a large multicenter trial showing a significant and independent association between microcirculatory perfusion parameters and the combined clinical endpoint of all-cause death and renal replacement therapy at 30 days follow-up.
12. \* Arnemann PH, Hessler M, Kampmeier T, et al. Resuscitation with hydroxyethyl starch maintains hemodynamic coherence in ovine hemorrhagic shock. *Anesthesiology* 2020; 132:131–139.  
Study showing that hemodynamic coherence might be influenced by the choice of resuscitation fluid, as resuscitation with hydroxyethyl starch-maintained coherence in hemorrhagic shock whereas physiological saline only improved macrocirculation but not microcirculation.
13. Zhou B, Tian R. Mitochondrial dysfunction in pathophysiology of heart failure. *J Clin Invest* 2018; 128:3716–3726.
14. Eguchi Y, Shimizu S, Tsujimoto Y. Intracellular ATP levels determine cell death fate by apoptosis or necrosis. *Cancer Res* 1997; 57:1835–1840.
15. Jiang X, Wang X. Cytochrome C-mediated apoptosis. *Annu Rev Biochem* 2004; 73:87–106.
1. Rizzuto R, De Stefani D, Raffaello A, Mammucari C. Mitochondria as sensors and regulators of calcium signalling. *Nat Rev Mol Cell Biol* 2012; 13:566–578.
2. Baughman JM, Perocchi F, Girgis HS, et al. Integrative genomics identifies MCU as an essential component of the mitochondrial calcium uniporter. *Nature* 2011; 476:341–345.
3. De Stefani D, Raffaello A, Teardo E, et al. A forty-kilodalton protein of the inner membrane is the mitochondrial calcium uniporter. *Nature* 2011; 476:336–340.
4. Chandel NS, Maltepe E, Goldwasser E, et al. Mitochondrial reactive oxygen species trigger hypoxia-induced transcription. *Proc Natl Acad Sci U S A* 1998; 95:11715–11720.
5. Redza-DutorDolr M, Averill-Bates DA. Activation of apoptosis signalling pathways by reactive oxygen species. *Biochim Biophys Acta* 2016; 1863:2977–2992.
6. Filomeni G, De Zio D, Cecconi F. Oxidative stress and autophagy: the clash between damage and metabolic needs. *Cell Death Differ* 2015; 22:377–388.
7. Wefers Bettink MA, Arbous MS, Raat NJ, Mik EG. Mind the mitochondria! *J Emerg Crit Care Med* 2019; 3:1–13.
8. Balestra GM, Mik EG, Eerbeek O, et al. Increased in vivo mitochondrial oxygenation with right ventricular failure induced by pulmonary arterial hypertension: mitochondrial inhibition as driver of cardiac failure? *Respir Res* 2015; 16:6.
9. Matkovich SJ, Al Khiami B, Efimov IR, et al. Widespread down-regulation of cardiac mitochondrial and sarcomeric genes in patients with sepsis. *Crit Care Med* 2017; 45:407–414.
10. Piel DA, Gruber PJ, Weinheimer CJ, et al. Mitochondrial resuscitation with exogenous cytochrome c in the septic heart. *Crit Care Med* 2007; 35:2120–2127.
11. Poulson R. The enzymic conversion of protoporphyrinogen IX to protoporphyrin IX in mammalian mitochondria. *J Biol Chem* 1976; 251:3730–3733.
12. Georges JF, Valeri A, Wang H, et al. Delta-aminolevulinic acid-mediated photodiagnoses in surgical oncology: a historical review of clinical trials. *Front Surg* 2019; 6:45.
13. Mik EG, Stap J, Sinaasappel M, et al. Mitochondrial PO<sub>2</sub> measured by delayed fluorescence of endogenous protoporphyrin IX. *Nat Methods* 2006; 3:939–945.
14. Mik EG. Special article: measuring mitochondrial oxygen tension: from basic principles to application in humans. *Anesth Analg* 2013; 117:834–846.
15. Mik EG, Donkersloot C, Raat NJ, Ince C. Excitation pulse deconvolution in luminescence lifetime analysis for oxygen measurements in vivo. *Photochem Photobiol* 2002; 76:12–21.
16. Mik EG, Johannes T, Zuurbier CJ, et al. In vivo mitochondrial oxygen tension measured by a delayed fluorescence lifetime technique. *Biophys J* 2008; 95:3977–3990.
17. Mik EG, Ince C, Eerbeek O, et al. Mitochondrial oxygen tension within the heart. *J Mol Cell Cardiol* 2009; 46:943–951.
18. Bodmer SI, Balestra GM, Harms FA, et al. Microvascular and mitochondrial PO<sub>2</sub> simultaneously measured by oxygen-dependent delayed luminescence. *J Biophotonics* 2012; 5:140–151.

19. Romers LH, Bakker C, Dollee N, et al. Cutaneous mitochondrial PO<sub>2</sub>, but not tissue oxygen saturation, is an early indicator of the physiologic limit of hemodilution in the pig. *Anesthesiology* 2016; 125:124–132.
20. Wefers Bettink MA, Harms FA, Dollee N, et al. Noninvasive versus ex vivo measurement of mitochondrial function in an endotoxemia model in rat: Toward monitoring of mitochondrial therapy. *Mitochondrion* 2020; 50:149–157.
21. Harms FA, de Boon WM, Balestra GM, et al. Oxygen-dependent delayed fluorescence measured in skin after topical application of 5-aminolevulinic acid. *J Biophotonics* 2011; 4:731–739.
22. Harms FA, Bodmer SI, Raat NJ, et al. Validation of the protoporphyrin IX-triplet state lifetime technique for mitochondrial oxygen measurements in the skin. *Opt Lett* 2012; 37:2625–2627.
23. Dantzer DR. The gastrointestinal tract. The canary of the body? *JAMA* 1993; 270:1247–1248.
24. Harms FA, Stolker RJ, Mik EG. Cutaneous respirometry as novel technique to monitor mitochondrial function: a feasibility study in healthy volunteers. *PLoS One* 2016; 11:e0159544.
25. Ubbink R, Bettink MAW, Janse R, et al. A monitor for Cellular Oxygen METabolism (COMET): monitoring tissue oxygenation at the mitochondrial level. *J Clin Monit Comput* 2017; 31:1143–1150.
26. van Diemen MPJ, Berends CL, Akram N, et al. Validation of a pharmacological model for mitochondrial dysfunction in healthy subjects using simvastatin: a randomized placebo-controlled proof-of-pharmacology study. *Eur J Pharmacol* 2017; 815:290–297.
27. \* Baumbach P, Neu C, Derlien S, et al. A pilot study of exercise-induced changes in mitochondrial oxygen metabolism measured by a cellular oxygen metabolism monitor (PICOMET). *Biochim Biophys Acta Mol Basis Dis* 2019; 1865:749–758.  
First independent publication showing the useability of COMET parameters mitoPO<sub>2</sub> and mitoVO<sub>2</sub> and the authors even introduced a new parameter, mitoDO<sub>2</sub>.
28. Mik E, Kortlever R, Ter Horst M, Harms F. Mitochondrial oxygen availability and regional saturation during CPB. *Critical Care* 2019; 23(Suppl 2):175.
29. \* van Dijk LJD, Ubbink R, Terlouw LG, et al. Oxygen-dependent delayed fluorescence of protoporphyrin IX measured in the stomach and duodenum during upper gastrointestinal endoscopy. *J Biophotonics* 2019; 12:e201900025.  
Study in healthy volunteers showing that protoporphyrin IX-based delayed fluorescence measurements can be safely performed in the gastrointestinal tract.
30. Fiddian-Green RG. Associations between intramucosal acidosis in the gut and organ failure. *Crit Care Med* 1993; 21(2 Suppl):S103–S107.
31. Hsia CC, Schmitz A, Lambert M, et al. Evolution of air breathing: oxygen homeostasis and the transitions from water to land and sky. *Compr Physiol* 2013; 3:849–915.
32. Nathan AT, Singer M. The oxygen trail: tissue oxygenation. *Br Med Bull* 1999; 55:96–108.
33. Balestra GM, Aalders MC, Specht PA, et al. Oxygenation measurement by multiwavelength oxygen-dependent phosphorescence and delayed fluorescence: catchment depth and application in intact heart. *J Biophotonics* 2015; 8:615–628.
34. De Santis V, Singer M. Tissue oxygen tension monitoring of organ perfusion: rationale, methodologies, and literature review. *Br J Anaesth* 2015; 115:357–365.
35. \*\*Keeley TP, Mann GE. Defining Physiological Normoxia for Improved Translation of Cell Physiology to Animal Models and Humans. *Physiol Rev* 2019; 99:161–234. A recent and very extensive review about various aspects of oxygen. Although the prime goal of the review is defining oxygen levels for cell culture purposes, the article gives an excellent overview of oxygen measurements in various tissues. A must read!
36. Ellsworth ML, Pittman RN. Arterioles supply oxygen to capillaries by diffusion as well as by convection. *Am J Physiol* 1990; 258(4 Pt 2):H1240–H1243.
37. Chandra S, Kulkarni H, Westphal M. The bloody mess of red blood cell transfusion. *Crit Care* 2017; 21(Suppl 3):310.
38. Ferraris VA, Davenport DL, Saha SP, et al. Surgical outcomes and transfusion of minimal amounts of blood in the operating room. *Arch Surg* 2012; 147:49–55.
39. Kozlov AV, Lancaster JR Jr, Meszaros AT, Weidinger A. Mitochondria-mediated pathways of organ failure upon inflammation. *Redox Biol* 2017; 13:170–181.
55. Gattinoni L, Brazzi L, Pelosi P, et al. A trial of goal-oriented hemodynamic therapy in critically ill patients. SvO<sub>2</sub> Collaborative Group. *N Engl J Med* 1995; 333:1025–1032.
40. Hayes MA, Timmins AC, Yau EH, et al. Oxygen transport patterns in patients with sepsis syndrome or septic shock: influence of treatment and relationship to outcome. *Crit Care Med* 1997; 25:926–936.
41. \*\* Kohoutova M, Dejmek J, Tuma Z, Kuncova J. Variability of mitochondrial respiration in relation to sepsis-induced multiple organ dysfunction. *Physiol Res* 2018; 67(Suppl 4):S577–S592.  
Recent and comprehensive review discussing the controversies about the role of mitochondrial dysfunction in the pathogenesis of sepsis-induced multiple organ failure.
42. Jeger V, Djafarzadeh S, Jakob SM, Takala J. Mitochondrial function in sepsis. *Eur J Clin Invest* 2013; 43:532–542.
43. Harms FA, Voorbeijtel WJ, Bodmer SI, et al. Cutaneous respirometry by dynamic measurement of mitochondrial oxygen tension for monitoring mitochondrial function in vivo. *Mitochondrion* 2013; 13:507–514.
44. Harms FA, Bodmer SI, Raat NJ, Mik EG. Noninvasive monitoring of mitochondrial oxygenation and respiration in critical illness using a novel technique. *Crit Care* 2015; 19:343.
45. Harms FA, Bodmer SI, Raat NJ, Mik EG. Cutaneous mitochondrial respirometry: noninvasive monitoring of mitochondrial function. *J Clin Monit Comput* 2015; 29:509–519.

# CHAPTER

# 6

## Mitochondrial oxygen tension within the heart

Mik EG  
Ince C  
Eerbeek O  
Heinen A  
Stap J  
Hooibrink B  
Schumacher CA  
Balestra GM  
Johannes T  
Beek JF  
Nieuwenhuis AF  
Horssen P  
Spaan JA  
Zuurbier CJ.

## ABSTRACT

By using a newly developed optical technique which enables non-invasive measurement of mitochondrial oxygenation (mitoPO<sub>2</sub>) in the intact heart, we addressed three long-standing oxygenation questions in cardiac physiology: 1) what is mitoPO<sub>2</sub> within the in vivo heart?, 2) is mitoPO<sub>2</sub> heterogeneously distributed?, and 3) how does mitoPO<sub>2</sub> of the isolated Langendorff-perfused heart compare with that in the in vivo working heart? Following calibration and validation studies of the optical technique in isolated cardiomyocytes, mitochondria and intact hearts, we show that in the in vivo condition mean mitoPO<sub>2</sub> was 35 ± 5 mm Hg. The mitoPO<sub>2</sub> was highly heterogeneous, with the largest fraction (26%) of mitochondria having a mitoPO<sub>2</sub> between 10 and 20 mm Hg, and 10% between 0 and 10 mm Hg. Hypoxic ventilation (10% oxygen) increased the fraction of mitochondria in the 0–10 mm Hg range to 45%, whereas hyperoxic ventilation (100% oxygen) had no major effect on mitoPO<sub>2</sub>. For Langendorff-perfused rat hearts, mean mitoPO<sub>2</sub> was 29 ± 5 mm Hg with the largest fraction of mitochondria (30%) having a mitoPO<sub>2</sub> between 0 and 10 mm Hg. Only in the maximally vasodilated condition, did the isolated heart compare with the in vivo heart (11% of mitochondria between 0 and 10 mm Hg). These data indicate 1) that the mean oxygen tension at the level of the mitochondria within the heart in vivo is higher than generally considered, 2) that mitoPO<sub>2</sub> is considerably heterogeneous, and 3) that mitoPO<sub>2</sub> of the classic buffer-perfused Langendorff heart is shifted to lower values as compared to the in vivo heart.

## 1. INTRODUCTION

Mitochondria figure prominently in cardiac physiology by powering virtually all forms of mechanical and chemical work of the heart. These organelles can also play a decisive role in cell death and survival signaling. Oxygen is the underlying, ultimate molecule used by the mitochondria, thus giving it the essential role in dictating life or death. The partial pressure of oxygen within the mitochondria (mitoPO<sub>2</sub>) is hypothesized to have a regulatory function in important physiological processes such as energy production, radical production, oxygen sensing, and gene expression [1–5]. Surprisingly, no direct quantitative data concerning the in vivo mitoPO<sub>2</sub> within the intact heart are available in the literature.

MitoPO<sub>2</sub> can be estimated from PO<sub>2</sub> values reported for other compartments such as the cytosolic, tissue or vascular compartments. Interestingly, most studies report rather low PO<sub>2</sub> values ranging from 10 – 17 mm Hg for vascular and interstitial compartments [6–8] to 3 – 7 mm Hg for the cytosolic compartment [9–11]. Such low values suggest that the oxygen tension at the mitochondria, being at the lowest end of the diffusion pathway which oxygen must travel, is below 5 mm Hg, making it likely that oxygen regulates energy production [1,3,5]. These values deviate largely from other studies, however, which report cardiac microvascular PO<sub>2</sub> values of 50 – 70 mm Hg [12] or interstitial values of 45 mm Hg [13]. Using these latter, higher values, mitoPO<sub>2</sub> is estimated to be between 20 and 40 mm Hg. To resolve these conflicting estimated data on such an important (patho-)physiological parameter of the heart, our first goal of the present study was to provide a direct determination of mitoPO<sub>2</sub> within the intact heart. To this end, we employed a novel optical technique using oxygen-dependent quenching of the delayed fluorescence lifetime from mitochondrial protoporphyrin IX (PpIX) [14,15].

In addition, although spatial heterogeneity of blood flow, oxygen delivery and oxygen metabolism within the heart is well accepted [12,16,17], it is not known whether such heterogeneity extends to the oxygenation status of mitochondria. Aside from heterogeneity dictated by blood flow distribution, heterogeneity may also exist due to the distribution of mitochondria within the cardiomyocyte, i.e., subsarcolemmal and interfibrillar mitochondria [18]. When mitoPO<sub>2</sub> heterogeneity is present, the determination of a single averaged mitoPO<sub>2</sub> for the whole heart is misleading in that a significant, albeit small, part of all mitochondria within the heart may still be oxygen limited. Thus, a second goal of the present study entailed the determination of mitoPO<sub>2</sub> heterogeneity using a lifetime-deconvolution algorithm developed by Golub et al. [19].

Finally, we wanted to compare the mitochondrial oxygenation status in the isolated, Langendorff-perfused heart with that in the in vivo working heart. Investigations with isolated hearts are numerous, and the results obtained have been used to further our understanding of heart physiology, so that the validity of this model is of utmost importance [20]. We are not aware of other studies that have directly compared the

mitochondrial oxygenation status of the isolated heart with that of the *in vivo* heart, and as such, this direct comparison will aid in answering questions concerning the validity of the isolated heart model.

In the present study we used a novel optical technique [14,15], which allowed for the first time quantitative and non-invasive measurements of mitoPO<sub>2</sub> in the intact heart. Following validation of our technique for determination of mitoPO<sub>2</sub> within the heart, our observations demonstrated rather high mean mitoPO<sub>2</sub> values of 35 mm Hg in the *in vivo* heart. However, cardiac mitoPO<sub>2</sub> was considerably heterogeneous, such that 10% of mitochondria in the *in vivo* condition and 30% of mitochondria in the isolated Langendorff-perfused condition still had a mitoPO<sub>2</sub> between 0 and 10 mm Hg, despite the relatively high mean mitoPO<sub>2</sub>. Only in the maximal vasodilated condition did the mitochondrial oxygenation status of the isolated heart mimic that of the *in vivo* heart.

## 2. MATERIALS AND METHODS

### 2.1. Animals

Male Wistar rats (Charles River, Wilmington, MA), 38 animals in total with body weight of 351 ± 7 g, were anesthetized with 60 mg/kg pentobarbital and received 5-aminolevulinic acid (ALA; 200 mg/kg dissolved in PBS (100 mg/ml)) through the tail vein, 2–5 h before experimentation or saline (controls). The protocol was approved by the Animal Research Committee of the Academic Medical Center at the University of Amsterdam. Animal care and handling were performed in accordance with the guidelines for Institutional and Animal Care and Use Committees (IACUC).

### 2.2. Isolated cardiomyocytes

Hearts (n = 4) were excised from pentobarbital-anesthetized animals and cardiomyocytes isolated according to previous reports [21]. Cardiomyocytes were kept in albumin-free, low Ca<sup>2+</sup>-containing Krebs–Henseleit solution until measurements.

### 2.3. Fluorescence microscopy

Fluorescence microscopy was performed using a Leica fluorescence microscope (DM RA HC) with a cooled CCD camera (KX1400, Apogee Instruments, Roseville, CA) and CY3 band pass filter set. Detection of protoporphyrin IX (PpIX) and MitoTracker Green was similar to that previously reported [15]. Cardiomyocytes were incubated with MitoTracker Green (27 nM for 30 min) and con-

traction inhibited with butanedione monoxime (BDM; 20 mM). PpIX bleaches rapidly, and we used this property to separate PpIX fluorescence from other sources of autofluorescence [15]. Two successive illuminations of 30 s were performed while integrating the fluorescence images on the cooled CCD. The second image was subtracted

from the first image using Image-Pro Plus software (Media Cybernetics, Bethesda, MD). The resulting “bleached image” represented the true PpIX signal. MitoTracker Green images were acquired with a 2 s integration time.

### 2.4. Flow cytometry

Cardiomyocytes were isolated from hearts of either ALA-treated or saline-treated animals (control). The PpIX fluorescence was studied in control and ALA cells with a LSRII flow cytometer (LSRII, BD Bioscience San Jose, CA). To study PpIX fluorescence, the viable cardiomyocytes were gated from a FSC (forward scatter) and SSC (side scatter) dotplot, and PpIX was excited by the blue laser (488 nm) and fluorescence was detected at 695 nm.

### 2.5. Imaging cryomicrotome

Hearts from ALA-treated and saline-treated animals were rinsed with saline solution and submerged together in a solution of carboxymethylcellulose sodium solvent (Brunschwig Chemie, Amsterdam) and Indian ink (Royal Talens, Apeldoorn) and frozen at –20 °C in an imaging cryomicrotome [22]. The frozen hearts were serially sectioned from base to apex into 17 μm slices. After each cut, images were taken from the cutting plane of the remaining bulk using a 4000 × 4000 pixel camera (ALTA U16, Apogee Instruments, Roseville, CA) equipped with a 70–180 mm Nikon lens, with excitation set at 510/20 nm and fluorescence detected at 635/30 nm.

### 2.6. Calibration of the PpIX delayed fluorescence lifetime with partial oxygen tension in cardiomyocytes

A cardiomyocyte suspension of 2 ml was placed in a custom-made cell oxygenator [15]. An adjustable gas-mixture of O<sub>2</sub>, N<sub>2</sub> and 5% CO<sub>2</sub> was blown over the cell suspension with %O<sub>2</sub> set at 0, 1, 2, 3, 4 or 5%. Oxygen consumption was inhibited using KCN (10 mM), rotenone (4 μM) and diphenyleioidonium (DPI; 40 μM).

### 2.7. Evaluation of the calibration of the PpIX delayed fluorescence lifetime in isolated hearts

To test the feasibility of the calibration of PpIX delayed fluorescence lifetime obtained in isolated cardiomyocytes for use in the intact heart, we performed PpIX lifetime measurements in Langendorff-perfused hearts (n = 3) perfused with 2 mM potassium cyanide, 25 mM KCl and 0 mM CaCl<sub>2</sub> to prevent contraction and oxygen consumption of the heart. For each heart, the perfusate was equilibrated with two different %O<sub>2</sub> levels between 0 and 7%, balanced with N<sub>2</sub> and 5% CO<sub>2</sub>. Oxygen tension was measured in the inflow just above the heart using a needle-type fiber-optic microsensor (World Precision Instruments, Sarasota, FL).

### 2.8. Isolated mitochondria and effects of ALA administration

Mitochondria were isolated from hearts of animals treated with ALA (200 mg/kg) dissolved in PBS (n = 3) or with PBS only (n = 3), 3–5 h before isolation. Procedures of isolation were as reported previously [23]. In short, hearts were placed in isolation buffer (200 mM mannitol, 50 mM sucrose, 5 mM KH<sub>2</sub>PO<sub>4</sub>, 5 mM MOPS, 1 mM EGTA, and 0.1% BSA) and minced into small pieces; then 5 U/ml protease was added, and the mixture was homogenized. The homogenate was centrifuged at 3220 g for 10 min, and the pellet was resuspended in isolation buffer and centrifuged at 800 g for 10 min. The remaining supernatant was centrifuged at 3220 g for 10 min. The final pellet was resuspended in isolation buffer and kept on ice, and the protein content was determined by the Bradford method.

All procedures were performed at 4 °C. Mitochondrial oxygen consumption was measured polarographically at 37 °C in a respirometer using mitochondria (0.3 mg protein/ml) resuspended in respiration buffer [23]. Respiration was initiated with 10 mM succinate + 10 μM rotenone (state 2 respiration), followed by the addition of 200 μM ADP (state 3 respiration). The respiratory control index (RCI) was calculated as the state-3 to state-4 ratio.

### 2.9. In vivo hearts

Animals (n = 5) were anesthetized with s-ketamine (150 mg/kg) and diazepam (1.5 mg/kg), and maintenance anesthesia was provided through i.v. administration of α-chloralose (30 mg/kg/h). Mechanical ventilation (70 breaths per min, 0.4 inspiration phase, 5 mm Hg PEEP) was started following intubation, and a left thoracotomy was performed to expose the heart [24]. Mean arterial pressure and heart rate were monitored through a fluid-filled catheter positioned in the cannulated carotid artery. Body temperature was maintained at 37 °C. Inspiration oxygen fraction was initially set at 40% and subsequently switched to 100% and finally 10% O<sub>2</sub>. The 40% FiO<sub>2</sub> step was deliberately chosen instead of 20% FiO<sub>2</sub> to ensure compensation for ventilation-perfusion defects due to mechanical ventilation [25] resulting in arterial PO<sub>2</sub> values in the physiological range reported for spontaneously air-breathing animals (~ 120 mm Hg).

### 2.10. Microvascular PO<sub>2</sub> of the in vivo hearts

To compare the mitoPO<sub>2</sub> with other indices of cardiac oxygenation, cardiac microvascular PO<sub>2</sub> (μPO<sub>2</sub>) of the in vivo heart was determined in separate animals (n=4) by the method of oxygen-dependent quenching of the phosphorescence lifetime of intravenously injected Pd-porphyrin (Pd-meso-tetra(4-carboxyphenyl)porphine, Frontier Scientific Inc, Logan, UT). To this end Pd-porphyrin was bound to albumin according to Sinaasappel et al. [26] and intravenously injected (12 mg/kg). Phosphorescence signals were obtained from the in vivo rat heart using a fiber based phosphorimeter [27]. These measurements were performed in a similar in vivo heart model as used for the PpIX determinations, at

FiO<sub>2</sub> of 40%, 100% and 10%, respectively (see description above).

### 2.11. Isolated Langendorff-perfused hearts

Hearts were isolated from pentobarbital-anesthetized animals and perfused at constant flow at 80 mm Hg according to previous reports [28]. Hearts (n = 6) were paced at 300 beats/min, and a balloon was inserted in the left ventricle to record left ventricular pressure. The perfusate contained glucose (10 mM/l), pyruvate (0.1 mM/l), lactate (1 mM/l), and glutamine (0.5 mM/l) as substrates. Venous oxygen tension was measured in the pulmonary artery using a needle-type fiber-optic microsensor (World Precision Instruments, Sarasota, FL). Perfusate was equilibrated with either 95%/0%/5%, 70%/25%/5% or 45%/ 50%/5% of O<sub>2</sub>/N<sub>2</sub>/CO<sub>2</sub>, respectively, using separate calibrated gas bottles. In a separate series (n = 6), the effect of maximal vasodilatation (100 μM adenosine and 1 μM nitroprusside) on the oxygenation status was studied.

### 2.12. Delayed fluorescence setup

The setup was essentially the same as that described previously [14]. In short, the excitation source was a tunable laser providing pulses of 2–4 ns (510 nm, 0.2 mJ/pulse). The detector was a red-sensitive photomultiplier tube combined with a monochromator set at 640 nm. Signal processing was done with a home-built integrator with an integration time of 3.5 μs and a reset time of 0.5 μs. A PC-based data-acquisition system sampled the signal at 250 kHz and averaged 64 laser pulses (repetition rate 20 Hz) prior to analysis. Controller and data-acquisition software was written in LabView (Version 7.1, National Instruments, Austin, TX).

### 2.13. Recovery of mitoPO<sub>2</sub> histograms

In case of a non-homogenous mitoPO<sub>2</sub>, the delayed fluorescence signal can be described generally by an integral over an exponential kernel:

$$y(t) = \int_0^t \exp(-\lambda t) f(\lambda)$$

where  $f(\lambda)$  denotes the spectrum of reciprocal lifetimes that should be determined from the finite data set  $y(t)$ . According to Golub et al. [19], a detailed recovery of the underlying oxygen distribution can be obtained by assuming that the delayed fluorescence signal can be described by a sum of rectangular distributions with adequately small chosen width ( $2\delta$ ), resulting in the following fit equation:

$$Y^*(t) = Y(t) [\exp(k_0 t) k_q \delta t / \sinh(k_0 \delta t)] = \sum w_i \exp(-k_q Q_i t)$$

where  $Y(t)$  is the normalized phosphorescence data,  $k_0$  is the first-order rate constant for delayed fluorescence decay in the absence of oxygen,  $k_q$  is the quenching constant,

and  $w_i$  is the weight factor for the according bin with central  $PO_2Q_i$  and width  $2\delta$  ( $w_i \geq 0$  and  $\sum w_i = 1$ ). Recently, this approach was successfully used by our group for the recovery of microvascular  $PO_2$  histograms from phosphorescence lifetime measurements [29] and mito $PO_2$  histograms from delayed fluorescence lifetime measurements in rat liver in vivo [14]. Recovery of oxygen histograms from the photometric signal was performed with the GraphPad Prism package (Version 4, GraphPad Software Inc, San Diego, CA). Mean mito $PO_2$  values were calculated from the retrieved mito $PO_2$  histograms.

### 2.14. Chemicals

MitoTracker Green was obtained from Invitrogen (Carlsbad, CA). Pentobarbital was obtained from Ceva (Sante Animale B.V., Maassluis, The Netherlands), Diazepam from Centrafarm (Etten-Leur, The Netherlands), S-ketamine from Pfizer B.V. (Capelle a/d IJssel, The Netherlands) and PBS was obtained from Baxter. ALA,  $\alpha$ -chloralose, KCN, rotenone, DPI, BDM,  $KH_2PO_4$ , MOPS, EGTA, BSA, protease, mannitol, succinate, pyruvate, sucrose, lactate, glucose, glutamine, adenosine, nitroprusside and the compounds for the Krebs–Henseleit buffer were all obtained from Sigma (St. Louis, MO).

### 2.15. Presentation of data

The data are presented as mean  $\pm$  SEM, unless stated otherwise.

## 3. RESULTS

### 3.1. Subcellular location of PpIX

Four hours after ALA administration, we observed a similar nonhomogeneous cellular distribution of PpIX fluorescence and MitoTracker Green signals in isolated cardiomyocytes (Fig. 1A). The very high colocalization of both images indicates the mitochondrial localization of the PpIX signal.

### 3.2. Calibration of the mitochondrial signal

Oxygen-dependent delayed fluorescence traces were clearly detectable from cardiomyocyte suspensions subjected to various oxygen levels. The calibration curve of reciprocal lifetime versus partial oxygen pressure for cardiomyocytes demonstrated a quenching constant ( $k_q$ ) that was similar to the  $k_q$  obtained in hepatocytes [14], indicating the general applicability of the calibration constant across organs (Fig. 1B). Lifetime under zero oxygen conditions ( $\tau_0$ ) was 0.8 ms.

### 3.3. ALA treatment does not affect mitochondrial oxygen consumption (Fig. 1C)

In order to examine whether ALA-induced mitochondrial accumulation of PpIX affected mitochondrial oxygen consumption, mitochondria were isolated from ALA-treated and

vehicle-treated animals. PpIX accumulation had no effect on respiration, coupling ratio or oxidative phosphorylation of the mitochondria, demonstrating that ALA-treatment did not disturb oxygen consumption.

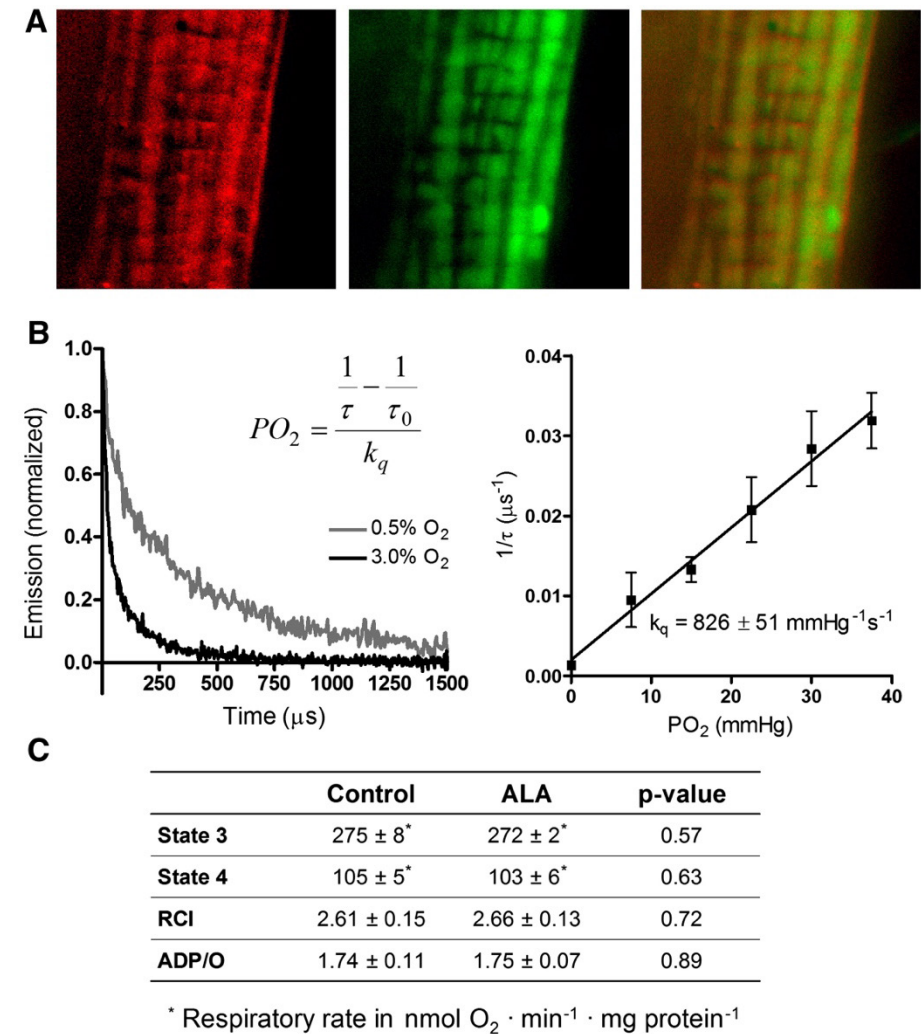


**Figure 1.** PpIX in cardiomyocytes and mitochondria. (A) Fluorescence microscopy showing (from left to right) PpIX fluorescence, MitoTracker Green fluorescence and colocalization of PpIX and Mitotracker Green fluorescence in isolated cardiomyocyte. (B) In vitro calibration experiments showing two examples of delayed fluorescence traces recorded at two different oxygen concentrations and the reciprocal delayed fluorescence lifetime ( $1/\tau$ ) versus  $PO_2$  in suspensions of isolated cardiomyocytes. Inserted is the Stern–Volmer equation in which  $k_q$  is the quenching constant and  $\tau_0$  is the lifetime at zero oxygen. Lifetimes were retrieved from the data by a mono-exponential non-linear Marquart–Levenberg fitting procedure. Shown are the mean and SD. (C) Function of mitochondria isolated from hearts of control or ALA-treated animal showing state 3 and 4 respiration, respiratory control index (RCI) and the P/O ratio.



### 3.4. Validation of the calibration constants in isolated rat heart

To test the validity of the calibration constants obtained from the isolated cardiomyocytes in intact heart we measured the delayed fluorescence lifetime in isolated Langendorff-perfused hearts from ALA treated animals. Oxygen consumption was blocked by addition of cyanide and measurements were performed at varying oxygen tensions in the perfusate. Blockage of oxygen consumption abolishes the oxygen gradients in the tissue and  $\text{mitoPO}_2$  should equal the  $\text{PO}_2$  in the perfusate. Mono-exponential fitting of the delayed fluorescence signals showed clearly oxygen-dependent delayed fluorescence lifetimes (Fig. 2A). Conversion of the lifetimes into  $\text{mitoPO}_2$  values using the calibration constants  $kq = 826 \text{ mm Hg} \cdot 1 \text{ s}^{-1}$  and  $\tau_0 = 0.8 \text{ ms}$  obtained from cardiomyocyte suspensions resulted in excellent agreement between  $\text{mitoPO}_2$  and the  $\text{PO}_2$  in the perfusate (Fig. 2B).

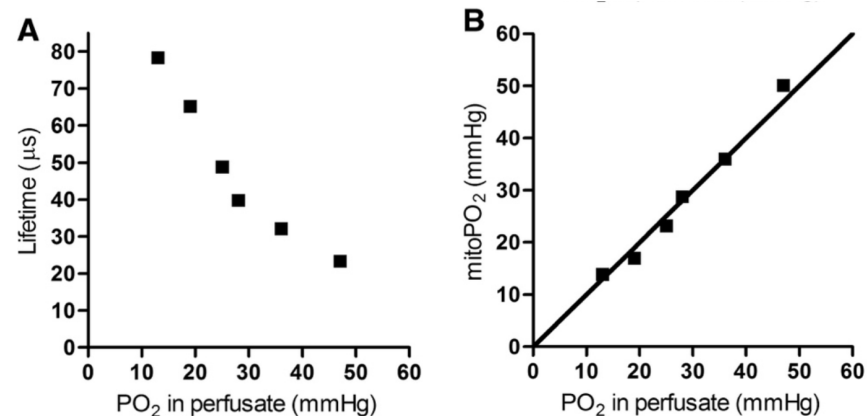


**Figure 2.** Evaluation of the calibration constants in isolated rat heart. (A) Measured delayed fluorescence lifetime versus the  $\text{PO}_2$  in the perfusate after cessation of mitochondrial oxygen consumption by addition of cyanide. Lifetimes were retrieved from the data by a mono-exponential non-linear Marquart–Levenberg fitting procedure. (B)  $\text{mitoPO}_2$  versus the  $\text{PO}_2$  in the perfusate.  $\text{mitoPO}_2$  was calculated from the delayed fluorescence lifetimes in panel A using the quenching constants obtained in suspensions of cardiomyocytes. The solid line is the line of equality.

### 3.5. Distribution of ALA enhanced PpIX

Our analysis method assumes that PpIX is homogeneously distributed in the measurement volume. For proper interpretation of our data it is essential to know to what extent this assumption holds in practice. Images from the cryomicrotome clearly showed increased, diffuse and near homogeneous red fluorescence throughout the entire myocardium after ALA administration (Fig. 3A). Some local differences in fluorescence intensity were visible, but this comprised relatively large areas also visible in the control heart. Therefore, these differences might be due to fixation and cutting artifacts instead

of true heterogeneities in the PpIX distribution. This was indeed confirmed by the flow cytometry experiments, which showed a uniform emergence of red fluorescence after administration of ALA (Fig. 3B).

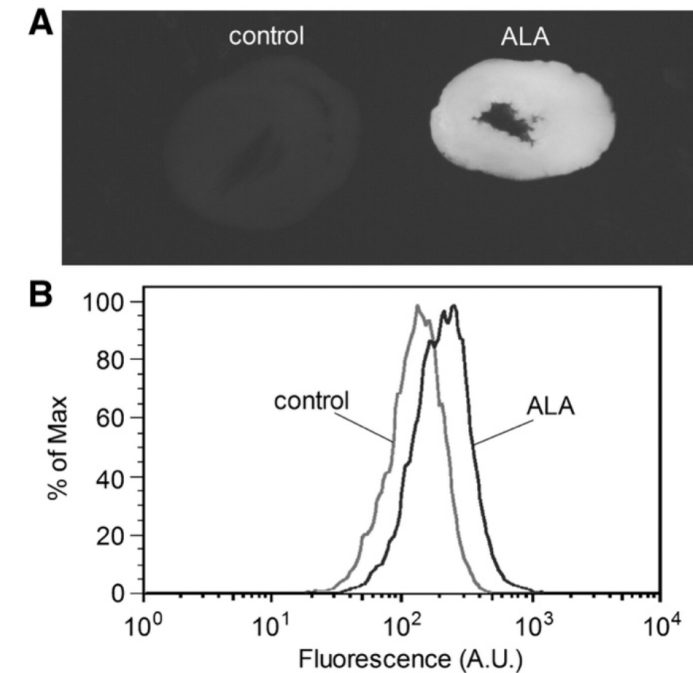


**Figure 3.** Distribution of ALA enhanced PpIX in the myocardium. (A) Typical example of an image obtained in the cryomicrotome showing PpIX fluorescence in hearts from a control (saline treated) and an ALA treated animal. Excitation at 510 nm, emission at 630 nm. (B) Flow cytometry in cardiomyocytes isolated from a control and ALA treated animal. Excitation at 488 nm, emission at 695 nm. The histograms are normalized to the maximal counted number of cells having equal fluorescence intensity (% of Max), i.e. the peaks of the individual histograms.

### 3.6. $\text{mitoPO}_2$ in the in vivo heart

$\text{FiO}_2$ -dependent delayed fluorescence signals were obtained from in vivo rat heart (Fig. 4A). At 40%  $\text{FiO}_2$ , the largest fraction (26%) of mitochondria was found in the range of 10 – 20 mm Hg, with a mean  $\text{mitoPO}_2$  of  $35 \pm 5$  mm Hg (Fig. 4B). Increasing  $\text{FiO}_2$  to 100% had no major effect on the  $\text{mitoPO}_2$  distribution; however, reducing  $\text{FiO}_2$  to 10% resulted in large changes: 46% of the mitochondria were in the lowest oxygen range of 0 – 10 mm Hg (Fig. 4B). The imposed  $\text{FiO}_2$  changes were accompanied by alterations in arterial oxygen tension and blood pressure, without changes in arterial  $\text{CO}_2$  tension (Table 1).

In separate experiments, we measured microvascular  $\text{PO}_2$  ( $\mu\text{PO}_2$ ) using the exogenous dye Pd-porphyrin for the three different  $\text{FiO}_2$ .  $\mu\text{PO}_2$  amounted to  $67 \pm 3$ ,  $108 \pm 9$  and  $22$

$\pm 4$  mm Hg, at 40%, 100% and 10%  $\text{FiO}_2$ , respectively.

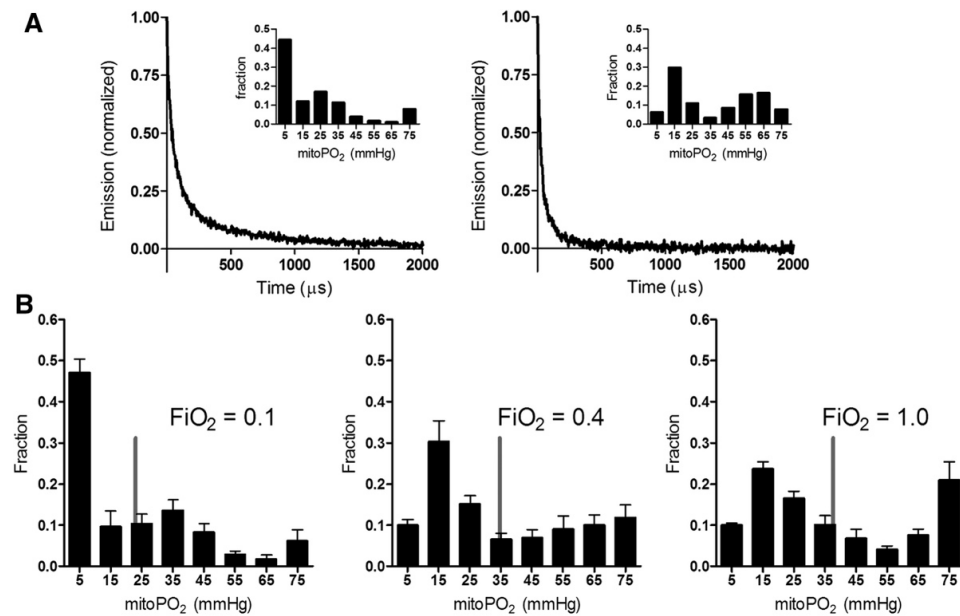


**Figure 4.** MitoPO<sub>2</sub> in the in vivo heart. (A) Delayed fluorescence traces from the heart of an animal ventilated with 10% oxygen (left panel) and 40% oxygen (right panel). (B) Distributions of mitoPO<sub>2</sub> at different  $\text{FiO}_2$  ( $n = 5$ ). The grey lines denote the mean mitoPO<sub>2</sub>.

**Table 1.** Hemodynamics and blood gas values of rats in vivo ( $n = 5$ )

$\text{FiO}_2$	MAP	Heart rate	$\text{PaO}_2$	$\text{PaCO}_2$	tHb
%	mm Hg	Beats/min	mm Hg	mm Hg	mmol/l
40	$99 \pm 5$	$351 \pm 21$	$115 \pm 5$	$41 \pm 3$	$6.9 \pm 0.5$
100	$103 \pm 6$	$336 \pm 20$	$331 \pm 20$	$43 \pm 6$	$6.2 \pm 0.7$
10	$50 \pm 5$	$305 \pm 15$	$39 \pm 3$	$40 \pm 2$	$6.2 \pm 0.7$

$\text{FiO}_2$  = inspiration oxygen %; MAP = mean arterial pressure;  $\text{PaO}_2$  = partial arterial oxygen tension;  $\text{PaCO}_2$  = partial arterial carbon dioxide tension; tHb = total hemoglobin. Values are given as mean  $\pm$  SEM.

### 3.7. MitoPO<sub>2</sub> in the Langendorff-perfused heart

Delayed fluorescence signals were obtained from isolated hearts, showing decreasing decay times (shorter  $\tau$ ) with increasing percentage of oxygen ( $\%O_2$ ) in the perfusate or with increased flow (going from the normal vasodilated to the maximal vasodilated condition) (Fig. 5A). The recovery of mitoPO<sub>2</sub> histograms provides a detailed view of the effects of  $\%O_2$  and vasodilatation on mitochondrial oxygenation (Fig. 5B). Only at maximal oxygenation (95%) and maximal vasodilatation did mitoPO<sub>2</sub> start to approach

a normal distribution in the isolated heart, with a mean mitoPO<sub>2</sub> of  $40 \pm 3$  mm Hg. The normally perfused Langendorff-condition had a mean mitoPO<sub>2</sub> of  $29 \pm 5$  mm Hg (at 95% oxygen). A dichotomous distribution was observed, with the largest fraction of mitochondria falling into the lowest oxygen range (0 – 10 mm Hg). The fraction of mitochondria in the lowest oxygen range increased further as the  $\%O_2$  was decreased to 70% and 45%.

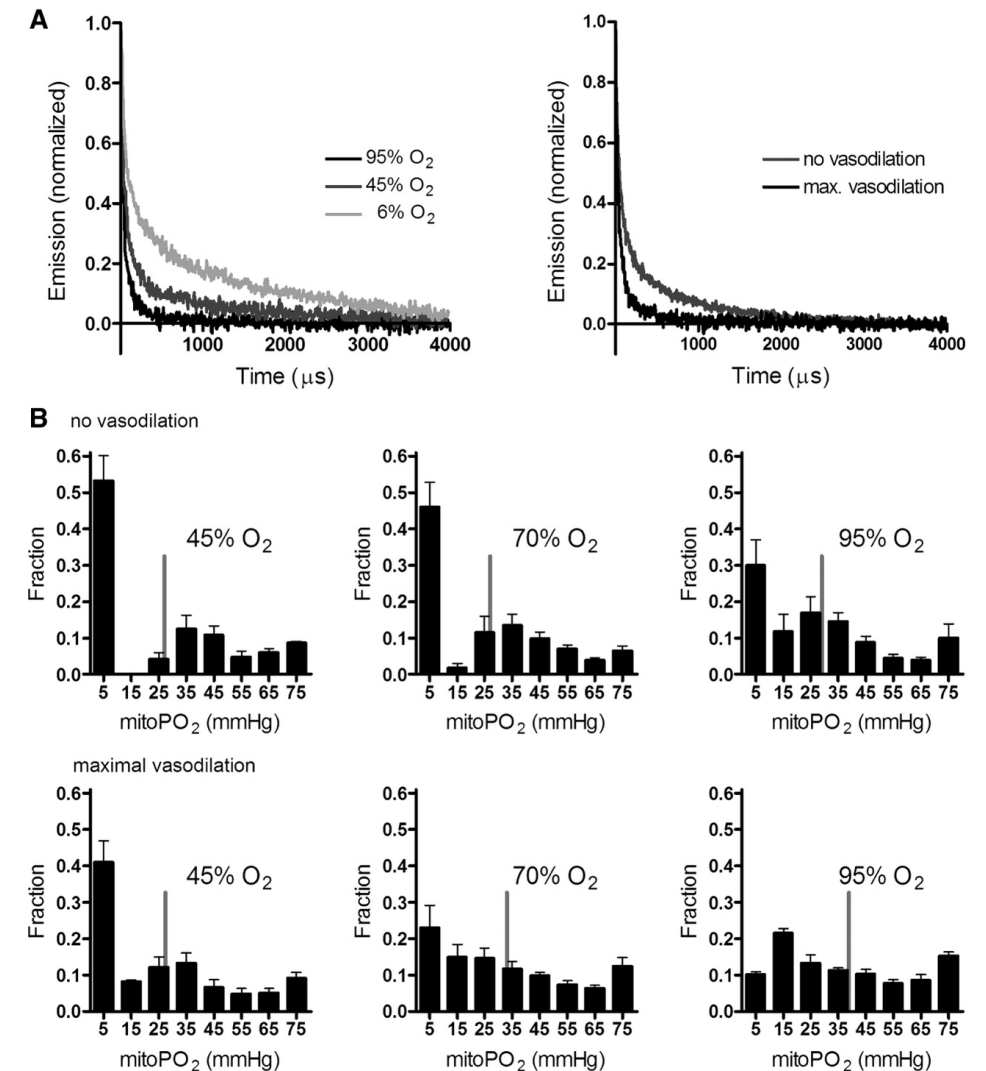


**Figure 5.** MitoPO<sub>2</sub> in the isolated Langendorff-perfused heart. (A) Examples of delayed fluorescence traces for 95%, 45%, and 6% oxygen saturated perfusate in a vasodilated heart (left panel) and delayed fluorescence traces of a normal and maximally vasodilated heart (right panel). (B) Distributions of mitoPO<sub>2</sub> at different  $\%O_2$  in perfusate for normal ( $n = 6$ ) and maximally vasodilated hearts ( $n = 6$ ). The grey lines denote the mean mitoPO<sub>2</sub>.

Decreasing %O<sub>2</sub> was associated with decreased mechanical performance and oxygen consumption of the hearts, whereas maximal vasodilatation increased mechanical performance and oxygen consumption (Table 2). It should be noted that oxygen consumption increased with vasodilatation due to the large coronary flow increases, despite the increase in venous PO<sub>2</sub> with vasodilatation for each level of % O<sub>2</sub> perfusate. Increasing the heart rate from 300 to 400 BPM did not change the mitoPO<sub>2</sub> distribution in hearts without vasodilatation (Fig. 6). In hearts with maximal vasodilatation there appeared to be a tendency towards lower mitoPO<sub>2</sub> values at higher heart rate without reaching significance in any of the bins (paired non-parametric testing).

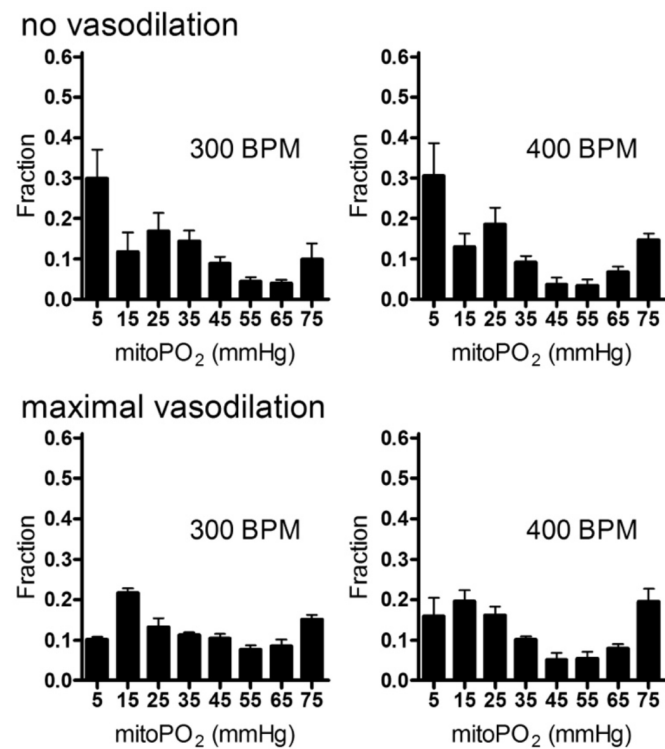


**Figure 6.** Response of mitoPO<sub>2</sub> to a heart rate step in the Langendorff-perfused heart. Distributions of mitoPO<sub>2</sub> at 300 and 400 beats per minute (BPM) with and without maximal vasodilatation and with 95% oxygen saturated perfusate.

**Table 2.** Functional characteristics of isolated Langendorff-perfused rat hearts

O <sub>2</sub>	Flow	P <sub>perf</sub>	P <sub>sys</sub>	P <sub>dia</sub>	VPO <sub>2</sub>	MVO <sub>2</sub> mol/min/G <sub>ww</sub>	RPP(× 10 <sup>3</sup> )
% perfusate	ml/min/G <sub>ww</sub>	mm Hg	mm Hg	mm Hg	mm Hg	μmol/min/G <sub>ww</sub>	mm Hg/min
95	13.3 ± 0.8	78 ± 2	117 ± 7	2 ± 1	153 ± 9	9.3 ± 0.5	35.1 ± 2.2
70	13.3 ± 0.8	80 ± 5	105 ± 12	2 ± 1	82 ± 7	7.4 ± 0.4	31.6 ± 3.5
45	13.3 ± 0.8	89 ± 11	71 ± 7	2 ± 1	36 ± 4	5.1 ± 0.2	21.4 ± 2.2
95	23.1 ± 0.7	79 ± 1	138 ± 5	2 ± 1	295 ± 21	11.8 ± 0.8	41.4 ± 1.5
70	23.1 ± 0.7	83 ± 4	123 ± 7	2 ± 1	205 ± 14	9.1 ± 0.6	35.1 ± 1.9
45	23.1 ± 0.7	96 ± 7	106 ± 8	2 ± 1	91 ± 11	7.1 ± 0.5	31.7 ± 2.1

Values are given for hearts ( $n = 6$ ) perfused at normal vasodilatation (normal flow) and at maximal vasodilatation ( $n = 6$ ; high flow) for different % oxygen in the perfusate.

G<sub>ww</sub> = gram, wet weight; P<sub>perf</sub> = perfusion pressure; P<sub>sys</sub> = systolic pressure; P<sub>dia</sub> = diastolic pressure; VPO<sub>2</sub> = venous oxygen tension; MVO<sub>2</sub> = oxygen consumption, RPP = rate pressure product (P<sub>sys</sub> × heart rate). Values are given as mean ± SEM.

## 4. DISCUSSION

This study is, to our knowledge, the first to describe direct measurements of mitochondrial oxygen tension within the intact heart. The main findings provide evidence that mean cardiac mitoPO<sub>2</sub> in vivo has a relatively high value of 35 mm Hg. Importantly, we found that mitoPO<sub>2</sub> was heterogeneously distributed within the rat heart in vivo, such that even when mean mitoPO<sub>2</sub> was 35 mm Hg, 10% of mitochondria still had a low PO<sub>2</sub> between 0 and 10 mm Hg. In addition, the frequently used isolated heart preparation operates at a lower mitochondrial oxygenation status than that of the in vivo heart.

### 4.1. In vivo myocardial PO<sub>2</sub> and mitoPO<sub>2</sub> heterogeneity

Because oxygen transport to the mitochondria is driven by a concentration gradient determined by consumption in the mitochondria, the oxygen tension in the mitochondrial compartment should be at the lowest end of oxygen tensions present compared to other [4] compartments (vascular, interstitial, cytosolic) of the intact heart. The mean mitoPO<sub>2</sub> value of 35 ± 5 mm Hg reported here is in accordance with tissue PO<sub>2</sub> values of 45 ± 8 mm Hg [13] and microvascular PO<sub>2</sub> values of 50 – 70 mm Hg found in the present and past studies [12], but is much higher than anticipated from estimates derived from cytosolic/interstitial/vascular measurements of 3 – 17 mm Hg [6 – 11]. Interestingly, this observation coincides with recent findings of oxygen pressure in tissues other than heart [30]. Myoglobin saturation studies in in vivo pig hearts, using either optical reflectance spectroscopy [31] or 1H NMR [32], were unable to detect desaturation of myoglobin. Knowing that these techniques can detect myoglobin desaturation only when intracellular PO<sub>2</sub> falls below 22 mm Hg [32], and that only an average myoglobin saturation is detected, these studies indicate an average cytosolic PO<sub>2</sub> above 22 mm Hg. Thus, the values obtained

with myoglobin saturation techniques are commensurate with our averaged mitoPO<sub>2</sub> of 35 mm Hg. Only recently has consensus been reached that the levels of oxygen in the tissue are much higher than originally thought of, due to the development of new techniques with increased accuracy [30]. The present study with the use of a novel technique clearly indicates that this new consensus may also hold for the heart.

Although the averaged mitoPO<sub>2</sub> observed in vivo was higher than anticipated, it is important to take into account the heterogeneity of mitoPO<sub>2</sub> within the heart. The observed heterogeneity in mitoPO<sub>2</sub> in the present study extends previously observed heterogeneities in, for example, blood flow and oxygen consumption down to the level of the mitochondria [12,16,17]. In addition, the mitoPO<sub>2</sub> heterogeneity indicates that approximately 10% of the mitochondria in the in vivo heart are exposed to a PO<sub>2</sub> between 0 and 10 mm Hg. Isolated mitochondria studies have demonstrated that mitochondrial oxidative phosphorylation is dependent on oxygen concentrations at PO<sub>2</sub> < 12-15 mm Hg [1,3,5]. This implies that some fraction of the mitochondria within the in vivo heart may well be partially controlled by the prevailing oxygen tension. That myocardial oxygen may be limiting is also supported by studies in myoglobin-knockout mice. Although the first studies in these mice concluded that myoglobin is of no physiological consequence for cardiac function [33], subsequent studies demonstrated that multiple compensatory mechanism in these mice were present [34], indicating an important role for myoglobin in oxygen delivery. Considering the major role that mitochondria play in cellular oxygen sensing [4], the quantitative determination of mitoPO<sub>2</sub> in the in vivo condition provides important information for the design of oxygen critical experiments.

#### 4.2. Isolated versus in vivo hearts

In non-vasodilated Langendorff-perfused isolated hearts, the fraction of mitochondria with oxygen tensions between 0 and 10 mm Hg increased to 30%, as compared to the 10% observed in the in vivo condition. Interestingly, studies using three-dimensional microvascular modeling together with myoglobin saturation information [35,36] have also concluded that approximately 15–30% of the myocardium in the Langendorff-perfused heart was hypoxic. Alleviating the 30% “hypoxic mitochondrial area” to 10% by increasing perfusate flow was indeed accompanied by increased myocardial oxygen consumption and mechanical performance, suggesting at least that the normal perfused isolated heart was oxygen limited. This data agree with older literature suggesting that the isolated heart is partially hypoxic [37,38]. Our data indicate that the oxygenation status of the isolated Langendorff-perfused heart model is comparable to that of the in vivo heart only in the maximally vasodilated condition.

#### 4.3. Methodological considerations

The PpIX delayed fluorescence technique provides a powerful tool for monitoring mitoPO<sub>2</sub> in cardiac muscle. The underlying lifetime technology is highly robust in that

it needs no recalibration and is immune to changes in tissue optical properties and tissue geometry, important features in a beating heart. A practical advantage is also that the technique does not need a physical contact with the heart, like oxygen electrodes, and is not locally destructive. As an optical technique it is scalable from microscopic to macroscopic implementations providing extensive opportunities for study of the heterogeneity of mitoPO<sub>2</sub> and its cause. Because of its resemblance to phosphorescence lifetime measurements further technological developments could provide e.g. imaging [39], 3-dimensional scanning by two-photon excitation [40] and multi-wavelength excitation [29]. The main disadvantage is the relatively small penetration depth of light in tissues. Therefore, the technique is not non-invasive for the whole organism (like e.g. MRI), but one always needs to make the organ or tissue accessible to the optical device. In the present study we converted lifetime distribution to oxygen histograms, based on the assumption that the heterogeneity in delayed fluorescence lifetimes arises from a volume with homogeneous distribution of PpIX and heterogeneous concentration of oxygen [19]. Such an assumption is generally relied on when converting phosphorescence lifetime distributions into quencher distributions [19,41,42]. In the present study, fluorescence microscopy of freshly isolated cardiomyocytes from ALA-treated animals showed the typical mitochondrial fluorescence patterns well known from NADH autofluorescence microscopy [43,44], indicating that PpIX synthesis is not sequestered within a cardiomyocyte. On a more macroscopic level, ALA administration induces a diffuse and near homogenous PpIX fluorescence throughout the heart as observed by the cryomicrotome and flow cytometry experiments.

Based on the work of Gandjbakhche et al. [45] the measurement depth with excitation at 510 nm is estimated to be between 400 and 500 μm, due to absorption and scatter of the excitation light. Sinaasappel et al. [46] estimated a catchment depth of 500 μm, using Monte-Carlo simulations on the penetration depth of 520 nm excitation light in phosphorescence lifetime measurements in the intestine. Assuming a left ventricular free wall thickness of 1.5 mm during diastole and 2.5–3.0 mm during systole, our mitoPO<sub>2</sub> measurements mainly reflect the oxygenation of the epicardium. Therefore, the mitoPO<sub>2</sub> distributions are unlikely to be caused by differences in endocardial and epicardial oxygenation. We previously demonstrated in rat liver that diffusion of ambient oxygen into the tissue has limited influence on the shape of mitoPO<sub>2</sub> histograms [14]. Oxygen in the ambient atmosphere marginally contributes to the highest PO<sub>2</sub> bins without altering the overall shape of the histograms. Exposure of epicardial surface to air is therefore very likely not the cause of the observed heterogeneity in mitoPO<sub>2</sub>.

The delayed fluorescence lifetime in vivo may also be affected by bound versus unbound PpIX and pH. Theoretically, unbound PpIX could mimic a very high PO<sub>2</sub> and distort the mitoPO<sub>2</sub> histograms. Unbound PpIX has a lifetime which is too short to be resolved with our current setup and therefore will not contribute to our signal. Furthermore, binding of PpIX with different environments could affect the lifetime

measurements by introducing additional lifetimes at a homogenous  $PO_2$ . However, the linear relationship between reciprocal delayed fluorescence lifetime and  $PO_2$  after abolishing oxygen gradients by addition of cyanide, as predicted by the Stern–Volmer equation [26,47] and obtained by monoexponential fitting on the data, argues against such influence. Physiological changes in pH have in general only minor effects on the quenching constants of phosphorescence [26,48,49] and delayed fluorescence [15]. Overall, despite the assumptions made in the current analysis and the possible caveats this introduces into the interpretation of the data, we regard PpIX delayed fluorescence as a valuable addition to the arsenal of techniques that allows new insight into myocardial oxygenation.

In summary, the data of the present study revealed that the amount of oxygen present within the mitochondria of the intact heart is higher than previously anticipated, is heterogeneously distributed and is lower in the often-used tyrode perfused isolated heart model as compared to the in vivo heart. Together, these results provide a first quantitative characterization of mitochondrial oxygenation within the intact heart in both the in vivo and isolated condition.

#### Acknowledgments

This work was partly sponsored by The Netherlands Organization for Scientific Research (ZON-MW 911-05-008) and in part by a Technological Collaboration Grant (TSGE 1048) from the Dutch Ministry of Economic Affairs. J. Stap was funded in part by a grant from the Dutch Cancer Society.

## REFERENCES

- Hoffman DL, Salter JD, Brookes PS. Response of mitochondrial reactive oxygen species generation to steady-state oxygen tension: implications for hypoxic cell signaling. *Am J Physiol, Heart Circ Physiol* 2007;292:H101–8.
- Maxwell PH, Wiesener MS, Chang GW, Clifford SC, Vaux EC, Cockman ME, et al. The tumour suppressor protein VHL targets hypoxia-inducible factors for oxygen-dependent proteolysis. *Nature* 1999;399:271–5.
- Rumsey WL, Schlosser C, Nuutinen EM, Robiolio M, Wilson DF. Cellular energetics and the oxygen dependence of respiration in cardiac myocytes isolated from adult rat. *J Biol Chem* 1990;265:15392–402.
- Ward JP. Oxygen sensors in context. *Biochim Biophys Acta* 2008;1777:1–14.
- Wilson DF, Rumsey WL, Green TJ, Vanderkooi JM. The oxygen dependence of mitochondrial oxidative phosphorylation measured by a new optical method for measuring oxygen concentration. *J Biol Chem* 1988;263:2712–8.
- Rumsey WL, Pawlowski M, Lejavardi N, Wilson DF. Oxygen pressure distribution in the heart in vivo and evaluation of the ischemic “border zone”. *Am J Physiol* 1994;266:H1676–80.
- Trochu JN, Bouhour JB, Kaley G, Hintze TH. Role of endothelium-derived nitric oxide in the regulation of cardiac oxygen metabolism: implications in health and disease. *Circ Res* 2000;87:1108–17.
- Zhao X, He G, Chen YR, Pandian RP, Kuppusamy P, Zweier JL. Endothelium-derived nitric oxide regulates postischemic myocardial oxygenation and oxygen consumption by modulation of mitochondrial electron transport. *Circulation* 2005;111:2966–72.
- Gayekski TE, Honig CR. Intracellular  $PO_2$  in individual cardiac myocytes in dogs, cats, rabbits, ferrets, and rats. *Am J Physiol* 1991;260:H522–31.
- Gnaiger E, Lassnig B, Kuznetsov A, Rieger G, Margreiter R. Mitochondrial oxygen affinity, respiratory flux control and excess capacity of cytochrome c oxidase. *J Exp Biol* 1998;201:1129–39.
- Wittenberg BA, Wittenberg JB. Transport of oxygen in muscle. *Annu Rev Physiol* 1989;51:857–78.
- Zuurbier CJ, van Iterson M, Ince C. Functional heterogeneity of oxygen supply–consumption ratio in the heart. *Cardiovasc Res* 1999;44:488–97.
- Al-Obaidi MK, Etherington PJ, Barron DJ, Winlove CP, Pepper JR. Myocardial tissue oxygen supply and utilization during coronary artery bypass surgery: evidence of microvascular no-reflow. *Clin Sci (Lond)* 2000;98:321–8.
- Mik EG, Johannes T, Zuurbier CJ, Heinen A, Houben-Weerts JH, Balestra GM, et al. In vivo mitochondrial oxygen tension measured by a delayed fluorescence lifetime technique. *Biophys J* 2008;95:3977–90.
- Mik EG, Stap J, Sinaasappel M, Beek JF, Aten JA, van Leeuwen TG, et al. Mitochondrial  $PO_2$  measured by delayed fluorescence of endogenous protoporphyrin IX. *Nat Methods* 2006;3:939–45.
- Decking UK. Spatial heterogeneity in the heart: recent insights and open questions. *News Physiol Sci* 2002;17:246–50.
- Yipintsoi T, Dobbs Jr WA, Scanlon PD, Knopp TJ, Bassingthwaite JB. Regional distribution of diffusible tracers and carbonized microspheres in the left ventricle of isolated dog hearts. *Circ Res* 1973;33:573–87.
- Takahashi E. Anoxic cell core can promote necrotic cell death in cardiomyocytes at physiological extracellular  $PO_2$ . *Am J Physiol, Heart Circ Physiol* 2008;294: H2507–15.

19. Golub AS, Popel AS, Zheng L, Pittman RN. Analysis of phosphorescence in heterogeneous systems using distributions of quencher concentration. *Biophys J* 1997;73:452–65.
20. Kammermeier H. Isolated, (Langendorff) hearts perfused with an aqueous buffer (should) have excess oxygen availability. *Basic Res Cardiol* 1994;89:545–8.
21. ter Welle HF, Baartscheer A, Fiolet JW, Schumacher CA. The cytoplasmic free energy of ATP hydrolysis in isolated rod-shaped rat ventricular myocytes. *J Mol Cell Cardiol* 1988;20:435–41.
22. Spaan JA, ter Wee R, van Teeffelen JW, Streekstra G, Siebes M, Kolyva C, et al. Visualisation of intramural coronary vasculature by an imaging cryomicrotome suggests compartmentalisation of myocardial perfusion areas. *Med Biol Eng Comput* 2005;43:431–5.
23. Heinen A, Camara AK, Aldakkak M, Rhodes SS, Riess ML, Stowe DF. Mitochondrial Ca<sup>2+</sup>-induced K<sup>+</sup> influx increases respiration and enhances ROS production while maintaining membrane potential. *Am J Physiol, Cell Physiol* 2007;292:C148–56.
24. Heinen A, Huhn R, Smeele KM, Zuurbier CJ, Schlack W, Preckel B, et al. Helium- induced preconditioning in young and old rat heart: impact of mitochondrial Ca (2+)-sensitive potassium channel activation. *Anesthesiology* 2008;109:830–6.
25. Nunn JF, Bergmann NA, Coleman AJ. Factors influencing the arterial oxygen tension during anaesthesia with artificial ventilation. 1965. *Br J Anaesth* 1998;80:860–76.
26. Sinaasappel M, Ince C. Calibration of Pd-porphyrin phosphorescence for oxygen concentration measurements in vivo. *J Appl Physiol* 1996;81:2297–303.
27. Mik EG, Donkersloot C, Raat NJ, Ince C. Excitation pulse deconvolution in luminescence lifetime analysis for oxygen measurements in vivo. *Photochem Photobiol* 2002;76:12–21.
28. Zuurbier CJ, Ince C. Post-ischaemic changes in the response time of oxygen consumption to demand in the isolated rat heart are mediated partly by calcium and glycolysis. *Pflugers Arch* 2002;443:908–16.
29. Johannes T, Mik EG, Ince C. Dual-wavelength phosphorimetry for determination of cortical and subcortical microvascular oxygenation in rat kidney. *J Appl Physiol* 2006;100(4):1301–10.
30. Wilson DF. Quantifying the role of oxygen pressure in tissue function. *Am J Physiol, Heart Circ Physiol* 2008;294:H11–3.
31. Arai AE, Kasserra CE, Territo PR, Gandjbakhche AH, Balaban RS. Myocardial oxygenation in vivo: optical spectroscopy of cytoplasmic myoglobin and mitochondrial cytochromes. *Am J Physiol* 1999;277:H683–97.
32. Murakami Y, Zhang Y, Cho YK, Mansoor AM, Chung JK, Chu C, et al. Myocardial oxygenation during high work states in hearts with postinfarction remodeling. *Circulation* 1999;99:942–8.
33. Garry DJ, Ordway GA, Lorenz JN, Radford NB, Chin ER, Grange RW, et al. Mice without myoglobin. *Nature* 1998;395:905–8.
34. Godecke A, Fogel U, Zanger K, Ding Z, Hirchenhain J, Decking UK, et al. Disruption of myoglobin in mice induces multiple compensatory mechanisms. *Proc Natl Acad Sci U S A* 1999;96:10495–500.
35. Beard DA, Schenkman KA, Feigl EO. Myocardial oxygenation in isolated hearts predicted by an anatomically realistic microvascular transport model. *Am J Physiol, Heart Circ Physiol* 2003;285:H1826–36.
36. Ejike JC, Arakaki LS, Beard DA, Ciesielski WA, Feigl EO, Schenkman KA. Myocardial oxygenation and adenosine release in isolated guinea pig hearts during changes in contractility. *Am J Physiol, Heart Circ Physiol* 2005;288:H2062–7.
37. Heineman FW, Kupriyanov VV, Marshall R, Fralix TA, Balaban RS. Myocardial oxygenation in the isolated working rabbit heart as a function of work. *Am J Physiol* 1992;262:H255–67.
38. van Beek JH, Bouma P, Westerhof N. Oxygen uptake in saline-perfused rabbit heart is decreased to a similar extent during reductions in flow and in arterial oxygen concentration. *Pflugers Arch* 1989;414:82–8.
39. Rumsey WL, Vanderkooi JM, Wilson DF. Imaging of phosphorescence: a novel method for measuring oxygen distribution in perfused tissue. *Science* 1988;241: 1649–51.
40. Mik EG, van Leeuwen TG, Raat NJ, Ince C. Quantitative determination of localized tissue oxygen concentration in vivo by two-photon excitation phosphorescence lifetime measurements. *J Appl Physiol* 2004;97:1962–9.
41. Vinogradov SA, Fernandez-Seara MA, Dupan BW, Wilson DF. A method for measuring oxygen distributions in tissue using frequency domain phosphorometry. *Comp Biochem Physiol A Mol Integr Physiol* 2002;132:147–52.
42. Vinogradov SA, Wilson DF. Phosphorescence lifetime analysis with a quadratic programming algorithm for determining quencher distributions in heterogeneous systems. *Biophys J* 1994;67:2048–59.
43. Eng J, Lynch RM, Balaban RS. Nicotinamide adenine dinucleotide fluorescence spectroscopy and imaging of isolated cardiac myocytes. *Biophys J* 1989;55:621–30.
44. Takahashi E, Endoh H, Doi K. Intracellular gradients of O<sub>2</sub> supply to mitochondria in actively respiring single cardiomyocyte of rats. *Am J Physiol* 1999;276: H718–24.
45. Gandjbakhche AH, Bonner RF, Arai AE, Balaban RS. Visible-light photon migration through myocardium in vivo. *Am J Physiol* 1999;277:H698–704.
46. Sinaasappel M, van Iterson M, Ince C. Microvascular oxygen pressure in the pig intestine during haemorrhagic shock and resuscitation. *J Physiol* 1999;514: 245–53.
47. Vanderkooi JM, Berger JW. Excited triplet states used to study biological macromolecules at room temperature. *Biochim Biophys Acta* 1989;976:1–27. [48] Dunphy I, Vinogradov SA, Wilson DF. Oxyphor R2 and G2: phosphors for measuring oxygen by oxygen-dependent quenching of phosphorescence. *Anal Biochem* 2002;310:191–8.
48. Lo LW, Koch CJ, Wilson DF. Calibration of oxygen-dependent quenching of the phosphorescence of Pd-meso-tetra (4-carboxyphenyl) porphine: a phosphor with general application for measuring oxygen concentration in biological systems. *Anal Biochem* 1996;236:153–60.

# CHAPTER

# 7

Increased in vivo mitochondrial  
oxygenation with right  
ventricular failure induced by  
pulmonary arterial hypertension:  
mitochondrial inhibition as driver  
of cardiac failure?

Balestra GM  
Mik EG  
Eerbeek O  
Specht PAC  
van der Laarse WJ  
Zuurbier CJ

## ABSTRACT

### Background

The leading cause of mortality due to pulmonary arterial hypertension (PAH) is failure of the cardiac right ventricle. It has long been hypothesized that during the development of chronic cardiac failure the heart becomes energy deprived, possibly due to shortage of oxygen at the level of cardiomyocyte mitochondria. However, direct evaluation of oxygen tension levels within the in vivo right ventricle during PAH is currently lacking. Here we directly evaluated this hypothesis by using a recently reported technique of oxygen-dependent quenching of delayed fluorescence of mitochondrial protoporphyrin IX, to determine the distribution of mitochondrial oxygen tension (mitoPO<sub>2</sub>) within the right ventricle (RV) subjected to progressive PAH.

### Methods

PAH was induced through a single injection of monocrotaline (MCT). Control (saline-injected), compensated RV hypertrophy (30 mg/kg MCT; MCT30), and RV failure (60 mg/kg MCT; MCT60) rats were compared 4 wk after treatment. The distribution of mitoPO<sub>2</sub> within the RV was determined in mechanically-ventilated, anaesthetized animals, applying different inspired oxygen (FiO<sub>2</sub>) levels and two increment dosages of dobutamine.

### Results

MCT60 resulted in RV failure (increased mortality, weight loss, increased lung weight), MCT30 resulted in compensated RV hypertrophy. At 30% or 40% FiO<sub>2</sub>, necessary to obtain physiological arterial PO<sub>2</sub> in the diseased animals, RV failure rats had significantly less mitochondria (15% of total mitochondria) in the 0-20 mmHg mitoPO<sub>2</sub> range than hypertrophied RV rats (48%) or control rats (54%). Only when oxygen supply was reduced to 21% FiO<sub>2</sub>, resulting in low arterial PO<sub>2</sub> for the MCT60 animals, or when oxygen demand increased with high dose dobutamine, the number of failing RV mitochondria with low oxygen became similar to control RV. In addition, metabolic enzyme analysis revealed similar mitochondrial mass, increased glycolytic hexokinase activity following MCT, with increased lactate dehydrogenase activity only in compensated hypertrophied RV.

### Conclusions

Our novel observation of increased mitochondrial oxygenation suggests down-regulation of in vivo mitochondrial oxygen consumption, in the absence of hypoxia, with transition towards right ventricular failure induced by pulmonary arterial hypertension.

## INTRODUCTION

Severe pulmonary arterial hypertension (PAH) is associated with poor prognosis. The development of PAH induces hypertrophy of the right ventricle (RV) that often transition into RV failure. Heart failure of the right ventricle during chronic PAH is the most common cause of mortality in severe PAH, with metabolic and energetic derangements as a prominent signature of heart failure [1]. In the hypertrophied and failing heart, the increased systolic wall stress in the ventricular wall would be expected to increase the energy demand, whereas the increased size of the cardiomyocyte and the decreased capillary density is anticipated to diminish the oxygen supply. These observations have led to the suggestion that there is an imbalance between oxygen/energy supply-demand in the hypertrophied heart, which possibly contributes to the transition to the decompensated, failing heart [2]. The often-observed decreased PCr/ATP ratio, increased reliance on glucose metabolism and elevated lactate levels [3,4] are in support of such a mismatch, and suggest that the failing heart is an engine out of fuel [5]. One possible cause for reduced ATP production in the failing heart could be the lack of enough oxygen provided to the mitochondria. Hitherto, this question has only been indirectly evaluated through <sup>1</sup>H NMR techniques which estimate the ratio of deoxygenated to oxygenated myoglobin. Examining several heart failure models using this technique it was concluded that reduced oxygen availability does not play a role in heart failure [3,6,7]. The sensitivity of this technique, however, is such that a signal can only be detected when the entire myocardial tissue investigated reaches an intracellular PO<sub>2</sub> < 20 mmHg [3]. Since the mean PO<sub>2</sub> at the level of the mitochondria in intact healthy heart is approximately 35 mmHg [8], the myoglobin technique can only detect large decreases (>40%) in myocardial oxygenation. Thus, relatively smaller decreases or any increase in myocardial oxygenation will go unnoticed with the <sup>1</sup>H NMR technique. In addition, the mitoPO<sub>2</sub> within the heart is highly heterogeneous, such that at a mean mitoPO<sub>2</sub> of 35 mmHg a significant portion of mitochondria may have a mitoPO<sub>2</sub> < 20 mmHg [8]. These mitochondria may become oxygen-limited, as studies in isolated mitochondria have demonstrated decreased oxygen consumption when PO<sub>2</sub> drops down in the 10-20 mmHg range [9,10].

Alternatively, ATP production could also diminish due to intrinsic mitochondrial remodelling resulting in suppression of mitochondrial energy production. Suppression of mitochondrial energy metabolism through mitochondrial metabolic reprogramming together with increased glycolysis was recently proposed as intrinsic mechanism in the development of heart failure [11]. In addition, mitochondrial oxygen consumption may also be inhibited through competition of increased levels of NO with O<sub>2</sub> at the level of cytochrome c oxidase during hypertrophy and heart failure [12]. Irrespective of the precise mechanism, suppression of mitochondrial energy metabolism should be reflected by elevated mitoPO<sub>2</sub>. Therefore, the non-invasive determination of



oxygenation within the intact heart may shed light on the important question whether the development of cardiac hypertrophy and the subsequent transition to heart failure is associated with increased hypoxia or suppressed mitochondrial energy production. Since mitochondria are the principal sites of ATP generation, they are the ideal site of determining the prevailing oxygen tension. Our group recently developed a non-invasive technique which allows, for the first time, the quantitative determination of the distribution of mitochondrial PO<sub>2</sub> within the heart [8,13-15]. Validation studies in several cell lines have demonstrated that the delayed fluorescence signal and its lifetime is determined by mitochondrial PpIX and the amount of mitochondrial oxygen present [15]. Subsequent studies, extending from cells to isolated organs to the *in vivo* organ for liver [14] and heart [8], validated that the lifetime of the specific delayed fluorescence signal measured in all these conditions did indeed reflect the mitochondrial oxygen tension. In the current project we now apply this novel technique to examine the *in vivo* mitochondrial oxygenation in the right ventricle during the development of cardiac hypertrophy and failure due to pulmonary arterial hypertension.

## METHODS

The experiments of this study were approved by the ethical committee for animal subjects of the Academic Medical Center at the University of Amsterdam and Erasmus Medical Center at the University of Rotterdam. Care and handling of the animals were in accordance with the guidelines for Institutional and Animal Care and Use Committees. Male Wistar rats (n=22; 7-8 wk, 180-220 g, Harlan, Netherlands) were attributed to either receive an intraperitoneal injection of monocrotaline (MCT) at a dose of 30 mg/kg (n=7) or 60 mg/kg (n=9), or normal saline (n=6). Body weight was monitored for the next 28 days.

### Animal preparation

Invasive measurements were performed on 28 days after intraperitoneal injection. We selected 28 days post MCT administration, because in our hands RV heart failure and sharp reductions in body weight then starts to develop before most of the animals die. Premedication was done with subcutaneous buprenorphine (Temgesic, Schering-Plough, Netherlands; 0.05 mg/kg), 30 minutes before intraperitoneal injection of NaOH-buffered 5-aminolevulinic acid (ALA; 200 mg/kg). ALA was administered to increase mitochondrial PpIX concentration. 30 minutes before instrumentation of the animals a further equal dose of buprenorphine was administered. Anesthesia was induced by isoflurane. 5% isoflurane in oxygen was used for controls, and 3% isoflurane for monocrotaline treated animals (pilot experiments showed increased sensitivity of MCT animals to isoflurane induction). Anesthesia was then similarly maintained for all groups by pentobarbital at

60 mg/kg initial dose followed hourly by 60% of the initial dose. Body temperature was rectally measured and kept at 37±0.5°C with a heating pad. The airway was secured by tracheal intubation following which the animals were ventilated in pressure-controlled mode at 40% oxygen with a positive end-expiratory pressure of 2.5 mbar. The ventilator settings were checked by capnography and blood gases. The carotid artery and jugular vein were cannulated for blood pressure and heart rate monitoring and infusion of fluid (Ringer's lactate at 10 ml/kg/h) and drugs, respectively. A median upper laparotomy was performed, the diaphragm incised and the pericardium opened. The fiber optic probe for mitoPO<sub>2</sub> measurements was positioned transdiaphragmally at approximately 1 mm from the right ventricle (RV) of the beating heart.

### Experimental protocol

The measurements of the mitochondrial oxygen partial pressures (mitoPO<sub>2</sub>) were started at 2 hours after ALA injection, to allow sufficient increases in mitochondrial PpIX for the delayed fluorescence measurements. The experimental protocol consisted in the measurement of mitoPO<sub>2</sub> at varying inspiratory oxygen fraction (40%, 30%, 21%, 40%) and at two dosages of dobutamine (Centrafarm, Etten-Leur, Netherlands), 2.5 µg/kg/min and 5 µg/kg/min. All measurements during the infusion of dobutamine were made at an inspiratory oxygen fraction of 40%. The 30 and 40% FiO<sub>2</sub> are necessary to prevent non-physiological low arterial oxygen tension in the MCT animals, probably because in these animals the lung damage impaired ventilation/perfusion matching within the lungs. Every step of the protocol was maintained for 10 minutes before any measurement was performed. At each step 0.2 ml blood was sampled from the cannulated carotid artery and analyzed with a blood gas analyzer (ABL800 flex, Radiometer, Copenhagen). At the end of the experiment, right ventricular pressure was measured by transmural puncture using a 23-gauge needle connected to a pressure transducer and automatic flushing system. After termination of the experiment, heart and lungs were excised and weighed. The heart was subsequently dissected into right and left ventricle, after a small apical part of the heart was removed for histological and biochemical processing. The tissue was immediately frozen in liquid nitrogen and stored at -80°C.

### Mitochondrial PO<sub>2</sub> measurements

The principle and setup for *in vivo* mitoPO<sub>2</sub> measurements was previously reported [8,14,15], and a detailed description of the used setup was recently published [13]. In brief, mitochondrial oxygen tension is measured with the Protoporphyrin IX (PpIX) – Triplet State Lifetime technique. Application of ALA results in the mitochondrial accumulation of PpIX. PpIX displays oxygen-dependent quenching of delayed fluorescence lifetime. Mitochondrial PpIX is excited at 510 nm through an excitation fiber coupled to a tunable laser, and delayed fluorescence at 630-700 nm is detected by an emission fiber connected to a gated microchannel plate photomultiplier. A PC-based data-acquisition

system sampled the signal at 1 MHz and averaged 64 laser pulses (repetition rate 20 Hz) prior to analysis. The delayed fluorescence signal was then used to recover the different mitoPO<sub>2</sub> histograms from fitting the signal by a sum of rectangular distributions of delayed fluorescence lifetimes. Three separate series of 64 pulses were analyzed and averaged at each experimental condition.

### Tissue analysis

Three sections of the apex, 5 μm thick, were cut in a cryostat, collected on slides, fixed in 4% formaldehyde, stained with hematoxylin and eosin, dehydrated and mounted in Entellan (Merck). Images were obtained with a 40x objective, and cross-sectional area of individual myocytes was determined at the level of the nucleus using Image J (imagej.nih.gov/ij/), taking the pixel to aspect ratio into account [16]. Within each section the cross-sectional area was determined for 6-12 cardiomyocytes. RV and LV homogenates were obtained by grinding the frozen tissue into powder in liquid nitrogen, dissolving the powder in 1 ml ice-cold homogenization buffer (0.5% Triton X-100, 250 mM sucrose, 20 mM Hepes (pH 7.4), 10 mM KCl, 1.5 mM MgCl<sub>2</sub>, 1 mM EDTA, 1 mM dithiothreitol, 0.1 mM PMSF, 5 μg/ml leupeptin and aprotinin and 1 μg/ml pepstatin), 15 min incubation, sonication and finally 1 min 10,000 g centrifugation to obtain the supernatant. Citrate synthase activity, as marker of mitochondrial content, and hexokinase and lactate dehydrogenase activities, as markers of glycolysis, were determined in the supernatant according to published spectrophotometric techniques [17,18], and normalised to protein content (Bradford technique).

### Statistics

The data are presented as mean ± SEM. One way analysis was performed followed by Fisher's probable least-significant-difference post hoc analysis between groups (SPSS Statistics 20). A value of P < 0.05 was considered statistically significant.

## RESULTS

### General characterization of MCT animals

Two 60 mg/kg MCT animals (MCT60) died before 4 wk. One 30 mg/kg (MCT30) and one MCT60 animal died at induction of anesthesia. 6 animals of each MCT group completed the experimental protocol. Body weight developed to a similar degree for all three groups up to 3 wk. Thereafter the MCT60 group started to lose weight, such that at 4 wk body weight was significantly reduced for the MCT60 group as compared to control and MCT30 (Figure 1A). In addition, MCT60 demonstrated increased lung weight at 4 wk (Figure 1B). RV hypertrophy was similar in both MCT groups (Figure 1C and D), whereas peak RV pressure almost tripled in MCT60 rats (Figure 1E). These data indicate

compensated RV hypertrophy for the MCT30 group, and the start of right heart failure for the MCT60 group.

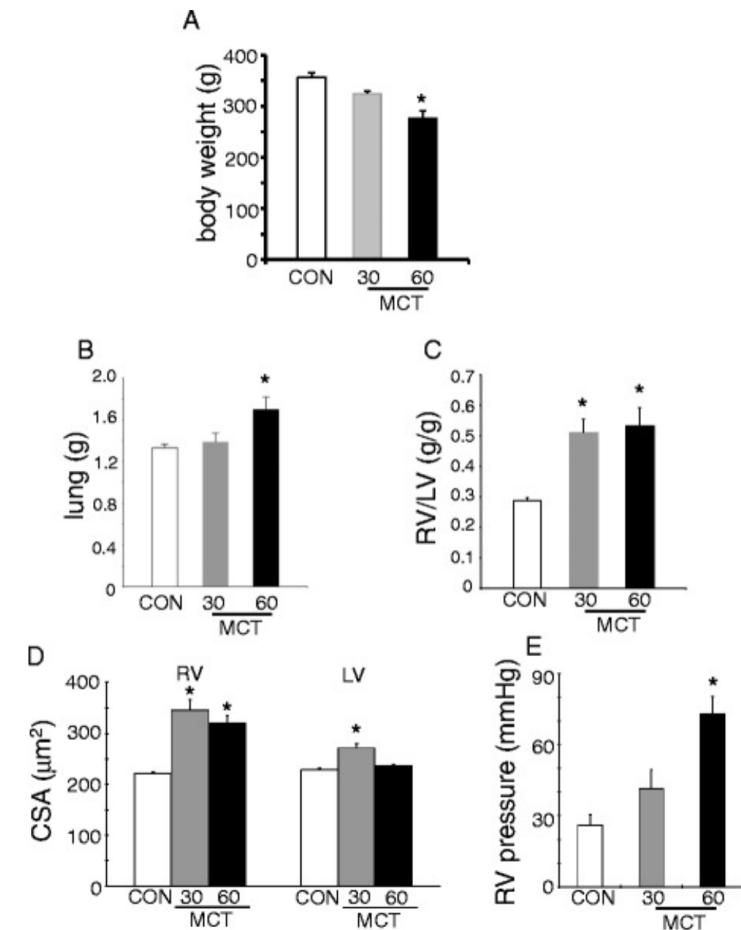


**Figure 1.** Body weight and anatomical and functional characteristics of right ventricle of control and MCT treated animals. **A.** body weight after 28 d following MCT administration. **B-D.** lung mass, right ventricle (RV) mass relative over left ventricle (LV) mass, and cross-sectional area (CSA) of cardiomyocytes in RV and LV, respectively, at end of 28 d following MCT treatment. **E.** systolic RV pressure measured at end experimental protocol (n=6 per group).

### Hemodynamics and blood oxygenation

Physiology of the animals during the experimental protocol is depicted in Figure 2. Although there was a trend that MCT in general lowers hemodynamics in the anesthetized animals, this only reached significance for heart rates (Figure 2A) during the dobutamine

infusions; no significant depression of MAP (Figure 2B) was observed following MCT treatment. Reducing FiO<sub>2</sub> was paralleled with reductions in arterial PO<sub>2</sub> for both control and MCT animals, whereas arterial PO<sub>2</sub> was in most conditions significantly higher for control versus MCT animals (Figure 2C). At 30% FiO<sub>2</sub> the arterial oxygen tension was still at a normal physiological level (~100 mmHg) for the MCT60 group, whereas at 21% FiO<sub>2</sub> arterial oxygen tension dropped below normal arterial oxygenation levels (<70 mmHg), indicating that at least 30% FiO<sub>2</sub> was necessary to maintain physiological PaO<sub>2</sub> in the MCT60 animals. There also was a non-significant trend for decreased oxygen saturation of hemoglobin in MCT animals at 21% FiO<sub>2</sub> (Figure 2D).

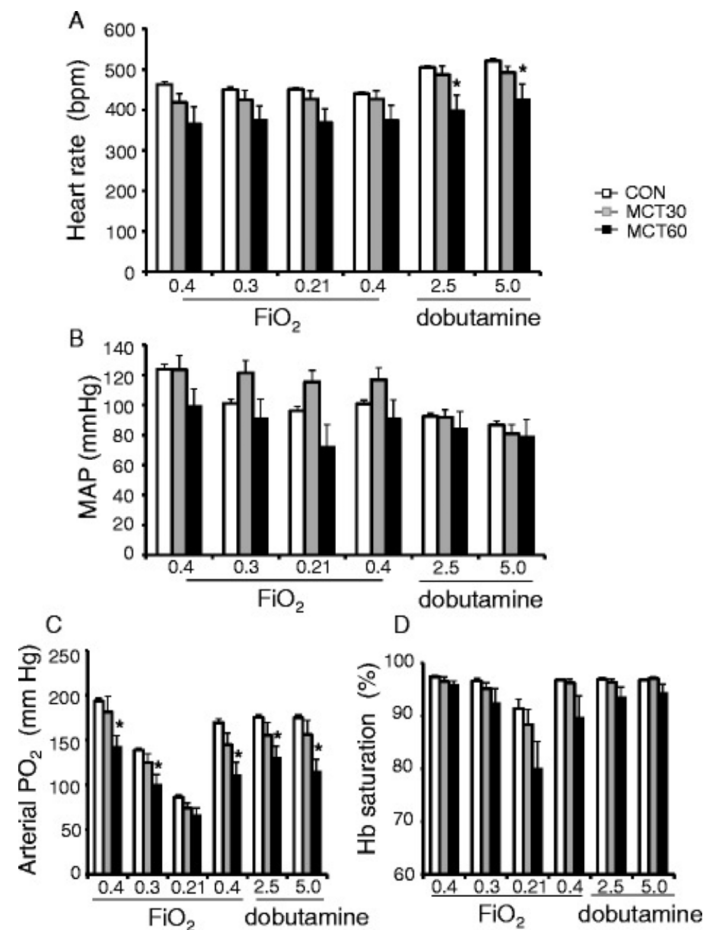


**Figure 2.** Hemodynamics (A: heart rate; B: mean arterial pressure (MAP)) and blood oxygenation (C: arterial oxygen tension; D: oxygen saturation of haemoglobin(Hb)) during the changes in inspiration oxygen (FiO<sub>2</sub>) and the administration of two dobutamine infusion rates. \* p < 0.05 relative to CON (control). (n=6 per group).

### Mitochondrial oxygen tension

FiO<sub>2</sub>-dependent PpIX delayed fluorescence signals were obtained in vivo from the RV of control and MCT animals and the distribution of mitoPO<sub>2</sub> histograms determined (Figure 3). At 40% FiO<sub>2</sub>, the distribution of mitoPO<sub>2</sub> showed a rightward shift towards higher values for the MCT60 RV as compared to control RV (Figure 3A). The fraction of mitochondria with PO<sub>2</sub> values below 20 mm Hg, assumed to be oxygen limited, was similar between control (54 ± 11%) and the MCT30 group (48 ± 12). However, significant less mitochondria within the RV of the MCT60 group (15 ± 10%) were observed in this low oxygen range as compared to control (Figure 3B). A similar pattern exists when FiO<sub>2</sub> was reduced to 30% oxygen (Figures 3C-D). Only when inspired oxygen supply was further reduced to 21%, the fraction of mitochondria within the 0-20 mmHg PO<sub>2</sub> range of the RV MCT60 group (42 ± 13%) increased to values similar as control (53 ± 5%) (Figure 3E-F). Resetting FiO<sub>2</sub> again to 40% restored oxygenation to the initial 40% inspiration conditions, indicating reversibility of the phenomenon (Figures 3G-H).

We next analyzed the responses of RV oxygenation towards increases in energy demand by using two different doses of dobutamine infusions (Figure 4). At a dobutamine dose of 2.5 μg/kg/min the differences observed in oxygenation between MCT60 and control RV persisted (Figure 4A-B); only at the highest dobutamine dose did the fraction of mitochondria in the 0-20 mmHg range in the MCT RV (32 ± 16%) become similar to that in control RV (49 ± 10%) (Figure 4C-D).

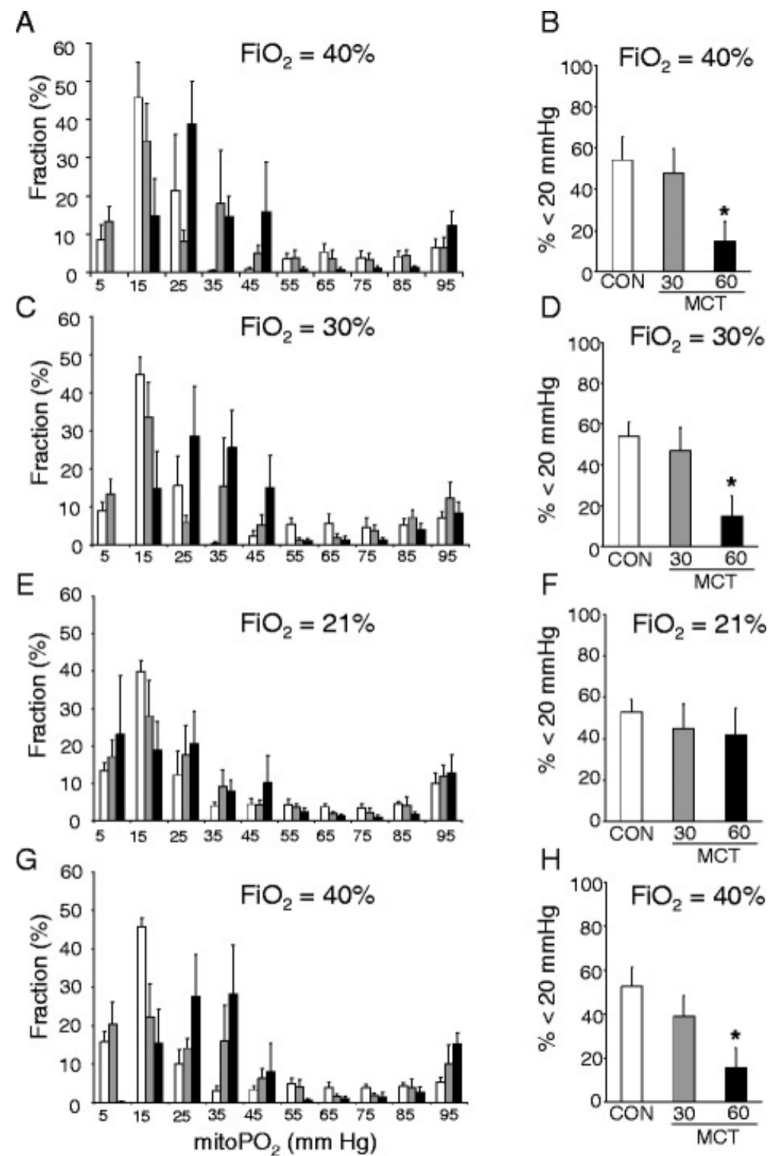


**Figure 3.** Right ventricle mitoPO<sub>2</sub> measurements during changes in inspiration oxygen content (FiO<sub>2</sub>) for control (CON) and monocrotaline-treated animals (MCT). **A, C, E, and G:** total distribution of mitoPO<sub>2</sub> during the different FiO<sub>2</sub> settings. **B, D, F, and H:** the fraction of mitochondria displaying a mitoPO<sub>2</sub> < 20 mmHg during the different FiO<sub>2</sub> settings. \* p < 0.05 relative to CON (control). (n = 6 per group).

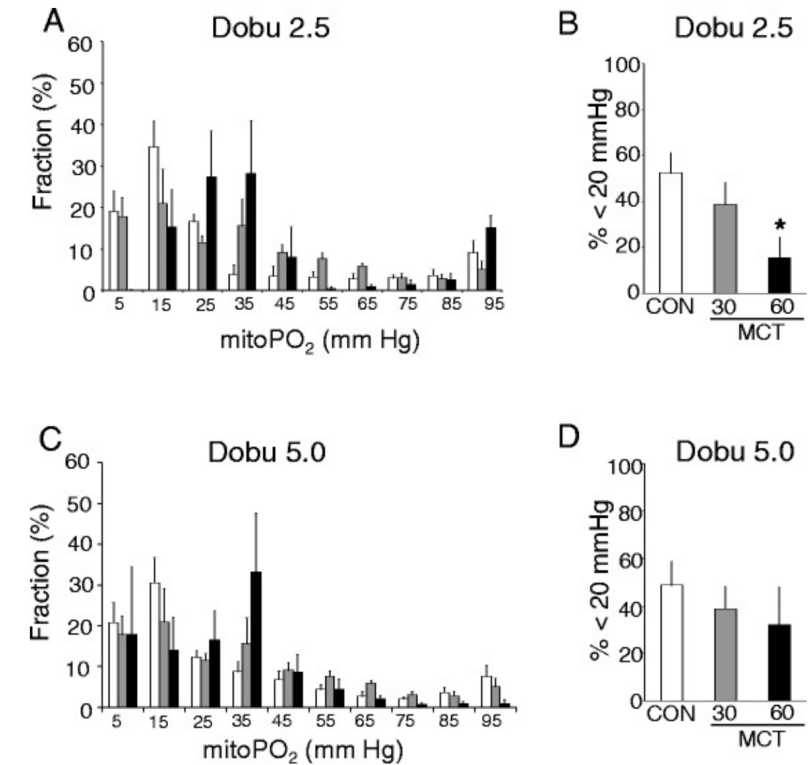


**Figure 4.** Right ventricle mitoPO<sub>2</sub> measurements during administration of two doses of dobutamine (dobu) for control (CON) and monocrotaline-treated animals (MCT). **A, C:** total distribution of mitoPO<sub>2</sub> within RV. **B, D:** the fraction of mitochondria displaying a mitoPO<sub>2</sub> < 20 mmHg. \* p < 0.05 relative to CON (control). (n = 6 per group).

#### Post-experimental metabolic analysis

Finally, we examined metabolic changes within RV and LV at the different stages of pulmonary hypertension (Figure 5). Citrate synthase activity was unaffected by MCT treatment in RV and LV, indicating similar mitochondrial mass among groups. Hexokinase (HK) activity was increased in the RV of both MCT groups. No change in HK activity was observed in LV. In contrast, lactate dehydrogenase (LDH) activity was only increased in the RV of the MCT30 group, but not in the RV of the MCT60 group. LDH activity in LV was unaltered (Figure 5). These data indicated a differential response of glycolytic enzymes to the development of RV failure.

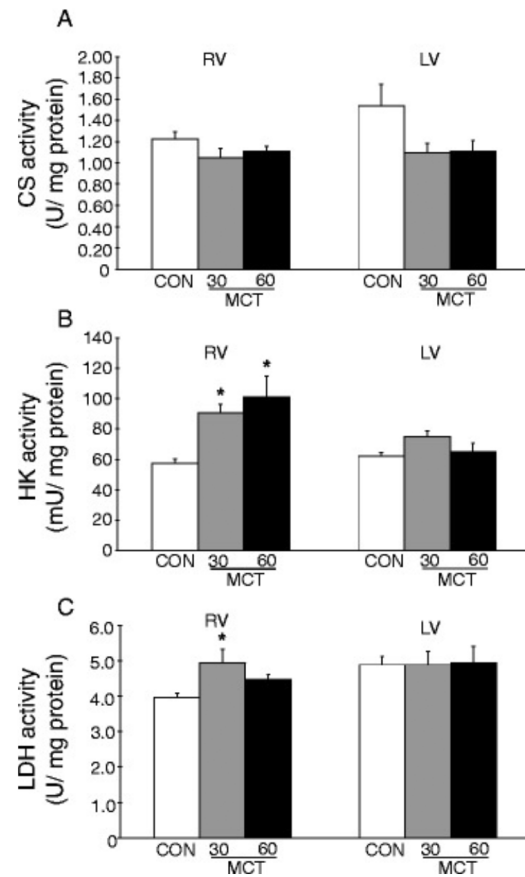


**Figure 5.** Metabolic marker enzyme activities in RV and LV of control and MCT treated animals 28 d following MCT administration. **A.** citrate synthase (CS) as mitochondrial marker; **B.** hexokinase (HK) as glycolytic marker; **C.** lactate dehydrogenase (LDH), as lactate metabolism marker. \* $p < 0.05$  relative to the respective CON (control). ( $n = 6$  per group).

## DISCUSSION

Hypoxia at the level of the cardiomyocyte mitochondria is hypothesized as an important contributing factor in the development of cardiac failure [2,5,19,20]. A critical evaluation of this hypothesis has been missing due to the lack of a technique enabling quantitative measurements of mitochondrial oxygenation within the in vivo working heart. In the present study, through application of a recently developed technique by our group, we show that at the initiation of cardiac failure, mitochondrial oxygenation is higher (under baseline conditions) or equal (under decreased oxygen supply or increased work demand conditions) as compared to healthy hearts. No decreased cardiac mitochondrial oxygenation was observed, arguing against hypoxia being an important contributor to

the development of right heart failure.

### Mitochondrial oxygenation and cardiac metabolic signature of RV failure

Our observation of less mitochondria with low oxygen in the RV failure developing animals, suggests decreased mitochondrial oxygen consumption in the transition from compensated hypertrophy towards cardiac failure. Decreased oxygen consumption has indeed been directly measured 4-6 wk after MCT administration, although not in intact hearts but in permeabilized cardiac fibers or minced heart tissue [19-21]. Suppression of mitochondrial metabolism together with increased glycolysis was recently proposed as intrinsic mechanism underlying the development of pulmonary arterial hypertension and heart failure [11]. This data would suggest that impairments in energy production (ATP synthesis) in RV heart failure, as reported by different groups [19,22], are mainly metabolically mediated, and not through impairment of oxygen delivery. Theoretically, mitoPO<sub>2</sub> can also be elevated as a consequence of increases in oxygen supply when going from the hypertrophied to the failing condition. However, such evidence cannot be found in literature. On the contrary, capillary density or coronary blood flow or angiogenesis are commonly decreased in hypertrophy or with the transition towards heart failing [11,16,23]. The increased mitochondrial PO<sub>2</sub> measured in this study is also not a result from a decrease in mitochondrial capacity, since citrate synthase activities were similar between control and MCT RV. Previous work from our group also demonstrated unaltered mitochondrial capacity in RV of MCT-treated animals [16,24]. We did find elevated HK activities in the hypertrophied and failing RV, consistent with other studies [25-27]. Interestingly, increases in hexokinase were recently also noted as metabolic hallmark of a right heart failure program [28]. The increase in HK is probably an adaptive mechanism, attenuating structural and maladaptive remodelling with pressure-overload [29]. Interestingly, LDH activity was only increased in the compensated hypertrophied RV, but not in the failing RV. Thus, decreased number of mitochondria with low oxygen tension and loss of LDH increase are the specific metabolic markers observed in the present study that sets the developing failing RV apart from the compensated hypertrophied RV. Although increased cardiac HK has been associated with decreased cardiac oxygen consumption [29-31], or decreased LDH may decrease oxygen consumption considering lactate as important substrate for the heart [32,33], further in-depth studies directed at these metabolic hypotheses are needed before any affirmative statements can be made. Alternatively, although not examined in the present study, mitochondrial oxygen consumption may also decrease due to cytochrome c oxidase inhibition by NO, which levels were shown to be increased in congestive heart failure [12,34]. Irrespective of the exact molecular mechanism, our novel observation of higher in vivo mitochondrial oxygenation suggests impaired in vivo mitochondrial metabolism as a possible trigger for the development of RV failure.

In the current work the chemical substance MCT was used to induce pulmonary

hypertension; however, pulmonary hypertension can have several different etiologies (chronic thromboembolic, pre-versus postcapillary pulmonary hypertension, connective tissue disease, etc.). Although we anticipate that, independent of the etiology, any increase in pulmonary arterial pressure will increase RV afterload and thereby most likely start the metabolic, mitochondrial, remodelling phase as described here for the MCT model, further research is warranted to state this more definitively for different pulmonary hypertension etiologies.

### Methodological considerations

Under baseline conditions the animals were mechanically ventilated with 30-40% inspiration oxygen, which is above the ambient air content of oxygen (21%) with spontaneously breathing. The higher inspiration oxygen levels are necessary to compensate for the known ventilation-perfusion defects caused by anesthesia and mechanical ventilation in especially diseased humans and animals [35,36] and are the recommended inspiration oxygen levels with mechanical ventilation used in the clinical arena. Mechanical ventilation in our healthy animals with a FiO<sub>2</sub> of 21% resulted in an arterial tension of approximately 80 mmHg, below the 100 mmHg normally obtained with spontaneous breathing, indicating that the use of ambient air oxygen levels with mechanical ventilation and anesthesia is indeed associated with insufficient blood oxygenation. In addition, we needed at least a FiO<sub>2</sub> of 30% to obtain a physiological normal arterial tension of 100 mmHg in the MCT60 animals. Most importantly, even with the lower arterial oxygen tension of the MCT60 animals as compared to healthy controls at 30% or 40% FiO<sub>2</sub>, there were still less mitochondria with pO<sub>2</sub><20 mmHg in the MCT60 RV, illustrating that the fewer mitochondria with low oxygen are not simple a result of higher arterial oxygen in these sick animals.

The present study used the monocrotaline-induced pulmonary arterial hypertension intervention as a model to study RV hypertrophy and failure. Because almost all animal models are not fully mimicking the clinical features of human pathologies, studies in different models of heart failure, e.g. infarction- or aortic constriction-induced models, will need to be examined to more definitely establish whether increased mitochondrial oxygenation is in general a signature of HF. In addition, although we did not fully characterise RV function with e.g. echocardiography, other studies demonstrated RV dysfunction with 60 mg/kg MCT at 3-6 weeks after MCT administration [11,19,20,37,38]. Together with the reported decreased body weight and increased mortality in the present study it is likely that the MCT60 animals at 4 wk after MCT administration are in the critical transition phase of RV decompensation. However, the use of full RV function characterization with mitoPO<sub>2</sub> measurements is needed in future studies to describe in more detail the relation between RV dysfunction and RV mitochondrial oxygenation.

## REFERENCES

1. Vonk-Noordergraaf A, Haddad F, Chin KM, Forfia PR, Kawut SM, Lumens J, et al. Right heart adaptation to pulmonary arterial hypertension: physiology and pathobiology. *J Am Coll Cardiol*. 2013;62:D22–33.
2. Katz AM. Cardiomyopathy of overload: a major determinant of prognosis in congestive heart failure. *N Engl J Med*. 1989;322:100–10.
3. Murakami Y, Zhang Y, Cho YK, Mansoor AM, Chung JK, Chu C, et al. Myocardial oxygenation during high work states in hearts with postinfarction remodelling. *Circulation*. 1999;99:942–94.
4. Van Bilsen M, Smeets PJH, Gilde AJ, Van der Vusse GJ. Metabolic remodelling of the failing heart: the cardiac burn-out syndrome? *Cardiovasc Res*. 2004;2004(61):218–26.
5. Neubauer S. The failing heart-an engine out of fuel. *N Engl J Med*. 2007;356:1140–51.
6. Bache RJ, Zhang J, Murakami Y, Zhang Y, Cho YK, Merkle H, et al. Myocardial oxygenation at high workloads in hearts with left ventricular hypertrophy. *Cardiovasc Res*. 1999;42:616–27.
7. Traverse JH, Melchert P, Pierpont GL, Jones B, Crampton M, Bache RJ. Regulation of myocardial blood flow by oxygen consumption is maintained in the failing heart during exercise. *Circ Res*. 1999;84:401–8.
8. Mik EG, Ince C, Eerbeek O, Heinen A, Stap J, Hooibrink B, et al. Mitochondrial oxygen tension within the heart. *J Mol Cell Cardiol*. 2009;46:943–51.
9. Hoffman DL, Salter JD, Brookes PS. Response of mitochondrial reactive oxygen species generation to steady-state oxygen tension: implications for hypoxic cell signalling. *Am J Physiol Heart Circ Physiol*. 2007;292:H101–8.
10. Wilson DF. Regulation of cellular metabolism: programming and maintaining metabolic homeostasis. *J Appl Physiol*. 2013;115:1583–8. DOI: 10.1152/jappphysiol.00894.2013.
11. Sutendra G, Dromparis P, Paulin R, Zervopoulos S, Haromy A, Nagendran J, et al. A metabolic remodeling in right ventricular hypertrophy is associated with decreased angiogenesis and a transition from a compensated to a decompensated state in pulmonary hypertension. *J Mol Med*. 2013;91:1315–27.
12. Brookes PS, Zhang J, Dai L, Parks DA, Darley-Usmar VM, Anderson PG. Increased sensitivity of mitochondrial respiration to inhibition by nitric oxide in cardiac hypertrophy. *J Mol Cell Cardiol*. 2001;33:69–82.
13. Harms FA, Voorbeijtel WJ, Bodmer SI, Raat NJ, Mik EG. Cutaneous respirometry by dynamic measurement of mitochondrial oxygen tension for monitoring mitochondrial function in vivo. *Mitochondrion*. 2013;13:507–14.
14. Mik EG, Johannes T, Zuurbier CJ, Heinen A, Houben-Weerts JH, Balestra GM, et al. In vivo mitochondrial oxygen tension measured by a delayed fluorescence lifetime technique. *Biophys J*. 2008;95:3977–90.
15. Mik EG, Stap J, Sinaasappel M, Beek JF, Aten JA, van Leeuwen TG, et al. Mitochondrial PO<sub>2</sub> measured by delayed fluorescence of endogenous protoporphyrin IX. *Nat Methods*. 2006;3:939–45.
16. Des Tombe AL, Van Beek-Harmsen BJ, Lee-De Groot MB, Van der Laarse WJ. Calibrated histochemistry applied to oxygen supply and demand in hypertrophied rat myocardium. *Microsc Res Tech*. 2002;58:412–20.
17. Gürel E, Smeele KM, Eerbeek O, Koeman A, Demirci C, Hollmann MW, et al. Ischemic preconditioning affects hexokinase activity and HKII in different subcellular compartments throughout cardiac ischemia-reperfusion. *J Appl Physiol*. 2009;106:1909–16.

18. Zuurbier CJ, Eerbeek O, Meijer AJ. Ischemic preconditioning, insulin, and morphine all cause hexokinase redistribution. *Am J Physiol Heart Circ Physiol.* 2005;289:H496–9.
19. Daicho T, Yagi T, Abe Y, Ohara M, Marunouchi T, Takeo S, et al. Possible involvement of mitochondrial energy-producing ability in the development of right ventricular failure in monocrotaline-induced pulmonary hypertensive rats. *J Pharmacol Sci.* 2009;111:33–43.
20. Piao L, Fang YH, Cadete VJJ, Wietholt C, Urboniene D, Toth PT, et al. The inhibition of pyruvate dehydrogenase kinase improves impaired cardiac function and electrical remodeling in two models of right ventricular hypertrophy: resuscitation the hibernating right ventricle. *J Mol Cell Cardiol.* 2010;88:47–60.
21. Piao L, Marsboom G, Archer SL. Mitochondrial metabolic adaptation in right ventricular hypertrophy and failure. *J Mol Med.* 2010;88:1011–20.
22. Lamberts RR, Caldenhoven E, Lansink M, Witte G, Vaessen RJ, St Cyr JA, et al. Preservation of diastolic function in monocrotaline-induced right ventricular hypertrophy in rats. *Am J Physiol Heart Circ Physiol.* 2007;293:H1869–976.
23. Traverse JH, Chen Y, Hou M, Li Y, Bache RJ. Effects of K<sup>+</sup>ATP channel and adenosine receptor blockade during rest and exercise in congestive heart failure. *Circ Res.* 2007;100:1643–9.
24. Van der Laarse WJ, Des Tombe AL, van Beek-Harmsen BJ, Lee-de Groot MB, Jaspers RT. Krogh's diffusion coefficient for oxygen in isolated *Xenopus* skeletal muscle fibers and rat myocardial trabeculae at maximum rates of oxygen consumption. *J Appl Physiol.* 2005;99:2173–80.
25. Do E, Baudet S, Verdys M, Touzeau C, Bailly F, Lucas-heron B, et al. Energy metabolism in normal and hypertrophied right ventricle of the ferret heart. *J Mol Cell Cardiol.* 1997;29:1903–13.
26. Fang YH, Piao L, Hong Z, Toth PT, Marsboom G, Bache-Wig P, et al. Therapeutic inhibition of fatty acid oxidation in right ventricular hypertrophy: exploring Randle's cycle. *J Mol Med.* 2012;90:31–43.
27. Zhang WH, Qiu MH, Wang XJ, Sun K, Zheng Y, Jing ZC. Up-regulation of hexokinase 1 in the right ventricle of monocrotaline induced pulmonary hypertension. *Respir Res.* 2014;15:119.
28. Drake JI, Bogaard HJ, Mizuno S, Clifton B, Xie B, Gao Y, et al. Molecular signature of a right heart failure program in chronic severe pulmonary hypertension. *Am J Respir Cell Mol Biol.* 2011;45:1239–47.
29. Nederlof R, Eerbeek O, Hollmann MW, Southworth R, Zuurbier CJ. Targeting hexokinase II to mitochondria to modulate energy metabolism and reduce ischemia-reperfusion injury in heart. *Brit J Pharmacol.* 2014;171:2067–79.
30. Nederlof R, Chaoqin X, Gurel E, Koeman A, Hollmann MW, Southworth R, et al. Hexokinase II binding to mitochondria suppress irreversible ischemia reperfusion injury in the beating heart by respiratory inhibition and reduced ROS levels. *Circ Res.* 2012;111(Suppl):217.
31. Ong SG, Hee Lee W, Theodorou L, Kodo K, Lim SY, Shukla DH, et al. HIF-1 reduces ischaemia-reperfusion injury in the heart by targeting the mitochondrial permeability transition pore. *Cardiovasc Res.* 2014;104:24–36.
32. Chatham JC. Lactate-the forgotten fuel. *J Physiol.* 2002;542:333.
33. Chatham JC, Gao ZP, Forder JR. Impact of 1 wk of diabetes on the regulation of myocardial carbohydrate and fatty acid oxidation. *Am J Physiol Endocrinol Metab.* 1999;277:E342–51.
34. Traverse JH, Chen Y, Hou M, Bache RJ. Inhibition of NO production increases myocardial blood flow and oxygen consumption in congestive heart failure. *Am J Physiol Heart Circ Physiol.* 2002;282:H2278–83.
35. Nunn JF. Factors influencing the arterial oxygen tension during halothane anaesthesia with spontaneous respiration. *Brit J Anaesth.* 1964;36:327–41. DOI: 10.1093/bja/36.6.327.
36. Nunn JF, Bergman NA, Coleman AJ. Factors influencing the arterial oxygen tension during anaesthesia with artificial ventilation. *Brit J Anaesth.* 1965;37:898–914.
37. Handoko ML, de Man FS, Happe CM, Schalij I, Musters RJP, Westerhof N, et al. Opposite effects of training rats with stable and progressive pulmonary hypertension. *Circulation.* 2009;12:42–9.
38. Korstjens IJM, Rouws CHFC, van der Laarse WJ, van der Zee L, Stienen GJM. Myocardial force development and structural changes associated with monocrotaline induced cardiac hypertrophy and heart failure. *J Muscl Res Cell Motil.* 2002;23:93–102.

# CHAPTER

# 8

## Microcirculatory and mitochondrial oxygenation is preserved in endotoxic shock and resuscitation in rat hearts

Balestra GM  
Ince C  
Johannes T  
de Boon WMI  
Specht PAC  
Betz MJ  
Zuurbier CJ  
Stolker RJ  
Mik EG.

submitted.  
PMID: tbd DOI: tbd





## ABSTRACT

### Objectives

To test the hypothesis that myocardial microcirculatory and mitochondrial oxygenation is altered in endotoxemic shock and restored during resuscitation.

### Design

Prospective randomized laboratory study.

### Setting

University research laboratory.

### Subjects

Male Sprague-Dawley rat (n = 48).

### Interventions

Rats were challenged with lipopolysaccharide. After 90 min of untreated endotoxemic shock, rats were randomly assigned to 7 treatment groups: no resuscitation, fluid resuscitation only, fluid plus dobutamine, fluid plus levosimendan, fluid plus norepinephrine, fluid plus norepinephrine and dobutamine, fluid plus norepinephrine and levosimendan (n = 6 / group). A control group (n = 6) underwent all procedures as all other animals but was neither treated with lipopolysaccharide nor resuscitation protocol.

### Measurements and Main Results

Myocardial mitochondrial and microcirculatory  $pO_2$  were measured by oxygen-dependent quenching of phosphorescence. Hemodynamic parameters, mixed-venous and arterial oxygen partial pressures ( $pO_2$ ) and mitochondrial, superficial and deep microcirculatory  $pO_2$  were collected during the 5h experiment. Troponin was measured at end experiment.

Endotoxemic shock caused a transient increase of microcirculatory and but no change of mitochondrial oxygenation as compared to controls. No hypoxic  $pO_2$  (< 10 mmHg) were measured in endotoxemic animals. The increased microcirculatory oxygenation was temporarily preserved by fluid resuscitation, before it dropped to similar levels of non-resuscitated hearts after 90 min. All additional drug treatments were without effect on microcirculatory and mitochondrial oxygenation. Troponin levels were only elevated in norepinephrine treatment groups.

### Conclusions

Our study showed that after an initial transient increase of the microcirculatory

oxygenation, myocardial microcirculatory and mitochondrial oxygenation are preserved during endotoxemic shock. Resuscitation did not further affect myocardial oxygenation. However, norepinephrine-resuscitation resulted in troponinemia indicating its possible deleterious effect on the myocardial integrity.

### Key Points

#### Question

(1) Does endotoxemic shock cause hypoxia microcirculatory and mitochondrial oxygenation in rat hearts *in vivo*. (2) Do fluid, norepinephrine, dobutamine or levosimendan as single or combined drugs influence cardiac oxygenation or (3) cause myocardial injury?

#### Findings

After an initial transient increase of the microcirculatory oxygenation, myocardial microcirculatory and mitochondrial oxygenation are preserved during endotoxemic shock. Fluid resuscitation only caused a transient increase of cardiac oxygenation and additional drug treatments led to no further effect. Troponin levels were only elevated in norepinephrine treatment groups.

#### Meaning

Preserved cardiac oxygenation and absence of hypoxia in endotoxemic shock fuels the hypothesis of altered oxygen utilization and challenges the standard resuscitation approach. Norepinephrine treatment was associated with myocardial injury.

## INTRODUCTION

Great advances in the understanding of the pathophysiology of sepsis have been achieved. However, there is a manifest difficulty to consolidate the accumulated evidence into a comprehensive view. Even more challenging appears the translation of this knowledge into a more successful sepsis therapy [1]. Sepsis is currently defined as “life-threatening organ dysfunction caused by a dysregulated host response to infection” [2]. In the heart, sepsis causes left and right ventricular dysfunction [3]. Elevated troponin levels in septic cardiomyopathy indicate cellular injury and are related to higher catecholamine requirements and increased mortality [4]. The most frequently suggested cause for troponin release is shortage of oxygen (i.e. hypoxia and ischemia), and one of the commonly debated concepts for the explanation of sepsis-induced organ dysfunction. Moreover, it is the only concept translated into a clinical treatment strategy [5]. Although hypoxia is generally considered to contribute to cardiac dysfunction in sepsis, experimental evidence for this is very limited. The sole experimental data with direct myocardial  $O_2$  measurements corroborate this mechanism showing hypoxia in endotoxemic rat hearts in a normotensive model [6]. In earlier publications, this has been contended by contrary findings in studies searching for indirect evidence of cellular  $O_2$  deficit [7, 8]. Contemporary concepts support altered oxygen utilization over hypoxia as pathophysiological mechanism of organ dysfunction however direct proof of absence of hypoxia is still lacking [9-11].

Using a modern comprehensive optical approach, we aimed to answer the question whether endotoxemia changes myocardial oxygenation causing hypoxia. Neither of the earlier studies examined the effect of supportive treatments comparable to those being used in clinical practice on myocardial oxygenation. It remains to be elucidated whether these supportive therapies translate to improved oxygen delivery from the microcirculatory to the mitochondrial compartment, which represents the ultimate target of the intended increase of oxygen delivery. It has even been suggested that supportive measures might actually contribute to clinical worsening of septic patients [12]. In addition to our primary question, we studied the effects of fluid resuscitation, norepinephrine, dobutamine and levosimendan as singular interventions and as a conjunction of fluid plus vasopressor and/or inotrope therapy on myocardial oxygenation status and injury.

In an endotoxemic shock model we measured the microcirculatory and mitochondrial oxygen partial pressures ( $PO_2$ ) in rat hearts *in vivo*, using a multi-wavelength optical technique. Microcirculatory  $PO_2$  ( $\mu PO_2$ ) was measured with a phosphorescence quenching technique [13] and mitochondrial  $PO_2$  ( $mtPO_2$ ) with oxygen-dependent delayed fluorescence of mitochondrial protoporphyrin IX [14]. Firstly, we explored, whether endotoxemia causes myocardial hypoxia in non-resuscitated animals. Secondly, we examined the influence of protocol-based resuscitation with clinically relevant

supportive measures on myocardial microcirculatory and mitochondrial oxygenation as well as the occurrence of myocardial damage.

## MATERIALS AND METHODS

An extended Methods section can be found in the Supplemental Digital Content (**Supplemental Digital Content**).

### Oxygenation measurement

Mitochondrial ( $mtPO_2$ ), superficial and deep microcirculatory  $PO_2$  ( $\mu PO_2$ ) were measured by oxygen-dependent quenching of phosphorescence in rat hearts *in vivo* using a setup developed in our laboratory as published earlier [14-17]. Pd-meso-tetra-(4-carboxyphenyl)-tetrabenzoporphyrin (1 mg/kg; Oxyphor G2, Oxygen Enterprises, Philadelphia, PA), was used for  $\mu PO_2$  measurements. Protoporphyrin IX synthesis was increased by 5-aminolevulinic acid hydrochloride (200 mg/kg; ALA, Sigma-Aldrich, St. Louis, MO, USA) to measure  $mtPO_2$  [17]. Blood gas analysis (ABL 800 flex, Radiometer, Copenhagen) was performed as indicated (**Figure 1**).

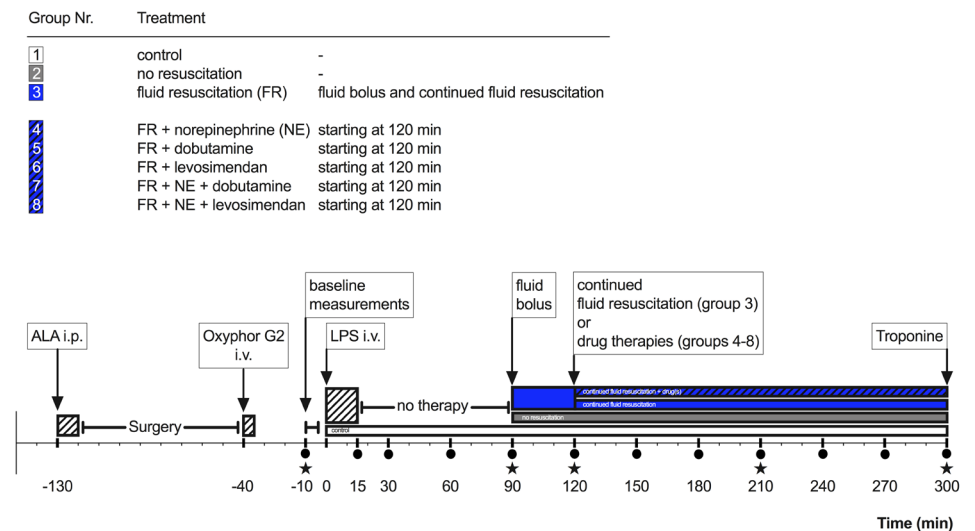


**Figure 1.** Schematic of the protocol

ALA: aminolaevulinic acid, i.p.: intra-peritoneal injection, i.v.: intravenous injection, LPS: lipopolysaccharide; NE: norepinephrine, Dobu: dobutamine, Levo: levosimendan, dots: measurement of  $mtPO_2$ , superficial and deep  $\mu PO_2$ ; stars: arterial and central-venous blood gas analysis including hemoglobin and measurement of cardiac output; hatched boxes represent duration of infusion.

### Experimental protocol

The Animal Research Committees of the Academic Medical Center Amsterdam and Erasmus Medical Center Rotterdam approved this study in 48 male Wistar rats. Care and handling of the animals were in accordance with the guidelines for Institutional and Animal Care and Use Committees.

Anesthesia was induced with isoflurane 5 % (Pharmachemie BV, Haarlem, The Netherlands) followed by intraperitoneal pentobarbital (60 mg/kg; Apotheek Faculteit Dierengeneeskunde Utrecht, NL) and sufentanil (20 µg/kg; Janssen-Cilag BV, Tilburg, NL). After surgery anesthesia was maintained with intravenous propofol (10 mg/kg/h; Fresenius Kabi, Nederland BV, Schelle, Belgium), midazolam (0.05mg/kg/h; Actavis Group PTC ehf, Hafnarfjordur, Iceland) and sufentanil (7.5 µm/kg/h). The animals were mechanically ventilated (Babylog 8000 plus, Draeger, Lübeck, Germany) in volume-controlled mode with a positive end-expiratory pressure (3 cmH<sub>2</sub>O). The inspired oxygen fraction was adjusted to a systemic (arterial) oxygenation of 100 mmHg and ventilation was corrected on end-tidal CO<sub>2</sub> and arterial PCO<sub>2</sub> (P<sub>a</sub>CO<sub>2</sub>). Animal preparation was performed as published earlier and detailed in the online supplement (**Supplemental Digital Content**)[15].

The experimental protocol was performed according to **Figure 1**. In short: oxygenation and hemodynamic measurements comprised: superficial and deep µPO<sub>2</sub>, mtPO<sub>2</sub>, heart rate, arterial pressure, cardiac output, and blood gas analysis. Lipopolysaccharide (LPS; 2.5 mg/kg; E. coli O127:B8, Sigma-Aldrich, St. Louis, MO) was infused over 15 min. Rats were randomly assigned to 8 groups. The 7 treatment groups were no resuscitation, fluid resuscitation only, fluid plus dobutamine, fluid plus levosimendan, fluid plus norepinephrine, fluid plus norepinephrine and dobutamine, fluid plus norepinephrine and levosimendan (n = 6 / group). Ringer's solution was given at 60 ml/kg/h (30 min), then 25 ml/kg/h. If applicable, norepinephrine was added at 3 µg/kg/min (Centrafarm BV, Etten-Leur, NL), dobutamine at 10 µg/kg/min (Centrafarm BV, Etten-Leur, NL) and levosimendan at 3 µg/kg/min (Orion Pharma, Zug, Switzerland). In the 8th group 6 control animals underwent all procedures as all other animals but were not treated with lipopolysaccharide or resuscitation protocol. After completion of the protocol animals were euthanatized by potassium overdose.

### Calculations

The deconvolution of the PO<sub>2</sub> signals was performed as published earlier [14, 18]. The calculation of PO<sub>2</sub> histograms allows deriving the hypoxic or hyperoxic fractions. We defined PO<sub>2</sub> ≤ 10 mmHg as hypoxia [6, 19]. Hyperoxia was defined as ≥ 140 mmHg in the microcirculation and ≥ 90 mmHg in the mitochondria. Systemic oxygen delivery, consumption, and extraction were calculated using standard formulae [20].

### Myocardial injury biomarker

Serum troponin levels were measured by enzyme-linked immunosorbent assay from plasma sampled at the end of the experiment.

### Statistics

Normality was assessed with D'Agostino & Pearson test. Group differences of hemodynamic and oxygenation parameters were analyzed with mixed-effects model with Dunnett's correction model (GraphPad Prism 8.4.3, GraphPad Software, San Diego, CA, USA). Troponin and oxygenation at 300 min. were analyzed with Kruskal-Wallis test with Dunn's correction multiple comparisons test. A p < 0.05 was considered statistically significant. Data are presented as mean ± SD if not stated otherwise.

## RESULTS

Whole body oxygenation parameters can be found in the **eTable 1** which illustrates the arterial, central-venous and derived global oxygenation parameters of controls and treatment groups.

### Effects of LPS and fluid resuscitation on hemodynamics and oxygenation

#### Hemodynamics

Endotoxemia without fluid resuscitation induced a state of hemodynamic deterioration as witnessed by the sharp decrease in blood pressure just after the LPS-infusion (52\* ± 7.5 mmHg and 54\* ± 8.3 mmHg versus 120 ± 15.4 mmHg in non- and fluid resuscitated animals versus controls; \*p < 0.0001 versus control) with only partial, temporary recovery and further deterioration towards the end of the experiment. Furthermore, endotoxemia depressed cardiac output in the last two hours of the experiment and induced a slight decrease in heart rate towards the end of the experiment (**Figure 2, eFigure 1**).

Fluid resuscitation initially increased blood pressure compared to non-resuscitation (89 ± 16 mmHg versus 57 ± 15.1 mmHg; p < 0.01) but at the end of the experiment this effect disappeared. The same pattern was observed for cardiac output (330 ± 40.5 ml/min versus 140 ± 44.4 ml/min in fluid and non-resuscitated animals, respectively; p < 0.0001), whereas fluid was without effect on heart rate (471 ± 12 /min versus 481 ± 27 /min, p = 0.6299).

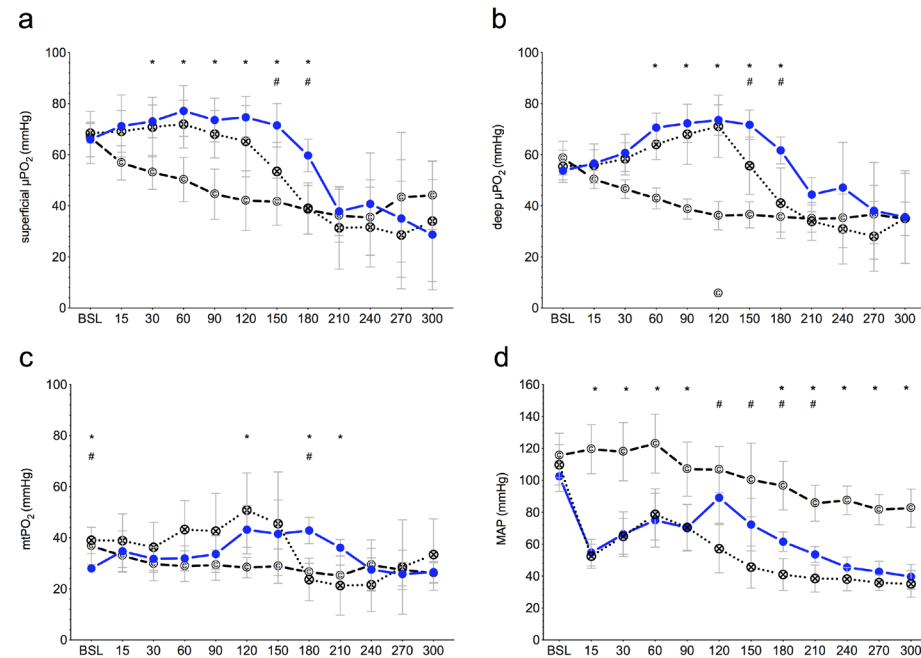


**Figure 2.** Hemodynamic and oxygenation measurements

Hemodynamic and oxygenation measurements of control (open circles and c), LPS-treated but non-resuscitated (crossed open circles) and LPS-treated and fluid resuscitated animals (blue dots). (a) superficial  $\mu\text{PO}_2$ , (b) deep  $\mu\text{PO}_2$ , (c) mt $\text{PO}_2$ , and (d) arterial pressure (MAP). Data are presented as mean  $\pm$  SD.  $p < 0.05$  (\*) fluid resuscitation versus control, (#) fluid resuscitation versus no resuscitation.

### Oxygenation

At baseline superficial  $\mu\text{PO}_2$  was  $67 \pm 7$  mmHg, deep  $\mu\text{PO}_2$   $56 \pm 6$  mmHg and mt $\text{PO}_2$   $35 \pm 7$  mmHg ( $n = 18$ ). During the first 90 minutes after infusion of endotoxin superficial and deep  $\mu\text{PO}_2$  were increased in the non-resuscitation and fluid resuscitation group as compared to control. At 90 min superficial and deep  $\mu\text{PO}_2$  in non-resuscitated, fluid resuscitated and control animals was  $74^* \pm 8.6$  mmHg and  $72^* \pm 7.4$  mmHg,  $68^\# \pm 9.3$  mmHg and  $68^* \pm 11.8$  mmHg,  $44.5 \pm 9.8$  mmHg and  $39 \pm 3.9$  mmHg, respectively ( $*p < 0.001$  and  $^\#p < 0.05$  versus control). Mitochondrial  $\text{PO}_2$  followed the same pattern of both, superficial and deep,  $\mu\text{PO}_2$  but to a lesser extent (Figure 2). Fluid resuscitation prolonged the period during which both superficial and deep  $\mu\text{PO}_2$  and mt $\text{PO}_2$  were higher than control values by about an hour and 30 minutes, respectively, as compared to the non-resuscitation group. Thereafter, superficial and deep  $\mu\text{PO}_2$  dropped back values similar to the control group for the later course. A compiled data set of the effect of fluid bolus resuscitation is shown in the Supplement (eFigure 2, which illustrates the effect of fluid bolus resuscitation on oxygenation, hemodynamics and derived oxygenation parameters).

The  $\text{PO}_2$  distribution obtained by deconvolution showed no increased microcirculatory

and mitochondrial hypoxia ( $\text{PO}_2 < 10$  mmHg) in the non-resuscitated LPS-treated animals (Figure 3). On the contrary, hypoxic fractions in the microcirculatory and mitochondrial compartments were even larger in the controls than in LPS-treated animals in the first 120 min. At 90 min the hypoxic fractions in controls were  $17 \pm 11\%$  (superficial  $\mu\text{PO}_2$ ),  $16 \pm 5\%$  (deep  $\mu\text{PO}_2$ ) and  $20 \pm 14\%$  (mt $\text{PO}_2$ ) whereas in LPS-treated animals, which all were unresuscitated by protocol at that time point, these fractions amounted to  $1 \pm 2\%$  in superficial  $\mu\text{PO}_2$  ( $p = 0.002$  versus controls),  $2 \pm 2\%$  in deep  $\mu\text{PO}_2$  ( $p = 0.002$ ) and  $2 \pm 3\%$  in mt $\text{PO}_2$  ( $p = 0.034$ ). Fluid bolus (at 120 min.) and fluid resuscitation had minor effects on hypoxic fractions in all three compartments, except for a trend to lowering of the hypoxic fractions at 210 min.

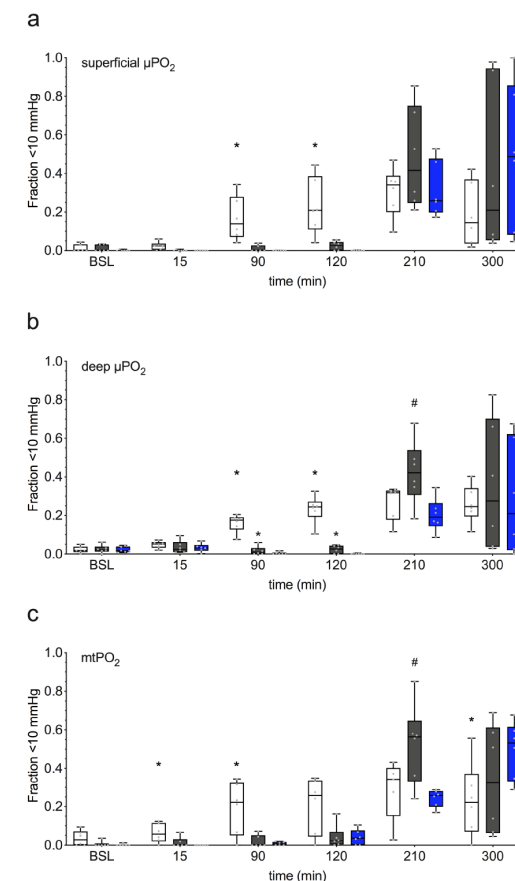


**Figure 3.** Hypoxic fractions in LPS-treated and control animals

Box plots (min. to max.) and readings of single animals (dots) representing the fractions  $< 10$  mmHg of deconvoluted (a) superficial  $\mu\text{PO}_2$ , (b) deep  $\mu\text{PO}_2$ , and (c) mt $\text{PO}_2$  measurements of control (white), non-resuscitated (black) and fluid resuscitated animals (blue).  $p < 0.05$  (\*) fluid resuscitation versus control, (#) fluid resuscitation versus no resuscitation.

### Effect of drug treatment in addition to fluid resuscitation

#### Hemodynamics

There was no difference in arterial pressure, cardiac output between any drug treatment group and fluid resuscitation only. Dobutamine, dobutamine plus norepinephrine and levosimendan plus norepinephrine led to a higher heart rate than in fluid only treated animals. The norepinephrine group led to a trend to higher arterial pressure as compared to fluid resuscitation only (**Figure 4, eFigure 3**).

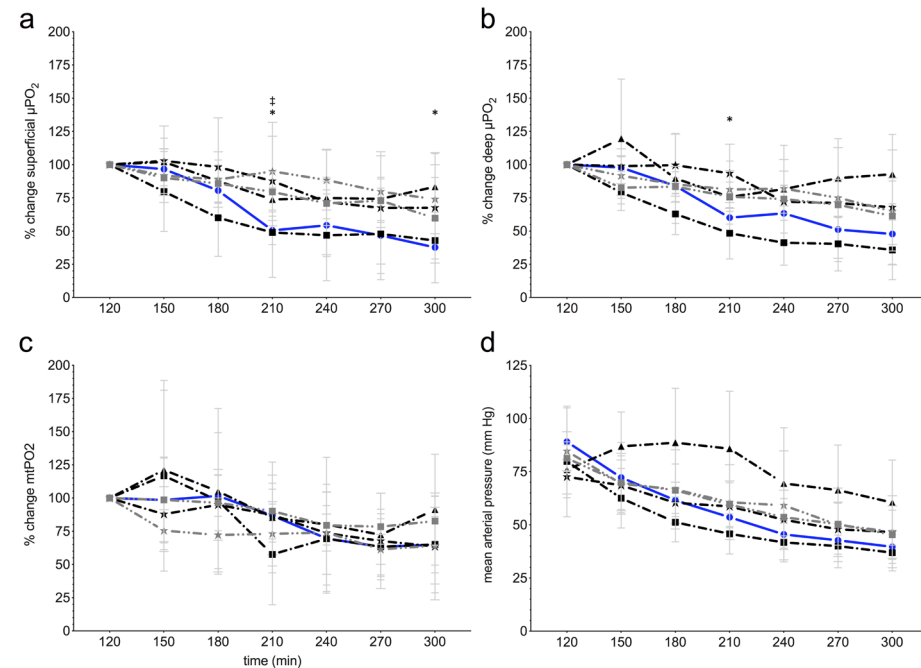


**Figure 4.** Effect of drug treatment on oxygenation and mean arterial pressure

(a) superficial  $\mu\text{PO}_2$ , (b) deep  $\mu\text{PO}_2$  and (c)  $\text{mtPO}_2$  plotted as percent change of the beginning of drug treatment (at 120 min), (d) mean arterial pressure. LPS-treated and fluid resuscitated (FR) animals (blue dots), FR plus norepinephrine (black triangle), FR plus dobutamine (black stars), FR plus levosimendan (black squares), FR plus norepinephrine and dobutamine (grey stars) and FR plus norepinephrine and levosimendan (grey squares).

Data are presented as mean  $\pm$  SD.  $p < 0.05$  (\*) fluid resuscitation (FR) versus FR plus norepinephrine and (†) FR versus FR plus norepinephrine and levosimendan.

#### Oxygenation

Addition of an inotrope, vasopressor or a combination of both had a very limited effect on both superficial and deep  $\mu\text{PO}_2$  and  $\text{mtPO}_2$  in comparison to fluid resuscitation alone, besides a trend to higher  $\mu\text{PO}_2$  values with norepinephrine as compared to fluid treatment only (**Figure 4**).

### Troponin

The troponin levels measured at the end of the experiment were elevated in all treatment groups containing norepinephrine ( $6.1 \pm 3.6 \mu\text{g/L}$ ,  $6.0 \pm 4.0 \mu\text{g/L}$  and  $5.2 \pm 2.5 \mu\text{g/L}$  in fluid plus norepinephrine, fluid plus norepinephrine and dobutamine and fluid plus norepinephrine and levosimendan versus  $1.1 \pm 0.7 \mu\text{g/L}$ ,  $1.4 \pm 0.8 \mu\text{g/L}$ ,  $1.5 \pm 0.5 \mu\text{g/L}$ ,  $2.3 \pm 1.2 \mu\text{g/L}$  and  $2.1 \pm 1.3 \mu\text{g/L}$  in controls, non-resuscitated, fluid resuscitated, fluid plus dobutamine and fluid plus levosimendan). The mitochondrial oxygenation and hypoxic fraction of  $\text{mtPO}_2$  of the norepinephrine groups were not different as compared to the other groups (**Figure 5**).

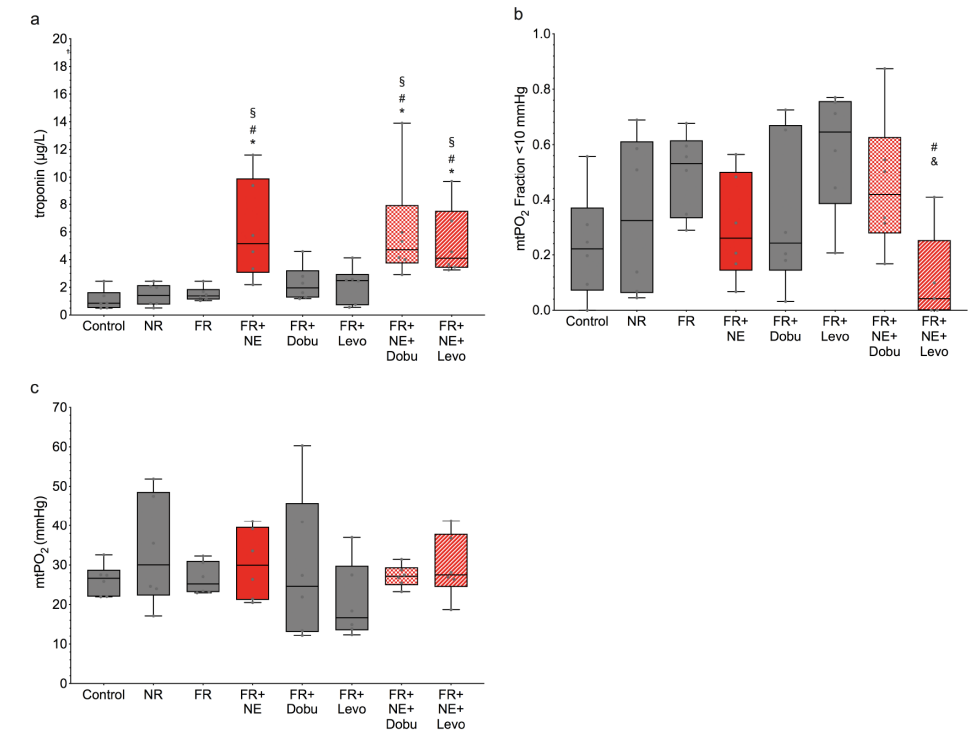


**Figure 5.** Troponinemia in norepinephrine-treated groups is not associated with hypoxia

Box plots (min. to max.) and readings of single animals (dots) at 300 min. (a) troponin levels, (b) fractions  $< 10$  mmHg of deconvoluted  $\text{mtPO}_2$ , (c)  $\text{mtPO}_2$ .  $p < 0.05$  (\*) versus control, (#) versus no resuscitation, (§) versus fluid resuscitation (FR), (&) versus FR plus levosimendan.

## DISCUSSION

In this study we investigated whether endotoxemic shock causes myocardial hypoxia. Further the effect of protocol-based resuscitation on microcirculatory and mitochondrial oxygenation in rat hearts was assessed. It is the first study addressing the oxygenation in the cardiac microcirculatory and mitochondrial compartment simultaneously *in vivo* in endotoxemia. Our study showed that myocardial microcirculatory and mitochondrial oxygenation is preserved during endotoxemic shock and not affected by various resuscitation procedures.

Our study underpins the conception of an unparalleled cardiac functional morphology with a high density of capillaries [21] and mitochondria [22] making hearts resilient to hypoxia even under severe conditions such as endotoxemic shock. In earlier studies we investigated the oxygen supply dependency of various organs in rats. Of all organs studied hearts could tolerate the lowest hematocrit when hemodiluted prior to becoming oxygen supply-dependent, with critical hematocrit being 30%, 20% and 5% respectively for the kidney, intestines and heart [23].

The supportive drug treatments with norepinephrine, dobutamine or levosimendan as well as their combination did not significantly alter the course of  $\mu\text{PO}_2$  and  $\text{mtPO}_2$ . However, norepinephrine entailed cellular damage, expressed as elevated troponin levels in all norepinephrine groups, not found in all other treatment groups. Our study suggests care should be taken with the use of norepinephrine as a vasopressor since it may lead to myocardial injury [24, 25].

In our study, we provide direct measurement of myocardial  $\mu\text{PO}_2$  and  $\text{mtPO}_2$ . We found no evidence of hypoxia during endotoxemic shock. Neither  $\mu\text{PO}_2$  nor  $\text{mtPO}_2$  dropped to 10 mmHg, let alone lower values, which could be interpreted as hypoxia [6, 19, 26]. Also, after adopting a deconvolution of the  $\text{PO}_2$  measurements, no hypoxia could be uncovered. In fact, we found sustained and even transiently increased microcirculatory oxygenation during endotoxemic shock. These findings are in line with our earlier indirect measurements of myocardial dysoxia. In isolated endotoxemic hearts we found no increased NADH fluorescence in endotoxemic hearts. However, in line with our present findings, the use of potent vasoconstrictor agents, in our previous study this were NO inhibitors and vasopressin, an increase of NADH fluorescence was seen [25].

There are several lines of investigation that indicate mitochondrial dysfunction as contributor to myocardial depression well known in sepsis. Our finding of unaltered, or even increased, mitochondrial oxygen levels fit in this concept. Very similar results have been described in isolated endotoxemic rat hearts, in which higher myoglobin saturations have been found than in controls. When oxygen shortage was applied, myoglobin desaturation was less in endotoxemic hearts, suggesting reduced oxygen consumption in endotoxemia [27]. The temporal impact on the alteration of myocardial mitochondrial function has been shown by others as well [28]. A reduced complex I

activity was found at 6h, but not at 2h after LPS injection [29]. Moreover, the type of inhibition changed over time transmuting the competitive inhibition of complex IV to non-competitive after 48h [30]. This gives an indication of the severity of the insult and foretells its consequences as well.

The apparently conflicting results of (non-) presence of decreased  $\mu\text{PO}_2$  or mitochondrial function found in the literature need to be interpreted in the light of the dynamicity of sepsis as well as varying mitochondrial sensitivity [31]. Reduced myocardial but not skeletal muscle, renal and liver mitochondrial function has been described in endotoxemia [28, 29, 32]. In common to the mentioned studies are the findings of either higher sensitivity to LPS-dose and/or earlier decrease of function of the myocardial mitochondria. Furthermore, comparability is apparently hampered not only the type of sepsis (model) but also its severity. Accordingly, we found hypoxic signals within the deconvoluted  $\mu\text{PO}_2$  of the renal cortex in severe endotoxemic shock but not in a normotensive version of the model. Yet, in both models mean  $\mu\text{PO}_2$  exceeded the hypoxic threshold. Even more interestingly, the animals in shock additionally developed a hyperoxic signal [20, 33].

### Effect of treatment

Fluid resuscitation yielded only a transient positive effect on  $\text{mtPO}_2$  and  $\mu\text{PO}_2$ , while additional inotrope, vasopressor or a combination therapy had no significant impact. Only levosimendan monotherapy led to a trend to lower  $\mu\text{PO}_2$  and  $\text{mtPO}_2$  and inotrope-vasopressor combination to slightly higher  $\mu\text{PO}_2$  values than other regimens.

The mechanistic model, that hypoperfusion or heterogenous perfusion at the microcirculatory level causes cellular hypoxia and as a consequence organ failure, has led to the strategy of reestablishing perfusion and oxygen delivery. The current sepsis treatment guidelines are based upon this assumption [34, 35]. As discussed above, ample evidence supports the notion that faulty oxygen delivery is most probably not the key-player in the pathogenesis of sepsis-induced organ dysfunction. Based on these thoughts the strategy of reestablishing perfusion, which represents currently the sole supportive therapy in sepsis, should be challenged. Moreover, early goal-directed therapy (EGDT) and “EGDT-like” usual care resuscitation protocols pursuing this goal have proved not to affect outcome beneficially, if not even causing harm [36, 37]. In fact, our study appears to corroborate this hypothesis. Hypoxia was not found. Furthermore, fluid resuscitation led to a superfluous increase of oxygen delivery expressed by a rise of  $\text{mtPO}_2$  to supra-normal levels.

### Myocardial damage

Troponin level elevation in the blood has been linked to septic cardiomyopathy. More importantly, it has been associated to higher requirements of catecholamines and worse outcome [3, 4, 38]. The exact mechanism of troponin release in septic cardiomyopathy

is still under investigation. Direct inflammatory and its secondary effects as regional heterogenous perfusion, hypoxia and altered oxygen utilization, but also direct impact of LPS and gram-positive bacterial toxins on cardiomyocytes are being debated [10, 39]. We therefore measured troponin levels in all animals after completion of the experimental protocol. Unexpectedly, animals treated with norepinephrine alone or in combination with dobutamine or levosimendan were found to have significantly higher troponin levels than animals of all other treatment groups. The macrohemodynamic parameters of norepinephrine-treated animals were closer to those of the controls. Furthermore, the  $mtPO_2$  values were neither lower nor the hypoxic fractions higher. Others have shown to be able to restore subendocardial flow even to supra-normal levels with norepinephrine [40]. In fact, in our norepinephrine- and norepinephrine-dobutamine-treated animals the difference between superficial and deep  $\mu PO_2$  was similar to controls. This suggests that endotoxin-associated flow redistribution could be corrected by these regimens in our model. Moreover, the restoration of a endotoxin-depressed complex I- and II-dependent respiratory control ratio by norepinephrine has been described [41]. Thus, no link to an insufficient, absolute or regional, oxygen supply or consumption appears to be present.

A causal connection of catecholamine therapy and elevation of troponin levels is increasingly recognized. Apoptosis and necrosis have been described in association to catecholamine use [42, 43]. Moreover, catecholamine therapy fueled LPS-induced apoptosis via multiple pathways in cardiomyocytes [44]. Cell culture and animal studies provided evidence that  $\beta_1$ -adrenoreceptor ( $\beta_1$ -AR) activation leads to protein kinase A activation, calcium entry via voltage-dependent calcium channels [45], increase of intracellular ROS and inflammatory mediators and finally, activation of caspase pathways [46]. Interestingly, no troponin increase was found in the group treated with dobutamine. This could be explained by the fact that norepinephrine seems to induce more harm than other catecholamines [42].

Even though some trials failed to prove the link between norepinephrine therapy and myocardial damage in septic patients [47] the use of catecholamines is more and more questioned [12, 48]. On the other hand, there is a need to ensure a sufficient perfusion pressure of all organs. An appealing alternative to changing vasopressor therapy to vasopressin and its analogues, which also have their drawbacks, is the selective blockade of the  $\beta_1$ -AR. This strategy has not only proven to diminish proinflammatory mediators and apoptosis but also seems to provide better outcomes [44, 49]. As much promising as this may appear in a rat model of sepsis induced by intraperitoneal injection of fecal slurry esmolol led to 50% reduction of the mortality of the animals predicted to be dying at the expense of doubling the mortality of the animals predicted to survive [50]. Thus, choosing the right patients will represent the forthcoming challenge.

### Limitations

The measurement of the beating heart *in vivo* and *in situ* confers the risk of measuring disparate points on the heart. Knowing that oxygen delivery and consumption are distributed heterogeneously [51], translational movement could potentially lead to differing readings. In order to minimize translation of the measuring point a microscrew-operated custom-made fibre holder, optimized surgical access and short fibre-myocardium distance were used.

Another issue is the real value of  $\mu PO_2$  and  $mtPO_2$ . Our  $\mu PO_2$  data match the measurements presented by others [52]. Invasive oxygenation measurements have yielded lower myocardial  $\mu PO_2$  than reported here [6]. Conjoint experiments of non- and invasive  $\mu PO_2$  measurements, however, demonstrated a good correlation of both methods [53]. For  $mtPO_2$  no comparative data exist. A wide range is given by other methods: 1.1 to 40.7 mmHg [54, 55]. Lower values tend to be found in single cell and invasive measurements. Even if we'd assume a 50% reduction of our values, if measured invasively, the here presented measurements were still above the hypoxic threshold.

Concerning the experimental design, it might be argued that treatment with inotropes led to hypotension and by consequence to lower  $PO_2$  values. For reasons of comparability of the animals we decided to administer fixed drug doses. In the clinical routine, however, the vasopressor dose would have been adapted accordingly to an arterial pressure target. This instance most probably would have prevented the lower  $PO_2$  values. Finally, endotoxemia models have attracted a series of criticism [56].

### CONCLUSION

Currently, treatment guidelines advocate a strategy of reestablishing perfusion pressure and oxygen delivery with the goal to prevent tissue hypoxia caused by septic shock. While resuscitation targets may be effective in rescuing vulnerable organs such as the kidney, they seem not effective to ameliorate myocardial injury. This finding is corroborated by the (supra-)normal  $\mu PO_2$  and sustained  $mtPO_2$  values found in our study. Moreover, fluid resuscitation led to a further rise of  $mtPO_2$  expressing the lack of need of additional  $O_2$  in the mitochondria. The treatment with norepinephrine, dobutamine or levosimendan as well as their combination did not significantly alter the course of  $\mu PO_2$  and  $mtPO_2$ . However, all treatments including norepinephrine had higher troponin levels suggesting drug-related cellular damage. Based on these observations we suggest the treatment target should be changed, away from the mechanistic cardiovascular resuscitation to one focused more on the cellular level.

## REFERENCES

1. Pettila V, Jakob SM, Takala J: The new sepsis/septic shock-3 definition is just not enough- more detailed research is needed. *Acta Anaesthesiol Scand* 2016; 60:1344–1346
2. Singer M, Deutschman CS, Seymour CW, et al.: The Third International Consensus Definitions for Sepsis and Septic Shock (Sepsis-3). American Medical Association; 2016. p. 801–810
3. Landesberg G, Jaffe AS, Gilon D, et al.: Troponin elevation in severe sepsis and septic shock: the role of left ventricular diastolic dysfunction and right ventricular dilatation\*. *Critical Care Medicine* 2014; 42:790–800
4. Bessière F, Khenifer S, Dubourg J, et al.: Prognostic value of troponins in sepsis: a meta-analysis. *Intensive Care Med* 2013; 39:1181–1189
5. Graetz TJ, Hotchkiss RS: Sepsis: Preventing organ failure in sepsis — the search continues. *Nature Publishing Group* 2016; 13:5–6
6. Bateman RM, Tokunaga C, Kareco T, et al.: Myocardial hypoxia-inducible HIF-1 $\alpha$ , VEGF, and GLUT1 gene expression is associated with microvascular and ICAM-1 heterogeneity during endotoxemia. *AJP: Heart and Circulatory Physiology* 2007; 293:H448–56
7. Cunnion RE, Schaer GL, Parker MM, et al.: The coronary circulation in human septic shock. *Circulation* 1986; 73:637–644
8. Hotchkiss RS, Rust RS, Dence CS, et al.: Evaluation of the role of cellular hypoxia in sepsis by the hypoxic marker [18F]fluoromisonidazole. *Am J Physiol* 1991; 261:R965–72
9. Alvarez S, Vico T, Vanasco V: Cardiac dysfunction, mitochondrial architecture, energy production, and inflammatory pathways: Interrelated aspects in endotoxemia and sepsis. *Int J Biochem Cell Biol* 2016; 81:307–314
10. Rudiger A, Singer M: Mechanisms of sepsis-induced cardiac dysfunction. *Critical Care Medicine* 2007; 35:1599–1608
11. Mokhtari B, Yavari R, Badalzadeh R, et al.: An Overview on Mitochondrial-Based Therapies in Sepsis-Related Myocardial Dysfunction: Mitochondrial Transplantation as a Promising Approach. *Can J Infect Dis Med Microbiol* 2022; 2022:3277274
12. Andreis DT, Singer M: Catecholamines for inflammatory shock: a Jekyll-and-Hyde conundrum. *Intensive Care Med* 2016; 42:1387–1397
13. Vanderkooi JM, Maniara G, Green TJ, et al.: An optical method for measurement of dioxygen concentration based upon quenching of phosphorescence. *J Biol Chem* 1987; 262:5476–5482
14. Mik EG, Ince C, Eerbeek O, et al.: Mitochondrial oxygen tension within the heart. *Journal of Molecular and Cellular Cardiology* 2009; 46:943–951
15. Balestra GM, Aalders MCG, Specht PAC, et al.: Oxygenation measurement by multi-wavelength oxygen-dependent phosphorescence and delayed fluorescence: catchment depth and application in intact heart. *J Biophotonics* 2015; 8:615–628
16. Bodmer SIA, Balestra GM, Harms FA, et al.: Microvascular and mitochondrial PO<sub>2</sub> simultaneously measured by oxygen-dependent delayed luminescence. *J Biophotonics* 2012; 5:140–151
17. Mik EG, Stap J, Sinaasappel M, et al.: Mitochondrial PO<sub>2</sub> measured by delayed fluorescence of endogenous protoporphyrin IX. *Nat Meth* 2006; 3:939–945
18. Mik EG, Johannes T, Zuurbier CJ, et al.: In vivo mitochondrial oxygen tension measured by a delayed fluorescence lifetime technique. *Biophys J* 2008; 95:3977–3990
19. Connett RJ, HONIG CR, Gayeski TE, et al.: Defining hypoxia: a systems view of VO<sub>2</sub>, glycolysis, energetics, and intracellular PO<sub>2</sub>. *J Appl Physiol* 1990; 68:833–842
20. Johannes T, Mik EG, Nohé B, et al.: Influence of fluid resuscitation on renal microvascular PO<sub>2</sub> in a normotensive rat model of endotoxemia. *Crit Care* 2006; 10:R88
21. Pathi VL, McPhaden AR, Morrison J, et al.: The effects of cardioplegic arrest and reperfusion on the microvasculature of the heart. *Eur J Cardiothorac Surg* 1997; 11:350–357
22. Vega RB, Horton JL, Kelly DP: Maintaining ancient organelles: mitochondrial biogenesis and maturation. *Circulation Research* 2015; 116:1820–1834
23. van Bommel J, Siegemund M, Henny CP, et al.: Heart, kidney, and intestine have different tolerances for anemia. *Transl Res* 2008; 151:110–117
24. Jozwiak M, Hamzaoui O: Adherence to surviving sepsis campaign guidelines 2016 regarding fluid resuscitation and vasopressors in the initial management of septic shock: The emerging part of the iceberg! *Journal of Critical Care* 2022; 68:155–156
25. Teboul J-L, Duranteau J, Russell JA: Intensive care medicine in 2050: vasopressors in sepsis. *Intensive Care Med* 2018; 44:1130–1132
26. Araki R, Tamura M, Yamazaki I: The effect of intracellular oxygen concentration on lactate release, pyridine nucleotide reduction, and respiration rate in the rat cardiac tissue. *Circulation Research* 1983; 53:448–455
27. Schenkman KA, Arakaki LSL, Ciesielski WA, et al.: Optical spectroscopy demonstrates elevated intracellular oxygenation in an endotoxic model of sepsis in the perfused heart. *Shock* 2007; 27:695–700
28. Trumbeckaite S, Opalka JR, Neuhofer C, et al.: Different sensitivity of rabbit heart and skeletal muscle to endotoxin-induced impairment of mitochondrial function. *Eur J Biochem* 2001; 268:1422–1429
29. Fukumoto K, Pierro A, Spitz L, et al.: Neonatal endotoxemia affects heart but not kidney bioenergetics. *Journal of Pediatric Surgery* 2003; 38:690–693
30. Levy RJ, Vijayasarathy C, Raj NR, et al.: Competitive and noncompetitive inhibition of myocardial cytochrome C oxidase in sepsis. *Shock* 2004; 21:110–114
31. Jeger V, Djafarzadeh S, Jakob SM, et al.: Mitochondrial function in sepsis. *Eur J Clin Invest* 2013; 43:532–542
32. Kozlov AV, Staniek K, Haindl S, et al.: Different effects of endotoxic shock on the respiratory function of liver and heart mitochondria in rats. *Am J Physiol Gastrointest Liver Physiol* 2006; 290:G543–9
33. Legrand M, Bezemer R, Kandil A, et al.: The role of renal hypoperfusion in development of renal microcirculatory dysfunction in endotoxemic rats. *Intensive Care Med* 2011; 37:1534–1542
34. Evans L, Rhodes A, Alhazzani W, et al.: Surviving sepsis campaign: international guidelines for management of sepsis and septic shock 2021. *Intensive Care Med* 2021; 47:1181–1247
35. Hollenberg SM: Inotrope and vasopressor therapy of septic shock. *Crit Care Clin* 2009; 25:781–802
36. PRISM Investigators, Rowan KM, Angus DC, et al.: Early, Goal-Directed Therapy for Septic Shock - A Patient-Level Meta-Analysis. *N Engl J Med* 2017; 376:2223–2234



37. Singer M, Glynn P: Treating critical illness: the importance of first DOIng no harm. *PLoS Med* 2005; 2:e167
38. Maeder M, Fehr T, Rickli H, et al.: Sepsis-associated myocardial dysfunction: diagnostic and prognostic impact of cardiac troponins and natriuretic peptides. *Chest* 2006; 129:1349–1366
39. Tavener SA: Immune Cell Toll-Like Receptor 4 Is Required for Cardiac Myocyte Impairment During Endotoxemia. *Circulation Research* 2004; 95:700–707
40. Lorigados CB, Ariga SK, Batista TR, et al.: Endotoxaemic myocardial dysfunction: the role of coronary driving pressure in subendocardial perfusion. *Crit Care Resusc* 2015; 17:12–22
41. Regueira T, Bänziger B, Djafarzadeh S, et al.: Norepinephrine to increase blood pressure in endotoxaemic pigs is associated with improved hepatic mitochondrial respiration. *Crit Care* 2008; 12:R88
42. Burniston JG, Ellison GM, Clark WA, et al.: Relative toxicity of cardiostimulant agents: some induce more cardiac and skeletal myocyte apoptosis and necrosis in vivo than others. *Cardiovasc Toxicol* 2005; 5:355–364
43. Schmittinger CA, Dünser MW, Torgersen C, et al.: Histologic Pathologies of the Myocardium in Septic Shock. *Shock* 2013; 39:329–335
44. Wang Y, Wang Y, Yang D, et al.:  $\beta_1$ -adrenoceptor stimulation promotes LPS-induced cardiomyocyte apoptosis through activating PKA and enhancing CaMKII and I $\kappa$ B $\alpha$  phosphorylation. *Crit Care* 2015; 19:76
45. Communal C, Singh K, Pimentel DR, et al.: Norepinephrine stimulates apoptosis in adult rat ventricular myocytes by activation of the beta-adrenergic pathway. *Circulation* 1998; 98:1329–1334
46. Fu Y-C, Chi C-S, Yin S-C, et al.: Norepinephrine induces apoptosis in neonatal rat endothelial cells via down-regulation of Bcl-2 and activation of beta-adrenergic and caspase-2 pathways. *Cardiovascular Research* 2004; 61:143–151
47. Mehta S, Granton J, Gordon AC, et al.: Cardiac ischemia in patients with septic shock randomized to vasopressin or norepinephrine. *Critical Care* 2013; 17:R117
48. Schmittinger CA, Wurzing B, Deutinger M, et al.: How to protect the heart in septic shock: a hypothesis on the pathophysiology and treatment of septic heart failure. *Med Hypotheses* 2010; 74:460–465
49. Morelli A, Ertmer C, Westphal M, et al.: Effect of heart rate control with esmolol on hemodynamic and clinical outcomes in patients with septic shock: a randomized clinical trial. *JAMA* 2013; 310:1683–1691
50. Andreis DT, Khaliq W, Singer M: Survival impact of  $\beta$ -blockade in a long-term model of fluid resuscitated sepsis depends on prognostic risk. *Intensive Care Med Exp* 2016; 4:454
51. Zuurbier CJ, van Iterson M, Ince C: Functional heterogeneity of oxygen supply-consumption ratio in the heart. *Cardiovascular Research* 1999; 44:488–497
52. Ranji M, Jaggard DL, Apreleva SV, et al.: Simultaneous fluorometry and phosphometry of Langendorff perfused rat heart: ex vivo animal studies. *Opt Lett* 2006; 31:2995–2997
53. Dyson A, Bezemer R, Legrand M, et al.: Microvascular and interstitial oxygen tension in the renal cortex and medulla studied in a 4-h rat model of LPS-induced endotoxemia. *Shock* 2011; 36:83–89
54. Richmond KN, Burnite S, Lynch RM: Oxygen sensitivity of mitochondrial metabolic state in isolated skeletal and cardiac myocytes. *Am J Physiol* 1997; 273:C1613–22
55. Kadatz R: Sauerstoffdruck und Durchblutung im gesunden und koronarinsuffizienten Myokard des Hundes und ihre Beeinflussung durch koronarweiternde Pharmaka. *Archiv für Kreislaufforschung* 1969; 58:263–293
56. Osuchowski MF, Ayala A, Bahrami S, et al.: Minimum quality threshold in pre-clinical sepsis studies (MQTiPSS): an international expert consensus initiative for improvement of animal modeling in sepsis. *Intensive Care Med Exp* 2018; 6:26

# CHAPTER

General discussion

# 9



## GENERAL DISCUSSION

Oxygen is essential in many cellular metabolic pathways. It plays a pivotal role for some signal transduction and defense mechanisms, but is most important in aerobic energy production [1]. Multiple evidence points towards involvement of oxygen in pathological processes of several diseases. In the heart this is particularly true for ischemic and septic cardiomyopathy as well as for acute and chronic heart failure [2-4]. Until now, in the heart, oxygen's role in these processes has mostly been assessed *ex vivo* [5], indirectly [6], with infrequent or invasive measurements [7]. Dual-wavelength phosphorimetry allowing measurements of microcirculatory PO<sub>2</sub> at two different depths {Johannes, 2006 32 /id} and a technique to measure mitochondrial oxygenation [8] opened up the opportunity to measure both microcirculatory *and* mitochondrial oxygenation *in vivo*, non-invasively, repetitively and (near-)simultaneously.

In this thesis, the focus was set on the further characterization of this measurement method, the application of these techniques to measure oxygen in the heart *in vivo*, and finally, on investigating the role of microcirculatory and mitochondrial oxygenation in two disease models.

Studies on the contribution of the microcirculation and mitochondria to the development and evolution of diseases, have accrued a growing amount of evidence on microcirculatory and mitochondrial dysfunction from laboratory experiments in the last decades. This is discussed in the **second chapter** with focus on sepsis-induced organ failure [9]. Until today, clinical human data are still sparse. This is mainly due to the fact that some diagnostic tools are available for evaluating the microcirculation but until lately no tool for assessing mitochondrial function existed. However, based on further development of the phosphorimetric method to measure mitochondrial oxygen described by our laboratory, a clinically applicable tool has now been developed [8,10]. The low number of clinically available tools is reflected by the fact that no microcirculatory or mitochondrial parameter is routinely measured other than lactate. The lack of such measurements in the clinical arena is probably the reason why none of these parameters are yet suggested as a treatment target in treatment guidelines. This is not exclusively due to technical limitations but also due to the fact that a thorough comprehensive concept and its translation to human clinic is still lacking. Some elements of a putative concept assert themselves: heterogeneous microcirculatory and mitochondrial dysfunction is a typical finding in sepsis and several cardiac diseases [11]. It remains unclear whether these findings are the result of a hibernation-like, self-protective process or fruit of a "maladaptive" dysfunction *per se* arising from direct damage (e.g. lipopolysaccharine, interleukine) or indirectly via hypoperfusion and hypoxia. The temporal span and magnitude of the insult (e.g. inoculum size, virulence, severity and duration of shock), however, appear to have a sizable impact on whether the dysfunction is temporary ("adaptive") or irreversible ("maladaptive"). The finding in

a murine cecal ligation and puncture model that inhibition of myocardial cytochrome c oxidase was reversible during early sepsis, but irreversible by 48h [12] gives rise to the assumption that there is a continuum between the self-protective and dysfunctional state. However, the interplay of microcirculatory and mitochondrial oxygenation and their contribution to diseases leaves still many unanswered questions. Hence, in order to match this need more experimental evidence and new technologies are required to provide new insights.

Vanderkooi first described measurement of oxygen by oxygen-dependent quenching of phosphorescence lifetime [13]. In our laboratory a further development of this technique led to a dual-wavelength phosphorimeter allowing measurements of microcirculatory oxygenation at two different depths {Johannes, 2006 32 /id}. The translation and modification of this technology led to a technique for measuring mitochondrial oxygenation [8]. The logical next step was the combination of the measurement of microcirculatory and mitochondrial oxygenation, which is described in the **third chapter** [14]. In this work we also showed the absence of crosstalk of the two retrieved measuring signals and analyzed the influence of noise on measurement accuracy. The method was feasible to measure hepatic microcirculatory and mitochondrial oxygenation *in vivo*. Evaluation of phosphorescence signal analysis proved the advantage of using a rectangular distribution method over mono-exponential analysis.

In this thesis the focus was set on microcirculatory and mitochondrial oxygenation measurements in the heart. Thus optical characterization of these oxygenation measurements was provided in the **fourth chapter** [15]. Monte Carlo simulations and *ex vivo* experiments found an excellent correlation of calculated and measured phosphorescence and provided the catchment depth of the superficial and deep microcirculatory and mitochondrial oxygenation measurements. For the first time the feasibility of measuring changes in microcirculatory and mitochondrial oxygen partial pressures in rat hearts *in vivo* in experiments lasting up to 5 hours was provided.

The novel measurement method of mitochondrial oxygen partial pressure using oxygen-dependent quenching of the phosphorescence in the heart required further characterization. This was reported in the **fifth chapter** [16]. In isolated cardiomyocytes we could prove, that the phosphorescence signal matched with the localization of MitoTracker Green-stained mitochondria, demonstrating the mitochondrial origin of the phosphorescence signal. Further, aminolevulinic acid, required to enhance protoporphyrin IX (PpIX) production and phosphorescence signal intensity, did not compromise oxygen consumption. Then lifetime under zero oxygen ( $\tau_0=0.8\text{ms}$ ) and time constant ( $kq = 826 \text{ mm Hg}^{-1}\text{s}^{-1}$ ) were determined in isolated cardiomyocytes. These values were used to convert lifetimes to calculate mitochondrial PO<sub>2</sub> in Langendorff-perfused hearts, in which oxygen consumption had been blocked with cyanide. These experiments showed consistency of the mitochondrial and the perfusate PO<sub>2</sub>. Moreover, the origin of the PpIX phosphorescence signal was homogeneously distributed in the

heart. Standard Langendorff-perfused hearts showed a slightly lower mean mitoPO<sub>2</sub> of 29 ± 5 mm Hg than the 40 ± 3 mm Hg that was observed with maximal vasodilatation (at 95% perfusate O<sub>2</sub>). The reason was found with deconvolution of the mitoPO<sub>2</sub> signal, which uncovered relevant fractions of mitochondria (30-55%) with a low mitoPO<sub>2</sub> (0-10mmHg) in standard Langendorff-perfused hearts when decreasing perfusate O<sub>2</sub> (95% to 45%). In maximally vasodilated state these fractions were smaller and matched those values retrieved from *in vivo* hearts with approximately 10% low mitoPO<sub>2</sub> at 95% perfusate O<sub>2</sub> or 40% inhaled O<sub>2</sub>, respectively [16]. These findings confirmed older data, which indicated that standard perfused, isolated hearts might be hypoxic, even when provided with 95% dissolved oxygen in the perfusate [17].

With these experiments we could show, that the mitochondrial oxygen tension was higher than earlier estimated from cytosolic, interstitial respectively vascular measurements, notably 35±5 mmHg instead of 3-17 mmHg [18-20]. Our measurements yielded microcirculatory PO<sub>2</sub> of 67±3 mmHg and were thus well in line with the new consensus that tissue oxygenation was not as low as suggested by Whalen and Clarke's experiments in the 70ies [21].

Based on these foundations, we further explored oxygen partial pressures in microcirculation and mitochondria in disease models. In particular in the clinical treatment of diseases the direct monitoring of the cellular state remains a pivotal missing piece of the puzzle – as discussed in **Chapter 6** [22]. In healthy subjects, the macrocirculation, microcirculation and mitochondria present an equilibrium, aiming at meeting the metabolic needs of the cells in terms of oxygen and nutrients (hemodynamic coherence). The loss of this coherence in disease has been shown to be associated with worse outcome [23]. Cellular, hence mitochondrial limitation of oxygen may lead to decreased function, hibernation and change of metabolic pathways as adaptive conformance to hypoxia with transition to dysfunction and (programmed) cellular death. Whether oxygen conformance is an adaptive consequence or the causative process of loss of hemodynamic coherence is currently unresolved.

In this light we investigated, in **Chapter 7**, the mitochondrial oxygen partial pressures in a model of pulmonary arterial hypertension leading to right ventricular hypertrophy and failure. The aim was to answer the long-standing question whether heart failure, an engine out of fuel [3], was caused by mitochondrial oxygen shortage [24].

In rats exposed to different dosages of monocrotaline (MCT), we could induce compensated right ventricular hypertrophy (low dose MCT) and right ventricular failure (high dose MCT). Strikingly, no evidence of cardiac mitochondrial hypoxia was observed in any stage of hypertrophy or heart failure. In the failing right hearts, mitochondrial oxygenation was similar under decreased oxygen supply or increased work demand conditions as compared to healthy hearts. At baseline condition mitochondrial oxygenation was even higher in failing right hearts with less mitochondria in the 0-20 mmHg mitoPO<sub>2</sub> range than in hypertrophied or control ventricles (15% vs. 48%

resp. 54%). This finding was matched with evidence of metabolic reprogramming. At a similar mitochondrial mass we found an increased glycolytic hexokinase activity at increasing MCT dose and increased lactate dehydrogenase activity only in compensated hypertrophied right ventricles. These findings suggested a down-regulation of *in vivo* mitochondrial metabolism because of increased anaerobic glycolysis. The decreased mitochondrial metabolism than resulted in decreased oxygen consumption and a rise in the number of mitochondria displaying higher oxygen levels. Most importantly, hypoxia in these severe diseased hearts was not observed. In fact, this had been postulated as mechanism of heart failure in pulmonary hypertension [25]. Supporting results of this thesis were found in permeabilized cardiac fibers and minced heart tissue in which reduced oxygen consumption was found after monocrotaline administration [26-28]. As oxygen availability is tightly linked to oxygen delivery in the heart the increased mitoPO<sub>2</sub> is either to be led back to decreased consumption or increased delivery. As in failing right hearts cardiac output is lower so is oxygen delivery. We did however, not measure cardiac output in our experiments. Heart rate and blood pressure were lower in animals with failing right heart. Others have demonstrated the presence of lower cardiac output in the same model and decreased myocardial blood flow reserve in hypertrophied right ventricles [29,30]. Moreover, decreased vessels density and larger diffusion distance further hamper oxygen availability in these hearts [31]. These findings support the assumption of reduced myocardial oxygen consumption. In a recent study, contrary to our findings, reduced microvascular oxygenation has been described in the right heart, but preserved PO<sub>2</sub> in the left heart [29]. Moreover, an increase of right but not left ventricular oxygenation was found after administration of myo-inositol pyrotriphosphate which increases oxygen release of hemoglobin. Some technical and experimental design limitations of this study appear. Reproducing the same depth of a 100 μm probe inserted into a beating right ventricle is very challenging. It is thus questionable whether comparable biologic compartments were measured in left, right and hypertrophied right ventricles. This might explain why control animals had a much higher microvascular oxygenation in the right ventricles than in the left ventricles (32 ± 5 and 15 ± 8 mmHg). Our own measurements of microcirculatory PO<sub>2</sub> revealed no significant difference between the right and left ventricle at comparable conditions (53 ± 10 mmHg and 66 ± 13 mmHg). The positive response to increased oxygen release in the right ventricle, however, corroborates the suggested oxygen limitation. In line with this are several experiments which showed an up-regulated hypoxia inducible-factor 1α (HIF-1α) expression in right ventricles of pulmonary hypertensive rats [32-34]. The upregulated HIF-1α pathway has been shown to lead to a metabolic shift towards glycolysis [35,36]. The increased hexokinase activity found in our study is thus well compatible with this finding. Now it could be hypothesized, that the increased mitochondrial oxygen partial pressures could be led back to decreased oxygen consumption due to the switch to glycolysis.

Decreased mitochondrial oxygen consumption and diminished production of ATP, resulting from mitochondrial dysfunction or adaptation to hypoperfusion and cellular oxygen shortage, was also a long-lasting hypothesis explaining sepsis-induced organ dysfunction. Thus, to investigate whether myocardial oxygen shortage is present in sepsis, we investigated, for the first time, the cardiac oxygenation of the microcirculation and mitochondria in endotoxemia and usual clinical supportive therapies in rat hearts *in vivo* (**Chapter 8**; Balestra et al. 2023 submitted). After induction of an endotoxemic shock rats were either not treated at all or received a protocol-based treatment with fluid, fluid plus dobutamine, fluid plus levosimendan, fluid plus norepinephrine, fluid plus norepinephrine and dobutamine or fluid plus norepinephrine and levosimendan. Additionally, hemodynamic parameters and troponin levels were measured.

In all these experiments, similar as for the right heart failure model, hypoxia was not observed. On the contrary, (supra-)normal microcirculatory PO<sub>2</sub> and sustained mitochondrial PO<sub>2</sub> values were actually found in endotoxemic rat hearts. Neither treatment regimen resulted in significant change of the course of the microcirculatory and mitochondrial oxygenation. However, in all norepinephrine-treated animals, elevated troponin levels were measured. Sustained microcirculatory and mitochondrial PO<sub>2</sub> levels excluded hypoxia as mechanism of myocardial damage and troponin release. Some experimental data from others have linked catecholamine therapy to  $\beta$ 1-adrenoreceptor mediated increased LPS-associated myocardial apoptosis but also to direct drug-induced apoptosis and necrosis [37-40]. This mechanism is further supported by the fact that selective blockade of the  $\beta$ 1-adrenoreceptors not only appeared to diminish proinflammatory mediators and apoptosis but also to provide better outcomes [41,42]. Our results show that the mechanistic assumption upon which clinical sepsis treatment guidelines are based on [43,44], namely that hypoperfusion or heterogenous perfusion at the microcirculatory level causes cellular hypoxia and as a consequence organ failure, could not be found and moreover, that the protocol-based resuscitation regimen, at least partly, caused harm. Caution must be applied not to generalize this finding to all sepsis types and in particular to the complete temporal evolution of sepsis [45]. Our results, however, suggest that dysfunction of metabolic pathways within the mitochondria, and not dysfunction of oxygen delivery, is the prevailing mechanism during the first hours of endotoxemic shock.

The same conclusion has been drawn by Schenkman *et al.* [46]. They found higher myoglobin saturations in LPS-treated isolated guinea pig hearts than in controls and slower and lesser decline of myoglobin saturation after application of a brief ischemia resulted in a. Both findings suggested reduced oxygen consumption in endotoxemia. An alteration of the mitochondrial function during the course of endotoxemia has also been shown [47,48]. Moreover, it appears, that the type of dysfunction gradually evolves from a reversible to an irreversible form [12] and goes hand in hand with sepsis severity and outcome [49-52].

Finally, as mentioned above, the reduction of oxygen consumption and a metabolic switch away from fatty acids towards glucose metabolism can be found in chronic heart failure, septic cardiomyopathy and coronary artery disease. Recent research has unraveled impaired mitochondrial bioenergetics in an increasing amount of diseases and organ systems such as insulin resistance, diabetes, obesity, artery disease in diabetic patients, chronic lung disease, hepatic disorders, Parkinson's disease and even mood disorders [53-56]. Thus, it could be even hypothesized that mitochondrial metabolic reprogramming, either to a hibernation-like state or to altered metabolism and function including oxygen consumption, might be a generic defense mechanism to severe cellular challenges.

## REFERENCES

1. Semenza GL. Life with oxygen. *Science*. 2007 Oct 5;318(5847):62–4.
2. Lucero García Rojas EY, Villanueva C, Bond RA. Hypoxia Inducible Factors as Central Players in the Pathogenesis and Pathophysiology of Cardiovascular Diseases 2021;8:709509.
3. Neubauer S. The failing heart--an engine out of fuel. *N Engl J Med* 2007 Mar 15;356(11):1140–51.
4. Hollenberg SM, Singer M. Pathophysiology of sepsis-induced cardiomyopathy. *Nat Rev Cardiol* 2021;18(6):424–34.
5. Ashruf JF, Ince C, Bruining HA. Regional ischemia in hypertrophic Langendorff-perfused rat hearts. *Am J Physiol*. 1999;277(4 Pt 2):H1532–9.
6. Tamura M, Oshino N, Chance B, Silver IA. Optical measurements of intracellular oxygen concentration of rat heart in vitro. *Arch Biochem Biophys*. 1978;191(1):8–22.
7. Benzing H, Lösse B, Schuchhardt S, Niederle N. Simultaneous measurement of regional blood flow and oxygen pressure in the dog myocardium during coronary occlusion or hypoxic hypoxia. *Adv Exp Med Biol*. 1973;37A:541–6.
8. Mik EG, Stap J, Sinaasappel M, Beek JF, Aten JA, van Leeuwen TG, et al. Mitochondrial PO<sub>2</sub> measured by delayed fluorescence of endogenous protoporphyrin IX. *Nat Meth*. 2006;3(11):939–45.
9. Balestra GM, Legrand M, Ince C. Microcirculation and mitochondria in sepsis: getting out of breath. *Current Opinion in Anaesthesiology* 2009;22(2):184–90.
10. Ubbink R, Bettink MAW, Janse R, Harms FA, Johannes T, Munker FM, et al. A monitor for Cellular Oxygen METabolism (COMET): monitoring tissue oxygenation at the mitochondrial level. *J Clin Monit Comput* 2017;31(6):1143–50.
11. Zuurbier CJ, van Iterson M, Ince C. Functional heterogeneity of oxygen supply-consumption ratio in the heart. *Cardiovascular Research*. 1999;44(3):488–97.
12. Levy RJ, Vijayasathay C, Raj NR, Avadhani NG, Deutschman CS. Competitive and noncompetitive inhibition of myocardial cytochrome C oxidase in sepsis. *Shock*. 2004;21(2):110–4.
13. Vanderkooi JM, Maniara G, Green TJ, Wilson DF. An optical method for measurement of dioxygen concentration based upon quenching of phosphorescence. *J Biol Chem* 1987;262(12):5476–82.
14. Bodmer SIA, Balestra GM, Harms FA, Johannes T, Raat NJH, Stolker RJ, et al. Microvascular and mitochondrial PO<sub>2</sub> simultaneously measured by oxygen-dependent delayed luminescence. *J Biophotonics* 2012;5(2):140–51.
15. Balestra GM, Aalders MCG, Specht PAC, Ince C, Mik EG. Oxygenation measurement by multi-wavelength oxygen-dependent phosphorescence and delayed fluorescence: catchment depth and application in intact heart. *J Biophotonics* 2015;8(8):615–28.
16. Mik EG, Ince C, Eerbeek O, Heinen A, Stap J, Hooibrink B, et al. Mitochondrial oxygen tension within the heart. *Journal of Molecular and Cellular Cardiology*. 2009;46(6):943–51.
17. Heineman FW, Kupriyanov VV, Marshall R, Fralix TA, Balaban RS. Myocardial oxygenation in the isolated working rabbit heart as a function of work. *Am J Physiol*. 1992;262(1 Pt 2):H255–67.
18. Gayeski TE, HONIG CR. Intracellular PO<sub>2</sub> in individual cardiac myocytes in dogs, cats, rabbits, ferrets, and rats. *Am J Physiol*. 1991;260(2 Pt 2):H522–31.
19. Gnaiger E, Lassnig B, Kuznetsov A, Rieger G, Margreiter R. Mitochondrial oxygen affinity, respiratory flux control and excess capacity of cytochrome c oxidase. *Journal of Experimental Biology* 1998;201(Pt 8):1129–39.
20. Zhao X, He G, Chen Y-R, Pandian RP, Kuppasamy P, Zweier JL. Endothelium-derived nitric oxide regulates postischemic myocardial oxygenation and oxygen consumption by modulation of mitochondrial electron transport. *Circulation* 2005;111(22):2966–72.
21. Wilson DF. Quantifying the role of oxygen pressure in tissue function. *AJP: Heart and Circulatory Physiology* 2008;294(1):H11–3.
22. Mik EG, Balestra GM, Harms FA. Monitoring mitochondrial PO<sub>2</sub>: the next step. *Current Opinion in Critical Care*. 2020;26(3):289–95.
23. Ince C. Hemodynamic coherence and the rationale for monitoring the microcirculation. *Crit Care* 2015;19 Suppl 3(Suppl 3):S8–13.
24. Balestra GM, Mik EG, Eerbeek O, Specht PAC, van der Laarse WJ, Zuurbier CJ. Increased in vivo mitochondrial oxygenation with right ventricular failure induced by pulmonary arterial hypertension: mitochondrial inhibition as driver of cardiac failure? *Respir Res* 2015 3;16(1):6.
25. Sutendra G, Dromparis P, Paulin R, Zervopoulos S, Haromy A, Nagendran J, et al. A metabolic remodeling in right ventricular hypertrophy is associated with decreased angiogenesis and a transition from a compensated to a decompensated state in pulmonary hypertension. *J Mol Med* 2013;91(11):1315–27.
26. Daicho T, Yagi T, Abe Y, Ohara M, Marunouchi T, Takeo S, et al. Possible involvement of mitochondrial energy-producing ability in the development of right ventricular failure in monocrotaline-induced pulmonary hypertensive rats. *J Pharmacol Sci* 2009;111(1):33–43.
27. Piao L, Marsboom G, Archer SL. Mitochondrial metabolic adaptation in right ventricular hypertrophy and failure. *J Mol Med* 2010;88(10):1011–20.
28. Piao L, Fang Y-H, Cadete VJJ, Wietholt C, Urboniene D, Toth PT, et al. The inhibition of pyruvate dehydrogenase kinase improves impaired cardiac function and electrical remodeling in two models of right ventricular hypertrophy: resuscitating the hibernating right ventricle. *J Mol Med* 2010;88(1):47–60.
29. Oknińska M, Zambrowska Z, Zajda K, Paterek A, Brodaczywska K, Mackiewicz U, et al. Right ventricular myocardial oxygen tension is reduced in monocrotaline-induced pulmonary hypertension in the rat and restored by myo-inositol trispyrophosphate. *Sci Rep* 2021;11(1):18002–9.
30. Saito D, Yamada N, Kusachi S, Tani H, Shimizu A, Hina K, et al. Coronary flow reserve and oxygen metabolism of the right ventricle. *Jpn Circ J* 1989;53(10):1310–6.
31. Graham BB, Kumar R, Mickael C, Kassa B, Koyanagi D, Sanders L, et al. Vascular Adaptation of the Right Ventricle in Experimental Pulmonary Hypertension. *Am J Respir Cell Mol Biol* 2018;59(4):479–89.
32. Pullamsetti SS, Mamazhakypov A, Weissmann N, Seeger W, Savai R. Hypoxia-inducible factor signaling in pulmonary hypertension. *J Clin Invest* 2020;130(11):5638–51.
33. Adão R, Mendes-Ferreira P, Santos-Ribeiro D, Maia-Rocha C, Pimentel LD, Monteiro-Pinto C, et al. Urocortin-2 improves right ventricular function and attenuates pulmonary arterial hypertension. *Cardiovascular Research*. 2018;114(8):1165–77.
34. Lai Y-L, Law TC. Chronic hypoxia- and monocrotaline-induced elevation of hypoxia-inducible factor-1 alpha levels and pulmonary hypertension. *J Biomed Sci* 2004;11(3):315–21.

35. Zeidan EM, Hossain MA, El-Daly M, Abourehab MAS, Khalifa MMA, Taye A. Mitochondrial Regulation of the Hypoxia-Inducible Factor in the Development of Pulmonary Hypertension. *J Clin Med* 2022;11(17):5219.
36. Fijalkowska I, Xu W, Comhair SAA, Janocha AJ, Mavrakis LA, Krishnamachary B, et al. Hypoxia inducible-factor1alpha regulates the metabolic shift of pulmonary hypertensive endothelial cells. *Am J Pathol*. 2010;176(3):1130–8.
37. Neri M, Cerretani D, Fiaschi AI, Laghi PF, Lazzerini PE, Maffione AB, et al. Correlation between cardiac oxidative stress and myocardial pathology due to acute and chronic norepinephrine administration in rats. *J Cellular Mol Med*. 2007;11(1):156–70.
38. Wang Y, Wang Y, Yang D, Yu X, Li H, Lv X, et al.  $\beta_1$ -adrenoceptor stimulation promotes LPS-induced cardiomyocyte apoptosis through activating PKA and enhancing CaMKII and I $\kappa$ B $\alpha$  phosphorylation. *Crit Care* 2015;19(1):76.
39. Communal C, Singh K, Pimentel DR, Colucci WS. Norepinephrine stimulates apoptosis in adult rat ventricular myocytes by activation of the beta-adrenergic pathway. *Circulation*. 1998;98(13):1329–34.
40. Fu Y-C, Chi C-S, Yin S-C, Hwang B, Chiu Y-T, Hsu S-L. Norepinephrine induces apoptosis in neonatal rat endothelial cells via down-regulation of Bcl-2 and activation of beta-adrenergic and caspase-2 pathways. *Cardiovascular Research*. 2004;61(1):143–51.
41. Mehta S, Granton J, Gordon AC, Cook DJ, Lapinsky S, Newton G, et al. Cardiac ischemia in patients with septic shock randomized to vasopressin or norepinephrine. *Critical Care* 2013;17(3):R117.
42. Lauzier F, Lévy B, Lamarre P, Lesur O. Vasopressin or norepinephrine in early hyperdynamic septic shock: a randomized clinical trial. *Intensive Care Med*. 2006;32(11):1782–9.
43. Evans L, Rhodes A, Alhazzani W, Antonelli M, Coopersmith CM, French C, et al. Surviving sepsis campaign: international guidelines for management of sepsis and septic shock 2021. *Intensive Care Med* 2021;47(11):1181–247.
44. Hollenberg SM. Inotrope and vasopressor therapy of septic shock. *Crit Care Clin*. 2009;25(4):781–802.
45. Jeger V, Djafarzadeh S, Jakob SM, Takala J. Mitochondrial function in sepsis. *Eur J Clin Invest*. 2013;43(5):532–42.
46. Schenkman KA, Arakaki LSL, Ciesielski WA, Beard DA. Optical spectroscopy demonstrates elevated intracellular oxygenation in an endotoxic model of sepsis in the perfused heart. *Shock*. 2007;27(6):695–700.
47. Trumbeckaite S, Opalka JR, Neuhofer C, Zierz S, Gellerich FN. Different sensitivity of rabbit heart and skeletal muscle to endotoxin-induced impairment of mitochondrial function. *Eur J Biochem*. 2001;268(5):1422–9.
48. Fukumoto K, Pierro A, Spitz L, Eaton S. Neonatal endotoxemia affects heart but not kidney bioenergetics. *Journal of Pediatric Surgery*. 2003;38(5):690–3.
49. Brealey D, Brand M, Hargreaves I, Heales S, Land J, Smolenski R, et al. Association between mitochondrial dysfunction and severity and outcome of septic shock. *Lancet* 2002 Jul;360(9328):219–23.
50. Carré JE, Orban J-C, Re L, Felsmann K, Iffert W, Bauer M, et al. Survival in critical illness is associated with early activation of mitochondrial biogenesis. *Am J Respir Crit Care Med* 2010;182(6):745–51.
51. Langley RJ, Tsalik EL, van Velkinburgh JC, Glickman SW, Rice BJ, Wang C, et al. An Integrated Clinico-Metabolomic Model Improves Prediction of Death in Sepsis. *Science Translational Medicine*. 2013;5(195):195ra95–5.
52. Hussain H, Vutipongsatorn K, Jiménez B, Antcliffe DB. Patient Stratification in Sepsis: Using Metabolomics to Detect Clinical Phenotypes, Sub-Phenotypes and Therapeutic Response. *Metabolites* 2022;12(5):376.
53. Giménez-Palomo A, Dodd S, Anmella G, Carvalho AF, Scaini G, Quevedo J, et al. The Role of Mitochondria in Mood Disorders: From Physiology to Pathophysiology and to Treatment. *Front Psychiatry* 2021;12:546801.
54. Auger C, Alhasawi A, Contavadoo M, Appanna VD. Dysfunctional mitochondrial bioenergetics and the pathogenesis of hepatic disorders. *Front Cell Dev Biol* 2015;3:40.
55. Rosca MG, Vazquez EJ, Kerner J, Parland W, Chandler MP, Stanley W, et al. Cardiac mitochondria in heart failure: decrease in respirasomes and oxidative phosphorylation. *Cardiovascular Research* 2008;80(1):30–9.
56. Caldeira D de AF, Weiss DJ, Rocco PRM, Silva PL, Cruz FF. Mitochondria in Focus: From Function to Therapeutic Strategies in Chronic Lung Diseases. *Front Immunol* 2021;12:782074.

# CHAPTER

Summary

# 10





## SUMMARY AND CONCLUSION

### Introduction

Handling and availability issues of oxygen are relevant processes fueling evolution of several diseases. Oxygen shortage is broadly acknowledged and investigated in ischemic heart disease. In acute coronary events ischemia may result in necrosis, apoptosis, stunning and hibernation. The latter can also be found as an adaptive reaction in chronic coronary syndrome. Thus, oxygen consumption is reduced in order to ensure cellular survival. Hibernation has not only been described in coronary syndromes but is also debated as a defense mechanism in sepsis. However, impaired oxygen handling due to mitochondrial dysfunction despite sufficient availability of oxygen and heterogeneous microcirculatory perfusion ensuing local oxygen shortage represent the predominant mechanisms for septic cellular and organ dysfunction.

Measuring oxygen in organs, at cellular and subcellular level bears several challenges. In response disparate technical methods have been developed with marked difference in accuracy, spatio-temporal resolution and invasiveness. Direct measurement of oxygen partial pressures is feasible using polarographic and mass spectrometric electrodes, electron paramagnetic resonance (EPR), and oxygen-dependent quenching of phosphorescence and fluorescence as well as chemiluminescence and spin label oximetry.

The largest number of measurements has been performed using polarographic and mass spectrometric probes. Invasiveness required to measure below organ surface and potential oxygen consumption have risen criticism. This led to the search of alternatives like EPR and phosphorimetry. EPR requires long acquisition times- a drawback not shared with phosphorimetry. That is why our group has chosen this technique for its versatility, minimal invasiveness and fast response. Earlier our group had developed dual-wavelength phosphorimeter allowing measurements of microcirculatory  $PO_2$  at two depths. Then, adaptation of this technique made the measurement of mitochondrial  $pO_2$  possible. The next logic step accomplished in this thesis was to combine both techniques. Before, few data on the transmural distribution of microcirculatory oxygen partial pressures ( $\mu PO_2$ ) and none of parallel measurements of microcirculation and mitochondria were available from *in vivo* studies.

### Thesis

The aim of the thesis was therefore to further develop and characterize this phosphorimetric method of near-simultaneous measurements of microcirculatory and mitochondrial oxygenation in the heart *in vivo*. Then in two animal models, namely endotoxemia and right ventricular pressure overload, we measured the oxygenation level in the microcirculation and mitochondria and investigated the changes induced by therapeutic interventions. We hypothesized that in sepsis hypoxia would be found

in non-resuscitated animals but no oxygen shortage would be found with supportive therapy indicating oxygen management issues arising from mitochondrial dysfunction. In pressure overload induced right heart failure we expected a switch increased anaerobic glycolysis without occurrence of hypoxia.

### Chapters

In the **second chapter** an overview of involvement and adaptive processes of the microcirculation in sepsis is given. Heterogeneous microcirculatory and mitochondrial dysfunction assert themselves as pathogenic mechanisms for septic organ dysfunction in experimental data. However, clinical human data are still sparse. No microcirculatory or mitochondrial parameter is routinely measured in the clinic other than lactate. Moreover, none of these parameters are yet suggested as a treatment target in treatment guidelines. This instance can be ascribed to the lack of a thorough pathophysiologic concept of sepsis and its translation to humans.

The **third chapter** describes of further development of the oxygen measurement technique by oxygen-dependent quenching of phosphorescence lifetime. Dual-wavelength phosphorimetry for measuring microcirculatory  $PO_2$  was combined with the measurement of delayed fluorescence for measuring mitochondrial  $PO_2$ . Absence of crosstalk of the signals, measurement accuracy and feasibility to assess hepatic microcirculatory and mitochondrial oxygenation *in vivo* was shown.

In this thesis the focus was set on myocardial microcirculatory and mitochondrial oxygenation measurements. Thus, optical characterization of these oxygenation measurements was provided in the **fourth chapter** by means of Monte Carlo simulations and *ex vivo* experiments. These experiments found an excellent correlation of calculated and measured phosphorescence. Furthermore, feasibility of near-simultaneous measurements of microcirculatory and mitochondrial  $PO_2$  in rat hearts *in vivo* was provided.

Further characterization of the measurement technique was reported in the **fifth chapter**. In isolated cardiomyocytes we could localize the origin of the phosphorescence signal, demonstrate that aminolevulinic acid is required to enhance protoporphyrin IX production and phosphorescence signal intensity without compromising oxygen consumption. Furthermore, characteristic measurement constants ( $\tau_0$  and  $k_q$ ) were determined and applied to convert lifetimes measured in Langendorff-perfused hearts to calculate mitochondrial  $PO_2$ . Our measurements yielded microcirculatory  $PO_2$  of  $67 \pm 3$  mmHg and mitochondrial  $PO_2$  of  $35 \pm 5$  mmHg. These values were well in line with the new consensus that tissue oxygenation was not as low as suggested by Whalen and Clarke's experiments in the 70ies and Gayeski and Honig in the 90ies.

In the clinical treatment of diseases, the direct monitoring of the cellular state remains a pivotal missing piece of the puzzle – as discussed in **Chapter 6**. In healthy subjects, the macrocirculation, microcirculation and mitochondria present an equilibrium with

cellular needs in terms of oxygen and nutrients (hemodynamic coherence). The loss of this coherence in disease has been shown to be associated with worse outcome. Hence, cellular and mitochondrial limitation of oxygen may lead to an adaptive decreased function, hibernation and metabolic reprogramming with transition to dysfunction and cellular death.

With these premises, in **Chapter 7**, we investigated mitochondrial  $PO_2$  in a model of pulmonary arterial hypertension leading to right ventricular hypertrophy and failure. We observed no hypoxia in any stage of hypertrophy or heart failure. At baseline condition mitochondrial oxygenation was even higher in failing right hearts and similar under decreased oxygen supply or increased work demand conditions as compared to healthy hearts. This finding was matched with evidence of metabolic reprogramming with an increased glycolytic hexokinase activity at increasing MCT dose and increased lactate dehydrogenase activity only in compensated hypertrophied right ventricles. These findings suggested a down-regulation of *in vivo* mitochondrial metabolism because of increased anaerobic glycolysis. This is in line with supporting results from others.

In **Chapter 8** we investigated whether oxygen shortage is present in sepsis. The cardiac oxygenation of the microcirculation and mitochondria in endotoxemia and usual clinical supportive therapies in rat hearts was measured for the first time *in vivo*. After induction of an endotoxemic shock rats were either not treated at all or received a protocol-based treatment with fluid, fluid plus dobutamine, fluid plus levosimendan, fluid plus norepinephrine, fluid plus norepinephrine and dobutamine or fluid plus norepinephrine and levosimendan. Additionally, hemodynamic parameters and troponin levels were measured. Hypoxia was not observed. On the contrary, (supra-) normal microcirculatory  $PO_2$  and sustained mitochondrial  $PO_2$  values were actually found in endotoxemic rat hearts. Neither treatment regimen resulted in significant change of the course of the microcirculatory and mitochondrial oxygenation. However, in all norepinephrine-treated animals, elevated troponin levels were measured. Some experimental data from others have linked catecholamine therapy to  $\beta_1$ -adrenoreceptor mediated increased LPS-associated myocardial damage. Our results show that the mechanistic assumption upon which clinical sepsis treatment guidelines are based on that hypoperfusion or heterogenous perfusion at the microcirculatory level causes cellular hypoxia and as a consequence organ failure, could not be found. Moreover, the protocol-based resuscitation regimen, at least partly, was associated with harm. Caution must be applied not to generalize this finding to all sepsis types and in particular to the complete temporal evolution of sepsis. Our results suggest that dysfunction of metabolic pathways within the mitochondria, and not dysfunction of oxygen delivery, is the prevailing mechanism during the first hours of endotoxemic shock.

## Conclusion

In this thesis we further developed and characterized our phosphorimetric method for near-simultaneous measurements of microcirculatory and mitochondrial oxygenation in the heart *in vivo*. In two animal models, right ventricular pressure overload and endotoxemia, we addressed the oxygenation level in the microcirculation and mitochondria. In both diseases no myocardial oxygen shortage was found. Our results suggest reprogramming of mitochondrial metabolic pathways and mitochondrial dysfunction as mechanisms for organ dysfunction in right ventricular pressure overload and endotoxemia, respectively. Elevated troponin levels were measured in animals treated with norepinephrine. Usual drug regimen according to sepsis treatment guidelines might therefore be associated with myocardial damage.

Finally, it could be hypothesized that the mitochondrial mechanisms with altered metabolism and function represent a generic defense mechanism to severe cellular challenges as they have been described in a large number of cardiac, pulmonary, hepatic, neurologic and psychiatric diseases.

# CHAPTER

# 11

Dutch summary  
(nederlandse samenvatting)



## NEDERLANDSE SAMENVATTING

### Introductie

Problemen met de beschikbaarheid en het verbruik van zuurstof spelen een belangrijke rol in het beloop van verschillende ziekten. Zuurstoftekort bij ischemische hartziekten is een algemeen bekend en belangrijk onderwerp van onderzoek. Acut zuurstoftekort in de hartspier kan leiden tot celdood, apoptose, stunning en hibernatie. Hibernatie kan ook aanwezig zijn als een fysiologische aanpassing bij chronisch coronair syndroom waardoor de zuurstofconsumptie verminderd is om de cel te laten overleven. Hibernatie is niet alleen beschreven bij coronaire syndromen maar zou ook een overlevingsstrategie kunnen zijn bij sepsis. Echter, verstoord mitochondriaal zuurstofgebruik door mitochondriale dysfunctie ondanks voldoende beschikbaarheid van zuurstof, en ongelijke lokale doorbloeding van de microcirculatie met lokale zuurstoftekorten tot gevolg, lijken de belangrijkste mechanismen te zijn voor cellulaire en orgaandysfunctie bij septische patiënten.

Het meten van zuurstof in organen op cellulair en subcellulair niveau kent verschillende uitdagingen. Daarom zijn er verschillende technische methodes ontwikkeld met aanzienlijke verschillen qua nauwkeurigheid, spatiële en temporele resolutie, en mate van invasiviteit. Er zijn verschillende methoden om de zuurstofspanning direct te meten, zoals met behulp van polarografische en massaspectrografische technieken, elektron paramagnetische resonantie (EPR), zuurstofafhankelijke uitdoving van fosforescentie en fluorescentie, alsmede chemiluminescentie.

De meeste metingen zijn gedaan met behulp van polarografische en massaspectrometrische technieken. De kritiek op deze methodes richt zich op het invasieve karakter van de zuurstof meting onder het orgaanoppervlak en de mogelijk problematische intrinsieke zuurstofconsumptie van de metingen. Dit heeft geleid tot het zoeken naar alternatieven als EPR en fosforimetrie. EPR heeft lange tijd nodig voor een bepaling, iets dat bij fosforimetrie geen probleem is. Daarom heeft onze onderzoeksgroep deze techniek gekozen op basis van de veelzijdige inzetbaarheid, het minimaal invasieve karakter en de snelle respons op veranderingen. In het verleden is door onze groep een dubbele-golflengte fosforimeter ontwikkeld die de zuurstofspanning in de microcirculatie op twee niveaus meten kan. Verdere ontwikkelingen hebben de meting van mitochondriale zuurstofspanning mogelijk gemaakt, door middel van zuurstofafhankelijke uitdoving van vertraagde fluorescentie van mitochondriaal protoporphyrine IX. De logische volgende stap was het combineren van beide technieken. Voorheen waren er bijna geen gegevens over zuurstofspanning in de microcirculatie in de verschillende delen van de hartspier. Er waren in het geheel geen *in vivo* verkregen gegevens over de parallele metingen in de microcirculatie en mitochondriën.

### Dit proefschrift

Het doel van dit proefschrift was derhalve het verder ontwikkelen en onderzoeken van de optische methode waarbij tegelijkertijd *in vivo* metingen van de microcirculatie en de mitochondriale oxygenatie van het hart verricht werden. Daarom maten we in twee diermodellen, een sepsis model en een rechter-kamer-overbelasting-model, de zuurstofspanning in de microcirculatie en de mitochondriën en onderzochten de effecten van de verandering ten gevolge van therapeutisch ingrijpen. Onze hypothese was dat bij sepsis wel hypoxie zou worden gevonden bij niet-geresusciteerde dieren, maar bij ondersteunende behandeling geen zuurstoftekort vastgesteld zou worden. Dit zou een aanwijzing voor problemen met het verbruik van zuurstof ten gevolge van mitochondriale dysfunctie zijn. In het rechter-kamer-overbelasting-model verwachtten we een verschuiving naar toegenomen anaerobe glucoseverbranding zonder het optreden van hypoxie.

### Chapters (Hoofdstukken)

In **hoofdstuk 2** wordt een overzicht gegeven van de rol van en de aanpassingen in de microcirculatie in sepsis. In experimenten wordt heterogene dysfunctie in zowel microcirculatie als mitochondriën beschreven die als ziekmakende mechanismen ten grondslag liggen aan septische orgaan dysfunctie. Gegevens verkregen bij mensen zijn er echter nog steeds nauwelijks. Dat komt omdat in de klinische situatie geen enkele parameter met betrekking tot de microcirculatie of mitochondriën routinematig gemeten wordt, behoudens lactaat. Bovendien wordt in de huidige richtlijnen geen van deze parameters genoemd als een potentieel aangrijpingspunt voor therapeutisch ingrijpen. Deze situatie kan toegeschreven worden als een gebrek aan een grondig pathofysiologisch concept van sepsis en de vertaling ervan naar de kliniek bij mensen.

**Hoofdstuk 3** beschrijft een verdere ontwikkeling van de meettechniek met behulp van de zuurstofafhankelijke uitdoving van de levensduur van fosforescentie. Dubbele-golflengte-fosforimetrie om zuurstofspanning in de microcirculatie te meten is gecombineerd met de meting van vertraagde fluorescentie voor het bepalen van de mitochondriale zuurstofspanning. Wij toonden aan dat de signalen elkaar onderling niet beïnvloedden, dat de metingen nauwkeurig waren en dat meten van de microcirculatie en van zuurstof in de mitochondriën in de lever *in vivo* goed mogelijk was.

In dit proefschrift is de nadruk gelegd op het meten van zuurstof in de microcirculatie en mitochondriën van het hart. In **hoofdstuk 4** worden de optische eigenschappen, met name de meetdiepte in hartspierweefsel, van deze zuurstofmetingen beschreven aan de hand van Monte Carlo simulaties en *ex vivo* experimenten. In deze experimenten werd een uitstekende relatie gevonden tussen de berekende en de gemeten fosforescentie signalen. Verder werd, in een andere serie experimenten, vastgesteld dat (bijna) gelijktijdige metingen in de microcirculatie en mitochondriën bij ratten *in vivo* praktisch goed mogelijk waren.

Verdere karakterisering van de meettechniek wordt beschreven in **hoofdstuk 5**. Wij konden in geïsoleerde hartspiercellen de oorsprong van het zuurstofafhankelijke signaal vaststellen en aantonen dat aminolevulinezuur nodig is om de protoporfyrine IX productie te verhogen en daarmee het vertraagde fluorescentie signaal zonder dat het zuurstofverbruik verstoord werd. Verder stelden wij de karakteristieke meet constanten vast ( $\tau_0$  en  $k_q$ ). Deze constanten konden worden toegepast om de uitdooftijd van het vertraagde fluorescentiesignaal in hartspiercellen, gemeten in een Langendorf-model, om te rekenen naar zuurstofspanning in de mitochondriën. Onze metingen toonden aan dat de zuurstofspanning in de microcirculatie  $67 \pm 3$  mmHg en in de mitochondriën  $35 \pm 5$  mmHg. Deze waarden zijn in lijn met de recente consensus dat zuurstofspanning in de weefsels niet zo laag is als vastgesteld in de experimenten van Whalen en Clark in de jaren zeventig en van Gayeski en Honig in de jaren negentig.

In **hoofdstuk 6** wordt besproken dat het ontbreken van directe monitoring op cellulair niveau een cruciaal missend onderdeel van de puzzel blijft bij de behandeling van ziektes. Bij gezonde mensen, zijn macrocirculatie, microcirculatie en mitochondriën met elkaar in evenwicht met betrekking tot zuurstof en voedingsstoffen. Dit wordt ook wel hemodynamische coherentie genoemd. Het verlies van coherentie is geassocieerd met een slechte uitkomst voor de patiënt. Daarom leidt een tekort aan cellulair en mitochondriaal zuurstof tot geadapteerde verminderde functie, hibernatie en metabole herprogrammering en daardoor uiteindelijk tot dysfunctie en celdood.

Met deze gedachten in het hoofd onderzochten wij in **hoofdstuk 7** de mitochondriale zuurstofspanning in een model van monocrotaline-geïnduceerde pulmonale hypertensie leidend tot hypertrofie en falen van de rechterhartkamer. Wij vonden in geen enkel stadium van hypertrofie of falen van de rechterkamer een tekort aan zuurstof. In de uitgangssituatie was de zuurstofspanning zelfs hoger bij een falende rechterkamers. In situaties waarbij er sprake was van een verminderd zuurstofaanbod of bij een verhoogde arbeid van het hart was de zuurstofspanning gelijk aan de waarde die gevonden werden bij gezonde harten. Deze bevinding past goed bij de aangetoonde metabole herprogrammering die gepaard gaat met een verhoogde glycolytische hexokinase activiteit die optreedt bij verhoging van de monocrotaline dosis en met een verhoogde lactaat dehydrogenase activiteit die uitsluitend optreedt bij gecompenseerde hypertrofische rechterkamers. De resultaten suggereren een down-regulering van het *in vivo* mitochondriale stofwisseling en toegenomen anaerobe verbranding van glucose. Onze onderzoeksresultaten zijn in lijn met die van anderen.

In **hoofdstuk 8** onderzochten we of er sprake is van een tekort aan zuurstof in het hart bij sepsis. De zuurstofspanning in de microcirculatie en in de mitochondriën van het hart werden onderzocht in een toestand van sepsis (endotoxemie), waarbij voor het eerst *in vivo* in het rattenhart gemeten werd wat het effect is van verschillende gebruikelijke behandelingen bij sepsis. Na het veroorzaken van een endotoxische shock werd een groep van de ratten niet behandeld, een groep kreeg volgens

protocol infuusvloeistoffen toegediend, een groep vloeistoffen plus dobutamine, een groep vloeistoffen met levosimendan, vloeistoffen met noradrenaline, vloeistoffen met noradrenaline en dobutamine en een groep vloeistoffen met noradrenaline en levosimendan. Tegelijkertijd werden hemodynamiek en troponinespiegels gemeten. Hypoxie werd niet gevonden. In tegendeel, wij vonden (supra)normale waarden voor de zuurstofspanning in microcirculatie en onveranderde zuurstofspanning in de mitochondriën van de rattenharten. Geen enkel therapeutisch regime leidde tot een significante verandering gedurende het experiment van het verloop van zowel de zuurstofspanning in de microcirculatie als in de mitochondriën. Echter, in alle groepen die noradrenaline toegediend kregen vonden wij verhoogde troponine spiegels. Experimenteel werk van anderen heeft een verband gelegd tussen de behandeling met catecholaminen en  $\beta_1$ -adrenoreceptor gemedieerde toegenomen LPS-geassocieerde beschadiging van hartcellen. Onze resultaten ondersteunen de mechanistische aannames waarop richtlijnen voor de behandeling van sepsis patiënten gebaseerd zijn niet. Volgens deze aannames leidt hypoperfusie of heterogene perfusie op niveau van de microcirculatie tot hypoxie van de cel en orgaanfalen. Sterker nog, de protocol-gebaseerde resuscitatiestrategieën waren, in elk geval ten dele, geassocieerd met schade. Er is voorzichtigheid geboden om deze bevindingen niet te extrapoleren naar alle soorten van sepsis en naar alle fasen in de evolutie van sepsis in de tijd. Onze resultaten suggereren dat dysfunctie van het metabolisme in de mitochondriën en niet zozeer verstoring van zuurstofaanbod het belangrijkste mechanisme is gedurende de eerste uren van endotoxische shock.

### Conclusie

In dit proefschrift hebben we onze *in vivo* fosforimetrische methode om (bijna) tegelijkertijd het zuurstofgehalte in de microcirculatie en de mitochondriën van de hartspiercellen verder ontwikkeld en gekarakteriseerd. In twee dierexperimentele modellen, rechter hartkamer overvulling en endotoxemie hebben we oxygenatie in de microcirculatie en de mitochondriën. In beide pathofysiologische modellen werd geen zuurstoftekort vastgesteld. Onze resultaten suggereren dat herprogrammering van het mitochondriaal metabolisme en mitochondriale dysfunctie als mechanismen van orgaandysfunctie respectievelijk bij rechterkamer overbelasting en endotoxemie een rol spelen. Bij de dieren die met noradrenaline behandeld werden werden verhoogde troponinewaarden vastgesteld. Dit betekent dat gebruikelijke behandelingen van sepsis mogelijk tot hartschade leiden. Tot slot kan gehypothetiseerd worden dat de mitochondriale mechanismen die leiden tot veranderd metabolisme en functie onderdeel zijn van een algemeen verdedigings mechanisme bij ernstige problemen op cellulair niveau, omdat ze beschreven zijn in vele cardiale, pulmonale, lever, neurologische en psychiatrische ziekten.

# CHAPTER

Acknowledgements

# 12



When a journey starts there is always an uncertainty of how the destination will be reached – if ever. Those who travel as a passion draw satisfaction of and strive for this thrill. Having travelled a the world somewhat I appreciate getting to know other cultures and landscapes. I wouldn't go as far as to indicate myself as an adventurous traveler though.

However, this thesis has been a colorful undertaking which has not followed the fastest path, was marked by hiccup's, delays and hibernation. The latter is wonderfully fitting the research topic of this thesis, but was by no means deliberately sought. Stories are far more frequently told when ending gloriously and successfully. Let's drop the glorious and keep the successful. This journey is the story of successfully knitting a network of clinicians and researchers, translating acquaintances to friendships, adopting innumerable intellectual and manual basic science skills, leading investigations on some challenging questions of basic (patho-)physiology and translating these into a couple of publications, and finally merging these achievements in this present work.

That this journey started I owe to Can. Your former PhD student and my ICU supervisor at that time Martin Siegemund as well as our current head of anesthesiology Luzius Steiner advised me to have a trip to Amsterdam if I wanted to learn something about microcirculation. You, Can, then introduced me to this "micro-world" and basically acted as the game maker. You brought me to become acquainted with several methods of microcirculatory imaging. Your large network of excellent collaborators and teachers of the techniques was unique. In the animal laboratory first steps of measuring microcirculatory oxygenation in the *in vivo* heart were achieved. There I was always striving after the example of the antecedent fellows who had done some great science, not at least after one who had further developed the phosphorimetric method in order to be able to measure the mitochondrial oxygenation. This fellow, I eventually met, was Bert.

That this journey came to a fruitful end is the merit of Robert Jan. You, Robert Jan, were the (pro-)motor of this work, with a lot of horse power. Your relentless positive energy is elating. You pushed and eventually dragged me and sometimes all of us further and beyond to the final achievement of this journey. Not only you sharp but always constructive analyses were invaluable but also your help for very down to earth issues was priceless and tremendously effective. Here I remind the 2-month daily contention with hospital and university bureaucracy. This challenge you mastered superbly. In analogy of your preferred Winston Churchill quote „*We shall fight on the beaches*“ I add the dictum of Peter Safar, one of the "fathers" of cardiopulmonary resuscitation: "*Bureaucracy is a challenge to be conquered with a righteous attitude, a tolerance for stupidity, and a bulldozer when necessary*".

This work would have gone nowhere without the inspiring enthusiasm and ingeniousness of Bert. It was an awesome task to found with you the experimental "rat ICU" in a 4 m<sup>2</sup> broom closet with nothing than a table in it. Finally stuffed with high end devices build from scratch by you and collected at the ICU's thrift shop hot science happened in this sweat bath. Eventually it was even brought to sustainable temperatures by an air conditioner which found its place- in the corridor. In this 1½ decades it was not alone your wits and scientific diligence but also thoughtfulness, humanity and friendship that kept this project going. For all this I'm much obliged to you!

And then, Coert, you were the scientific conscience of this work. From you I learned how one should do and write it right. If ever unsure it would be a clear point of orientation to think what you would do or say. Your thoughts and contributions were always sharp witted, precise, to the point, constructive and improving either planning, analyses or writing. For this I'm very grateful to you.

Patricia, you taught me all one needs to master to successfully carry out challenging rat experiments. Your surgical skills were unmet and of invaluable help for my work even though my experimental pace finally gave way to some despair. Thank you for facilitating, assisting and accompanying me on this industrious journey.

During my time at Can's laboratory, I met a promising young scintillatingly gifted student who was looking for some research experience – Wadim de Boon. Together we undertook an endeavor into microcirculatory response to cardiac resynchronization and a short excursus to a clinical pilot study on nocturnal alertness of intensive care fellows. Finally at the Erasmus with you help I could accelerate my experimental pace. It was an exciting and laborious time where you were a relentless, reliable and witty partner. However, we stretched our experimental race too thin and came to a full stop. Keeping our noses to the grindstone we fought our way back and even laid the foundations for another study.

At the Amsterdam Medical Center, I was sharing my office with Matthieu. Watching you doing science was inspiring. Complex and difficult were other expressions of "challenge accepted". You were rushing through experiments like a TGV working literally night and day. Highly gifted, sharp witted but convivial and sociable you were a fantastic companion though we were living on different "planets" – namely me on *heart* and you on *kidney*.

I'd like to thank all staff of Can's Amsterdam laboratory. In particular Rick Bezemer, Dan Milstein and posthumously Peter Goedhart. Rick, being an engineer, you added always a different view on how to assess the microcirculation. Dan, you taught me with great patience and skill how to acquire and analyze microcirculatory images. So, it was great

to tie in with our collaboration and have you over for the Micro-SOAP study to Basel. Peter, who sadly left us way too early, was the good soul of the department. Leading me into the viscera of the AMC when something needed to be arranged. Moreover, he introduced me into the Dutch way of living. I happily remind myself of the memorable evening boat trips through beautiful Waterland.

One more word goes to Matthias Betz and posthumous also to Jens Moll. Independently, both of you helped me to better understand my data. With Jens I had long discussions about statistics and how to setup the best analytic plan. Matthias you virtuously programmed in R and opened up to me inaccessible possibilities.

Last but not least, the biggest thanks go to my wife Krysia for her tolerance and understanding for this undertaking which separated us for 2 years and to our children Gianluca and Martina who had to do without me for many evenings and days.



# CHAPTER

# 13

Publication list



## IDENTIFIERS

## OCRID

<https://orcid.org/0000-0002-5862-0435>

## Web of Science

ResearcherID: JFJ-7657-2023, <https://www.webofscience.com/wos/author/record/JFJ-7657-2023>

## PUBLICATIONS

## Microcirculation;

## Microcirculatory and Mitochondrial Oxygenation, in particular of the Heart

1. **Balestra GM**, Mik EG, Eerbeek O, Specht PA, van der Laarse WJ, Zuurbier CJ. Increased in vivo mitochondrial oxygenation with right ventricular failure induced by pulmonary arterial hypertension: mitochondrial inhibition as driver of cardiac failure? **Respir Res.** 2015 Feb 3;16:6. PMID: 25645252, DOI: 10.1186/s12931-015-0178-6
2. **Balestra GM**, Aalders MC, Specht PA, Ince C, Mik EG. Oxygenation measurement by multi-wavelength oxygen-dependent phosphorescence and delayed fluorescence: catchment depth and application in intact heart. **J Biophotonics.** 2015 Aug;8(8):615-28. PMID: 25250821, DOI: 10.1002/jbio.201400054
3. **Balestra GM**, Bezemer R, Boerma EC, Yong ZY, Sjauw KD, Engstrom AE, Koopmans M, Ince C. Improvement of sidestream dark field imaging with an image acquisition stabilizer. **BMC Med Imaging.** 2010 Jul 13;10:15. PMID: 20626888, DOI: 10.1186/1471-2342-10-15
4. **Balestra GM**, Legrand M, Ince C. Microcirculation and mitochondria in sepsis: getting out of breath. **Curr Opin Anaesthesiol.** 2009 Apr;22(2):184-90. PMID: 19307893, DOI: 10.1097/ACO.0b013e328328d31a
5. **Balestra GM**, Ince C, Johannes T, de Boon, WMI, Specht PAC, Betz MJ, Zuurbier CJ, Stolker RJ, Mik EG. Microcirculatory and mitochondrial oxygenation is preserved in endotoxic shock and resuscitation in rat hearts. **submitted**
6. Hydroxyethyl starch and Ringer's lactate for volume resuscitation in sepsis and septic shock – The BaSES Trial. Hollinger A; von Felten S, **Balestra GM**, Dickenmann M, Steiner L; Marsch S; Pargger H, Siegemund S. **submitted**
7. Monitoring mitochondrial PO<sub>2</sub>: the next step. Mik EG, **Balestra GM**, Harms FA. **Curr Opin Crit Care.** 2020 Jun;26(3):289-295. PMID: 32348095, DOI: 10.1097/MCC.0000000000000719.
8. Bodmer SI, **Balestra GM**, Harms FA, Johannes T, Raat NJ, Stolker RJ, Mik EG.

- Microvascular and mitochondrial PO<sub>2</sub> simultaneously measured by oxygen-dependent delayed luminescence. **J Biophotonics.** 2012 Feb;5(2):140-51. PMID: 22114031, DOI: 10.1002/jbio.201100082
9. Bedside hand vein inspection for noninvasive central venous pressure assessment. Vogel F, Staub D, Aschwanden M, Siegemund M, Imfeld S, **Balestra G**, Keo HH, Uthoff H. **Am J Emerg Med.** 2020 Feb;38(2):247-251. PMID: 31088750, DOI: 10.1016/j.ajem.2019.04.044.
  10. Mildly elevated lactate levels are associated with microcirculatory flow abnormalities and increased mortality: a microSOAP post hoc analysis. Vellinga NAR, Boerma EC, Koopmans M, Donati A, Dubin A, Shapiro NI, Pearse RM, van der Voort PHJ, Dondorp AM, Bafi T, Fries M, Akarsu-Ayazoglu T, Pranskunas A, Hollenberg S, **Balestra G**, van Iterson M, Sadaka F, Minto G, Aypar U, Hurtado FJ, Martinelli G, Payen D, van Haren F, Holley A, Gomez H, Mehta RL, Rodriguez AH, Ruiz C, Canales HS, Duranteau J, Spronk PE, Jhanji S, Hubble S, Chierago M, Jung C, Martin D, Sorbara C, Bakker J, Ince C; microSOAP study group. **Crit Care.** 2017 Oct 18;21(1):255. PMID: 29047411, DOI: 10.1186/s13054-017-1842-7.
  11. Vellinga NA, Boerma EC, Koopmans M, Donati A, Dubin A, Shapiro NI, Pearse RM, Machado FR, Fries M, Akarsu-Ayazoglu T, Pranskunas A, Hollenberg S, **Balestra G**, van Iterson M, van der Voort PH, Sadaka F, Minto G, Aypar U, Hurtado FJ, Martinelli G, Payen D, van Haren F, Holley A, Pattnaik R, Gomez H, Mehta RL, Rodriguez AH, Ruiz C, Canales HS, Duranteau J, Spronk PE, Jhanji S, Hubble S, Chierago M, Jung C, Martin D, Sorbara C, Tijssen JG, Bakker J, Ince C; microSOAP Study Group. International study on microcirculatory shock occurrence in acutely ill patients. **Crit Care Med.** 2015 Jan;43(1):48-56. PMID: 25126880, DOI: 10.1097/CCM.0000000000000553
  12. Harms FA, de Boon WM, **Balestra GM**, Bodmer SI, Johannes T, Stolker RJ, Mik EG. Oxygen-dependent delayed fluorescence measured in skin after topical application of 5-aminolevulinic acid. **J Biophotonics.** 2011 Oct;4(10):731-9. PMID: 21770036, DOI: 10.1002/jbio.201100040
  13. Dyson A, Bezemer R, Legrand M, **Balestra G**, Singer M, Ince C. Microvascular and interstitial oxygen tension in the renal cortex and medulla studied in a 4-h rat model of LPS-induced endotoxemia. **Shock.** 2011 Jul;36(1):83-9. PMID: 21368713, DOI: 10.1097/SHK.0b013e3182169d5a
  14. Legrand M, Mik EG, **Balestra GM**, Lutter R, Pirracchio R, Payen D, Ince C. Fluid resuscitation does not improve renal oxygenation during hemorrhagic shock in rats. **Anesthesiology.** 2010 Jan;112(1):119-27. PMID: 19996951, DOI: 10.1097/ALN.0b013e3181c4a5e2
  15. Mik EG, Ince C, Eerbeek O, Heinen A, Stap J, Hooibrink B, Schumacher CA, **Balestra GM**, Johannes T, Beek JF, Nieuwenhuis AF, van Horssen P, Spaan JA, Zuurbier CJ. Mitochondrial oxygen tension within the heart. **J Mol Cell Cardiol.** 2009 Jun;46(6):943-51. PMID: 19232352, DOI: 10.1016/j.yjmcc.2009.02.002

16. Mik EG, Johannes T, Zuurbier CJ, Heinen A, Houben-Weerts JH, **Balestra GM**, Stap J, Beek JF, Ince C. In vivo mitochondrial oxygen tension measured by a delayed fluorescence lifetime technique. **Biophys J.** **2008** Oct;95(8):3977-90. PMID: 18641065, DOI: 10.1529/biophysj.107.126094

#### CARDIOLOGY

17. Krisai P, Ruperti-Repilado FJ, Goeldi A, Kraus D, De Alencar B, Sticherling C, Balestra G. Occurrence and predictors of severe arrhythmia in patients with myocarditis. **EP Europace.** **2022** 24(Suppl 1): euac053.117. <https://doi.org/10.1093/europace/euac053.117>
18. Use of a Protective Shield Successfully Prevents Exposure to Aerosols and Droplets during Transesophageal Echocardiography. **Balestra G**, Kaufmann BA, Zhou Q. **J Am Soc Echocardiogr.** **2020** Jul;33(7):908-909. PMID: 32624093, DOI: 10.1016/j.echo.2020.04.028.
19. Zimmerli M, Tisljar K, **Balestra GM**, Langewitz W, Marsch S, Hunziker S. Prevalence and risk factors for post-traumatic stress disorder in relatives of out-of-hospital cardiac arrest patients. **Resuscitation** **2014** Jun;85(6):801-8. PMID: 24598377, DOI: 10.1016/j.resuscitation.2014.02.022
20. Hunziker S, Bühlmann C, Tschan F, **Balestra G**, Legeret C, Schumacher C, Semmer NK, Hunziker P, Marsch S. Brief leadership instructions improve cardiopulmonary resuscitation in a high fidelity simulation: a randomized controlled trial. **Crit Care Med.** **2010** Apr;38(4):1086-91. Erratum in: *Crit Care Med.* 2010 Jun;38(6):1510. PMID: 20124886, DOI: 10.1097/CCM.0b013e3181cf7383
21. Di Valentino M, **Balestra GM**, Christ M, Raineri I, Oertli D, Zellweger MJ. Inverted Takotsubo cardiomyopathy due to pheochromocytoma. **Eur Heart J.** **2008** Mar;29(6):830. PMID: 17954493, DOI: 10.1093/eurheartj/ehm449

#### INFECTIOLOGY

22. Kuenzli E, Labhardt N, **Balestra G**, Weisser M, Zellweger MJ, Blum J. Staphylococcus aureus Endocarditis as a Complication of Toxocariasis-Associated Endomyocarditis With Fibrosis: A Case Report. **Open Forum Infect Dis.** **2016** Sep 7;3(3):ofw145. PMID: 27800525. DOI:10.1093/ofid/ofw145
23. Osthoff M, Siegemund M, **Balestra G**, Abdul-Aziz MH, Roberts JA. Prolonged administration of  $\beta$ -lactam antibiotics - a comprehensive review and critical appraisal. **Swiss Med Wkly.** **2016** Oct 10;146:w14368. PMID: 27731492, DOI: 10.4414/smw.2016.14368.
24. Osthoff M, Gürtler N, Bassetti S, **Balestra G**, Marsch S, Pargger H, Weisser M, Egli A. Impact of MALDI-TOF mass spectrometry based identification directly from positive blood cultures on patient management: A controlled clinical trial. **Clin Microbiol Infect.** **2016** Aug 25. pii: S1198-743X(16)30329-9. PMID: 27569710, DOI:10.1016/j.

cmi.2016.08.009

25. Schuetz P, Affolter B, Hunziker S, Winterhalder C, Fischer M, **Balestra GM**, Hunziker P, Marsch S. Serum procalcitonin, C-reactive protein and white blood cell levels following hypothermia after cardiac arrest: a retrospective cohort study. **Eur J Clin Invest.** **2010** Apr;40(4):376-81. PubMed PMID: 20192974, DOI: 10.1111/j.1365-2362.2010.02259.x
26. **Balestra GM**, Nüesch R. [Souvenirs from vacation. Rocky Mountain spotted fever]. **Praxis** (Bern 1994). **2005** Nov 23;94(47):1869-70.
27. Hess C, Klimkait T, Schlapbach L, Del Zenero V, Sadallah S, Horakova E, **Balestra G**, Werder V, Schaefer C, Battegay M, Schifferli JA. Association of a pool of HIV-1 with erythrocytes in vivo: a cohort study. **Lancet.** **2002** Jun 29;359(9325):2230-4. PubMed PMID: 12103286, DOI: 10.1016/S0140-6736(02)09291-7

#### TEACHING

28. Diagnostic Errors Induced by a Wrong a Priori Diagnosis: A Prospective Randomized Simulator-Based Trial. Meyer FML, Filipovic MG, **Balestra GM**, Tisljar K, Sellmann T, Marsch S. **J Clin Med.** **2021** Feb 18;10(4):826. PMID: 33670489, DOI: 10.3390/jcm10040826.
29. The introduction of a standardised national licensing exam as a driver of change in medical education: A qualitative study from Switzerland. Huwendiek S, Jung D, Schirlo C, Huber P, **Balestra G**, Guttormsen S, Berendonk C. **Med Teach.** **2020** Oct;42(10):1163-1170. PMID: 32772611, DOI: 10.1080/0142159X.2020.1798911.
30. Berendonk C, Schirlo C, **Balestra G**, Bonvin R, Feller S, Huber P, Jünger E, Monti M, Schnabel K, Beyeler C, Guttormsen S, Huwendiek S. The new final Clinical Skills examination in human medicine in Switzerland: Essential steps of exam development, implementation and evaluation, and central insights from the perspective of the national Working Group. **GMS Z Med Ausbild.** **2015** Oct 15;32(4):Doc40. PMID: 26483853 DOI: 10.3205/zma000982.

#### VARIA

31. «Diabetische Ketoazidose unter Empagliflozin». Pfefferkorn F, **Balestra GM**, Hepprich M, Betz M, Krähenbühl S, Rätz Bravo AE, Leuppi-Taegtmeier A. **Swiss Med Forum.** **2019**;19(2930):473-475. DOI: <https://DOI.org/10.4414/smf.2019.08247>
32. Sutter R, Bruder E, Weissenburg M, **Balestra GM**. Thyroid hemorrhage causing airway obstruction after intravenous thrombolysis for acute ischemic stroke. **Neurocrit Care.** **2013** Dec;19(3):381-4. PMID: 23975614, DOI: 10.1007/s12028-013-9889-z

# CHAPTER

Curriculum vitae

# 14



## GIANMARCO BALESTRA, MD

Unterburgweg 1  
4143 Dornach  
Switzerland

Mobile CH: +41 79 270 98 76  
E-mail: gianmarco.balestra@protonmail.ch

### Particulars

Surname Balestra  
Name Gianmarco Maria  
Date of birth January 1<sup>st</sup>, 1974  
Place of birth Basel  
Marital status Married, 2 children  
Nationality Swiss

### Education

1994-2000 Studies of human medicine  
Federal Medical Diploma, November 2000  
Faculty of Medicine, University of Basel, Switzerland

1990-1993 Matura type B (Latin), December 1993  
Diploma with distinction  
Gymnasium Münchenstein, Münchenstein, CH

### Post-graduate Education

2022 Specialist Diploma Cardiology FMH

2017 Good Clinical Practice (GCP) basic course for investigators by CTU  
University Hospital Basel, Advanced Studies of University of Basel,  
endorsed by *swissethics*

2010 Specialist Diploma Intensive Care Medicine FMH

2005 Specialist Diploma Internal Medicine FMH

2004 Course for Emergency Physicians, Schweizerische Gesellschaft für  
Notfall- und Rettungsmedizin (SGNOR)

2001 ACLS Provider Diploma

### Professional Experience

09.23-to date Senior staff, Deputy Head Echocardiography Laboratory and  
Interventional Echocardiography, Cardiology, University Hospital  
Basel

01.22-08.23 Attending, Cardiology, University Hospital Basel

09.19-12.21 Fellow, Cardiology, University Hospital Basel

03.11-05.19 Attending, Medical Intensive Care, University Hospital Basel

12.09-11.10 Fellow, Surgical Intensive Care, University Hospital Basel

10.09-11.09 Fellow, Medical Intensive Care, University Hospital Basel

04.06-09.07 Attending, Internal Medicine, University Hospital Basel  
assigned to ICU and ED

01.04-03.06 Fellow, Internal Medicine, University Hospital Basel  
(7mths Internal Medicine, 5mths Medical Outpatient Clinic, 6mths  
Bone Marrow Transplantation Unit, 6mths ICU/CCU)

01.03-12.03 Resident, Anesthesia and Intensive Care, Cardiocentro Ticino,  
Lugano

07.01-12.02 Resident, Internal Medicine Ospedale Regionale di Lugano  
(Civico)  
(9mths Internal Medicine, 5mths ICU, 4mths ED)

### Teaching

2023-to date Working group member for development of 1<sup>st</sup> Swiss Master  
Studies for "Cardiac Sonographer" in cooperation with University  
Hospital Zurich and University of Applied Sciences Northwestern  
Switzerland (FHNW)

2022-to date Examiner for Board Examina, Swiss Society of Cardiology on  
behalf of Foedertio Medicorum Helveticorum (FMH)

2017-to date Examiner for Board Examina, Swiss Society of Intensive Care  
on behalf of Foedertio Medicorum Helveticorum (FMH)

2022-to date and 2015-2019 Lecturer, Faculty of Medicine, University of Basel

2013-2019 Development and Implementation of a generic electronic  
platform for work-placed based assessment for pre- and post-  
graduate candidates endorsed by Swiss Institute of Medical  
Education (Schweizerisches Institut für ärztliche Weiter- und  
Fortbildung), Medical Faculty Basel and University Hospital Basel

2011-2019	Working group member for further development and innovation of the Swiss Federal Licensing Exam (FLE):
	- New FLE exam formats project group 2016-2019
	- Clinical skills (CS) working group 2011-2019
	- Computer-based assessment (CBA) group 2011-2016
2011-2019	Responsible for clinical skills exams of the FLE, Faculty of Medicine Basel on behalf of the Swiss Federal Office of Public Health
2010-2012	Responsible for clinical skills exams of the Faculty of Medicine, University of Basel
2007-2014	Lecturer, Critical Care Nursing School, University Hospital Basel

### Research Experience

01.09-09.09	Research Fellow, Laboratory of Experimental Anesthesiology, Department of Anesthesiology, Erasmus MC, Rotterdam, NL
10.07-12.08	Research Fellow, Laboratory of Translational Physiology, Department of Biomedical Engineering and Physics, Academic Medical Center Amsterdam, Amsterdam, NL
03.2002	Medical thesis: „Etablierung der Grundlagen für den Nachweis Erythrozyten assoziierter HIV bei chronisch HIV-infizierten Patienten“. Supervisor: Dr. Dr. Ch.Hess, Prof. Dr. J. A. Schifferli; Co-Supervisor: Prof. Dr. P. Erb; Faculty of Medicine, University Basel

### Awards

2015	Project Award by the Swiss Institute of Medical Education (Schweizerisches Institut für ärztliche Weiter- und Fortbildung) for the development and implementation of a generic electronic platform for work-place based assessments
2008	ECCRN Basic Science Award of the European Society of Intensive Care Medicine (ESICM) for the project “Microcirculatory and Mito-chondrial Oxygenation in Sepsis-Induced Myocardial Dysfunction”

### Membership / Scientific Societies

Foederation Medicorum Helveticorum (FMH)  
 Verein Schweizer Assistenz- und Oberärzte (VSAO)  
 European Society of Intensive Care Medicine (ESICM)

# CHAPTER

PhD portfolio

# 15



## PHD PORTFOLIO

Description	Organizer	EC
<b>Required</b>		
21th ESICM LIVES (2008)	ESICM	1.10
Minisymposium LET IT FLOW (2009)	Medisch Centrum Leeuwarden	0.25
8th Swiss ICU Network Meeting (2009)	Swiss ICU Network	0.65
9th Swiss ICU Network Meeting (2010)	Swiss ICU Network	0.65
OSCE Workshops (2010)		0.40
32nd ISICEM Bruxelles (2012)	ISICEM	1.05
FCCS Course (2014)	Dept. Intensive Care Medicine, Inselspital Bern	0.65
27th ESICEM LIVES (2014)	ESICM	0.90
35th ISICEM Bruxelles (2015)	ISICEM	1.10
Good Clinical Practice (GCP) basic course (2017)	Swissetics	0.50
Annual Congress Swiss Society of Intensive Care Medicine (2018)	SSI	0.20
31st ESICM LIVES (2018)	ESICM	1.30
<b>Optional</b>		
Site Responsible of the Medical Faculty of University for the Swiss Federal Licensing Exam (FLE)of Basel (2019)	University of Basel, Medical Faculty	188.70
Examinator for Swiss Intensive Care Medicine Board Exam (2023)	Swiss Society of Intensive Care Medicine	1.40
Examinator for Cardiology Board Exams (2023)	Swiss Society of Cardiology	0.55
<b>Total EC</b>		<b>199.40</b>